การวิเคราะห์แบบแรงกระทำด้านข้างแยกโหมดสำหรับการประเมินโครงสร้างสะพาน

นาย อาน ฮง เหงียน

วิทยานิพนธ์นี้เป็นส่วนหนึ่งของการศึกษาตามหลักสูตรปริญญาวิศวกรรมศาสตรดุษฎีบัณฑิต
สาขาวิชาวิศวกรรมโยธา ภาควิชาวิศวกรรมโยธา
คณะวิศวกรรมศาสตร์ จุฬาลงกรณ์มหาวิทยาลัย
ปีการศึกษา 2553

MODAL PUSHOVER ANALYSIS FOR SEISMIC EVALUATION OF BRIDGES

Mr. An Hong Nguyen

A Dissertation Submitted in Partial Fulfillment of the Requirements
for the Degree of Doctor of Philosophy Program in Civil Engineering
Department of Civil Engineering
Faculty of Engineering
Chulalongkorn University
Academic Year 2010

Thesis Title	MODAL PUSHOVER ANALYSIS FOR SEISMIC EVALUATION OF BRIDGES
By	Mr. An Hong Nguyen
Field of study	Civil Engineering
Thesis Advisor	Assistant Professor Chatpan Chintanapakdee, Ph.D.
Thesis Co-Advisor	Professor Toshiro Hayashikawa, D.Eng.

Accepted by the Faculty of Engineering, Chulalongkorn University in Partial Fulfillment of the Requirements for the Doctoral Degree

..... Dean of the Faculty of Engineering
(Associate Professor Boonsom Lerdhirunwong, Dr.Ing.)

THESIS COMMITTEE

..... Chairman
(Professor Panitan Lukkunaprasit, Ph.D.)

..... Advisor
(Assistant Professor Chatpan Chintanapakdee, Ph.D.)

..... Co-Advisor
(Professor Toshiro Hayashikawa, D.Eng.)

..... Examiner
(Assistant Professor Anat Ruangrassamee, Ph.D.)

..... External Examiner
(Assistant Professor Arnon Wongkaew, Ph.D.)

อาน ฮง เหงียน: การวิเคราะห์แบบแรงกระทำด้านข้างแยกโหมดสำหรับการประเมินโครงสร้างสะพาน (MODAL PUSHOVER ANALYSIS FOR SEISMIC EVALUATION OF BRIDGES) อ.ที่ปรึกษาวิทยานิพนธ์หลัก: ผศ. ดร. ฉัตรพันธ์ จินตนาภักดี, อ.ที่ปรึกษาวิทยานิพนธ์ร่วม: ศ. ดร. โตชิโร ฮายาชิกาวา, 172 หน้า.

การวิเคราะห์วิธีประวัติเวลาไม่เชิงเส้นจัดเป็นวิธีที่ให้คำตอบถูกต้องที่สุดในการวิเคราะห์หาการตอบสนองของโครงสร้างต่อแผ่นดินไหวแต่วิธีนี้ทำได้เฉพาะวิศวกรที่มีความรู้ความชำนาญสูงเท่านั้นและใช้เวลาในการคำนวณนานเกินไปไม่เหมาะที่จะใช้ในการออกแบบหรือประเมินโครงสร้างตามปกติ วิธีวิเคราะห์แบบสถิตไม่เชิงเส้นหรือวิธีแรงกระทำด้านข้าง จึงเป็นวิธีที่ได้รับความนิยมมากกว่าถึงแม้จะให้คำตอบแบบประมาณซึ่งไม่ถูกต้องเท่าวิธีประวัติเวลาไม่เชิงเส้น งานวิจัยนี้มีวัตถุประสงค์เพื่อปรับปรุงวิธีวิเคราะห์แบบสถิตไม่เชิงเส้นซึ่งเดิมพัฒนาขึ้นมาใช้วิเคราะห์อาคารให้สามารถนำไปใช้ในการวิเคราะห์สะพานได้ ถึงแม้สะพานจะมีความซับซ้อนและต้องวิเคราะห์แบบ 3 มิติ เมื่อไม่นานมานี้ได้มีการพัฒนาให้วิธีวิเคราะห์แบบสถิตไม่เชิงเส้นมีความถูกต้องมากขึ้น ยกตัวอย่างเช่น วิธีแรงกระทำด้านข้างแบบแยกโหมด (modal pushover analysis, MPA) ซึ่งพิจารณารวมผลการตอบสนองเนื่องจากโหมดที่สูงกว่าโหมดพื้นฐานด้วย รวมถึงวิธี MPA ที่ถูกปรับปรุง และวิธีแรงกระทำด้านข้างที่เป็นสัดส่วนกับมวล งานวิจัยนี้จึงเริ่มด้วยการเปรียบเทียบความถูกต้องของวิธีวิเคราะห์แบบสถิตไม่เชิงเส้นทั้ง 3 วิธีดังกล่าว เพื่อเลือกใช้วิธีที่ดีที่สุด โดยทดลองนำไปวิเคราะห์อาคารที่ยึดรั้งด้วยตัวยึดที่ถูกป้องกันไม่ให้โก่งเดาะซึ่งมีพฤติกรรมที่ดีเพราะไม่มีการเสื่อมถอยของกำลัง จากการเปรียบเทียบพบว่า วิธี MPA และวิธี MPA ถูกปรับปรุง มีความคลาดเคลื่อนต่ำกว่าวิธีแรงกระทำด้านข้างที่เป็นสัดส่วนกับมวล โดยวิธี MPA มีความยุ่งยากในการคำนวณน้อยกว่าจึงได้ถูกเลือกนำไปพัฒนาเพื่อใช้วิเคราะห์สะพาน งานวิจัยนี้เสนอวิธี MPA ใหม่ที่พิจารณาตำแหน่งของการกระจัดที่ใช้บ่งชี้การเคลื่อนที่ในแต่ละโหมด ตามลักษณะของรูปร่างโหมด โดยเลือกตำแหน่งที่มีการกระจัดสูงสุด เพื่อให้สามารถพิจารณารูปร่างการตอบสนองเช่น การเคลื่อนที่ในแนวดิ่งหรือการบิดตัวของพื้นสะพานได้ จากนั้นทดลองนำวิธี MPA ที่เสนอใหม่ไปวิเคราะห์สะพานจริงแห่งหนึ่งที่ตั้งอยู่ในประเทศญี่ปุ่น ซึ่งเป็นแบบที่ใช้คานหน้าตัด I คู่และปูพื้นด้วยแผ่นคอนกรีตอัดแรง ภายใต้แรงแผ่นดินไหว 20 คลื่นและพิจารณาสะพานแบบที่ใช้แท่นรองรับ 2 รูปแบบ คือ แบบเหล็กธรรมดา และแบบยางที่มีแกนตะกั่ว ผลการวิเคราะด้วยวิธี MPA ถูกนำไปเปรียบเทียบกับผลการวิเคราะห์ด้วยวิธีประวัติเวลาไม่เชิงเส้น พบว่า เมื่อแรงแผ่นดินไหวกระทำในทิศทางตามยาว วิธีวิเคราะห์แบบแรงกระทำด้านข้างให้คำตอบที่ถูกต้องถึงแม้จะพิจารณาเฉพาะโหมดพื้นฐาน แต่เมื่อแผ่นดินไหวกระทำในทิศทางขวาง การวิเคราะห์แบบแรงกระทำด้านข้างที่พิจารณาเฉพาะโหมดพื้นฐานจะมีความคลาดเคลื่อนมาก แต่ถ้าใช้วิธี MPA จะได้คำตอบที่ถูกต้องมากกว่าโดยมีความคลาดเคลื่อนไม่เกินร้อยละ10 สำหรับสะพานในกรณีศึกษานี้ การประมาณค่าการบิดตัวของพื้นสะพานจะมีความคลาดเคลื่อนมากกว่าการหาการกระจัดหรือการเคลื่อนตัวสัมพัทธ์ระหว่างฐานกับยอดของเสาสะพาน

ภาควิชา วิศวกรรมโยธา ลายมือชื่อนิสิต

สาขาวิชา วิศวกรรมโยธา ลายมือชื่อ อ.ที่ปรึกษาวิทยานิพนธ์หลัก

ปีการศึกษา 2553 ลายมือชื่อ อ.ที่ปรึกษาวิทยานิพนธ์ร่วม

507 18800 21: MAJOR CIVIL ENGINEERING
KEYWORDS: BRIDGE / EARTHQUAKE / MODAL PUSHOVER ANALYSIS / NONLINEAR RESPONSE HISTORY ANALYSIS / NONLINEAR STATIC PROCEDURE / SEISMIC DESIGN

AN HONG NGUYEN: MODAL PUSHOVER ANALYSIS FOR SEISMIC EVALUATION OF BRIDGES. THESIS ADVISOR: ASST. PROF. CHATPAN CHINTANAPAKDEE, Ph.D., THESIS CO-ADVISORS: PROF. TOSHIRO HAYASHIKAWA, D.Eng., 172 pp.

Although nonlinear response history analysis (NL-RHA) is considered to be the most rigorous method to determine responses of a structure due to a strong earthquake excitation, it can only be undertaken by highly qualified engineers and may be too time-consuming for typical structural design and evaluation projects. The nonlinear static procedure, or pushover analysis, thus became a popular method to estimate building responses considering inelastic behavior, although the results are not as accurate as those from NL-RHA. This research aims to extend the nonlinear static procedure, originally developed for analyzing buildings, to analyze bridges. In recent years, there have been attempts to improve the accuracy of nonlinear static procedures, for example, modal pushover analysis (MPA), which includes response contributions from higher modes, improved modal pushover analysis (IMPA), or mass proportional pushover (MPP) procedures. This research first assesses the accuracy of these available procedures when applied to simpler structures like buckling-restrained-braced frame buildings, which have non-degrading behavior. It was found that MPA and IMPA provide good estimates of structural responses, while MPA is slightly easier to implement, so it was chosen to be modified for application to bridges. An extension of MPA procedure was proposed in this study to estimate seismic responses of complex actual bridges that require 3D analyses. In particular, the displacement monitoring point for pushover analysis, which is usually the roof displacement when buildings are analyzed, was proposed to be the point of largest displacement in the vibration mode considered, so that the contributions of torsional and vertical vibrations can be taken into account. The bias and dispersion of the proposed extension of MPA procedure was investigated in a case study of analyzing an existing continuous twin I-girder bridge with PC slab due to a set of twenty large-magnitude-small-distance (LMSR) ground motions. Two types of bridge bearing supports were considered: (1) steel bearing and (2) rubber bearing with lead core. The MPA estimates were compared to reference 'exact' values computed by NL-RHA. The results show that the pushover analysis, despite considering only the fundamental 'mode,' can accurately estimate responses due to excitation in the longitudinal direction, but one 'mode' pushover analysis is inadequate when excitation is in the transverse direction. In this case, MPA can provide better estimates with bias less than 10% for the studied bridge. The bias in estimating deck rotations due to torsional vibration is larger than in estimating displacements of the deck, or drifts of column piers.

Department: Civil Engineering Student's Signature .....

Field of Study: Civil Engineering Advisor's Signature .....

Academic Year: 2010 Co-Advisor's Signature Toshiro Hayashikawa

ACKNOWLEDGEMENTS

First of all, I would like to express my heartfelt gratitude to my academic advisor Assist. Prof. Dr. Chatpan Chintanapakdee for his continuous support, constant guidance, and valuable suggestions through out the course of this research. He showed me different ways to approach a research problem and the need of persistence to accomplish any goal. Without him, I could not have finished this project. It is my pleasure and honor to work with him.

I wish to extend my sincere thanks to my co-supervisor, Prof. Dr. Toshiro Hayashikawa, for his valuable ideas and advices. He brought out the good ideas in me. He had confidence in me when I doubted myself. His enthusiasm sustained my research project through disappointments and difficulties. I also want to thank him for his helps in bringing my family to visit me during my time in Japan. It gave me strength and energy to continue on with my journey.

Besides my advisors, I would like to thank the members of the examination committee: Prof. Dr. Panitan Lukkunaprasit, Assist. Prof. Dr. Anat Ruangrassamee, and Assist. Prof. Arnon Wongkaew for their insightful comments and constructive criticism.

This research has been greatly benefited from the correspondence with Prof. Stephen A. Mahin of University of California, Berkeley and Dr. Sutat Leelataviwat of King Mongkut's University of Technology. I also would like to thank Assoc. Prof. Behrouz Asgarian and Mr. H.R. Shokrgozar of K.N. Toosi University of Technology for providing the data used in this study. My thanks must go to all of my colleagues in the Center of Excellence in Earthquake Engineering and Vibration for their open discussions and recommendations.

I gratefully acknowledge the generous financial support provided by Japan International Cooperation Agency (JICA) through the ASEAN University Network / Southeast Asia Engineering Education Development Network (AUN/SEED-Net) program. This support has provided me the precious opportunity to pursue my goal in education in Thailand and Japan. It helps to make my dream comes true.

A special thanks to my parents, brothers, and sisters for unconditional support and encouragement to fulfill my desire of higher learning, and for taking care of my little family when I am away.

Last, but not least, I want to thank my wife, Cam Nhung Truong, for her love, her understanding, and for everything she has been doing for me and our son. I am particularly indebted to her. I also need to thank my little child for being a good son and for his sacrifice throughout the years I am away from him.

Once again, thank you all. I am so grateful to have all your helps and supports.

CONTENTS

Page

Page

LIST OF TABLES

LIST OF FIGURES

Figure Page

Figure Page

Figure Page

Figure Page

Figure Page

LIST OF ABBREVIATIONS

2D	Two-Dimensional
3D	Three-Dimensional
AMC	Adaptive Modal Combination
ADRS	Acceleration-Displacement Response Spectra
BRBF	Buckling-Restrained Braced Frame
CDD	Capacity Demand Diagram
CPA	Conventional Pushover Analysis
CQC	Complete Quadratic Combination
CSM	Capacity Spectrum Method
DCM	Displacement Coefficient Method
ELF	Equivalent Lateral Force
IMPA	Improved Modal Pushover Analysis
IRSA	Incremental Response Spectrum Analysis
LMSR	Large Magnitude Small distance
LRB	Lead Rubber Bearing
MDOF	Multi-Degree-Of-Freedom
MMP	Multimode Pushover Procedure
MMPA	Modified Modal Pushover Analysis
MPA	Modal Pushover Analysis
MPP	Mass Proportional Pushover
NL-RHA	Nonlinear Response History Analysis
NSA	Nonlinear Static Analysis
NSP	Nonlinear Static Procedure
RC-SMRF	Reinforced Concrete Special Moment Resisting Frame
RSA	Response Spectrum Analysis
SB	Steel Bearing
SDF	Single-Degree-of-Freedom
SPA	Standard Pushover Analysis
SRSS	Square-Root-of-Sum-of-Squares
UMRHA	Uncoupled Modal Response History Analysis

NOTATIONS

Greek symbols

α	stiffness hardening ratio
α_n	participation factor of the *n*th 'mode'
Γ_n	modal participation factor
ζ_n	damping ratio of *n*th mode
$\boldsymbol{\iota}$	influence vector
δ	standard deviation
θ	hinge rotation
$\hat{x}$	geometric mean
Δ	story drift
Δ^*_{MPA}	drift ratio
μ	ductility factor
$\boldsymbol{\phi}_n$	*n*th natural vibration mode
ϕ_{mn}	value of *n*th natural vibration mode at the monitoring point
ϕ_{rn}	roof value of *n*th natural vibration mode; and
ω_n	modal frequency
β	ratio of the modal frequencies
ρ_{in}	correlation coefficient

Roman symbols

A	pseudo-acceleration spectrum ordinate
$\mathbf{c}$	classical damping matrix
D_n	peak value of deformation of SDF system
$D_n(t)$	deformation of SDF system
g	gravity acceleration
$\mathbf{k}$	stiffness matrix

h_j	height of *j*th floor
L_n	defined by Equation (1.3)
$\mathbf{m}$	mass matrix
M_n	defined by Equation (1.3)
M_n^*	effective modal mass
$\mathbf{p}_{eff}$	effective earthquake force vector
q_n	modal coordinate
r	response quantity
r_g	response due to gravity loads
r_0	peak modal response
R	response modification factor
S_a	pseudo-acceleration
$\mathbf{s}_n^*$	force distribution of *n*th mode
T_n	*n*th natural period
$\mathbf{u}$	vector of displacements
$\mathbf{u}_e$	deformation shape vector in elastic range
$\ddot{u}_g(t)$	ground acceleration
u_r	roof displacement
u_{mn}	monitoring displacement of *n*th mode
$u_{rn}(t)$	roof displacement of *n*th mode of MDF system
u_{rno}	peak roof displacement of *n*th mode of MDF system
$(u_r)_{SDF}$	target roof displacement predicted by SDF system
$(u_r^*)_{SDF}$	target roof displacement ratio
V_b	base shear
V_{by}	base shear at the yield point; and
$\mathbf{w}$	weight matrix

CHAPTER I

INTRODUCTION

1.1 Background and Motivations

Nonlinear Response History Analysis (NL-RHA) is a powerful tool for study of structural seismic responses. The seismic performance of structures when subjected to a set of ground motions can be estimated accurately. In spite of the accuracy and efficiency of the computational tools have increased substantially, there are still some reservations about the NL-RHA, which are mainly related to its complexity for practical design applications. Therefore, NL-RHA is an onerous task to estimate seismic demands.

Since the nonlinear dynamic analysis of structures is not feasible for most practical applications, many researchers are trying to develop more rational analysis methods that would achieve a satisfactory balance between required reliability and applicability for everyday design use. Consequently, approximate procedures, called Nonlinear Static Procedures (NSPs) which are rooted in structural dynamic theory, were developed as an alternative to rigorous NL-RHA. The main content of approximate procedures is to estimate seismic demands of multi-degree-of-freedom (MDOF) systems due to an earthquake by nonlinear static analysis of structure which is simpler and more practical for structural design.

The Nonlinear Static Procedure (NSP) described in FEMA-356 (ASCE, 2000) and ATC-40 (ATC, 1996) guidelines for seismic evaluation of buildings, seismic demands are computed by nonlinear static analysis of the structure subjected to monotonically increasing lateral forces with a specified, usually invariant, height-wise distribution until a pre-determined target displacement is reached. The target roof displacement is determined from the deformation of an equivalent single-degree-of-freedom (SDF) system. Also known as pushover analysis, these procedures are now standard in structural engineering practice. They provide a better assessment of the actual capacity and expected performance of the structure than traditional linear static analysis, but require much less computational effort compared to rigorous Nonlinear

Response History Analysis. A formulation of the pushover analysis can be found in Krawinkler and Seneviratna (1998). This procedure is obviously based on two major assumptions: (1) the response of the multi-degree-of-freedom (MDOF) system can be related to the response of an equivalent SDF system, implying that the response is controlled by a single 'mode' and this mode shape remains unchanged even after yielding occurs; and (2) the invariant later force distribution can represent and bound the distribution of inertia forces during an earthquake.

However, these NSPs based on invariant load patterns provide accurate seismic demand estimates only for low- and medium-rise moment-frame buildings where contributions of higher 'modes' response are not significant and inadequate to predict inelastic seismic demands in buildings when the higher 'modes' contribute to the response (Krawinkler and Seneviratna, 1998; Gupta and Krawinkler, 1999; Gupta and Kunnath, 2000; Chopra and Goel, 2002; Chintanapakdee and Chopra, 2003a; Chopra and Chintanapakdee, 2004a; Kunnath and Kalkan, 2004; Chintanapakdee *et al.*, 2009; and Nguyen *et al.*, 2010). To overcome these drawbacks, an improved pushover procedure, called Modal Pushover Analysis (MPA), was proposed by Chopra and Goel (2002) to include contributions of higher 'modes', where seismic demands due to individual terms in the modal expansion of the effective earthquake forces are determined by a pushover analysis using the inertia force distributions associated with each mode up to a modal target displacement. The MPA procedure has been demonstrated to increase accuracy of seismic demand estimation in taller moment-frame buildings, e.g., 9- and 12-story tall, compared to the conventional pushover analysis (Chopra and Goel, 2002; Chintanapakdee and Chopra, 2003a; Chopra and Chintanapakdee, 2004a; and Chopra *et al.*, 2004; and Nguyen *et al.*, 2010).

Another type of pushover method is the adaptive pushover procedures, where the force distributions are updated to consider changes in the structure during inelastic phase (Fajfar and Fischinger, 1989; Bracci *et al.*, 1997; and Gupta and Kunnath, 2000). In this procedure, equivalent seismic loads are calculated at each pushover step using the immediate 'mode' shape. Recently, a new adaptive pushover method, called Adaptive Modal Combination (AMC) procedure, has been developed by Kalkan and

Kunnath (2006) where a set of adaptive mode-shape based inertia force patterns is applied to the structure. This procedure has been validated for regular moment frame buildings (Kalkan and Kunnath 2006; 2007). It was shown that the AMC procedure provides more accuracy in estimating seismic demands than MPA in comparison with Nonlinear Response History Analysis. However, it is conceptually complicated and computationally demanding for routine application in structural engineering practice while the MPA method is generally simpler, and thus, more practical than adaptive pushover procedures for seismic design.

These researches focused mainly on two-dimensional (2D) analysis of buildings while corresponding works on three-dimensional (3D) analysis and bridges have been very limited. Recently, a three-dimensional pushover analysis procedure to estimate seismic demands of a collapsed reinforced concrete chimney was proposed by Huang and Gould (2007). Meanwhile, a new modal pushover analysis procedure was proposed by Chopra and Goel (2004) to account for the effect of torsional vibration of asymmetric-plan buildings. Subsequently, an extension of modal pushover analysis procedure to seismic assessment of bridges was proposed by Paraskeva *et al.* (2006). The main goal of their study is to propose the displacement monitoring points of the bridge which will be discussed in the next section. At the same time as Paraskeva *et al.* (2006), a displacement-based adaptive pushover for assessment of buildings and bridges was developed by Pinho *et al.* (2006). This method is an extended version of adaptive pushover which takes into account both the contributions of higher ‘modes’ to response and the redistribution of inertia forces due to structural yielding associated changes in vibration properties. A number of idealized bridges were analyzed to verify this procedure. However, the finite element models of the bridges were simplified in these studies. In addition, due to limitations of the software used in these investigations, the pushover analysis and the NL-RHA had to be performed to different finite element models. In particular, nonlinear rotational spring elements were used in the finite element models used in NL-RHA, while the built-in beam hinge properties were implemented in the models set up for pushover analysis. Therefore, these simple models may not be able to capture the torsional and vertical vibrations of the deck of the bridges and their seismic behaviors may not represent the actual bridges.

The main objective of this study is to extend the modal pushover analysis procedure for seismic evaluation of complex actual bridges that requires a three-dimensional analysis procedure. The spatial modal force distributions are applied to pushover analysis. Furthermore, the monitoring displacement, which is the roof displacements in building analysis procedure, is proposed in this study to take into account the contributions of torsional and vertical vibrations of bridges.

The work presented in this dissertation focused on the bias and accuracy of the proposed extension of MPA procedure for seismic assessment of actual bridges. Its applicability in estimating seismic demands of bridges is investigated. The contribution is therefore towards an extension of modal pushover analysis procedure which can be applied in evaluating or designing actual bridges due to an earthquake.

1.2 Review of Previous Researches

There are several studies regarding the Nonlinear Static Procedures for seismic evaluation of structures. Most of these procedures can be classified into two major groups: (1) the non-adaptive group, and (2) the adaptive group. The approach of the first group is to consider the contribution of higher ‘modes’ but neglecting any changes in the mode shapes during an earthquake and using invariant lateral force pattern. The second group considers the effect of higher ‘modes’ as well as their changes after the structure yields due to an earthquake. The variant lateral load patterns are updated in each step to consider the change in structure during inelastic phase.

1.2.1 Estimating Deformation of Inelastic SDF System

One of critical tasks of nonlinear static procedures is to predict the target displacement of inelastic multi-degree-of-freedom structures due to a ground motion. Several approaches were proposed to estimate the target displacement by using an equivalent SDF system. The methods described in the ATC-40 and FEMA-356 guidelines are now commonly used in practice.

According to the nonlinear static procedure described in ATC-40 and FEMA-356 documents, seismic demands are computed by nonlinear static analysis of a structure subjected to monotonically increasing lateral loads representing inertia forces due to an earthquake (pushover analysis) with a specified, usually invariant height-wise distribution until a pre-determined target displacement is reached. The target displacement of these procedures is estimated from the deformation *D* of an equivalent inelastic SDF system which is derived from relationship between base shear force and roof displacement known as the pushover curve.

The ATC-40 presents an approach, called Capacity Spectrum Method (CSM), to estimate seismic response of inelastic SDF systems where the deformation *D* of an inelastic SDF system is determined by an iterative method which requires analysis of a sequence of equivalent linear systems with successively updated values of period and damping ratio. This method is typically implemented graphically. However, the accuracy and convergence of the ATC-40 iterative procedure can be considerable (Chopra and Goel, 2000). The ATC-40 tends to underestimate the deformation over a wide range of periods.

Unlike the ATC-40 Capacity Spectrum Method, FEMA-356 presents an alternative approach, known as Displacement Coefficient Method (DCM), in which the target displacement, δ_t, at each floor level is estimated by multiplying the deformation of the corresponding linear system.

$$\delta_t = C_0 C_1 C_2 C_3 S_a \left(\frac{T_e}{2\pi} \right)^2 g \qquad (1.1)$$

C_0 is modification factor to relate spectral displacement of an equivalent SDF system to the roof displacement of the building MDOF system. The coefficient C_1 relates expected maximum inelastic deformation to deformation determined for linear elastic response. The coefficient C_2 accounts for the effect of pinched hysteretic shape, stiffness degradation and strength deterioration on maximum displacement response and modification factor. C_3 represents the increase in the deformation due to negative post-yield stiffness arising from $P-\Delta$ effects. T_e is

effective fundamental period and S_a is spectral acceleration at the effective fundamental period and damping ratio of the structure in the direction under consideration. Numerical values of these coefficients are based on research results.

The limitations on accuracy of ATC-40 Capacity Spectrum Method such as lack of convergence or large error in some cases (Chopra and Goel, 2000), and the lack on research results of coefficient C_1 of FEMA-356 Displacement Coefficient Method are specified and rectified in FEMA-440 report (ATC, 2005). Then, an investigation on accuracy of improved nonlinear static procedures in FEMA-440 was carried out by Akkar and Metin, (2007). It was found that both of these improved procedures provide fairly good deformation demand estimations.

To overcome the limitation of previously mentioned methods, several improved methods were proposed and investigated. An improved Capacity Demand Diagram (CDD) method, which was originally developed by Freeman *et al.* (1975) and Freeman (1978), based on inelastic design spectrum for estimating seismic deformation of inelastic structures using SDF systems was developed and illustrated by Chopra and Goel, (1999a-b). Subsequently, Chopra *et al.* (2001), and Chopra and Goel, (2002) suggested that the contribution of the *n*th vibration mode to the target roof displacement of an inelastic MDOF system in MPA procedure u_{rno} is

$$u_{rno} = \Gamma_n \phi_{rn} D_n \tag{1.2}$$

where ϕ_{rn} = value at the roof of the *n*th mode shape vector $\boldsymbol{\phi}_n$ and

$$\Gamma_n = \frac{L_n}{M_n} \qquad L_n = \boldsymbol{\phi}_n^T \mathbf{m} \boldsymbol{\iota} \qquad M_n = \boldsymbol{\phi}_n^T \mathbf{m} \boldsymbol{\phi}_n \tag{1.3}$$

where $\mathbf{m}$ = mass matrix and $\boldsymbol{\iota}$ is the influence vector whose each element is equal to unity; and D_n is peak value of deformation $D_n(t)$ of an equivalent inelastic SDF system of *n*th 'mode', determined rigorously by nonlinear response history analysis by solving the uncoupled modal response history analysis (UMRHA) governing equation for the *n*th 'mode':

$$\ddot{D}_n + 2\zeta_n \omega_n \dot{D}_n + \frac{F_{sn}\left(D_n, \operatorname{sign} \dot{D}_n\right)}{L_n} = -\ddot{u}_g\left(t\right) \tag{1.4}$$

where natural frequency ω_n and damping ratio ζ_n correspond to the MDOF system, and $F_{sn} / L_n - D_n$ relation between resisting force and modal coordinate obtained from pushover curve as described in Chopra and Goel, (2002). For planar analysis of symmetric-plan building, the peak modal responses u_{rno}, each determined by pushover analysis for modal force distribution and dynamic analysis of the *n*th 'mode' inelastic SDF system, may be combined using an appropriate modal combination rule such as the square-root-of-sum-of-squares (SRSS) rule to obtain a MPA estimate of the total roof displacement:

$$\left(u_r\right)_{MPA} = \sqrt{\sum_{n=1}^{N} u_{rno}^2} \tag{1.5}$$

Then, an investigation on accuracy of single-degree-of-freedom estimate of displacement for pushover analysis of buildings was carried out by Chopra *et al.* (2003). The statistics show that the roof displacement of a multi-story building can be determined from the deformation of an equivalent SDF system. The estimation considering first 'mode' SDF system overestimates the median roof displacement for systems subjected to large ductility demand μ, but underestimates for small μ. The bias and dispersion of this method tend to increase for longer period system for every value of μ and increasing when $P-\Delta$ effects are included due to gravity loads. On the other hand, considering the contribution of higher 'modes' by using Equation (1.5) of MPA procedure helps reduce the dispersion in the roof displacement, but it increases slightly the overestimation of roof displacement of buildings responding far into the inelastic range (Chopra *et al.*, 2003).

For further examination, inelastic deformation ratios for design and evaluation of structures using SDF bilinear systems was investigated by Chopra and Chintanapakdee, (2004b) to assess the relationship between the peak deformation of inelastic and corresponding linear SDF systems.

1.2.2 Nonlinear Static Analysis Procedure for Symmetric Structures

The nonlinear static procedure in FEMA-356 (ASCE, 2000), which is commonly used in engineering practice, requires development of a pushover curve, a relationship between base shear forces versus roof displacement, by nonlinear static analysis of structure subjected to gravity loads, followed by monotonically increasing lateral forces with a specified invariant heightwise distribution. At least two force distributions must be considered for this approach. The first is to be selected among the following: (1) first mode distribution: $s_j^* = m_j \phi_{j1}$, where m_j is the mass and ϕ_{j1} is the mode shape value at the *j*th floor; (2) equivalent lateral force (ELF) distribution: $s_j^* = m_j h_j^k$, where h_j is the height above the base of *j*th floor and k is a coefficient related to the vibration period T_1 as shown in Equation (1.6) below; and (3) response spectrum analysis (RSA) distribution: A vertical distribution proportional to the story shear distribution calculated by combining modal responses from a response spectrum analysis of the building; a vector of lateral forces at the various floor levels is $s_{jn}^* = \Gamma_n m_j \phi_{jn}$.

$$k = \begin{cases} 1 & T_1 \le 0.5 \\ (T_1 + 1.5)/2 & 0.5 \le T_1 \le 2.5 \\ 2 & T_1 \ge 2.5 \end{cases} \tag{1.6}$$

The second distribution is either the uniform distribution or an adaptive distribution. Each of these force distribution is applied to the building in the same direction over the height of the building. These four FEMA-356 force distributions for the Los Angeles 9-story building are illustrated as follow by Chopra (2007) (Figure 1.1).

Seismic demands of building are determined by extracting the responses from the pushover analysis when the target displacement estimated by displacement coefficient method as mentioned before is reached. The potential and limitations of FEMA-356 force distributions are demonstrated by Goel and Chopra (2004a); and Chopra and Chintanapakdee (2004a). The FEMA-356 force distributions provide a good estimate of story drifts for low-rise building, e.g., 3-story buildings. However, the first ‘mode’ distribution grossly underestimates the story drifts, especially in the

upper stories of tall building, e.g., 9-, and 20-story buildings, implying that the higher mode contributions are significant in the seismic demands for upper stories. Although the ELF and RSA force distributions in FEMA-356 are intended to account the contribution of higher ‘modes’, they do not provide satisfactory estimates of seismic demands for buildings that are deformed moderately or far into the inelastic range. On the other hand, the uniform load distribution seems to significantly overestimate story drifts in lower stories and significantly underestimate in upper stories (Goel and Chopra, 2004a; and Chopra and Chintanapakdee, 2004a).

Nevertheless, the above method is obviously limited by the assumption that response of the structure is controlled by its fundamental ‘mode’. As a result, both the invariant forces distributions and the target displacement do not account for higher ‘modes’ contribution, which can affect both, particularly in the inelastic range. Therefore, extension of the standard pushover analysis to consider higher ‘mode’ effects has attracted attention. Firstly, Sasaki *et al.* (1998) developed the Multimode Pushover Procedure (MMP) to identify the effects of higher ‘modes’ in pushover analysis of buildings by appropriately extending the Capacity Spectrum Method (CSM), which directly compares building capacity to earthquake demand; separate pushover curves were derived for each mode without an attempt to combine modal responses.

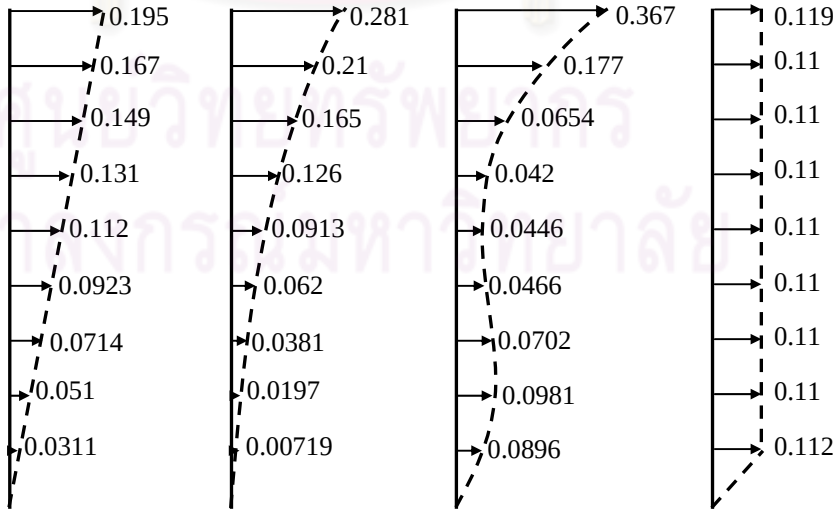

Figure 1.1 FEMA-356 force distributions for the Los Angeles 9-story building: (a) first ‘mode’; (b) ELF; (c) RSA; (d) uniform (Chopra, 2007).

To overcome the limitation of nonlinear static procedure in FEMA-356, an improved NSP known as Modal Pushover Analysis (MPA) was proposed by Chopra and Goel (2002) to account for the contribution of higher 'modes' in estimating seismic deformation demands for a symmetric-plan multistory building subjected to earthquake ground motion along an axis of symmetry. Seismic demands in MPA due to individual terms in the modal expansion of the effective earthquake forces are determined by a pushover analysis using the inertia force distributions associated with each 'mode' up to a modal target displacement. The peak value u_{rno} of $u_{rn}(t)$, the roof displacement of the inelastic MDF system due to earthquake forces $p_{eff,n}(t)$ can be estimated from Equation (1.2), where D_n is the peak value of deformation $D_n(t)$ of the *n*th 'mode' inelastic SDF system. It can be determined by solving Equation (1.4). Then, the peak modal responses r_{rno}, each determined by pushover analysis for force distribution $\mathbf{s}_n^* = \mathbf{m}\phi_n$ and dynamic analysis of the *n*th 'mode' inelastic SDF system, are combined using an appropriate modal combination rule, e.g., the SRSS, Equation (1.5), or CQC rule to obtain a MPA estimate of the total response. Although the rule of superposition of modal responses does not apply in the inelastic range of the response (because modes are not uncoupled anymore), Goel and Chopra (2004b) have shown that the error, taking the results of nonlinear response history analysis (NL-RHA) as the benchmark, is typically smaller than in the case that superposition is carried out at the level of loading (with fixed loading pattern) as recommended in FEMA-356. The lateral force distributions $\mathbf{s}_n^* = \mathbf{m}\phi_n$ of the SAC-Los Angeles 9-story building are illustrated as follow (Figure 1.2).

To assess the accuracy and classify the potential limitations of MPA procedure, an investigation on accuracy of MPA using generic frames was carried out by Chintanapakdee and Chopra (2003a-b); and an evaluation of modal and FEMA pushover analyses using vertically 'regular' and 'irregular' generic frames was done by Chopra and Chintanapakdee (2004a). Concurrently, an evaluation of modal and FEMA pushover analyses was carried out by Goel and Chopra (2004a). Then, the superiority of MPA method over the conventional dynamic analysis method recommended by the code, in a seismic evaluation of multi-storey RC frame was

brought out by Chandrasekaran and Roy (2006). The MPA procedure has been demonstrated to increase accuracy of seismic demand estimation in taller moment-frame buildings, e.g., 9- and 12-story tall, compared to the conventional pushover analysis.

Despite including the contribution of higher 'modes', MPA is conceptually no more difficult than standard procedures because higher 'modes' pushover analyses are similar to the first 'mode' pushover analysis. Moreover, MPA procedure considering the first few (two or three) 'modes' contribution are typically sufficient (Chintanapakdee and Chopra, 2003a; Chopra and Chintanapakdee, 2004a; and Chandrasekaran and Roy, 2006). Although MPA is sufficiently accurate to be useful in seismic evaluation of many buildings for many ground motions, and is much more accurate than FEMA-356 procedures, it may not be highly accurate for buildings subjected to very intense ground motions that deform the structure far into the inelastic range and the region of negative postyield stiffness (Goel and Chopra, 2004a; Chintanapakdee *et al.*, 2009).

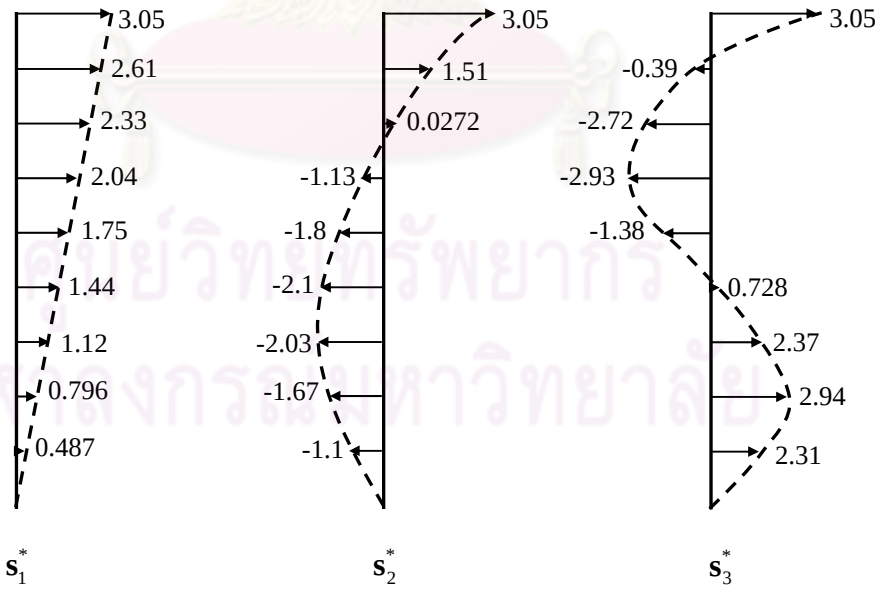

Figure 1.2 Lateral force distributions $\mathbf{s}_n^* = \mathbf{m}\boldsymbol{\phi}_n$, $n = 1$, 2 and 3 for first three 'modes' of the SAC-Los Angeles 9-story building (Chopra, 2007).

For further examination, an investigation on accuracy of MPA procedure for a different class of buildings, reinforced concrete special moment resisting frame (RC-SMRF) buildings, was carried out by Bobadilla and Chopra (2007). These RC-SMRF buildings were characterized by deterioration of strength and stiffness under cyclic deformation. The accuracy of MPA and FEMA-356 nonlinear static procedure in estimating seismic demands for RC-SMRF buildings was also compared in this research. It was concluded that even for intense ground motions that deform the buildings far into the inelastic range, the MPA procedure demonstrates a sufficient degree of accuracy, making it useful for practical application in estimating seismic demands for RC-SMRF structures.

To reduce the computational effort of MPA procedure in estimating seismic demands, a Modified Modal Pushover Analysis (MMPA) procedure was proposed by Chopra *et al*. (2004) in which the response contributions of higher vibration 'modes' are computed by assuming the building to be linearly elastic. It was found that the MMPA leads to a larger estimate of seismic demands, improving the accuracy of the MPA results in some cases (relative to nonlinear response history analysis). Although it is not necessarily more accurate than the MPA procedure, the MMPA approach provides a larger estimate of demand.

An alternative pushover method is the adaptive pushover procedure in which the load pattern distributions are redefined. The loading pattern is determined by modal combination rules (e.g. SRSS of modal loads) at each stage of the response during which the dynamic characteristics of the structure change, usually at each step when a new plastic hinge forms in inelastic range (Fajfar and Fischinger, 1987; Bracci *et al.*, 1997; and Gupta and Kunnath, 2000). In this procedure, equivalent seismic loads are calculated at each pushover step using the immediate 'mode' shape. Recently, a new adaptive pushover method, called Adaptive Modal Combination (AMC) procedure, has been developed by Kalkan and Kunnath (2006) where a set of adaptive mode-shape based on inertia force patterns is applied to the structure. This procedure has been validated for regular moment frame buildings (Kalkan and Kunnath, 2006; 2007). In recent development, an adaptive pushover analysis procedure called the Incremental Response Spectrum Analysis (IRSA) method was

proposed by Aydinoglu (2004) to take into account the influence of higher ‘modes’ as well as their changes in the mode shapes depending on the seismic intensity. In each pushover analysis, the effect of modal coupling on the formation of the plastic hinges is taken into account and each time a new hinge forms in the structure, elastic modal response spectrum analysis is performed to consider the change in the dynamic properties of the structure.

It was shown that the AMC procedure provides a higher accuracy in estimating seismic demands than MPA in comparison with Nonlinear Response History Analysis (NL-RHA). However, it is conceptually complicated and computationally demanding for routine application in structural engineering practice while the MPA method is generally simpler, and thus, more practical than adaptive pushover procedures for seismic design.

Back in the mid-1980s, a relatively simple nonlinear method, known as the N2 method (N stands for Nonlinear analysis and 2 for two mathematical models), was developed by Fajfar and Fischinger (1987, 1989). The method combines the nonlinear static pushover analysis of a MDOF system and the response spectrum analysis approach of an equivalent SDF system; similar to the capacity spectrum method, applied in ATC-40 and displacement coefficient method, applied in FEMA-356. It was initially based on the Q-model developed by Saiidi and Sozen (1981). This approach is based on two main assumptions: (1) the response of a structure is governed by one ‘mode’ and (2) this ‘mode’ does not change significantly when the structure is subjected to different seismic intensities. The N2 method has been included in the Eurocode 8 standards for the seismic analysis of structures (CEN, 2004a-b). Then, the method has been gradually improved by Fajfar and Gaspersic (1996) and its application has been extended to bridges (Fajfar *et al.*, 1997). The N2 method, for convenience, has been formulated in the acceleration-displacement $(A-D)$ format by Fajfar (1999). This version combines the advantages of the visual representation of the capacity spectrum method and the sound physical basis of inelastic demand spectra. Generally, the N2 method provides a reasonably accurate result for structures which oscillates predominantly in the first ‘mode’. The similarities and differences among the N2 method, the FEMA-273 (ATC, 1997), and

ATC-40 nonlinear static procedures for performance-based seismic design have been investigated and discussed by Fajfar (2000a). Subsequently, a practical version of the N2 method for seismic performance evaluation was developed by Fajfar (2000b). It was concluded that the applications of the methods are restricted to planar structures vibrating predominantly in the fundamental 'mode'; and can be used both for the seismic performance evaluation of newly designed or existing structures. However, the limitations of the N2 method as well as ATC-40 and FEMA-237 should be recognized as mentioned before.

Considering the influence of the higher 'modes' in the nonlinear pushover analysis of reinforced concrete single column bent viaducts, an investigation on ability of the N2 method (single mode procedure) and typical multimode approaches (MPA, adaptive pushover procedure, and IRSA) was carried out by Isakovic and Fishchinger (2006). It was concluded that the influence of higher 'modes' is typically small when the columns (substructure) do not hinder free deformation of the superstructure in transverse direction and the N2 method works well in these cases. Conversely, all multimode procedures provide good estimates in most cases, although the degree of accuracy was different among them. However, all the methods have limitations related to the higher 'modes' effect linked to the torsional flexibility in the transverse direction of the viaducts. It was also concluded that MPA is simpler and easier to apply than the other methods. On the other hand, IRSA is theoretically sound procedure but it requires considerable effort in application. Subsequently, an overview of the application of the N2 method and two typical multimode pushover procedures (MPA and IRSA) for the analysis of single column bent viaducts in the transverse direction was discussed by Isakovic *et al.* (2008). It shows that the N2 method is accurate enough for bridges where the effective modal mass of the fundamental mode is at least 80% of the total mass. On the contrary, both multi-mode procedures, MPA and IRSA, perform well in the case of the moderately irregular long viaducts, which are frequently used in construction design practice. Again, it was recommended that all pushover methods should be used with care for torsionally sensitive structures.

More recently, an Improved Modal Pushover Analysis (IMPA) procedure was proposed by Jianmeng *et al.* (2008) to consider the redistribution of inertia forces

after the structure yields. The structural stiffness changes after it yields, so the displacement shape vector also changes. The IMPA procedure uses the product of the time variant floor displacement vector (as the displacement shape vector) and the structural mass matrix as the lateral force distribution at each load step beyond the yield point of the structure. However, to avoid a large computation, only two phase lateral load distribution was recommended. In the first phase, the pushover analysis is performed by using the first few elastic natural 'modes' of structure, i.e., similar to the MPA. In the second phase, only for the first 'mode' the lateral load distribution is based on assumption that the floor displacement vector at the initial yielding point is the displacement shape vector.

An alternative pushover analysis procedure to estimate seismic displacement demands, referred to as the Mass Proportional Pushover (MPP) procedure, was recently proposed by Kim and Kurama (2008). The main advantage of MPP procedure over other approximate procedures is the use of a single pushover analysis for the structure with no need to conduct a modal analysis to capture the effect of higher 'modes'. The effects of higher 'modes' on the lateral displacement demands are lumped into a single invariant lateral force distribution that is proportional to the total seismic masses at the floor and roof levels, given by $\mathbf{m}g\iota = \mathbf{w}\iota$ where $\mathbf{m}$ is the mass matrix and $\mathbf{w}$ is weight matrix. This lateral force distribution is similar to uniform lateral force pattern described in FEMA-356. The floor/roof lateral displacement vector (normalized with respect to the roof displacement) obtained from the linear-elastic response range are used to replace 'mode' shape vector. This approximate approach is proposed for structures which are primarily governed by the first 'mode'; and thus, structures that develop weak/soft story mechanisms are outside the scope of this procedure.

1.2.3 Nonlinear Static Analysis Procedure for Unsymmetrical Structures

Nonlinear static pushover analysis procedures have attracted attentions of a lot of researchers since the mid-1980s. However, most of the work performed in the direction of improvement or extending the applicability of pushover analysis focused on planar frames or symmetrical buildings. Starting in 1997, various researchers have

extended pushover analysis to unsymmetrical-plan buildings. By applying a height-wise distribution of lateral forces, typical of standard planar pushover analysis at the floor centers of mass, an approximate nonlinear static analysis procedure was developed by Kilar and Fajfar (1997). Nevertheless, the procedure does not pretend to be very accurate by the authors' admission.

In the effort of extending the applicability of pushover analysis, an evaluation on the effect of multimode pushover analysis in three dimensional asymmetric frame structures was discussed by Barros and Almeida (2005). A different lateral force distribution was proposed for pushover analysis, based on a multimode combination of the vibration modes obtained from a linear elastic analysis of the structure. The proposed load pattern (LP) is proportional to the shape of the considered modes of vibration, each affected by the participation factor. The load pattern is defined in the following equation:

$$LP = \alpha_1 \phi_1 + \alpha_2 \phi_2 + ... + \alpha_n \phi_n = \sum_{i=1}^{n} \alpha_i \phi_i \tag{1.7}$$

where ϕ_n are the modes of vibration of the structure and α_n is the participation factor of the *n*th 'mode', that represents the contribution of each mode to the global response of the system using:

$$\alpha_n = \frac{R_n}{R_g} \tag{1.8}$$

The global dynamic response of a structure, R_g, subjected to a ground motion excitation is decomposed into modal contributions, R_n, using the equation:

$$R_g = \sum R_n \tag{1.9}$$

The proposed multi-mode load pattern was evaluated by comparing the results of the proposed pushover analysis with both the conventional pushover analysis (single mode pushover) and the results obtained from NL-RHA. It was concluded that the proposed multimodal load pattern improves the accuracy and reliability of the pushover analysis.

To consider the effect of torsional vibration of building, an extension of MPA procedure to unsymmetric-plan buildings, which respond in coupled lateral-torsional motions during earthquakes, was proposed by Chopra and Goel (2004). The force distribution $\mathbf{s}_n^*$ used in the pushover analysis for each 'mode' now includes two lateral forces and torque at each floor as:

$$\mathbf{s}_n^* = \begin{Bmatrix} \mathbf{m}\phi_{xn} \\ \mathbf{m}\phi_{yn} \\ \mathbf{I}_O\phi_{\theta n} \end{Bmatrix} \tag{1.10}$$

where $\mathbf{m}$ is a diagonal mass matrix with diagonal entry $m_{jj} = m_j$, the mass lumped at the *j*th floor diaphragm; I_O is a diagonal matrix with diagonal entry $I_{jj} = I_{Oj}$, the polar moment of inertia of the *j*th floor diaphragm about a vertical axis through the center of mass (CM); and ϕ_{xn}, ϕ_{yn} and $\phi_{\theta n}$ are three subvectors of the *n*th natural vibration mode of the structure, $\boldsymbol{\phi}_n$.

Between the two pushover curves obtained corresponding to two lateral directions, *x* and *y*, preferably choose the pushover curve in the dominant direction of the motion of the 'mode'. Gravity loads and their $P-\Delta$ effects are now included in pushover analysis for all 'modes'. The response due to the *n*th 'mode' is computed by $r_n = r_{n+g} - r_g$, where r_g is the contribution of gravity load alone. The total seismic demands are determined by combining gravity response and the peak 'modal' responses using the complete quadratic combination (CQC) rule, instead of the SRSS rule:

$$r \approx \max\left[r_g \pm \left(\sum_{i=1}^{J}\sum_{n=1}^{J} \rho_{in} r_i r_n \right)^{1/2} \right] \tag{1.11}$$

where the correlation coefficient ρ_{in} is given by:

$$\rho_{in} = \frac{8\sqrt{\zeta_i \zeta_n}\left(\beta_{in}\zeta_i + \zeta_n\right)\beta_{in}^{3/2}}{\left(1-\beta_{in}^2\right) + 4\zeta_i\zeta_n\beta_{in}\left(1+\beta_{in}^2\right) + 4\left(\zeta_i^2 + \zeta_n^2\right)\beta_{in}^2} \tag{1.12}$$

in which $\beta_{in} = \omega_i / \omega_n$ is the ratio of the *i*th and *n*th modal frequencies, and ζ_i and ζ_n are the damping ratios for these modes.

The extended MPA procedure to unsymmetric-plan buildings has been demonstrated to provide generally accurate seismic response estimates for unsymmetric systems to a similar degree as it was for a symmetric building (Chopra and Goel, 2004; Goel and Chopra, 2005).

Meanwhile, Fajfar and his co-workers have observed that the torsional effects of plan-asymmetric buildings are mostly pronounced in the elastic range and early stages of plastic behavior and tend to decrease with an increase in the plastic deformations. Hence, the amplifications in the displacement demands due to torsional effects computed from elastic dynamic analysis can be used as a rough and conservative estimate both in the elastic and inelastic range. Based on this observation, Fajfar *et al.* (2005) developed the extension of the N2 method, which was developed for the nonlinear static analysis of planar structures, to plan-asymmetric buildings. Pushover analysis of the three-dimensional (3D) mathematical model of the building is performed independently in two horizontal directions and the target roof displacement for each horizontal direction is computed using the N2 method. Then, a linear response spectrum analysis of the 3D model is carried out independently in two horizontal directions and the results are combined using the SRSS rule. The correction factors to be applied to the relevant results of pushover analysis are determined. After that, the correction factor is defined as the ratio between the normalized roof displacements obtained by elastic modal analysis and by pushover analysis. The normalized roof displacement is the ratio of the roof displacement at an arbitrary location to the roof displacement at the center of mass (CM).

Subsequently, a 3D pushover analysis procedure was developed by Huang and Gould (2007) to analyze a collapsed reinforced concrete chimney. The idea of this new approach is to apply two directional lateral forces to the structure to obtain the responses over the height. However, the lateral load patterns may be selected from those that were described in FEMA-356.

To evaluate the capability and applicability of the extension of N2 method (Fajfar *et al.*, 2005) and extension of MPA approach (Chopra and Goel, 2004) in capturing the torsional effects that arise from plan irregularities, an assessment of these procedures on the estimation of torsional effects in low-rise frame buildings was carried out by Erduran, (2008). Results of numerical analyses show that far-fault and near-fault ground motions have similar influences on the displacement demand of structures as far as torsional effects are concerned. These procedures proposed for asymmetric buildings were found to be effective in capturing torsional effects whereas the classical nonlinear static procedure developed originally for planar systems significantly underestimates torsional rotation demands in structures.

1.2.4 Nonlinear Static Analysis Procedure for Bridges

In view of previous considerations, most of researches performed in the direction of extending the applicability of pushover analysis to structures focused on buildings. Such works on bridges, on the other hand, have been implemented for a limited number of cases; although the contribution of higher ‘mode’ on bridges usually play a more critical role than in buildings.

The inelastic behavior of a highway concrete bridge (Greveniotikos bridge) was investigated by Abeysinghe *et al.* (2002) from the first pier hinging to the inelastic equilibrium condition during the design-level earthquake by using the conventional pushover analysis. The effects on the seismic demand of period lengthening and damping increase produced by structural deterioration were evaluated in this study. Pushover analysis is performed in both longitudinal and transverse directions in which invariant force patterns are applied separately. The capacity curve (pushover curve) and the initial curve (design spectrum) are both plotted in the acceleration-displacement response spectra (ADRS) domain. Then, the design of Greveniotikos was checked by using the well known capacity spectrum method.

Aydinoglu (2004) proposed the Incremental Response Spectrum Analysis (IRSA) as mentioned previously, which includes an application to a bridge structure, taking one or eight ‘modes’ into account, without any detailed discussion of the resulting differences. In the studies by Isakovic and Fishchinger (2006) and Isakovic

et al. (2008), investigations on ability of the N2 method (single mode procedure) and typical multimode approaches (MPA, adaptive pushover procedure, and IRSA) were carried out for the analysis of hypothetical irregular, torsionally sensitive bridges.

Recently, an extension of modal pushover analysis procedure to seismic assessment of bridges was proposed by Paraskeva *et al.* (2006). It was then examined the relative accuracy by comparing results with results obtained from NL-RHA as well as 'standard' pushover analysis (SPA) (single 'mode' load pattern) for a realistic case of highway bridge. In their study, the capacity spectrum method (CSM) was used to define the earthquake displacement demand associated with each of pushover curves, instead of NL-RHA of each SDF system proposed by Chopra and Goel (2002). The main goal of their study is to propose the displacement monitoring points of the bridges. It was suggested that the monitoring point may be the point of the deck that corresponds to the location of an equivalent SDF system (along the longitudinal axis of the bridge), x_n^*, defined by following relationship:

$$x_n^* = \frac{\sum_{j=1}^{N} x_j m_j \phi_{jn}}{\sum_{j=1}^{N} m_j \phi_{jn}} \tag{1.13}$$

in which, x_j is the distance of the *j*th mass from a selected point of the bridge, and ϕ_{jn} is the ordinate of the *n*th mode shape $\boldsymbol{\phi}_n$ at the *j*th mass. x_n^* is essentially independent of the way the 'mode' is normalized. It was concluded that comparative evaluation of the calculated response of the bridge illustrates the applicability and potential of the MPA approach for bridges.

At the same time as Paraskeva *et al.* (2006), a displacement-based adaptive pushover for assessment of buildings and bridges was developed by Pinho *et al.* (2006). This method is an extended version of adaptive pushover which takes into account both the contributions of higher 'modes' to response and the redistribution of inertia forces due to structural yielding and associated changes in vibration properties. A number of idealized 2D bridges were analyzed to verify this procedure. The results

show that the approach can lead to the attainment of significantly improved predictions.

More recently, to assess the suitability of various analysis methods and software tools for performing practical seismic analysis of structures, an evaluation of nonlinear static analysis methods and software tools [SAP2000 (CSi, 1997), GT-STRUDL (GT-STRUDL, 2000), ADINA 800-node (ADINA, 2000), and SC-Push3D (SC Solutions, 1998)] for seismic analysis of a two-span highway bridge was carried out by Shattarat *et al.* (2008). The analysis revealed that some software programs are well suited to perform nonlinear static analysis.

In these studies, the finite element models of the bridges were simplified. Therefore, these simple models may not able to capture the torsional and vertical vibrations of the deck of the bridges and their seismic behaviors may not represent for the actual bridges.

1.2.5 Displacement Monitoring Point

One of critical steps of multi-mode pushover procedures is to select the displacement monitoring point, which is usually the roof when buildings are analyzed. The selection of the monitoring point affects the shape of the pushover curve in the inelastic range. For bridges, intuitive selections for the displacement monitoring point are the centre of deck mass as recommendation by CEN (2004a-b). It can be also selected as the point of the deck which is determined from the properties of the structure using Equation (1.13) recommended by Paraskeva *et al.* (2006). However, the applicability of this approach in structural engineering practice seems to be unsuitable for complicated structures.

Another proposal for the displacement monitoring point of single column bent viaducts is at the maximum displacement of the superstructure as recommended by Isakovic and Fischinger (2006). The selection of the displacement monitoring point for multi-mode pushover analysis of bridge as recommendation of the previous mentioned researchers is not able to take into account the contributions of torsional and vertical vibrations of the bridge because the modal load patterns will not cause any displacements at that monitoring point. To overcome these drawbacks, relevant

displacement monitoring points for MPA procedure when it is applied to bridges will be proposed in Section 2.3 of this study.

1.3 Research Objectives

Based on a comprehensive literature review, the primary objective of this study is to develop an MPA procedure to analyze bridges that require a three-dimensional analysis. The objectives of this research are as follows:

(1) Investigation on the accuracy of current nonlinear static procedures for seismic assessment of steel structures such as buckling-restrained braced frames.

(2) To develop an MPA procedure which can be applied to three-dimensional analysis of bridges using spatial distribution force patterns.

(3) Relevant displacement monitoring points are proposed and evaluated for this pushover analysis procedure when it is applied to bridges.

(4) To evaluate the bias and accuracy of proposed MPA procedure for bridges by comparing the results obtained from MPA estimates with results determined by NL-RHA as well as conventional pushover analysis.

1.4 Scope of Research

The scopes of this research are stated as follows:

(1) An existing continuous twin I-girder bridge with PC slab is analyzed to evaluate the bias and accuracy of proposed MPA procedure.

(2) Both geometric and material non-linearities, which are crucial for understanding the complex structural behaviour under strong earthquake excitations, are accounted for.

(3) Two cases of bearing supports are considered in this study: (a) the superstructure is supported by steel bearings (SBs); and (b) the deck is seismically isolated by Lead Rubber Bearings (LRBs). A trilinear force-deformation model of the LRB bearings is used to accurately represent the influence of hardening of isolators at the high strains induced by intense earthquake ground motions.

(4) A set of Large-Magnitude-Small-distance (LMSR) ground motions (20 records) is used to evaluate the bias and accuracy of proposed MPA procedure for bridges.

(5) The bias and accuracy of the proposed extension of MPA procedure are evaluated by a comparison of the response quantities with results from Nonlinear Response History Analysis (NL-RHA) which can be considered as 'exact' results. Conventional pushover analysis procedure was also evaluated.

(6) The response quantities considered in this study are the peak deck displacements, pier (column) drifts, hinge rotations and internal forces, which are the main quantities used for assessing the bridges. The pier drift, which indicates deformation demand in the column, is defined as the displacement at top of the pier relative to its base divided by the pier height.

(7) Multiple-support excitations are not considered in this research.

1.5 Assumptions

The assumptions used in this study are stated as follows:

(1) Plastic hinges form at beam or column ends whereas the rest of each element remains elastic.

(2) The coupling of modal coordinates due to yielding of the structure is neglected in the proposed extension of MPA procedure.

1.6 Organization of the Contents

The dissertation contents are organized into six chapters. The first chapter presents the general introduction of this study including the research motivations, a brief review of previous researches and research objectives.

In Chapter 2, the theoretical backgrounds of nonlinear response history analysis and modal pushover analysis procedures to estimate seismic demands for inelastic systems are presented. Then, an extension of modal pushover analysis procedure for seismic evaluation of bridges is proposed.

With the increase in the number of alternative pushover analysis procedure proposed in recent years, it is useful to assess the accuracy and classify the potential limitations of these methods. Therefore, Chapter 3 provides an assessment of current nonlinear static procedures for seismic evaluation of buckling-restrained braced frame buildings.

Chapter 4 presents the configuration and the comprehensive three-dimensional analytical model of the continuous twin I-girder bridge which is selected to evaluate the bias and accuracy of the proposed extension of MPA procedure. Subsequently, the ensemble of 20 ground motions and statistical analysis are introduced.

In Chapter 5, the bias and accuracy of the proposed extension of MPA procedure in estimating peak displacements, pier drifts, internal forces and hinge rotations of studied bridge are evaluated by comparing with the results determined by NL-RHA which can be considered as ‘exact’ solutions. Moreover, the effects of bearing supports on the accuracy of the proposed extension of MPA procedure are investigated.

Finally, the significant findings and general conclusions obtained throughout this research are summarized in Chapter 6.

CHAPTER II

THEORETICAL BACKGROUND AND METHODOLOGY

2.1 Introduction

In recent years, nonlinear structural analysis has gained a greater momentum because of the need to assess inelastic structural behavior under earthquake loads. Common seismic design philosophies for buildings or bridges allow some degree of damage without collapse. To control and evaluate damage, a post-elastic nonlinear structural analysis is required (Moehle, 1995; and JSCE, 1996). Nonlinear Response History Analysis (NL-RHA) is usually performed for the safety evaluation of structures to determine their inelastic responses when subjected to strong earthquake ground motions. This method is a powerful tool and provides a realistic measure of structural responses.

Although the nonlinear response history analysis is not difficult in concept, it requires careful structural modeling and intensive computing effort. The NL-RHA of structures therefore is not feasible for most practical applications. On the other hand, the nonlinear static analysis procedures which are rooted in structural dynamic theory have advantages in that it is simpler and more practical than NL-RHA for structural design. These approaches have been demonstrated to provide reasonable results in estimating seismic demands for buildings. The Modal Pushover Analysis (MPA) procedure has been considered as one of the efficient methods of approximate procedures that would achieve a satisfactory balance between required reliability and applicability for everyday design use.

Theoretical approaches of the NL-RHA and the MPA procedure to estimate seismic demands for inelastic systems are presented in this chapter. First, the theoretical background of rigorous nonlinear response history analysis is reviewed. Then, the approximate MPA procedure for inelastic systems developed earlier for estimating seismic demands for buildings (Chopra and Goel, 2002) is presented. Finally, an extension of modal pushover analysis procedure for seismic evaluation of bridges is proposed.

2.2 Modal Pushover Analysis Procedures: Inelastic Systems

2.2.1 Nonlinear Response History Analysis (NL-RHA)

The governing equations of an inelastic system due to earthquake ground motion $\ddot{u}_g(t)$ are as follows:

$$\mathbf{m}\ddot{\mathbf{u}} + \mathbf{c}\dot{\mathbf{u}} + \mathbf{f}_s(\mathbf{u}, \operatorname{sign}\dot{\mathbf{u}}) = -\mathbf{m}\boldsymbol{\iota}\ddot{u}_g(t) \tag{2.1}$$

where $\mathbf{u}$ is the vector of displacements, $\mathbf{m}$, $\mathbf{c}$, and $\mathbf{k}$ are the mass, classical damping, and lateral stiffness matrices of the system; $\boldsymbol{\iota}$ is the influence vector whose each element equals to unity. These coupled equations can be solved directly to get 'exact' NL-RHA results.

The right hand side of Equation (2.1) can be considered as effective earthquake forces:

$$\mathbf{p}_{eff}(t) = -\mathbf{m}\boldsymbol{\iota}\ddot{u}_g(t) \tag{2.2}$$

The effective earthquake forces can then be expressed as

$$\mathbf{p}_{eff}(t) = \sum_{n=1}^{N} \mathbf{p}_{eff,n}(t) = \sum_{n=1}^{N} -\mathbf{s}_n \ddot{u}_g(t) \tag{2.3}$$

where $\mathbf{s}_n$ is modal inertia force distribution for the *n*th-mode

$$\mathbf{s}_n = \Gamma_n \mathbf{m}\boldsymbol{\phi}_n \tag{2.4}$$

and

$$\mathbf{m}\boldsymbol{\iota} = \sum_{n=1}^{N} \mathbf{s}_n = \sum_{n=1}^{N} \Gamma_n \mathbf{m}\boldsymbol{\phi}_n \tag{2.5}$$

in which $\boldsymbol{\phi}_n$ is the *n*th natural vibration mode of the structure, and

$$\Gamma_n = \frac{L_n}{M_n}; \qquad L_n = \boldsymbol{\phi}_n^T \mathbf{m}\boldsymbol{\iota}; \qquad M_n = \boldsymbol{\phi}_n^T \mathbf{m}\boldsymbol{\phi}_n \tag{2.6}$$

The contribution of the *n*th-mode to the effective earthquake forces (Equation 2.3) can then be rewritten as

$$\mathbf{p}_{eff,n}(t) = -\mathbf{s}_n \ddot{u}_g(t) \tag{2.7}$$

The effect of $\mathbf{p}_{eff,n}(t)$ to the response of the inelastic MDF system is entirely in the *n*th-mode, with no contributions from other modes.

The classical modal analysis is no longer valid for inelastic system because the coupling of modal co-ordinates due to yielding of the structure. The 'modes' other than the *n*th-'mode' will also contribute to the system response:

$$\mathbf{u}_n(t) = \sum_{r=1}^{N} \boldsymbol{\phi}_r q_r(t) \tag{2.8}$$

However, Chopra and Goel (2002) have demonstrated that the contributions of 'modes' other than the *n*th-mode are relatively small or weakly coupled. Expanding the displacements of the inelastic system in terms of the natural vibration modes of the corresponding linear system, we get

$$\mathbf{u}(t) = \sum_{n=1}^{N} \boldsymbol{\phi}_n q_n(t) \tag{2.9}$$

Substituting Equation (2.9) into Equation (2.1), and pre-multiplying both side by $\boldsymbol{\phi}_n^T$, then using the orthogonality of mass, and classical damping of modes gives

$$\ddot{q}_n + 2\zeta_n \omega_n \dot{q}_n + \frac{F_{sn}}{M_n} = -\Gamma_n \ddot{u}_g(t), \quad n = 1, 2, ..., N \tag{2.10}$$

Equation (2.10) represents *N* equations in the modal co-ordinates q_n. Unlike linearly elastic systems, these equations are coupled for inelastic systems.

2.2.2 Modal Pushover Analysis (MPA)

If the effect of coupling of modal coordinates for inelastic system is neglected, Equation (2.10) leads to the Uncoupled Modal Response History Analysis (UMRHA) procedure. This approximate RHA procedure was proposed by Chopra and Goel (2002) and used as a basis for developing an MPA procedure for inelastic systems.

Neglecting the coupling of modal coordinates, the displacements of system can be approximated as:

$$\mathbf{u}_n(t) = \sum_{r=1}^{N} \boldsymbol{\phi}_r q_r(t) \simeq \boldsymbol{\phi}_n q_n(t) \tag{2.11}$$

Substituting this approximation into Equation (2.1), and pre-multiplying by $\boldsymbol{\phi}_n^T$ gives Equation (2.10):

$$\ddot{q}_n + 2\zeta_n \omega_n \dot{q}_n + \frac{F_{sn}}{M_n} = -\Gamma_n \ddot{u}_g(t), \quad n = 1, 2, ..., N \tag{2.10}$$

where F_{sn} now depends only on one modal co-ordinate, q_n:

$$F_{sn} = F_{sn}(q_n, \operatorname{sign} \dot{q}_n) = \boldsymbol{\phi}_n^T \mathbf{f}_s(q_n, \operatorname{sign} \dot{q}_n) \tag{2.12}$$

The solution q_n of Equation (2.10) now can be expressed in similar form with linear elastic systems:

$$q_n(t) = \Gamma_n D_n(t) \tag{2.13}$$

Substituting Equation (2.13) into Equation (2.10) gives:

$$\ddot{D}_n + 2\zeta_n \omega_n \dot{D}_n + \frac{F_{sn}}{L_n} = -\ddot{u}_g(t) \tag{2.14}$$

and

$$F_{sn} = F_{sn}(D_n, \operatorname{sign} \dot{D}_n) = \boldsymbol{\phi}_n^T \mathbf{f}_s(D_n, \operatorname{sign} \dot{D}_n) \tag{2.15}$$

Equation (2.14) is the equation of motion for the *n*th-mode inelastic SDF system with vibration properties (natural frequency ω_n and damping ratio ζ_n) of the *n*th-mode of the corresponding linear MDF system subjected to $\ddot{u}_g(t)$.

Substituting Equation (2.13) into Equation (2.11) gives the displacements

$$\mathbf{u}_n(t) = \Gamma_n \boldsymbol{\phi}_n D_n(t) \tag{2.16}$$

Response quantities of inelastic system denoted as $r(t)$, e.g., story drifts, internal element forces, etc., can be expressed as

$$r_n(t) = r_n^{st} A_n(t) \tag{2.17}$$

where r_n^{st} denotes the modal static response which is determined by nonlinear static analysis due to lateral force pattern $\mathbf{s}_n$, and

$$A_n(t) = \omega_n^2 D_n(t) \tag{2.18}$$

is the pseudo-acceleration response of the *n*th-mode inelastic SDF system. Figure 2.1 shows the conceptual explanation of these approaches.

The response of the inelastic system to the total excitation $\mathbf{p}_{eff}(t)$ is given by:

$$\mathbf{u}(t) = \sum_{n=1}^{N} \mathbf{u}_n(t) = \sum_{n=1}^{N} \Gamma_n \boldsymbol{\phi}_n D_n(t) \tag{2.19}$$

$$r(t) = \sum_{n=1}^{N} r_n(t) = \sum_{n=1}^{N} r_n^{st} A_n(t) \tag{2.20}$$

Equations (2.17) to (2.20) are used to estimate seismic demands of inelastic system due to an earthquake and known as the UMRHA procedure.

Alternatively, the peak response r_n of the inelastic system to $\mathbf{p}_{eff,n}(t)$ can be determined by a nonlinear pushover analysis of the structure subjected to lateral forces $\mathbf{s}_n^* = \mathbf{m}\boldsymbol{\phi}_n$ with the forces increased to push the structure up to the target roof displacement u_{rno}.

$$u_{rno} = \Gamma_n \phi_{rn} D_n \tag{2.21}$$

in which D_n is determined by solving Equation (2.14) with dynamic properties (e.g., natural frequency ω_n and damping ratio ζ_n) are based on the *n*th-mode pushover curve, a relationship between base shear V_{bn} and roof displacement u_{rn} as shown in Figure 2.2a. This capacity curve is then idealized as a bilinear curve.

Subsequently, convert the idealize bilinear curve to the force-deformation $(F_{sn}/L_n - D_n)$ curve for the *n*th-mode inelastic SDF system, which is required in Equation (2.14) by:

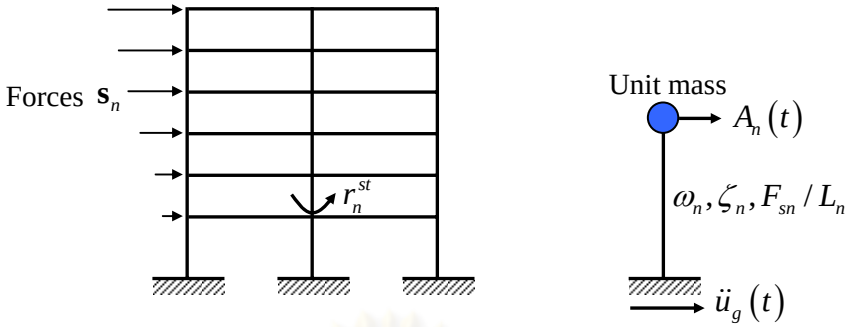

(a) Static analysis of structure

(b) Dynamic analysis of Inelastic SDF system

Figure 2.1 Conceptual explanation of uncoupled RHA of inelastic MDF system (Chopra and Goel, 2002).

$$\frac{F_{sn}}{L_n} = \frac{V_{bn}}{M_n^*} \quad ; \quad D_n = \frac{u_{rn}}{\Gamma_n \phi_{rn}} \tag{2.22}$$

The concept of this step is shown in Figure 2.2b, where the yield values of F_{sn}/L_n and D_n are

$$\frac{F_{sny}}{L_n} = \frac{V_{bny}}{M_n^*} \quad ; \quad D_{ny} = \frac{u_{rny}}{\Gamma_n \phi_{rn}} \tag{2.23}$$

in which $M_n^* = L_n \Gamma_n$ is the effective modal mass, and ϕ_{rn} is the value of the roof of $\boldsymbol{\phi}_n$.

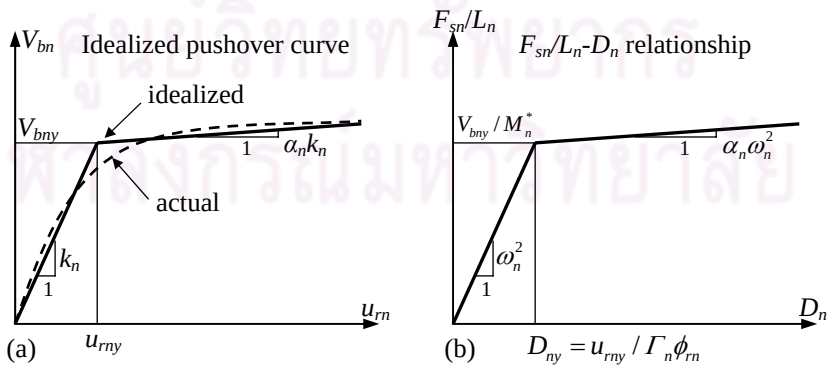

Figure 2.2 (a) Pushover curve and (b) Force and deformation relationship of SDF system.

The initial slope of this curve is equal to ω_n^2 indicating that the vibration period T_n of the inelastic SDF system is given by

$$T_n = 2\pi \left(\frac{L_n D_{ny}}{F_{sny}} \right)^{1/2} \tag{2.24}$$

in which subscript y indicates the yield values. This value of T_n, which may differ from the period of the corresponding linear system, should be used for estimating deformation of the inelastic SDF system.

The peak modal response are combined according to the Square-Root-Of-Sum-Of-Squares (SRSS) by Equation (2.25) or the Complete Quadratic Combination (CQC) rules.

$$r_o \approx \left(\sum_{n=1}^{N} r_{no}^2 \right)^{1/2} \tag{2.25}$$

More details of the this procedure can be found in Chopra and Goel (2002).

2.3 Proposed Extension of MPA Procedure for Seismic Evaluation of Bridges

The previously mentioned modal pushover analysis (MPA) procedure, which was proposed by Chopra and Goel (2002), is an extension of conventional pushover analysis to include contribution of higher ‘modes’. This approach was developed to estimate seismic demands for buildings. To extend the applicability of MPA procedure to the case of three-dimensional bridges, a step-by-step of proposed extension of MPA procedure to estimate the seismic demands for bridges is presented as a sequence of steps:

(1) Compute the natural frequencies, ω_n, and mode shape vectors, ϕ_n, for linearly elastic vibration modes of the three-dimensional structure. It is noted that in the case of bridges, the number of ‘modes’ whose masses contribute to at least 90% of the total mass of a complex bridge structure – a criterion commonly used in seismic codes- that have to be taken into account is significantly higher than in the case of buildings.

(2) Identify the most dominant modes that need to be considered in the MPA procedure based on the effective modal masses (as a fraction of the total mass) of the linearly elastic bridge in each direction (in the longitudinal, transverse and vertical directions). The most dominant modes are dependent on the response quantities under consideration (e.g., the peak displacements of the deck in transverse or longitudinal directions). The bridge modes may be categorized by their primary motion: longitudinal, transverse, vertical or torsional, or coupled motion such as longitudinal-vertical or transverse-torsional. Category of a mode shape may be identified from deformed shape of the bridge and effective modal masses. The effective modal mass determined by $M_n^* = \Gamma_n L_n$ in which $L_n = \boldsymbol{\phi}_n^T \mathbf{m}\boldsymbol{\iota}$, $\Gamma_n = \dfrac{\boldsymbol{\phi}_n^T \mathbf{m}\boldsymbol{\iota}}{\boldsymbol{\phi}_n^T \mathbf{m}\boldsymbol{\phi}_n}$, and $\boldsymbol{\iota}$ is the influence vector and each element of the influence vector $\boldsymbol{\iota}$ corresponding to the direction of the ground motion is equal to unity.

(3) For the *n*th-dominant 'mode', develop the pushover curve (capacity curve), which is the relationship between the base-shear and the displacement of the monitoring point ($V_{bn} - u_{mn}$), by nonlinear static analysis of the bridge using the spatial force distribution $\mathbf{s}_n^* = \mathbf{m}\boldsymbol{\phi}_n$ where $\mathbf{m}$ is the mass matrix of the structure. Gravity loads are applied before each pushover analysis, and $P-\Delta$ effects are included. The value of the desired dynamic response of the bridge due to gravity loads is denoted as r_g.

The displacement monitoring point of the bridge for the *n*th-dominant 'mode' is proposed to be at the degree of freedom where mode shape value is maximum in the direction of applied ground motion. This proposed monitoring point can take into account the contributions of torsional and vertical vibrations of bridges, and this approach is no more complicated than before because the mode shape was already computed in Step 1.

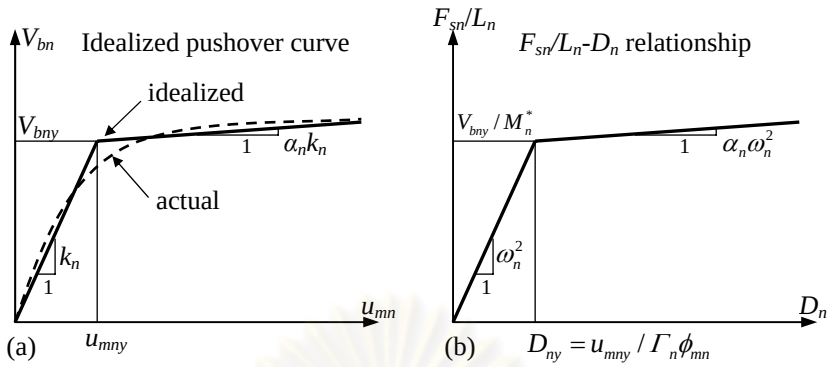

Figure 2.3 (a) Pushover curve and (b) the *n*th-mode inelastic SDF system curve.

(4) Idealize the pushover curve as a bilinear curve (Figure 2.3a). There are several ways to idealize this curve. The implementation of bilinear idealization in this study adopted the criterion specified in FEMA-356 that: (a) the first linear segment shall intersect the actual curve at 60% of the (idealized) yield force; and (b) the energy (area under the curve) associated with the peak response has to be the same as for the actual curve. More details of this approach can be found in Appendix A.

(5) Convert the idealized pushover curve to the force–deformation $\left(F_{sn}/L_n - D_n\right)$ relation of the *n*th-dominant 'mode' inelastic SDF system by using $F_{sny}/L_n = V_{bny}/M_n^*$; $D_{ny} = u_{mny}/\Gamma_n \phi_{mn}$ in which ϕ_{mn} is the value of ϕ_n at the displacement monitoring point; and determine the elastic modal frequency ω_n. The *n*th-dominant 'mode' inelastic SDF system is defined by the force–deformation curve of Figure 2.3b (with post-yield stiffness ratio α_n) and damping ratio ζ_n specified for the *n*th 'mode'.

(6) Peak value of deformation, $D_n \equiv \max_{\forall t} \left|D_n(t)\right|$, of an equivalent inelastic SDF system of *n*th 'mode' (with force–deformation relation of Figure 2.3b) due to ground excitation $\ddot{u}_g(t)$, are determined rigorously by nonlinear response history analysis (NL-RHA) (Equation 2.14). The reason for choosing this approach is mentioned in Section 1.2.1.

(7) Calculate the peak monitoring displacement u_{mno} associated with the nth-dominant 'mode' inelastic SDF system from

$$u_{mno} = \Gamma_n \phi_{mn} D_n \tag{2.26}$$

(8) The response quantities of interest (e.g., displacements of deck, piers; plastic hinge rotations; and internal forces), r_{no}, are evaluated by extracting from the pushover database when the displacement of monitoring point equals to u_{mno}.

(9) Repeat Steps 3–8 for as many 'modes' as required for sufficient accuracy. For seismic evaluation of buildings, usually the first two or three 'modes' will suffice for buildings shorter than 10 stories (Chintanapakdee and Chopra, 2003a; Chopra and Chintanapakdee, 2004a). On the other hand, as mentioned in Step 1, the required number of 'modes' may be far in the case of bridges.

(10) Compute the dynamic response due to the nth-dominant mode: $r_n = r_{n+g} - r_g$, where r_g is the contribution of gravity load alone.

(11) Determine the total response r_{MPA} by combining the peak 'modal' responses using appropriate modal combination rule, e.g., Square-Root-of-Sum-of-Squares (SRSS) by Equation (2.27) or Complete Quadratic Combination (CQC) rule by Equation (2.28)

$$r \approx \max\left[r_g \pm \left(\sum_{n=1}^{J} r_n^2 \right)^{1/2} \right] \tag{2.27}$$

$$r \approx \max\left[r_g \pm \left(\sum_{i=1}^{J} \sum_{n=1}^{J} \rho_{in} r_i r_n \right)^{1/2} \right] \tag{2.28}$$

where the correlation coefficient ρ_{in} is given by:

$$\rho_{in} = \frac{8\sqrt{\zeta_i \zeta_n}\left(\beta_{in}\zeta_i + \zeta_n\right)\beta_{in}^{3/2}}{\left(1-\beta_{in}^2\right) + 4\zeta_i\zeta_n\beta_{in}\left(1+\beta_{in}^2\right) + 4\left(\zeta_i^2 + \zeta_n^2\right)\beta_{in}^2} \tag{2.29}$$

in which $\beta_{in} = \omega_i / \omega_n$ is the ratio of the *i*th and *n*th modal frequencies, and ζ_i and ζ_n are the damping ratios for these modes.

CHAPTER III

ASSESSMENT OF CURRENT NONLINEAR STATIC PROCEDURES FOR SEISMIC EVALUATION OF BUILDINGS

3.1 Introduction

Steel moment-resisting frames are vulnerable to large lateral displacements during severe earthquakes. In response to many practical and economic issues involved, conventional braced frames have been widely used as lateral-force resisting systems in seismic resistant design; however, their post-elastic behavior is susceptible to rapid stiffness and strength degradation after the braces buckle due to compression forces. That was observed in past earthquakes, such as the 1985 Mexico (Osteraas and Krawinkler, 1989), 1989 Loma Prieta (Kim and Goel, 1992), 1994 Northridge (Krawinkler *et al.*, 1995; and Mahin, 1998), and 1995 Hyogo-Ken Nanbu (Tremblay *et al.*, 1996) earthquakes. Thus, their energy dissipation capacity is limited when subjected to earthquake loading (Figure 3.1a). Alternatively, Buckling-Restrained Braced Frame (BRBF) is an innovative structural system that prevents buckling of the braces by using a steel core and an outer casing filled with concrete for the brace. Brace axial force is resisted only by the steel core, which is restrained from buckling by the outer shell and the infill mortar. This results in a stable hysteresis loop like a bilinear relationship (Figure 3.1b) where significant hysteretic energy dissipation can be achieved. The system is considered to have favorable seismic performance over traditional braced frames, making it an attractive option to structural engineers. Moreover, lateral-force-resisting systems with buckling restrained braces can yield significant structural cost saving over conventional special concentrically braced frame systems. This saving is resulted from decreased material quantities and foundation demands due to the reduced base shear and required brace cross-section areas. The saving increases with building height, as the greater quantities of materials offset the more expensive braces (DASSE, 2007). A more comprehensive background on this system can be found in (Kumar *et al.*, 2007; and Uang and Nakashima, 2003). Therefore, BRBF has become a preferable system in seismic resistant design recently.

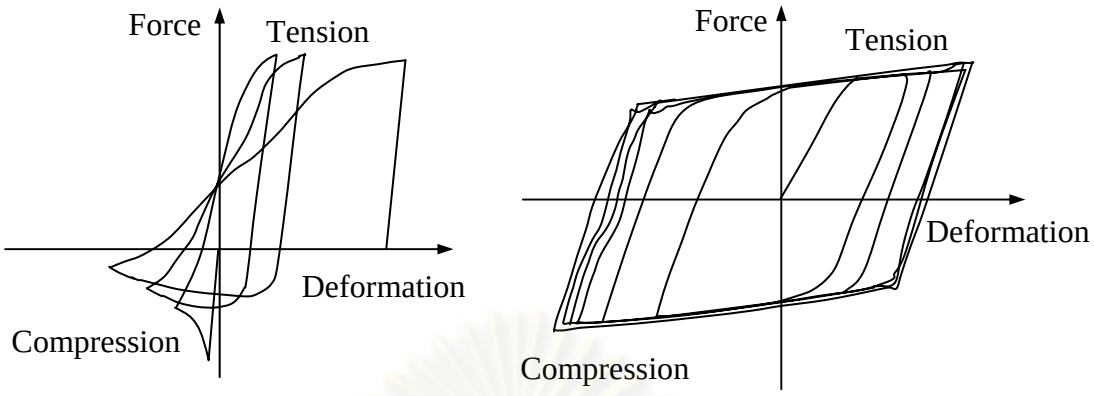

(a) Conventional bracing (b) Buckling-restrained bracing

Figure 3.1 Hysteretic behavior of conventional bracing and buckling-retrained bracing under cyclic loading (Kumar *et al.*, 2007).

To estimate seismic demands in the design and evaluation of buildings, the Nonlinear Static Procedures (NSPs) using the lateral force distributions recommended in ATC-40 (ATC, 1996) and the FEMA-356 (ASCE, 2000) documents are now standard in engineering practice. The nonlinear static procedure in these documents is based on the Capacity Spectrum Method (ATC-40) and Displacement Coefficient Method (FEMA-356), and assumes that the lateral force distribution for the pushover analysis and the conversion of the results to the capacity diagram are based on the fundamental vibration mode of the elastic structure. Consequently, these NSPs based on invariant load patterns provide accurate seismic demand estimates only for low- and medium-rise moment-frame buildings where the contributions of higher 'modes' response are not significant and inadequate to predict inelastic seismic demands in buildings when the higher 'modes' contribute to the response (Krawinkler and Seneviratna, 1998; Gupta and Krawinkler, 1999; Chopra and Goel, 2002; Chintanapakdee and Chopra, 2003a; Kunnath and Kalkan, 2004; Bobadilla and Chopra, 2007).

To overcome these drawbacks, an improved pushover procedure, called Modal Pushover Analysis (MPA), was proposed by Chopra and Goel, (2002) to include the contributions of higher 'modes'. The MPA procedure has been demonstrated to increase the accuracy of seismic demand estimation in taller moment-frame buildings, e.g., 9- and 12-stories tall, compared to the conventional pushover analysis (Chopra

and Chintanapakdee, 2004a; and Chopra *et al.*, 2004). In spite of including the contribution of higher 'modes', MPA is conceptually no more difficult than standard procedures because higher 'modes' pushover analyses are similar to the first 'mode' pushover analysis. Moreover, MPA procedure considering for the first few (two or three) 'modes' contribution are typically sufficient (Chintanapakdee and Chopra, 2003a; and Chopra and Chintanapakdee, 2004a).

Another pushover method is the adaptive pushover procedures, where the load pattern distributions are updated to consider the change in structure during the inelastic phase (Fajfar and Fischinger, 1989; Bracci and Kunnath, 1997; and Gupta and Kunnath, 2000). In this type of procedure, equivalent seismic loads are calculated at each pushover step using the immediate 'mode' shape. Recently, a new adaptive pushover method, called the Adaptive Modal Combination (AMC) procedure, has been developed by Kalkan and Kunnath, (2006) where a set of adaptive mode-shape based inertia force patterns is applied to the structure. This procedure has been validated for regular moment frame buildings (Kalkan and Kunnath, 2006; 2007). However, it is conceptually complicated and computationally demanding for routine application in structural engineering practice while the MPA method is generally simpler, and thus, more practical than adaptive pushover procedures for seismic design.

More recently, an Improved Modal Pushover Analysis (IMPA) procedure was proposed by Jianmeng *et al.* (2008) to consider the redistribution of inertia forces after the structure yields. The structural stiffness changes after it yields, so the displacement shape vector also changes. The IMPA procedure uses the product of the time variant floor displacement vector (as the displacement shape vector) and the structural mass matrix as the lateral force distribution at each applied-load step beyond the yield point of the structure. However, to avoid a large computation, only two phase lateral load distribution was recommended. In the first phase, the pushover analysis is performed by using the first few elastic natural 'modes' of structure, i.e., similar to the MPA. In the second phase, only for the first 'mode' the lateral load distribution is based on assumption that the floor displacement vector at the initial yielding point is the displacement shape vector.

An alternative pushover analysis method to estimate the seismic displacement demands, referred to as the Mass Proportional Pushover (MPP) procedure, was proposed by Kim and Kurama (2008). The main advantage of the MPP is that the effects of higher 'modes' on the lateral displacement demands are lumped into a single invariant lateral force distribution that is proportional to the total seismic masses at the floor and roof levels. However, the accuracy of both IMPA and MPP procedures has been verified for a limited number of cases.

With the increase in the number of alternative pushover analysis procedure proposed in recent years, it is useful to assess the accuracy and classify the potential limitations of these methods. An assessment on accuracy of MPA and FEMA pushover analyses for moment resisting frame buildings was investigated by Chopra and Chintanapakdee (2004a). Then, an investigation on the accuracy of improved nonlinear static procedures in FEMA-440 was carried out by Akkar and Metin (2007). Meanwhile, the ability of FEMA-356, MPA and AMC in estimating seismic demands of a set of existing steel and reinforced concrete buildings was examined by Kalkan and Kunnath (2007). More recently, an investigation into the effects of nonlinear static analysis procedures which are the Displacement Coefficient Method (DCM) recommended in FEMA 356 and the Capacity Spectrum Method (CSM) recommended in ATC 40 to performance evaluation on low-rise RC buildings was carried out by Irtem and Hasgul (2009).

To assess the ability of current procedures, this chapter aims to investigate comparatively the bias and accuracy of MPA, IMPA and MPP procedures when applied to buckling-restrained braced frames (BRBFs).

3.2 Review of Selected Nonlinear Static Procedures

This section briefly introduces the modal, improved modal pushover analysis (MPA, IMPA) and mass proportional pushover (MPP) procedures in estimating seismic demands for building design.

3.2.1. Modal Pushover Analysis (MPA)

The Modal Pushover Analysis (MPA), which has been proposed by Chopra and Goel (2002), is an extension of conventional pushover analysis to include contribution of higher 'modes'. A step-by-step summary of the MPA procedure to estimate the seismic demands for building is presented as a sequence of steps:

(1) Compute the natural frequencies, ω_n , and mode shape vectors, $\boldsymbol{\phi}_n$, for linearly elastic vibration modes of the building.

(2) For the *n*th-'mode', develop the base-shear—roof-displacement ($V_{bn} - u_{rn}$) pushover curve by nonlinear static analysis of the building using the force distribution $\mathbf{s}_n^* = \mathbf{m}\boldsymbol{\phi}_n$ where $\mathbf{m}$ is the mass matrix.

(3) Idealize the pushover curve as a bilinear curve (Figure 3.2a).

(4) Convert the idealized pushover curve to the force–deformation ($F_{sn}/L_n - D_n$) relation of the *n*th-'mode' inelastic SDF system and determine the elastic modal frequency ω_n, and yield deformation D_{ny}. The *n*th-'mode' inelastic SDF system is defined by the force–deformation curve of Figure 3.2b (with post-yield stiffness ratio α_n) and damping ratio ζ_n specified for the *n*th 'mode'. Where $M_n^* = \Gamma_n L_n$ is the effective modal mass, $L_n = \boldsymbol{\phi}_n^T \mathbf{m}\boldsymbol{\iota}$, $\Gamma_n = \dfrac{\boldsymbol{\phi}_n^T \mathbf{m}\boldsymbol{\iota}}{\boldsymbol{\phi}_n^T \mathbf{m}\boldsymbol{\phi}_n}$, and each element of the influence vector $\boldsymbol{\iota}$ is equal to unity.

(5) Compute the peak deformation, $D_n \equiv \max_{\forall t} |D_n(t)|$, of the *n*th-'mode' inelastic SDF system with the force–deformation relation of Figure 3.2b due to ground excitation $\ddot{u}_g(t)$ by solving:

$$\ddot{D}_n + 2\zeta_n \omega_n \dot{D}_n + \frac{F_{sn}\left(D_n, \dot{D}_n\right)}{L_n} = -\ddot{u}_g(t) \tag{3.1}$$

(6) Calculate the peak roof displacement u_{rno} associated with the *n*th-'mode' inelastic SDF system from

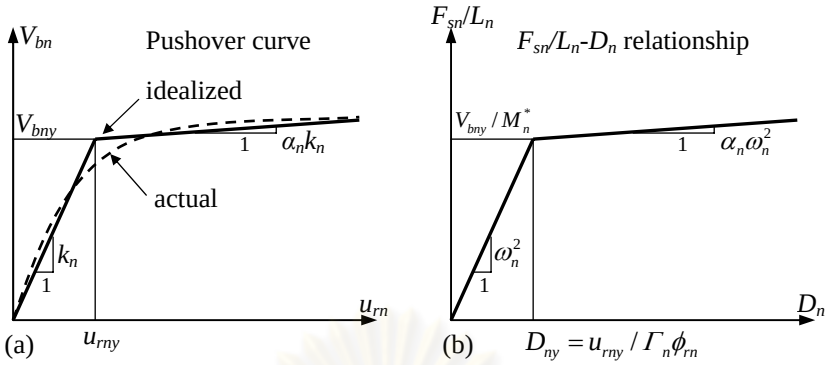

Figure 3.2 (a) Pushover curve and (b) Force and deformation relationship of SDF system.

$$u_{rno} = \Gamma_n \phi_{rn} D_n \tag{3.2}$$

(7) Extract other desired responses, r_{no}, from the pushover database when roof displacement equal to u_{rno}.

(8) Repeat Steps 2–7 for as many 'modes' as required for sufficient accuracy; usually the first two or three 'modes' will suffice for buildings shorter than 10 stories.

(9) Determine the total response r_{MPA} by combining the peak 'modal' responses using appropriate modal combination rule, e.g., Square-Root-of-Sum-of-Squares (SRSS) as shown by Equation (3.3) or Complete Quadratic Combination (CQC) rule:

$$r_{MPA} = \sqrt{\sum_{n=1}^{j} r_{no}^2} \tag{3.3}$$

where j is the number of 'modes' included.

The MPA procedure summarized in this paper is developed for symmetric buildings (Chopra and Goel, 2002).

3.2.2 Improved Modal Pushover Analysis (IMPA)

Unlike the MPA procedure where the response is obtained from invariant multi-mode lateral load pattern vectors, the improved modal pushover analysis (IMPA) proposed by Jianmeng *et al.* (2008) considering the redistribution of inertia

forces after the structure yields. The principal improvement of the IMPA is to use deflection shape of structure after yielding as an invariant later load pattern. However, to avoid a large computation, a two-phase lateral load distribution is suggested for the first 'mode' while the force patterns for higher 'modes' are similar to the MPA approach. The IMPA procedure is summarized by following steps:

(1) Implement the Steps 1-3 of the MPA procedure described in previous section for first 'mode'. The lateral force distribution $\mathbf{s}_1^* = \mathbf{m}\boldsymbol{\phi}_1$ is considered as the first-phase load pattern.

(2) Determine the displacements vector of structure, $\boldsymbol{\psi}_{1y}$, at the yielding point with the pushover analysis obtained from Step 1.

(3) Continue pushover analysis from the structure yielding point by applying the load distribution $\mathbf{s}_{1y}^* = \mathbf{m}\boldsymbol{\psi}_{1y}$, which is considered as the second-phase lateral load pattern to obtain new pushover curve. Then, this new pushover curve is used for determining the response of the structure by Steps 4-7 of MPA procedure described in Section 3.2.1.

(4) Determine the total response r_{IMPA} with SRSS or CQC combination rules by combining the response for the first 'mode' obtained from Step 3 and the responses due to other higher 'modes' obtained from MPA procedure.

3.2.3 Mass Proportional Pushover (MPP) Procedure

An alternative pushover analysis procedure, called the Mass Proportional Pushover (MPP), was proposed by Kim and Kurama (2008) to estimate the peak seismic lateral displacement demands for buildings. The main advantage of the MPP procedure over other approximate procedures is the use of a single pushover analysis for the structure with no need to conduct a modal analysis to capture the effect of higher 'modes'. A summary of the mass proportional pushover procedure, whose details can be found in Kim and Kurama (2008), is as follows:

(1) Determine the multi-degree-of-freedom (MDOF) base shear force versus the roof displacement ($V_b - u_r$) relationship using the force distribution given by $\mathbf{m}g\iota = \mathbf{w}\iota$ where $\mathbf{m}$ is the mass matrix and $\mathbf{w}$ is weight matrix.

(2) Idealize the pushover curve as a bilinear curve.

(3) Convert the idealized pushover curve to the pseudo-acceleration versus the displacement ($A - D$) relationship of an equivalent SDF system using:

$$A = \frac{V_b}{M} \quad ; \quad D = \frac{u_r}{\Gamma} \tag{3.4}$$

where M is the total mass and Γ is the participation factor calculated as: $\Gamma = \frac{\mathbf{u}_e^T \mathbf{m}\iota}{\mathbf{u}_e^T \mathbf{m}\mathbf{u}_e}$; $\mathbf{u}_e$ is the lateral floor displacement vector (normalized with respect to the roof) obtained from the linear-elastic response range of the pushover analysis using the $\mathbf{m}g\iota = \mathbf{w}\iota$ force distribution which is the same as uniform distribution of FEMA-356.

(4) Determine the maximum SDF displacement, $D_{\max}$ by solving Equation (3.1) with $F_s/L = A$.

(5) Calculate the maximum MDOF roof and floor displacements of structure as: $\mathbf{u}_{\max} = D_{\max}\Gamma\mathbf{u}_e$

3.3 Structural Systems and Analytical Models

Analyses of 3-, 6-, 10-, and 14-story BRBF buildings are presented to evaluate the bias and accuracy of MPA, IMPA and MPP procedures. Building designs for the BRBF system in both the 3-story and 6-story cases adhered to the criteria for the 3vb2 and 6vb2 model cases studied by Sabelli *et al.* (2003). These office buildings are assumed to be located in downtown Los Angeles on site class D. Figure 3.3 shows floor plans of the 3- and 6-story buildings. Models 3vb2 and 6vb2 were designed using response modification factor, R = 8, which was recommended by Structural

Engineers Association of California (SEAOC, 2001) for buckling restrained braced frame design. The typical story height is 4 m, except for the first story of the 6-story building, which has a story height of 5.5 m. The floor plan dimensions are 36.6 m × 54.9 m for the 3-story building and 45.8 m × 45.8 m for the 6-story building. Both buildings have beam spans equal to 9.15 m in each direction. Each floor slab and the roof is a 76-mm metal deck with normal-weight concrete topping. The 3-story building has eight bays of bracing, four in each direction, while the 6-story building has twelve bays of bracing, six in each direction. The elevation view of all BRBF systems is shown in Figure 3.4.

Braces were designed for the force calculated based on equivalent static base shear. Brace sizes were set to be within 2% of computed required cross-sectional area based on a nominal yield stress of 248 MPa for the yielding core without using any strength-reduction factor. Table 3.1 lists brace yield forces and axial stiffnesses for each story, sizes of beams and columns determined for 3-and 6-story are also shown. To calculate brace stiffness, yielding of buckling-restrained brace core was assumed to occur in 70% of the brace length and the cross-sectional area of non-yielding zone is three to six times that of the yielding zone.

The characteristics of the 10- and 14-story buildings are adopted from Asgarian and Shokrgozar (2009). Figure 3.5 shows the floor plan of these buildings. The floor plan dimensions are 18 m × 18 m for both buildings with the beam spans equal to 6 m in each direction. Each building has eight bays of bracing, four in each direction. The story height of both models is 3.2 m. The dead load of 6 kN/m^2 was used for gravity load. The buildings were designed as per the requirement of Iranian Earthquake Resistance Design Code and Iranian National Building Code which is similar to AISC-89. The importance factor of I = 1, seismic zone factor of A = 0.35 and preliminary response modification factor of R = 9.5 were considered for frame design. Asgarian and Shokrgozar (2009) concluded that response modification factor of 9.4, very close to 9.5, is suitable for inverted-V buckling-restrained braced frames designed per the Iranian National Building Code. Braces were designed to sustain 100 percents of the lateral load. Sizes of members determined for the 10-story building are shown in Table 3.2.

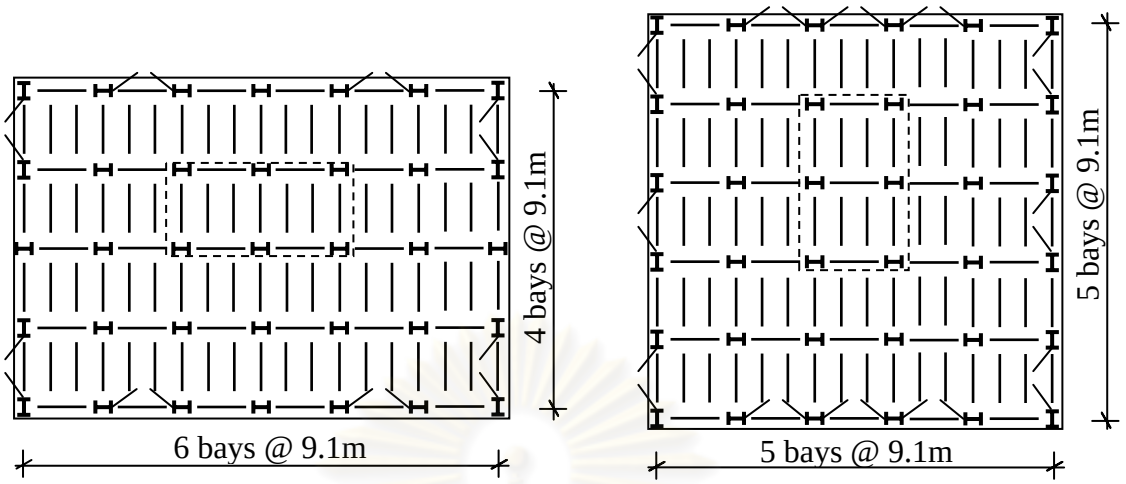

(a) 3-story building (b) 6-story building

Figure 3.3 Floor plans of 3- and 6-story BRBF buildings.

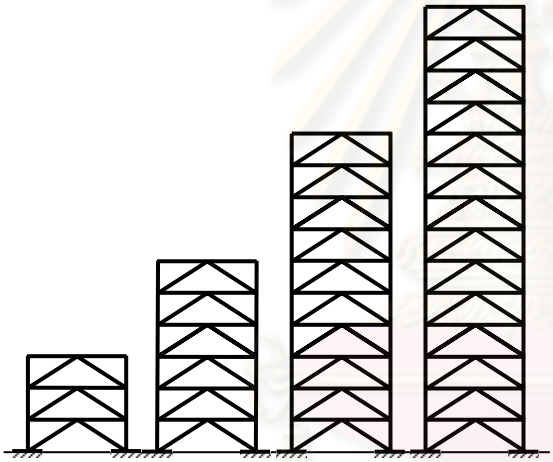

(a) 3-story (b) 6-story (c) 10-story (d) 14-story

Figure 3.4 Frame elevations of 3-, 6-, 10-, and 14-story buildings.

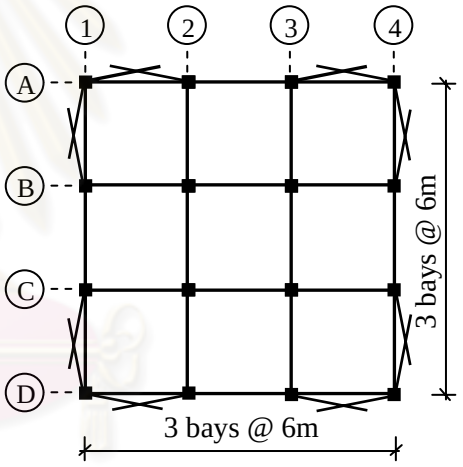

Figure 3.5 Floor plans of 10- and 14-story BRBF buildings.

Table 3.1 Member properties for the 3- and 6-story buildings.

Building model	Story	Buckling-restrained braces		Beams	Columns
		Tensile yield force (kN)	Axial stiffness (kN/cm)		
3-story	3	520	1030	W14x48	W12x96
	2	872	1651		
	1	1081	1905		
6-story	6	391	799	W14x48	W14x132
	5	712	1419		
	4	961	1881		
	3	1161	2238		W14x211
	2	1299	2482		
	1	1699	2501		

Table 3.2 Member properties for the 10-story building.

Story	Buckling-restrained braces		Beams	Columns D-1, D-4	Columns D-2, D-3
	Tensile yield force (kN)	Axial stiffness (kN/cm)			
10	198	521	IPE300	B100x100x10	B125x125x10*
9	273	717			
8	322	847		B125x125x12	B150x150x15
7	372	977			
6	397	1042		B175x175x15	B225x225x15
5	422	1107	IPE360		
4	446	1172		B250x250x15	B250x250x20
3	471	1238			
2	496	1303		B275x275x22	B300x300x25
1	521	1368			

*B125x125x10 is a square tube with 125 x 125mm cross section and 10mm thickness.

Table 3.3 Natural periods of building models in this study.

Mode	Modal natural periods T_n (sec)			
	3-story	6-story	10-story	14-story
1	0.504	0.797	0.982	1.274
2	0.197	0.296	0.338	0.423
3	0.120	0.174	0.187	0.230

In this study, compressive yield strengths of the braces are 110% of their tensile yield strengths (Sabelli *et al.*, 2003) and the post-yield stiffness was taken as 1/1000 of the elastic stiffness (Kumar *et al.*, 2007). Section nonlinear properties of beams and columns were defined using bilinear moment-rotation relationships with 3% post-yield stiffness ratio (Chintanapakdee and Chopra, 2003a).

The analysis of a three-dimensional building was simplified to analysis of a single two-dimensional BRBF. Seismic masses for each BRBF were calculated by dividing the total mass per floor by the number of BRBFs in each principal direction, which are the floor level masses used in the analysis to account for horizontal inertia forces. Global P–Δ effect was considered by a gravity column carrying vertical loads based on the tributary area of the frame, i.e., total gravity load divided by number of BRBFs in each direction. The stiffness of this gravity column represents the equivalent stiffness for all non-frame columns in the building (Kiggins and Uang, 2006). A Rayleigh damping model was used with 5% critical damping ratios for the

first two modes, according to common practice for code designed steel structures (Sabelli *et al.*, 2003; and Kiggins and Uang, 2006). Nonlinear static and dynamic analyses were carried out using the nonlinear dynamic analysis computer program DRAIN-2DX (Prakash *et al.*, 1993). The natural periods of all models are shown in Table 3.3.

3.4 Ground Motions and Response Statistics

Two sets of ground motions, referred as LA2/50 and LA10/50, corresponding to 2% and 10% probabilities of exceedence in a 50-year period are used in this study. These ground motions were compiled by the SAC Phase II Steel Project for a site in Los Angeles, California (Somerville *et al.*, 1997). These acceleration time histories were derived from historical recordings or from simulations of physical fault rupture processes. Each set of ground motions consists of 20 records which are the fault-normal and fault-parallel components of 10 recordings. The records in these suites include near-fault and far-fault records. The ground acceleration time histories of the LA10/50 and LA2/50 ensembles are shown in Figures 3.6 and 3.7, respectively. The pseudo-acceleration spectra for the two sets of ground motions are shown in Figure 3.8 together with the median spectra (black solid lines). Tables 3.4 and 3.5 provide the information of LA10/50 and LA2/50 sets of records including: recording station, earthquake magnitude, distance, scaling factor, and peak ground acceleration (PGA).

To determine the seismic demands of a building due to a set of ground motions, each record was scaled such that the spectral acceleration at the fundamental natural period of the building is equal to the median spectral acceleration for that period (Table 3.6). This method of scaling helps reduce the dispersion of results (Shome and Cornell, 1997). The pseudo-acceleration spectra of scaled LA10/50 and LA2/50 sets of ground motions for analyzing 3-, 6-, 10-, and 14-story models are shown in Figures 3.9.

Table 3.4 Set of ground motions having 10% probability of being exceeded in 50 years (LA10/50).

Record	Earthquake/Recording station	Earthquake Magnitude	Distance (km)	Scaling Factor	PGA (cm/sec^2)
LA01	1940 Imperial Valley, El Centro	6.9	10	2.01	452
LA02	1940 Imperial Valley, El Centro	6.9	10	2.01	662
LA03	1979 Imperial Valley, Array #05	6.5	4.1	1.01	386
LA04	1979 Imperial Valley, Array #05	6.5	4.1	1.01	478
LA05	1979 Imperial Valley, Array #06	6.5	1.2	0.84	295
LA06	1979 Imperial Valley, Array #06	6.5	1.2	0.84	230
LA07	1992 Landers, Barstow	7.3	36	3.20	412
LA08	1992 Landers, Barstow	7.3	36	3.20	417
LA09	1992 Landers, Yermo	7.3	25	2.17	509
LA10	1992 Landers, Yermo	7.3	25	2.17	353
LA11	1989 Loma Prieta, Gilroy	7.0	12	1.79	652
LA12	1989 Loma Prieta, Gilroy	7.0	12	1.79	950
LA13	1994 Northridge, Newhall	6.7	6.7	1.03	664
LA14	1994 Northridge, Newhall	6.7	6.7	1.03	644
LA15	1994 Northridge, Rinaldi RS	6.7	7.5	0.79	523
LA16	1994 Northridge, Rinaldi RS	6.7	7.5	0.79	568
LA17	1994 Northridge, Sylmar	6.7	6.4	0.99	558
LA18	1994 Northridge, Sylmar	6.7	6.4	0.99	801
LA19	1986 North Palm Springs	6.0	6.7	2.97	999
LA20	1986 North Palm Springs	6.0	6.7	2.97	967

Table 3.5 Set of ground motions having 2% probability of being exceeded in 50 years (LA2/50).

Record	Earthquake/Recording station	Earthquake magnitude	Distance (km)	Scaling factor	PGA (cm/sec^2)
LA21	1995 Kobe	6.9	3.4	1.15	1258
LA22	1995 Kobe	6.9	3.4	1.15	903
LA23	1989 Loma Prieta	7.0	3.5	0.82	410
LA24	1989 Loma Prieta	7.0	3.5	0.82	464
LA25	1994 Northridge	6.7	7.5	1.29	854
LA26	1994 Northridge	6.7	7.5	1.29	925
LA27	1994 Northridge	6.7	6.4	1.61	909
LA28	1994 Northridge	6.7	6.4	1.61	1304
LA29	1974 Tabas	7.4	1.2	1.08	793
LA30	1974 Tabas	7.4	1.2	1.08	973
LA31	Elysian Park (simulated)	7.1	17.5	1.43	1271
LA32	Elysian Park (simulated)	7.1	17.5	1.43	1164
LA33	Elysian Park (simulated)	7.1	10.7	0.97	767
LA34	Elysian Park (simulated)	7.1	10.7	0.97	668
LA35	Elysian Park (simulated)	7.1	11.2	1.10	973
LA36	Elysian Park (simulated)	7.1	11.2	1.10	1079
LA37	Palos Verdes (simulated)	7.1	1.5	0.90	698
LA38	Palos Verdes (simulated)	7.1	1.5	0.90	761
LA39	Palos Verdes (simulated)	7.1	1.5	0.88	491
LA40	Palos Verdes (simulated)	7.1	1.5	0.88	613

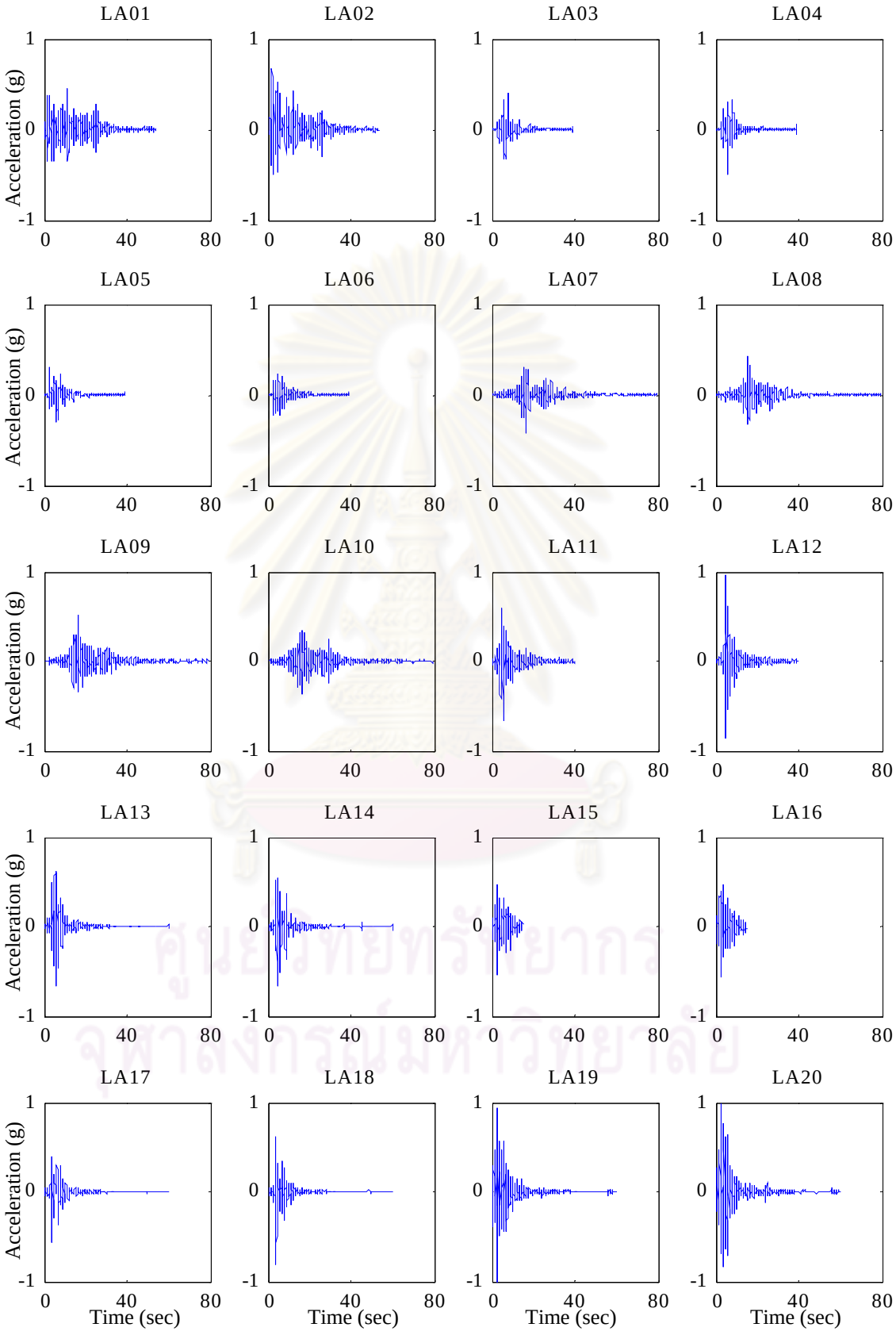

Figure 3.6 LA10/50 ensemble of 20 ground motions: ground accelerations.

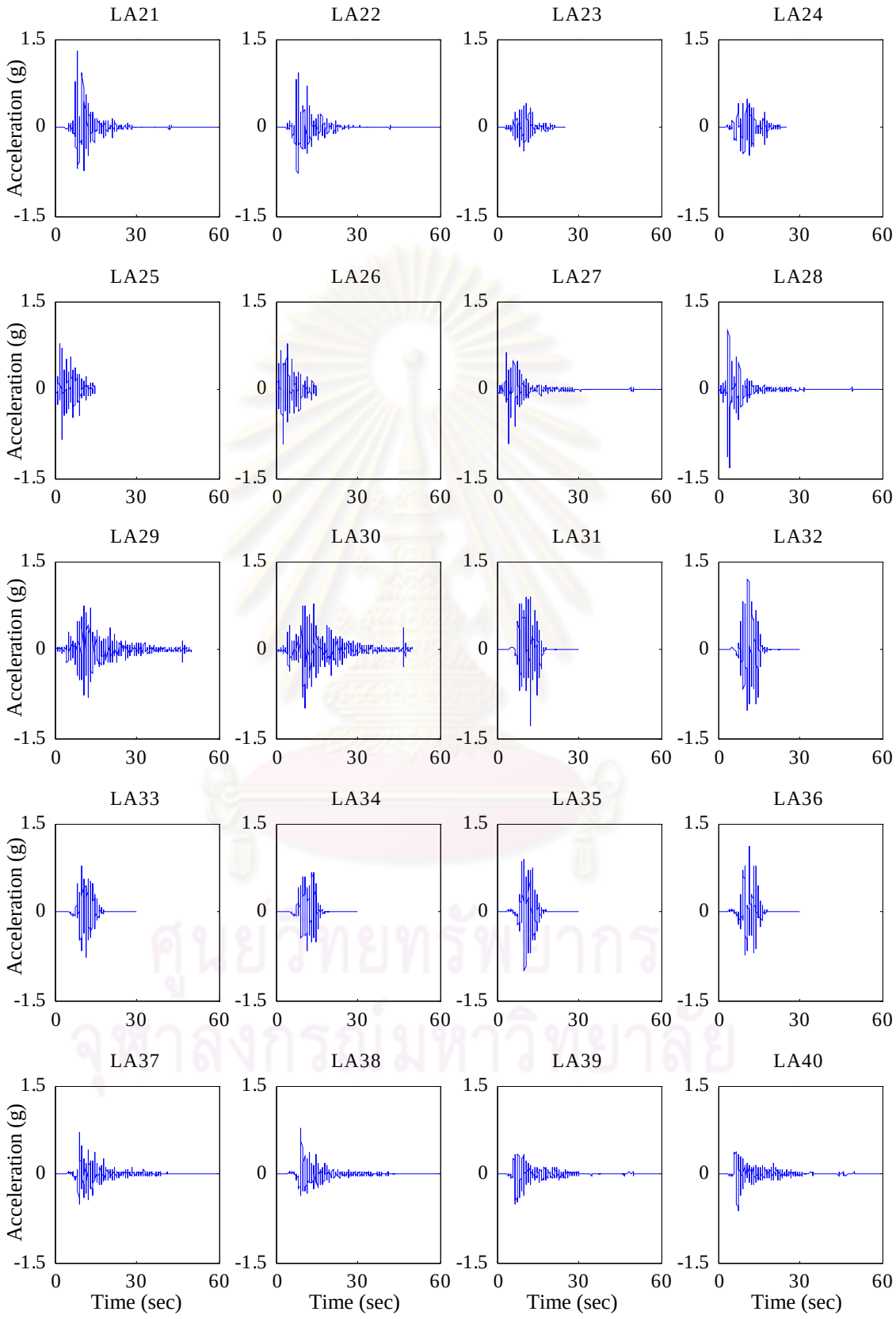

Figure 3.7 LA2/50 ensemble of 20 ground motions: ground accelerations.

The response of each building to each set of the ground motions was determined by nonlinear response history analysis (NL-RHA), and a nonlinear static procedure (NSP), e.g., MPA, IMPA and MPP. The peak value of inter-story drift, Δ, determined by NL-RHA is denoted by Δ_{NL-RHA} , and from NSP by Δ_{NSP}. From these data for each ground motion, a response ratio was determined from the following equation: $\Delta^{*}_{NSP} = \Delta_{NSP} / \Delta_{NL-RHA}$. The median values, $\hat{x}$, defined as the geometric mean, of n observed values (x_i) of Δ_{NSP}, Δ_{NL-RHA} and Δ^{*}_{NSP}; and the dispersion measures δ of Δ^{*}_{NSP} defined as the standard deviation of logarithm of the n observed values were calculated:

$$\hat{x} = \exp\left[\frac{\sum_{i=1}^{n} \ln x_i}{n}\right] \tag{3.5}$$

$$\delta = \sqrt{\frac{\sum_{i=1}^{n} \left(\ln x_i - \ln \hat{x}\right)^2}{n-1}} \tag{3.6}$$

An advantage of using the geometric mean as the estimator of median is that the ratio of the median of Δ_{NSP} to the median of Δ_{NL-RHA} is equal to the median of the ratio Δ^{*}_{NSP}, i.e., the bias of NSP in estimating the median response is equal to the median of bias in estimating response to individual excitation.

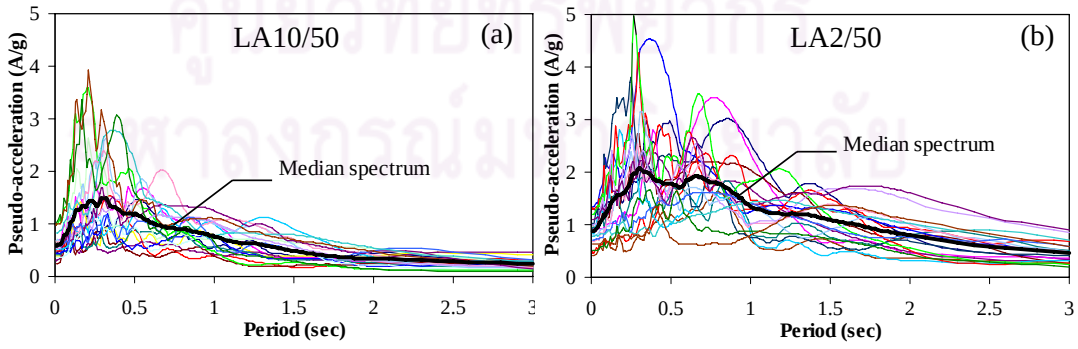

Figure 3.8 Pseudo-acceleration spectra of (a) LA10/50, and (b) LA2/50 set of ground motions.

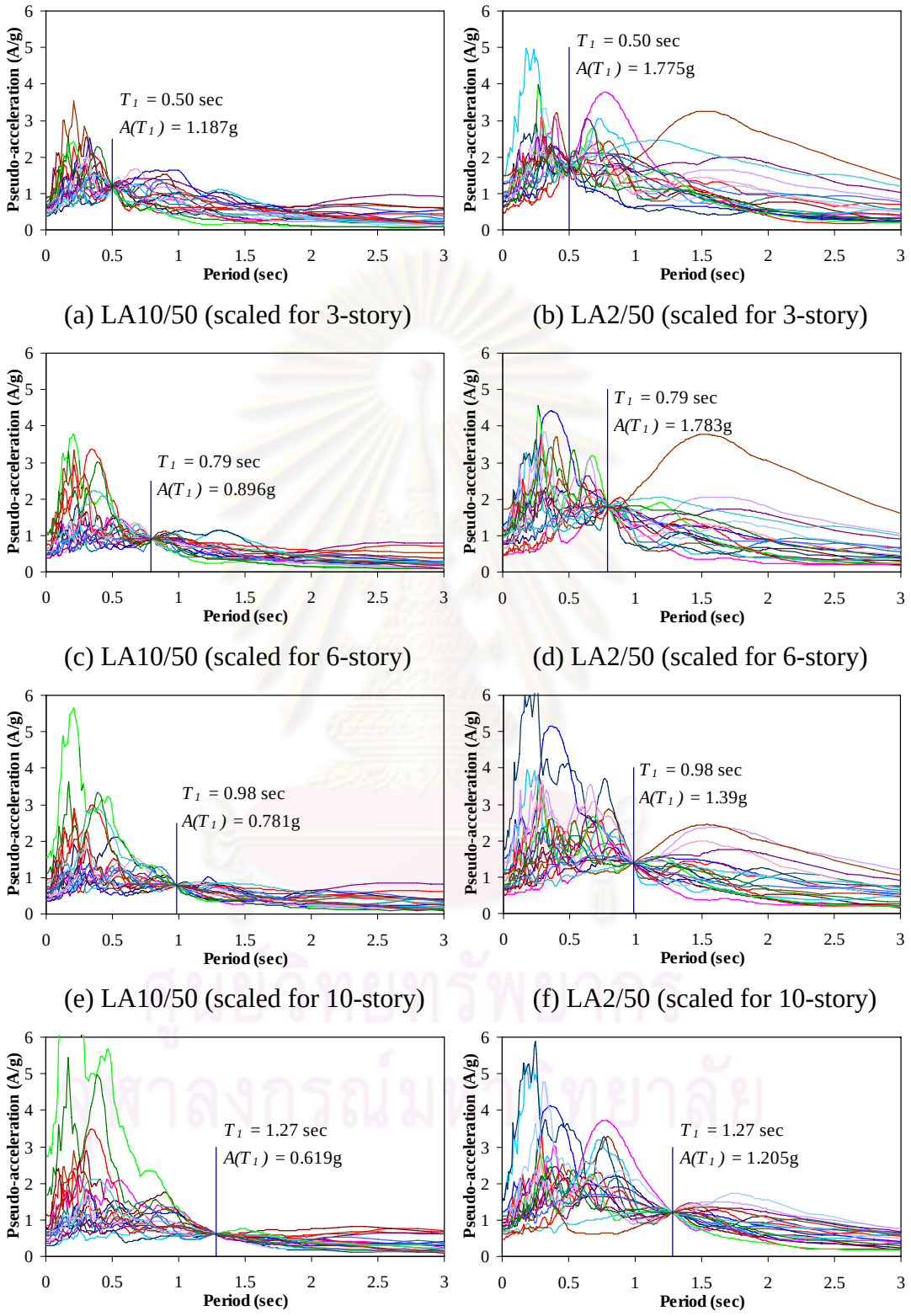

(a) LA10/50 (scaled for 3-story) (b) LA2/50 (scaled for 3-story)

(c) LA10/50 (scaled for 6-story) (d) LA2/50 (scaled for 6-story)

(e) LA10/50 (scaled for 10-story) (f) LA2/50 (scaled for 10-story)

(g) LA10/50 (scaled for 14-story) (h) LA2/50 (scaled for 14-story)

Figure 3.9 Pseudo-acceleration spectra of scaled LA10/50 and LA2/50 sets of ground motions for analyzing 3-, 6-, 10-, and 14-story buildings.

Table 3.6 Median spectral acceleration at the fundamental period $A(T_1)/g$ of each building.

Set of records	Median spectral acceleration $A(T_1)/g$			
	3-story	6-story	10-story	14-story
LA10/50	1.187	0.896	0.781	0.619
LA2/50	1.775	1.783	1.390	1.205

3.5 Evaluation of Selected Nonlinear Static Procedures

The bias and accuracy of the MPA, IMPA and MPP procedures applied to BRBF buildings are evaluated by comparing the target roof displacements, peak floor (or roof) displacements and inter-story drifts compared to more accurate results from nonlinear response history analysis (NL-RHA).

3.5.1 Target Roof Displacements

Pushover curves, which show the relationship between the base shear force and the roof displacement, for the 3-, 6-, 10- and 14-story BRBF buildings due to the first 'mode' load pattern (MPA), variable lateral force distribution (IMPA) and seismic mass (or weight) distribution (MPP) are plotted in Figure 3.10. The pushover curves for these frames are approximately tri-linear in nature whose details were discussed by Chintanapakdee *et al.* (2009). The variable lateral force distribution of IMPA procedure in this study is taken as a three-phase load pattern, which changes at the first and second yielding points of the pushover curve. Figure 3.10 shows that the pushover curve of IMPA is similar to MPA. This results in nearly identical estimates of target roof displacements of both procedures. It implies that the changes of lateral load distribution of IMPA procedure are not significant whereas the $\mathbf{m}g\iota = \mathbf{w}\iota$ force distribution of MPP leads to different results. Pushover curves of MPP are always higher and stiffer than both MPA's and IMPA's for all cases.

On each pushover curve, diamond (MPA), star (IMPA) and circle (MPP) markers show the peak roof displacements of buildings determined by NL-RHA of the equivalent single-degree-of-freedom (SDF) system due to 20 records in each set of ground motions. The ductility factors of the first 'mode', defined here as the ratio between median of peak roof displacements determined by NL-RHA and yield roof

displacement estimated by first ‘mode’ load pattern, are about 1.94 to 6.02 for LA10/50 and 2.93 to 14.85 for LA2/50 ground motions, respectively. Table 3.7 shows the median ductility factors for these BRBF buildings calculated from NL-RHA estimate. The median ductility factor noticeably decreases when the building height increases.

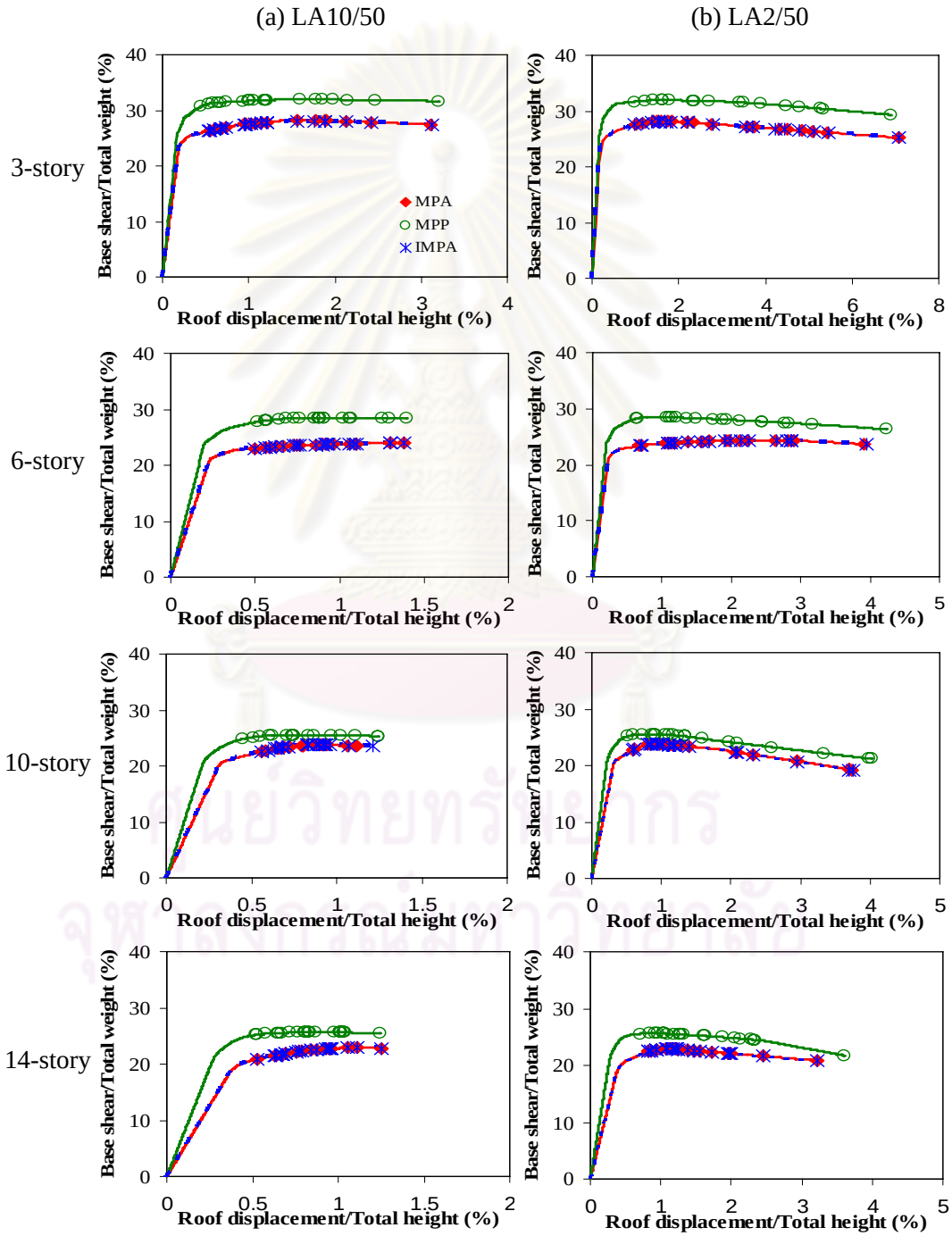

Figure 3.10 First ‘mode’ pushover curves of 3-, 6-, 10-, and 14-story BRBF buildings due to (a) LA10/50 and (b) LA2/50 ground motions.

Table 3.7 Median ductility factors for building models calculated from NL-RHA estimate of peak roof displacement.

Set of records	Building model			
	3-story	6-story	10-story	14-story
LA10/50	6.02	3.25	2.20	1.94
LA2/50	14.85	7.29	3.52	2.93

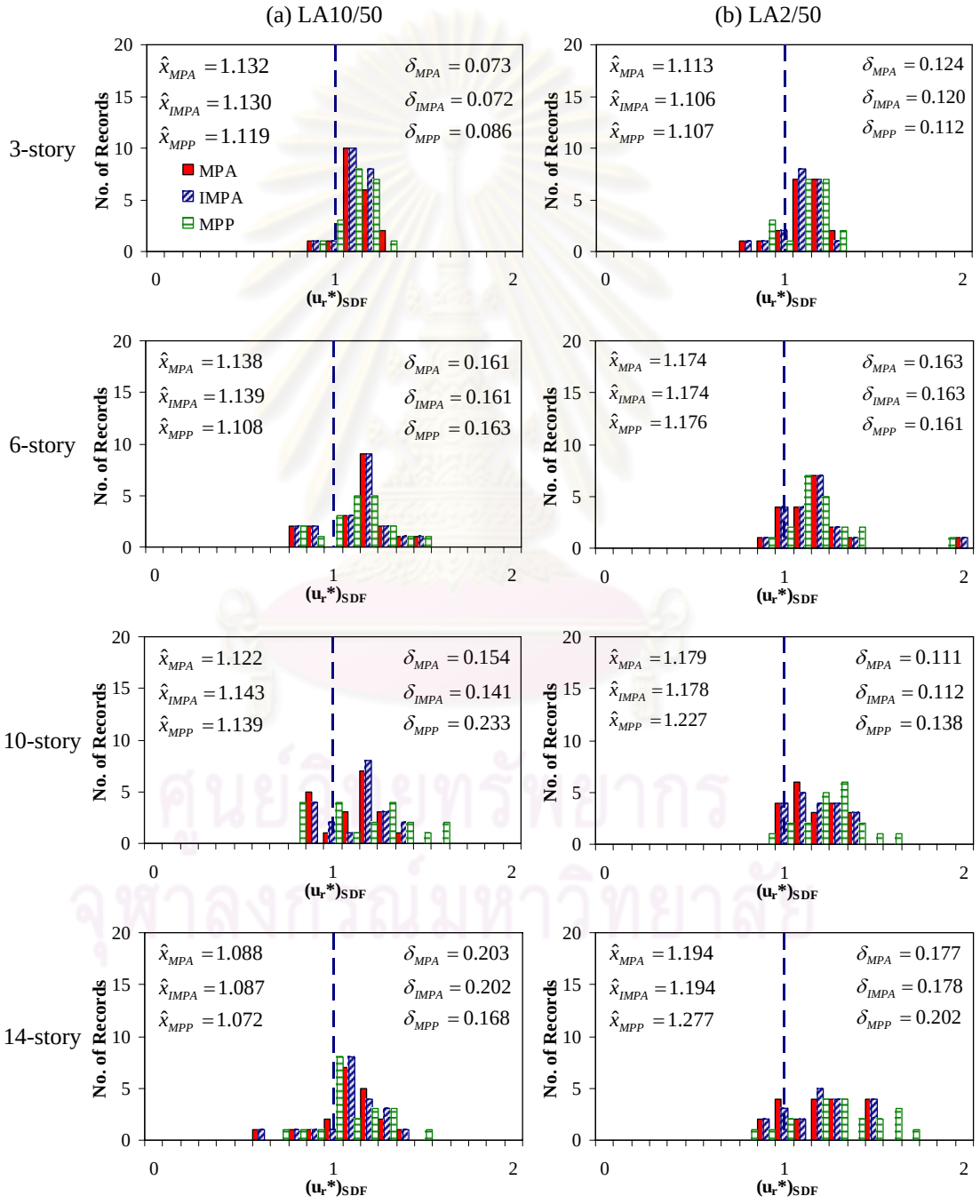

Figure 3.11 Histograms of ratio $\left(u_r^*\right)_{SDF}$ for 3-, 6-, 10-, and 14-story BRBF buildings due to (a) LA10/50 and (b) LA2/50 ground motions.

The accuracy of target maximum roof displacements predicted by displacement of the equivalent SDF systems: $(u_r)_{SDF} = \Gamma_1 \phi_{r1} D_1$ for MPA and IMPA or $(u_r)_{SDF} = \Gamma D_{\max}$ for MPP are examined by calculating the ratio between the SDF system's estimate and roof displacement determined from NL-RHA: $(u_r^*)_{SDF} = (u_r)_{SDF} / (u_r)_{NL-RHA}$. The ratio $(u_r^*)_{SDF}$ being close to 1 indicates good accuracy. The histograms of these ratios are shown in Figure 3.11. The median and dispersion of the peak roof displacements are also noted. Figure 3.11 shows that the SDF systems of these nonlinear static procedures slightly over-estimate the maximum roof displacements but the bias of MPA and IMPA is no larger than 15% for set of LA10/50 ground motions and 19% for stronger ground motions LA2/50 while the bias of MPP is 14% and 28% for LA10/50 and LA2/50 records, respectively. The IMPA tends to predict the median and dispersion of target roof displacements better than MPA; however, the difference is not significant while the MPP tends to estimate the maximum roof displacements slightly more accurate than both MPA and IMPA for set of LA10/50 but less accurate for stronger records LA2/50.

3.5.2 Peak Floor/Roof Displacements

The responses of the BRBF buildings studied to the two sets of ground motions were determined by MPA, IMPA, MPP nonlinear static procedures and by nonlinear response history analysis (NL-RHA). The MPA and IMPA were considered as many modes as to include participating mass at least 95% of the total mass. For the structures in this study, the contribution of the first two 'modes' for a 3-story building, three 'modes' for 6- and 10-story buildings, and four 'modes' for a 14-story building were considered to estimate the seismic demands. The combined values of floor displacements and story drifts were computed by using the SRSS modal combination rule.

The peak floor/roof displacement demands from the four methods are compared in Figure 3.12; the results from modal pushover analysis (MPA) including only the fundamental 'mode' are also shown by the dashed line. These results lead to the following observations for the BRBF system. The contributions of higher 'modes'

of MPA and IMPA procedures to floor displacements are not significant. One ‘mode’ pushover analysis, MPA, and IMPA can estimate the peak floor displacements reasonably well with a tendency to slightly overestimate the floor/roof displacement compared to NL-RHA while the MPP tends to significantly overestimate peak floor displacements of lower stories (Figure 3.12).

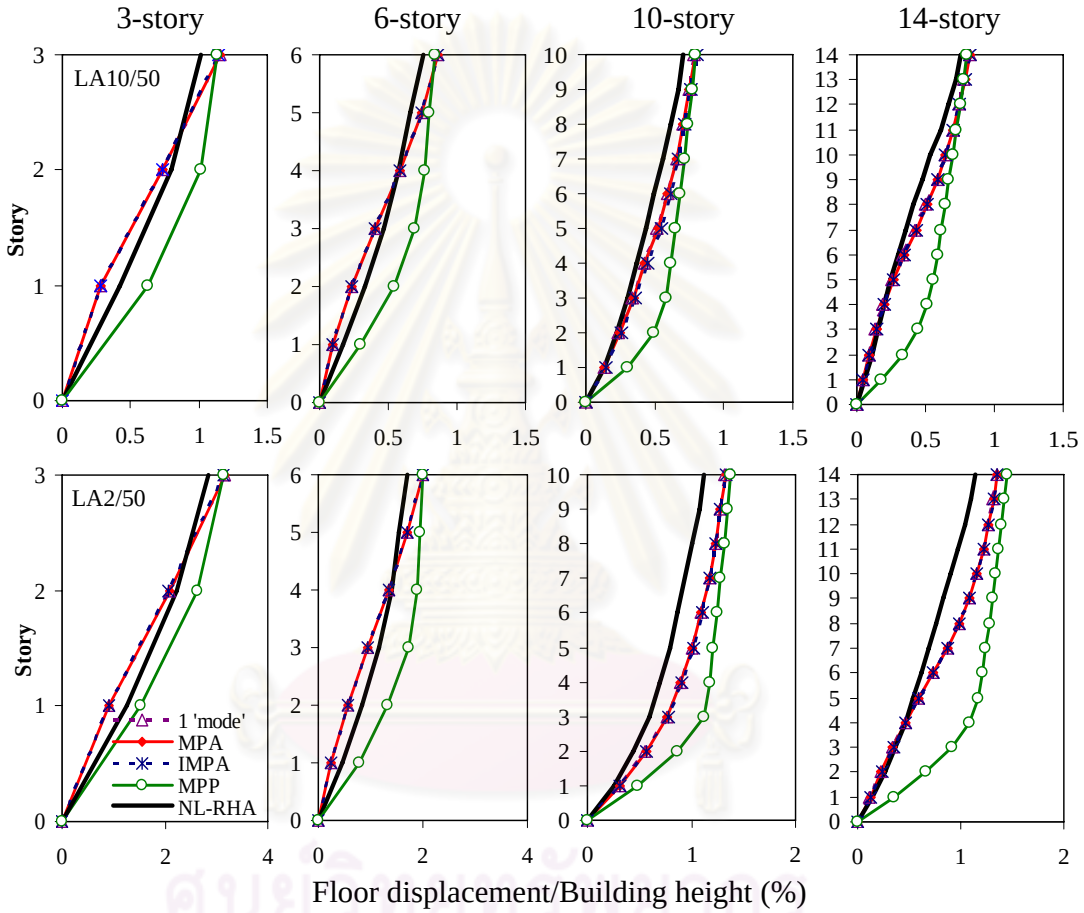

Figure 3.12 Median floor displacements of 3-, 6-, 10- and 14-story BRBF buildings determined by one ‘mode’ pushover analysis, MPA, IMPA, MPP and NL-RHA due to LA10/50 (first row), and LA2/50 (second row) ground motions.

Figure 3.13 shows the median floor displacement ratio, $u^{*}_{NSP} = u_{NSP} / u_{NL-RHA}$, due to the two sets of ground motions. It can be seen that the MPA procedure can accurately estimate floor displacements of the 3-, 6-, 10-, and 14-story BRBF buildings; the bias is generally less than 20% and 30% for LA10/50 and LA2/50 ground motions, respectively. The IMPA tends to overlap the MPA with slight difference whereas the MPP tends to much overestimate peak floor displacements of

lower stories with increasing bias when the building height increases. The bias of MPP is very large for BRBF buildings taller than 6 stories considered in this study.

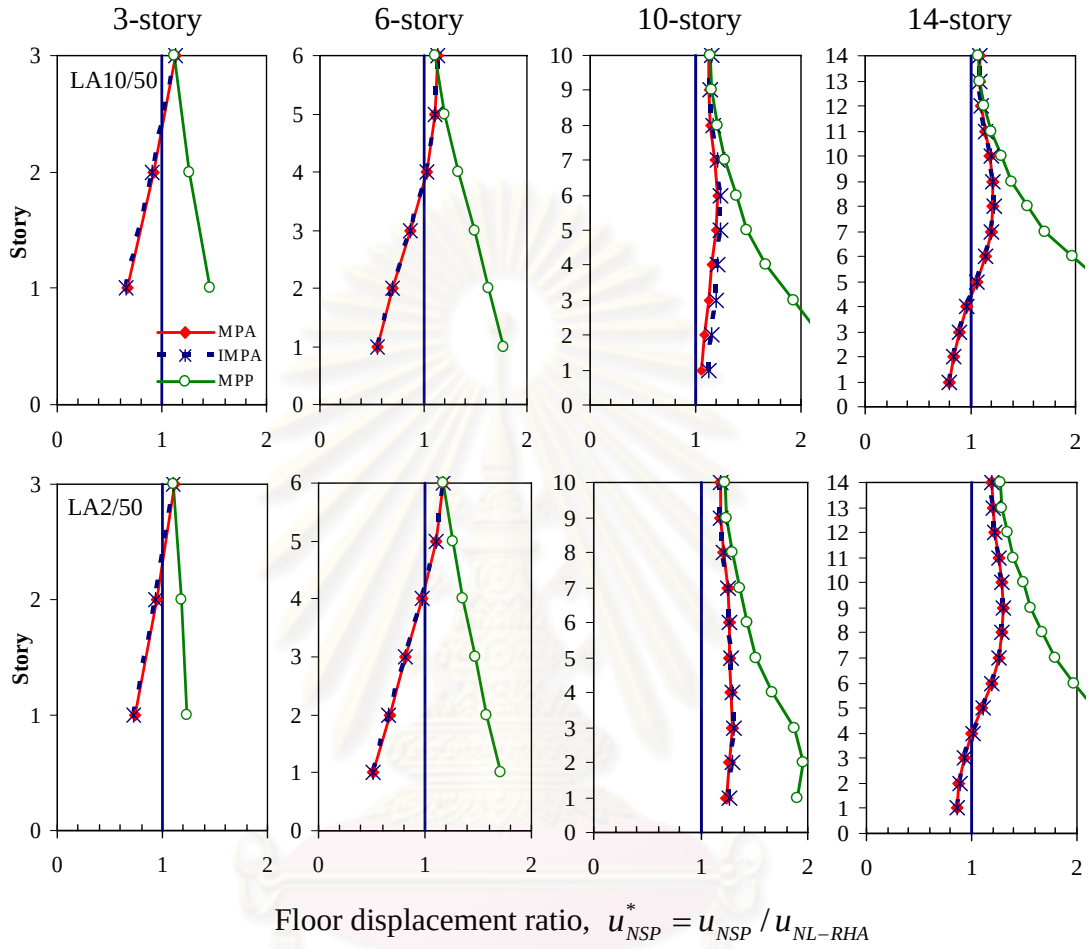

Figure 3.13 Floor displacement ratio of 3-, 6-, 10- and 14-story BRBF buildings due to LA10/50 (first row) and LA2/50 (second row) ground motions.

3.5.3 Story Drift Demands

Unlike the floor/roof displacements, the contributions of higher 'modes' in estimating the story drifts of MPA and IMPA procedures are more significant, especially in upper stories of tall BRBF buildings. Figure 3.14 shows that the story drift demands of 10-, and 14-story BRBF buildings predicted by MPA are able to follow the NL-RHA results whereas the first 'mode' alone is inadequate. With three or four 'modes' included, the story drifts estimated by MPA are generally similar to the results from nonlinear RHA. However, the MPA story drift results including two

'modes' for 3-story and three 'modes' for 6-story BRBF buildings are close to the one 'mode' results indicating that the contributions of higher 'modes' are not significant for these buildings. Both one 'mode' pushover analysis and MPA can estimate the response of structures reasonably well, although their results differ from the NL-RHA results at some stories. Similar to investigations of peak floor/roof displacements, IMPA estimates tend to overlap the MPA estimates in estimating story drift demands. The MPP excessively overestimates story drifts in the lower stories but underestimates the story drifts in the upper stories in these cases. Moreover, the story drifts predicted by the MPP procedure seem to be uniform in the upper stories, especially for 10- and 14-story BRBF buildings.

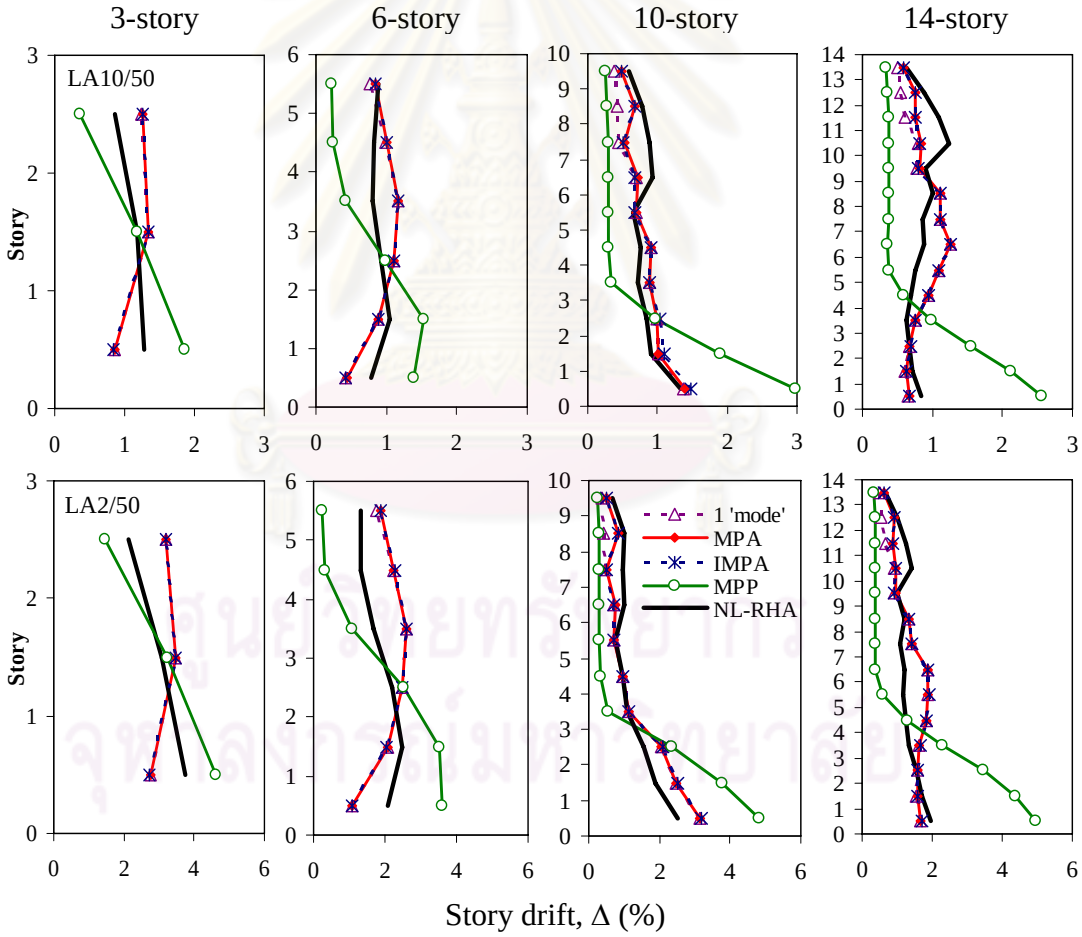

Figure 3.14 Median story drifts of 3-, 6-, 10- and 14-story BRBF buildings determined by one 'mode' pushover analysis, MPA, IMPA, MPP and NL-RHA due to LA10/50 (first row), and LA2/50 (second row) ground motions.

Figure 3.15 shows the median story drift ratio, $\Delta^{*}_{NSP} = \Delta_{NSP} / \Delta_{NL-RHA}$, due to the two sets of ground motions. The bias of MPA, IMPA and MPP nonlinear static procedures in estimating seismic demands tends to increase for stronger excitations and the variation of the NSP bias in estimating seismic demands along building height primarily depends on the building height rather than the intensity of ground motions. The bias of MPA and IMPA in estimating peak story drifts at an individual story can be as large as 50% and 60% at certain locations for LA10/50 and LA2/50 ground motions, respectively. Meanwhile, the bias of MPP in peak story drifts estimation at an individual story can be as large as 80% for two sets of ground motions; however, it overestimates story drifts by as much as 200% for the lower stories of 14-story building. This is because the MPP significantly overestimates floor displacements for lower stories due to the total seismic mass (or weight) load pattern (Figure 3.12).

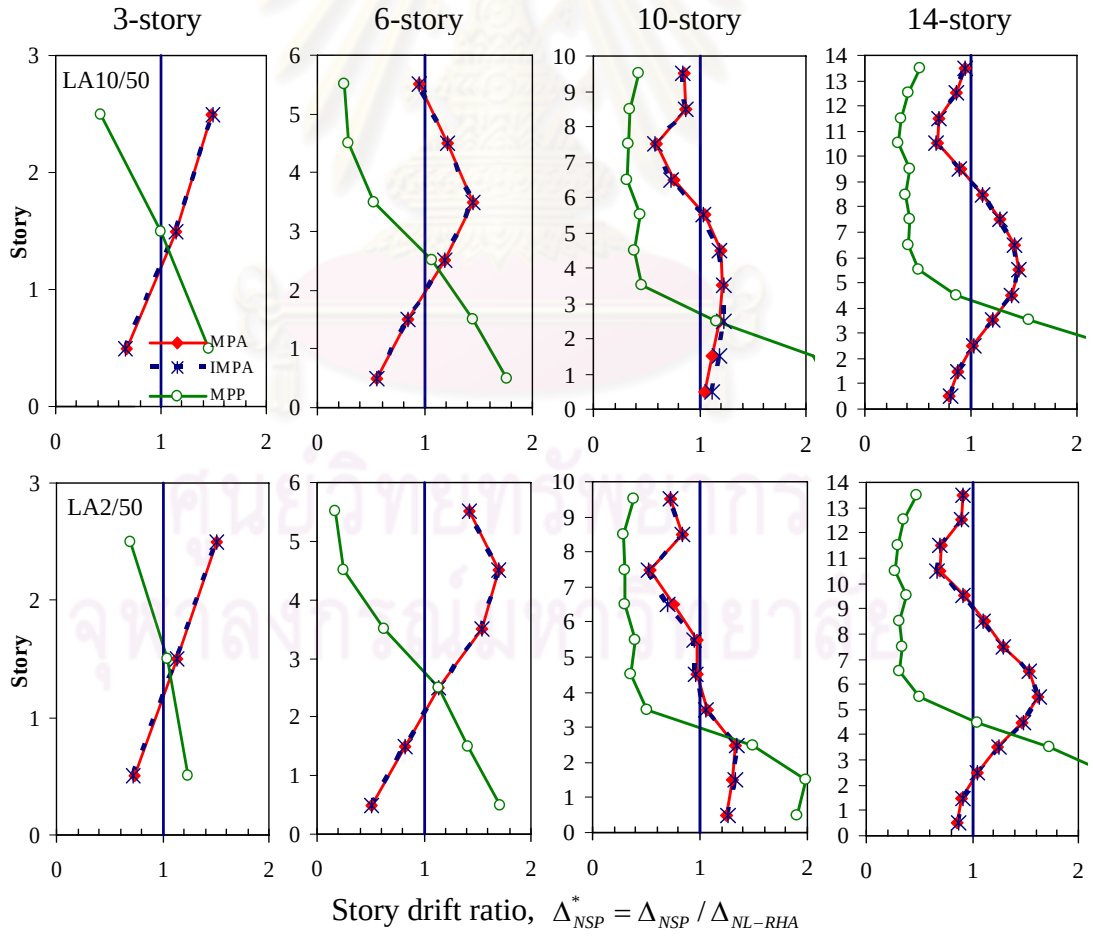

Figure 3.15 Story drift ratio of 3-, 6-, 10- and 14-story BRBF buildings due to LA10/50 (first row) and LA2/50 (second row) ground motions.

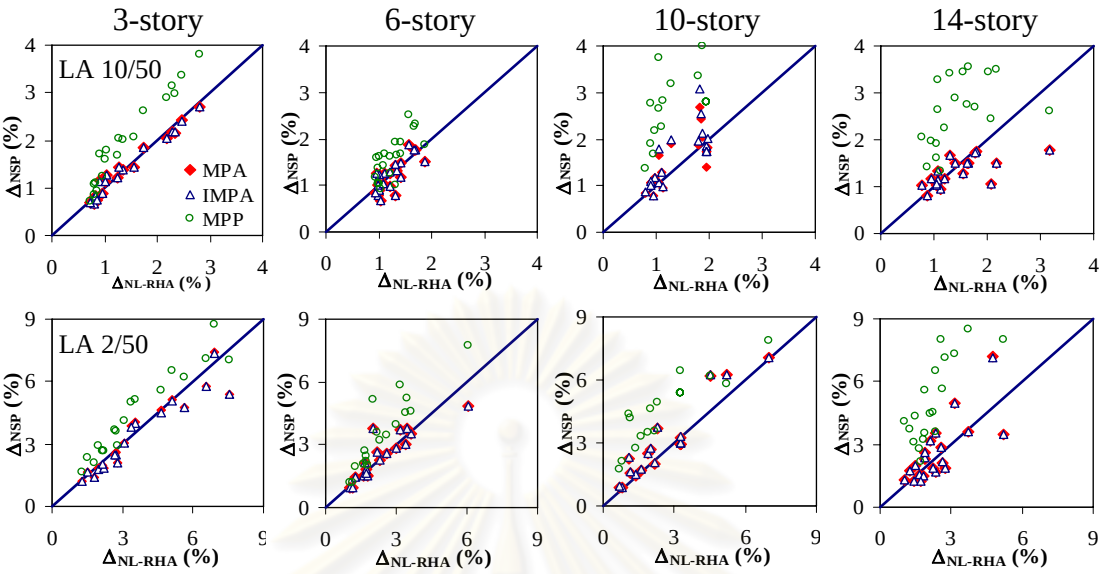

Figure 3.16 Maximum story drifts over all stories determine by NSP, Δ_{NSP}, versus 'exact' values Δ_{NL-RHA}, for 3-, 6-, 10- and 14-story BRBF buildings due to LA10/50 (first row), and LA2/50 (second row) ground motions.

To verify a building design or to evaluate an existing structure, building codes usually require the maximum story drift in any stories to be less than its allowable value. Figure 3.16 plots the maximum story drifts over all stories determined by NL-RHA and NSP as abscissa and ordinate, respectively, with diamond markers for MPA, star markers for IMPA and circle markers for MPP. The MPA and IMPA data points are clustered along the diagonal line indicating that the maximum story drifts over all stories estimated by MPA and IMPA are close to the value from NL-RHA. The median and dispersion of story-drift ratio Δ^*_{NSP} considering maximum story drift over all stories are also shown in Table 3.8. The median story-drift ratios of MPA, Δ^*_{MPA}, range from 0.93 to 1.14 while the median story-drift ratios of IMPA, Δ^*_{IMPA}, from 0.92 to 1.16 indicating that both MPA and IMPA procedures predict maximum story drifts over all stories with a bias less than 14% and 16% for these BRBF buildings, respectively. On the contrary, the bias in estimating the maximum story drifts over all stories of MPP can be considerable in the range from 1.22 to 2.26. This implies that MPP significantly overestimates the maximum story drift over all stories.

Table 3.8 Median and dispersion of maximum story drift ratios over all stories determine by MPA, IMPA and MPP, Δ_{NSP}, versus 'exact' values, Δ_{NL-RHA}.

Set of records	3-story	6-story	10-story	14-story
LA10/50	Δ^*_{MPA} =0.982; δ =0.119	Δ^*_{MPA} =0.949; δ =0.205	Δ^*_{MPA} =1.058; δ =0.214	Δ^*_{MPA} =0.986; δ =0.248
	Δ^*_{IMPA} =0.983; δ =0.117	Δ^*_{IMPA} =0.952; δ =0.206	Δ^*_{IMPA} =1.101; δ =0.220	Δ^*_{IMPA} =0.987; δ =0.249
	Δ^*_{MPP} =1.353; δ =0.163	Δ^*_{MPP} =1.244; δ =0.209	Δ^*_{MPP} =2.154; δ =0.284	Δ^*_{MPP} =1.831; δ =0.317
LA2/50	Δ^*_{MPA} =0.926; δ =0.132	Δ^*_{MPA} =1.013; δ =0.203	Δ^*_{MPA} =1.143; δ =0.226	Δ^*_{MPA} =1.046; δ =0.298
	Δ^*_{IMPA} =0.922; δ =0.128	Δ^*_{IMPA} =1.015; δ =0.202	Δ^*_{IMPA} =1.161; δ =0.227	Δ^*_{IMPA} =1.048; δ =0.297
	Δ^*_{MPP} =1.225; δ =0.149	Δ^*_{MPP} =1.422; δ =0.212	Δ^*_{MPP} =1.839; δ =0.364	Δ^*_{MPP} =2.256; δ =0.287

The dispersion δ of story-drift ratios of MPA and IMPA range from 0.117 for 3-story building to 0.298 for a 14-story building with a tendency to increase as the building becomes taller or ground motions become stronger. Meantime, the dispersion δ of story-drift ratios of MPP range from 0.149 to 0.364 for these BRBF buildings. This implies that the accuracy of NSPs in predicting the response due to an individual ground motion deteriorates when applied to taller BRBF buildings or subjected to stronger ground motions. Among these cases, the dispersion is still small, less than 0.298 for MPA and IMPA and 0.364 for MPP, when NSPs are used to estimate the maximum story drift over all stories. Moreover, the dispersion of story-drift ratios of MPP is always larger than both MPA's and IMPA's. Thus, MPA and IMPA can be a useful analysis tool to estimate the peak story drift over all stories in evaluating existing buildings or design of new buildings using BRBFs. Both of these procedures provide practically the same results but MPA is simpler and more practical than IMPA because it involves an invariant load pattern. On the contrary, the MPP method is simple with no need to conduct a modal analysis to capture the effects of higher 'modes' but it may be inaccurate in estimating seismic demands for BRBF tall buildings due to strong ground motions.

CHAPTER IV

STRUCTURAL SYSTEM, GROUND MOTIONS AND RESPONSE STATISTICS

4.1 Introduction

Bridges are extremely important components in modern transportation networks. Bridges play the role of critical lifeline facilities due to their significance in the economic development of a nation and their importance in supporting the daily functions. Unfortunately, such essential systems often become the victims of earthquakes. Society suffers a tremendous cost and inconvenience due to the collapse of a bridge. Even non-collapsed, the temporary lost of post-earthquake serviceability of important bridges may cause very costly disruption to vehicle traffic on major transportation arteries and is simply unacceptable (Zhang, 1999; and Hashimoto *et al.*, 2005). Additionally, the direct economic loss, attributed to replacement or repair cost of the damaged bridges, forms only a minor portion of the total losses. The major cost, which is often difficult to estimate accurately, is associated with the disruption of vehicular movement immediately following the earthquakes and during the long reconstruction phase (Rose and Lim, 2002). In order to ensure the functionality and operationally of bridges, it is therefore essential to design them to safely withstand the devastating forces of earthquake ground motions.

With the rapid development of highway systems, steel bridges have become a viable option of highway viaducts, urban expressways, valley- or river-crossings and widely used in Japan because of the simplicity of fabrication and construction, speed of erection as well as low cost for maintenance. They are considered specially advantageous in regions of high seismic activity (Usami and Kumar, 1998; and Hsu and Chang, 2001). Recent strong earthquakes have caused collapse or severe damage to a considerable number of steel bridges. For instance, a steel girder bridge named South Fork Eel was damaged due to the 1992 Petrolia Earthquake, as reported by Itani *et al.* (2004). Local failures or total collapses of bridges represent not only immediate concern for loss of life and repair costs, but also financial restrictions and major

economic impact due to the temporary suspension of traffic serviceability (Menoni, 2001; Chang and Nojima, 2001; and Rose and Lim, 2002).

Japan is one of the most seismically prone countries in the world and has often suffered significant damage from large earthquakes. More than 3000 bridges have sustained seismic damage since the 1923 Kanto earthquake (Unjoh, 1999). The 1995 Hyogoken Nanbu earthquake supposed an inflexion point in seismic design of bridges in Japan. Seismic design of bridge structures has greatly evolved in the last decade in response to the serious damage to bridges observed in the 1995 Hyogoken-Nanbu earthquake. The simply-supported bridges are vulnerable by the failure due to deck unseating (Dicleli and Bruneau, 1995; and Rashidi and Saadeghvaziri, 1997). As a positive fact, the Hyogoken-Nanbu earthquake provided a stimulus to investigate the seismic response of highway bridges. Immediately after the earthquake the Japanese Specifications for Highway Bridges were revised in 1996 (JRA, 1996). To improve the seismic performance of bridges due to deck unseating in the particular case of simply-supported superstructures, a possible solution consists in making girders continuous over the piers by linking the webs together with tie-plates (Keady *et al.*, 1999).

It is widely recognized that bridges are complex structures which consist of many structural members. Therefore, an accurate prediction of the bridge dynamic responses requires the adoption of three-dimensional models instead of two-dimensional analytical approaches. These three-dimensional models can provide accurate estimates of seismic nonlinear behaviors of bridges due to both material and geometrical nonlinearities of the structures.

One of irregularities of bridges is found at the weak connection between deck superstructure and substructure members. This link is considerably fragile due to the vulnerability of bearing supports. Several examples of bearing failures can be found in the 1995 Hyogoken Nanbu earthquake (Wilson, 2003). Figure 4.1 shows several examples of various types of structural damages to steel bearings of bridges occurred in Hokkaido during the 2003 Tokachi Oki Earthquake (Julian, 2005).

(a) Concrete pedestal failure

(b) Residual bearing displacement

(c) Dislodgement of roller bearing

(d) Destruction of bearing assembly

Figure 4.1 Seismic damages to steel bearing supports (Julian, 2005).

Based on the above considerations, it should be clear how the necessity of accurately assessing the state of existing bridges or estimating seismic demands in design new bridges has become a deeply felt issue. For this reason, the study presented proposes an extension of MPA procedure in estimating seismic demands for bridges. This chapter presents a structural system which is analyzed to assess the bias and accuracy of the proposed extension of MPA procedure. Different bearing supports of the bridge are also considered in this study.

4.2 Structural System

In recent decades, steel bridges have become widely used to support highway viaducts in urban areas, valley- or river-crossings, and considered specially advantageous in regions of high seismic activity. Twin I-girders steel bridges have been considered as one of the most popular bridge types for short and medium span bridges in Japan with span length of more than 50 m. This type of steel bridge has

advantageous in relation to the simplicity of its fabrication, design and low cost for maintenance, speed of erection as well as construction. However, these I-girders have lower structural damping and less torsional stiffness than conventional plate girder bridges and may cause problems related to vibration due to earthquakes, especially when the span length of the bridges becomes longer. For these reasons, an actual twin I-girder bridge is selected and analyzed due to a set of 20 strong ground motions to assess the bias, accuracy, efficiency, and also the practicality of the proposed extension of MPA procedure in this study.

4.2.1 Description of the Bridge

The bridge selected in this study is an existing continuous steel twin I-girder bridge with PC slab that has structural characteristics of typical highway viaducts in Japan, with bridge components designed in compliance with the Japanese Code (JRA, 1996). The bridge considered is the Chidorinosawa river bridge which has four spans with two steel main girders and concrete slab (Tamura *et al.*, 1998). The selected bridge is 194 m total length divided into four spans varying from 41 m to 53 m. The bridge superstructure consists of a concrete deck slab that rests on two I-shape steel girders. The two main I-girders are 2.9 m deep and spaced transversely 5.7 m apart. The girders are interconnected by end-span diaphragms as well as intermediate diaphragms spacing of 5.0 m to 6.0 m. The deck weight is supported by three piers whose height varies from 32 m to 34 m along the length. The elevation view of this bridge is shown in Figure 4.2. The global coordinate system for the bridge is shown in the figure, in which the x-axis refers to the longitudinal direction of the bridge along the centerline of the road, the y-axis indicates the transverse horizontal direction, and the z-axis is vertical.

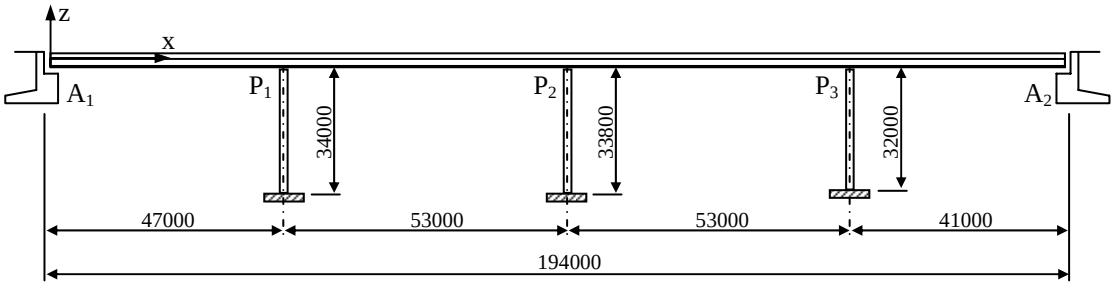

Figure 4.2 Elevation view of Chidorinosawa river bridge.

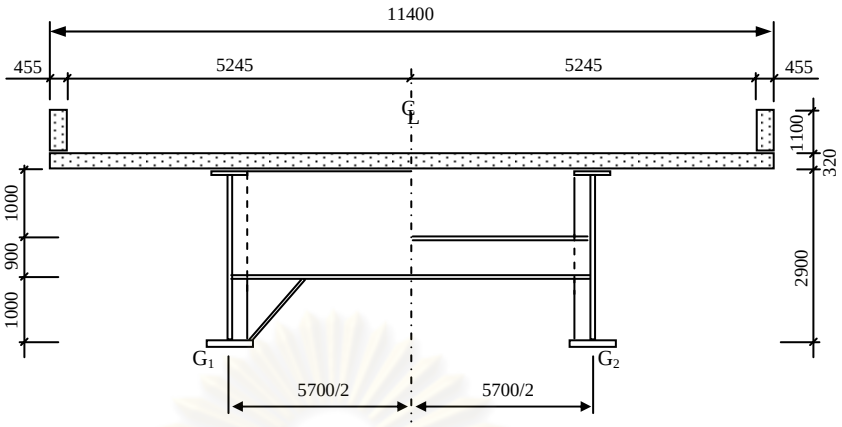

Figure 4.3 End and intermediate cross sections of the bridge studied.

The cross sections of the two main girders are uniform throughout the bridge's spans. These main girders are interconnected with each other by a reinforced concrete bridge deck, which acts compositely with the steel main girders, and transverse members (e.g., the cross beams). The cross beams are connected to the webs of main girders through transverse stiffeners of 250mm wide and 25mm thick. The cross section the basic geometric properties of the studied bridge are presented in Figure 4.3 and Table 4.1, respectively.

Seismic forces at the deck are transmitted from the cross beams to arrive at the top of the bearings, to reach the substructure and finally the ground. In this study the effect of soil-structure interaction is not taken into account, and the base of piers are considered as fixed supports on the ground.

Table 4.1 Basic geometric properties of cross section of the studied bridge.

Deck width x thickness (m)	11.4x0.32
Dimensions of the main girders (mm)	Upper flange 500x30
	Web 2900x24
	Lower flange 800x50
Dimensions of the cross beam (mm)	Web 900x16
	Flange 300x25
Dimensions of the end cross beam (mm)	Web 1900x16
	Flange 300x25

4.2.2 Bearing Supports

To consider the influence of bearing supports to the bias and accuracy of the proposed extension of MPA procedure in estimating seismic responses of the bridges. Two cases of bearing supports are considered in this study: (1) the superstructure is supported by steel bearings (SB), and (2) the deck is seismically isolated by Lead Rubber Bearings (LRBs).

4.2.2.1 Steel Bearing Supports

Steel bearings have been extensively installed in bridges to transfer vertical and horizontal forces from the superstructure to the substructure. An adequate combination of fixed and roller steel bearings is considered optimal to support the superstructure weight, providing accommodation for thermal expansion, contraction and rotation to the deck superstructure. However, recent strong earthquakes, including the Hyogoken-Nanbu earthquake, have clearly demonstrated the poor performance of steel bearings under seismic loads and the disastrous consequences that a bearing failure can have on the overall earthquake performance of a bridge (Tanimura *et al.*, 2002). Therefore, it emphasized that the bearing support is one of the essential structural members of a bridge.

In the bridge equipped with steel bearings (SB) in this study, steel fixed bearings are installed on all piers (P1, P2 and P3 as shown in Figure 4.2) and steel roller bearings are applied at both end of the bridge to allow for movement in the longitudinal direction while restrained by stoppers in the transverse direction.

A typical steel fixed bearing consists of a metal casing with each part welded to the top and bottom steel plates. The top steel plate of the bearing is connected to the deck girder by connection bolts and the bottom steel plate is connected to the pier by anchor bolts. Steel roller bearings have similar details of fixed bearings, except the casings, which have a special configuration to allow for some movement of the supported deck in longitudinal direction. Roller supports are free to translate along the surface upon which the roller rests, allowing the bridge structure to move under seismic and non-seismic loadings. Therefore, both steel bearings are considered transversally fixed in the 3D model.

4.2.2.2 Lead-Rubber Bearing Isolation System

Steel bearings have performed poorly and have been damaged by relatively minor seismic shaking (DesRoches *et al.*, 2004). Therefore, many innovative systems are being developed for the purpose of seismic isolation of bridges. One of the most widely adopted isolation system is the Lead Rubber Bearing (LRB) shown in Figure 4.4. Lead-Rubber Bearings (LRB) have found wide application in bridge structures to replace the vulnerable steel bearing supports (Pan *et al.*, 2005). LRB bearings are steel reinforced elastomeric bearings in which a lead plug is inserted to provide hysteretic damping as well as rigidity against minor earthquakes, wind and service loads. The lead plug yields at relatively low shearing stress resulting in significant dissipation of seismic energy and reduction of earthquake response (Turkington *et al.*, 1989). It has been demonstrated that the bridges equipped with LRB support perform effectively in reducing the seismic responses during earthquake (Bessason and Haflidason, 2004).

4.2.2.2.1 Components of LRB bearings

Under normal conditions, LRB bearings behave like regular bearings. The isolation device, represented in Figure 4.5, is characterized by a high initial stiffness provided by the lead plug inserted in the bearing to avoid undesirable displacements under service requirements, wind action and minor earthquakes. However, the shear stiffness decreases favorably for moderate levels of deformation, allowing the isolator to uncouple the bridge from the damaging action of earthquake ground motions. Therefore, the seismic damage of the structure is minimized through the reduction of the seismic inertial loads.

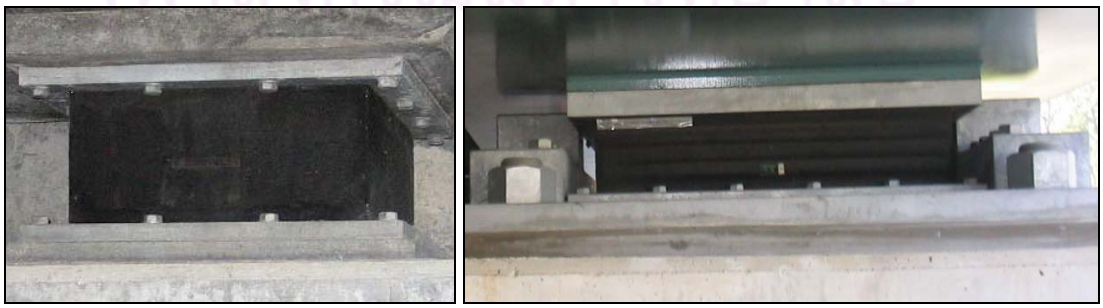

Figure 4.4 LRB isolation devices installed in bridge structures.

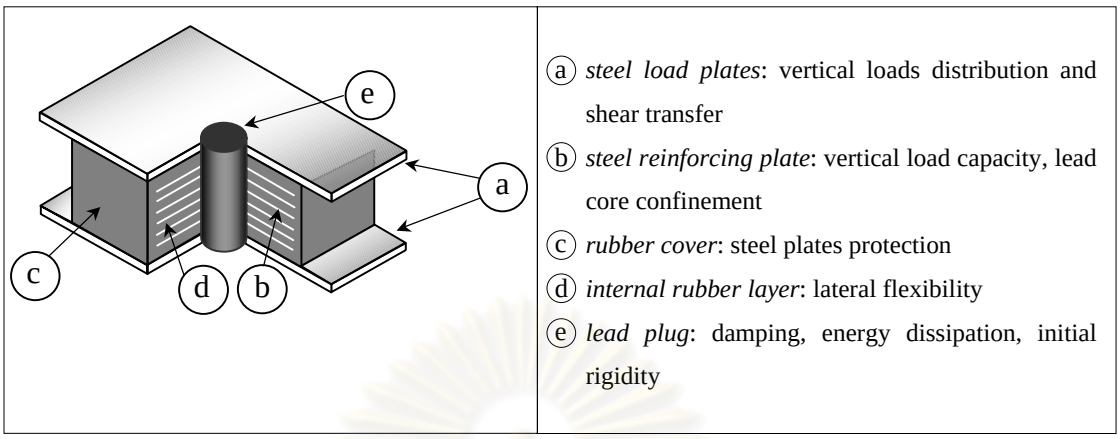

Figure 4.5 Components of LRB bearing supports.

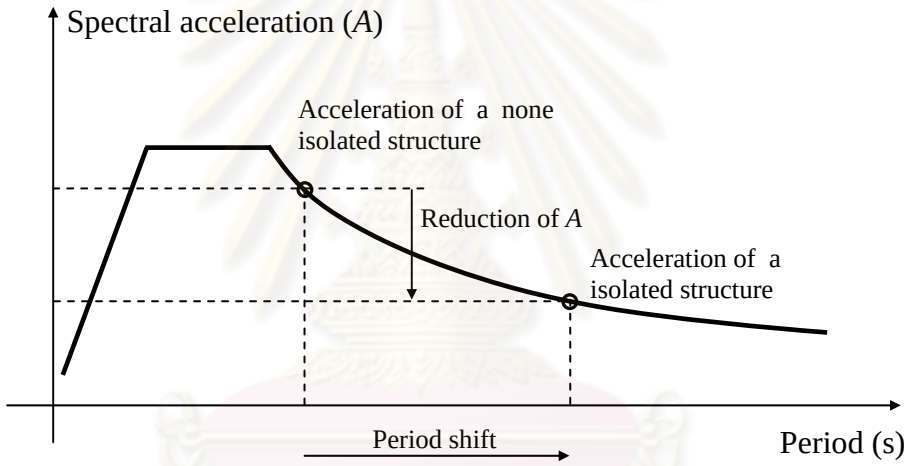

Figure 4.6 Response spectrum of bridge.

Bridges are ideal candidates for the adoption of base isolation technology due to the convenience of installation, inspection and maintenance of isolation devices. The seismic isolation bearing protects the bridge by increasing the fundamental natural period and also by dissipation of seismic energy through the additional hysteretic damping due to yielding of the lead core (Robinson, 1982). Thus the natural vibration period of the bridge is moved away from the high-energy seismic ground period and seismic energy transfer to the structure is minimized (Figure 4.6). Therefore usage of seismic isolation on soft or weak soil conditions, where long period ground motion is dominant, reduces the benefits offered by the technology (Yoshikawa *et al.*, 2000). Another consideration is related to the large deformations

that may occur in the seismic base-isolation bearings during an intense ground motion, which causes large displacements of the deck (Roberts, 2005).

4.2.2.2.2 LRB Analytical Model

LRB bearings can be modeled in a variety of ways, ranging from very simple models to rather sophisticated finite element models (Hwang *et al.*, 1996; Salomon *et al.*, 1999). Nevertheless, the most widely used analytical model is the bilinear idealization due to its simplicity and accuracy to estimate the force-displacement relationship of the isolation systems (Ali *et al.*, 1995). Figure 4.7a presents the bilinear force-displacement hysteresis loop of LRB bearing supports. It has been demonstrated that the bilinear analytical model can provide a good estimate of LRB behaviour under low-to-moderate earthquake ground motions. However, this analytical model is not able to capture the hardening behaviour at large strain ranges of LRB system due to strong ground motions (Julian *et al.*, 2007).

Sato *et al.* (2002) showed that the LRB supports display significant hardening behaviour beyond certain high strain levels. This hardening behaviour is caused by geometric effects and rubber material properties. Due to hardening effect on the LRB supports, the seismic response of the bridges are affected when subjected to strong earthquake ground motions. For this reason, a trilinear analytical model shown in Figure 4.7b was introduced to represent the strain hardening effect at high strain levels, and thus to accurately reproduce the hysteresis loop obtained from experimental tests on LRB bearings. This trilinear analytical model can accurately capture the large strain hardening behaviour with relatively easy implementation (Morishita *et al.*, 2002).

For the isolated case considered in this study, the superstructure is supported on three piers (P1, P2 and P3) by LRB bearings. The structural properties of LRB bearing supports used in this study is L1 representing the small bearing (Table 4.2). The characteristics of L1 LRB can be found in Julian *et al.* (2007). The orientation of the LRBs is such that they allow for longitudinal and transverse movements. The LRBs are represented by the trilinear force-displacement hysteresis loop shown in Figure 4.7b.

Table 4.2 Structural properties of LRB bearings considering hardening effect.

Bearing type	Pier location	K_1 (MN/m)	K_2 (MN/m)	K_3 (MN/m)	F_1 (MN)	F_2 (MN)
L1	P1, P2, P3	24.50	2.45	7.35	0.245	0.833

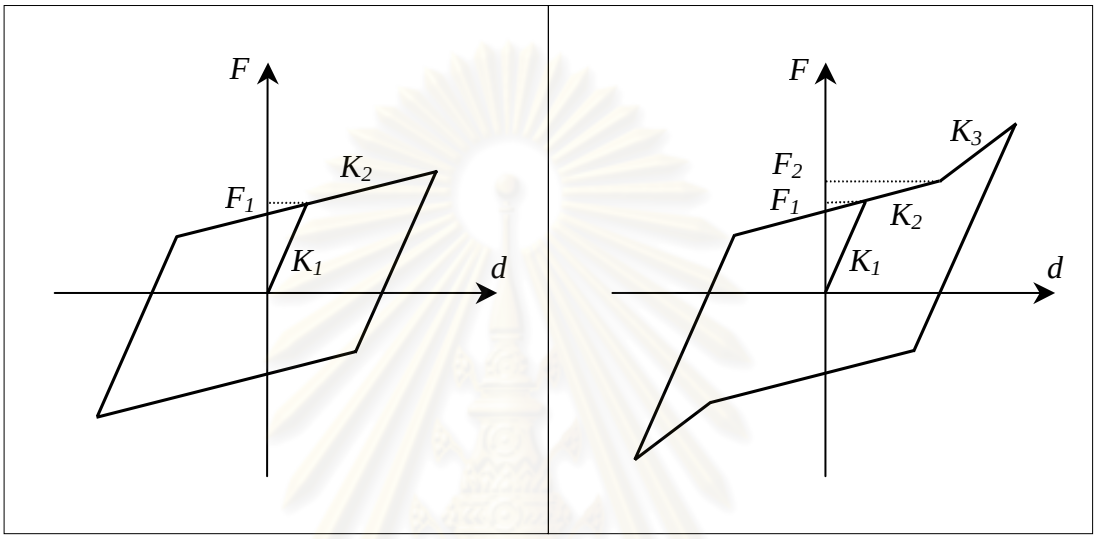

(a) Bilinear model (b) Trilinear model

Figure 4.7 Bilinear and trilinear analytical models of LRB bearing supports.

4.2.3 Finite Element Model of the Bridge

A bridge can be modeled in a variety of ways, ranging from very simple models to rather sophisticated finite element models (Ali and Abdel-Ghaffar, 1995; Chen, 1996; Jangid, 2004; Nasim *et al.*, 2008; and Ngo-Tran *et al.*, 2008). The dynamic analysis of complex structural systems, like bridges, for earthquake loads often entails simplifying assumptions. Regardless of the type of models adopted, reasonable results can be obtained if all important behavioral aspects of the bridge are properly accounted for. For instance, two-dimensional (2D) plane-frame structural models have been often used in the recent past to study the vibration and dynamic responses of bridges. These 2D models are still widely required for the preliminary seismic assessment of bridges when only approximate solutions are needed or when detailed models are not warranted. Despite its simplicity and ease of application, these

simple models may not be able to capture the dynamic responses of the bridges and their seismic behaviors may not represent the actual bridges.

For this reason, in making the refinement, three-dimensional (3D) analytical models have become necessary in design of complex structures, since 2D models can not capture important seismic response characteristics. For instance, a 3D model allows for consideration of the torsional vibration of the bridge deck or coupling between lateral and torsional responses of actual bridges.

The three-dimensional finite element model of the selected bridge is created by using appropriate elements. The piers are modeled as a series of frame elements. ATC-32 (1996a-b) suggested that a minimum of three elements per bent should be used. However, the piers are modeled by using twenty elements to represent long piers in this study. The three-dimensional frames is used to simulate the seismic behavior of bridge structures. In the analytical model, the material nonlinear behavior is modeled by plastic hinges using moment-rotation ($M-\theta$) relation (Chintanapakdee and Chopra, 2003a; Paraskeva *et al.*, 2006; and Banerjee and Shinozuka, 2007). Plastic hinges and shear failures are considered for all girder, pier and crossbeam elements. The three-dimensional P-M-M interaction yield surface proposed by El-Tawil and Deierlein (2001a-b) was used. Cross-section properties of girders and piers were defined using bilinear moment-rotation relationships for each P-M plane with 1% post-yield stiffness ratio. A finite element mesh of steel main girders and crossbeam elements are modeled at the bottom surface of the deck slabs. The mass of the superstructure is divided and lumped on nodes of the steel main girder elements, and the mass of the substructure is similarly divided and lumped on nodes of elements (Murakoshi *et al.*, 2006; Fumoto *et al.*, 2006; and Julian *et al.*, 2007). Rayleigh damping was used with 2% damping ratios for the first two modes, according to common practice for code designed steel structures (Julian *et al.*, 2007). *P*–Δ effect was also considered for this study. Nonlinear static and dynamic analyses were carried out using computer program PERFORM 3D (CSi, 2006) and MATLAB (2007) was used for pre and post processing. The finite element model of the studied bridge is shown in Figure 4.8.

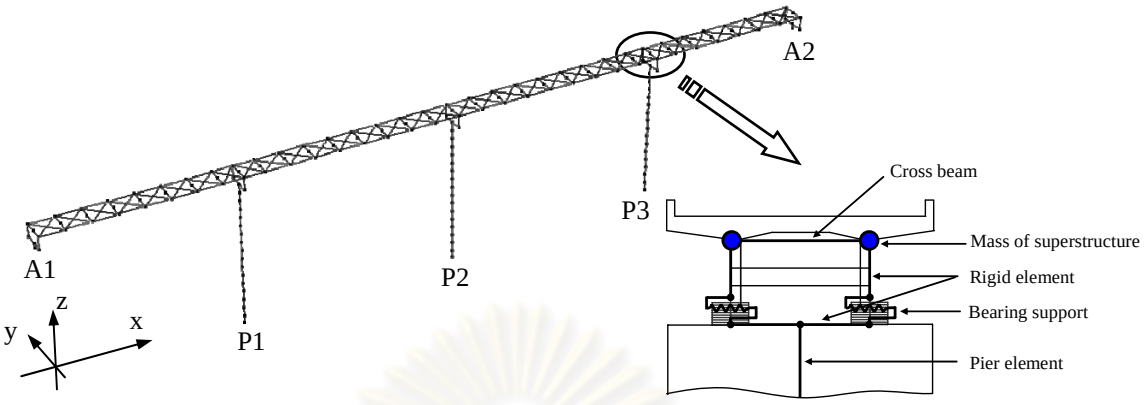

Figure 4.8 Finite element model of the studied bridge.

4.3 Ground motions

The seismic excitation used in this study is defined by a set of 20 LMSR (Large-Magnitude-Small-distance) records. Table 4.3 provides the information of the LMSR set of records including: name of record, recording station, earthquake magnitude, distance, peak ground acceleration (PGA), peak ground velocity (PGV) and peak ground displacement (PGD). These ground motions were obtained from California earthquakes of magnitude ranging from 6.6 to 6.9 recorded at distances of 13 to 30 km on firm soil (NEHRP site class D) and used by Chintanapakdee and Chopra (2003b). The ground acceleration, velocity and displacement time histories of the LMSR ensemble are shown in Figures 4.9, 4.10 and 4.11. Note that although this set of 20 records is binned for the given earthquake scenario, there is large variability from record to record. The pseudo-acceleration, pseudo-velocity and deformation spectra for the set of ground motions with damping ratio 2% are shown in Figures 4.12, 4.13 and 4.14 together with the median spectra (black solid lines). These ground motions are applied in both horizontal directions of the bridge, namely transverse and longitudinal directions.

Table 4.3 List of ground motions in LMSR ensemble.

No.	Earthquake Name	Record	Location	Magnitude	R^* (km)	$\ddot{u}_{go}$ (cm/s^2)	$\dot{u}_{go}$ (cm/s)	u_{go} (cm)
1	1989 Loma Prieta	LP89agw	Agnews State Hospital	6.9	28.2	169	25.9	12.6
2	1989 Loma Prieta	LP89cap	Capitola	6.9	14.5	435	29.2	5.5
3	1989 Loma Prieta	LP89g03	Gilroy Array #3	6.9	14.4	360	44.7	19.3
4	1989 Loma Prieta	LP89g04	Gilroy Array #4	6.9	16.1	208	37.9	10.1
5	1989 Loma Prieta	LP89gmr	Gilroy Array #7	6.9	24.2	221	16.4	2.5
6	1989 Loma Prieta	LP89hch	Hollister City Hall	6.9	28.2	242	38.5	17.7
7	1989 Loma Prieta	LP89hda	Hollister Diff. Array	6.9	25.8	274	35.6	13.0
8	1989 Loma Prieta	LP89svl	Sunnyvale - Colton Ave.	6.9	28.8	203	37.3	19.1
9	1994 Northridge	NR94cnp	Canoga Park - Topanga Canyon	6.7	15.8	412	60.7	20.3
10	1994 Northridge	NR94far	LA - N Faring Rd	6.7	23.9	268	15.8	3.3
11	1994 Northridge	NR94fle	LA - Fletcher Dr	6.7	29.5	236	26.2	3.6
12	1994 Northridge	NR94glp	Glendale - Las Palmas	6.7	25.4	202	7.40	1.8
13	1994 Northridge	NR94hol	LA - Hollywood Stor FF	6.7	25.5	227	18.2	4.8
14	1994 Northridge	NR94nya	La Crescenta - New York	6.7	22.3	156	11.3	3.0
15	1994 Northridge	NR94stc	Northridge-Saticoy St	6.7	13.3	361	28.9	8.4
16	1971 San Fernando	SF71pel	LA - Hollywood Stor Lot	6.6	21.2	171	14.8	6.3
17	1987 Superstition Hills	SH87bra	Brawley	6.7	18.2	153	13.9	5.3
18	1987 Superstition Hills	SH87icc	El Centro Imp. Co. Center	6.7	13.9	351	46.3	17.6
19	1987 Superstition Hills	SH87pls	Plaster City	6.7	21.0	182	20.6	5.4
20	1987 Superstition Hills	SH87wsm	Westmorland Fire Station	6.7	13.3	169	23.5	13.1

*The closest distance to fault rupture.

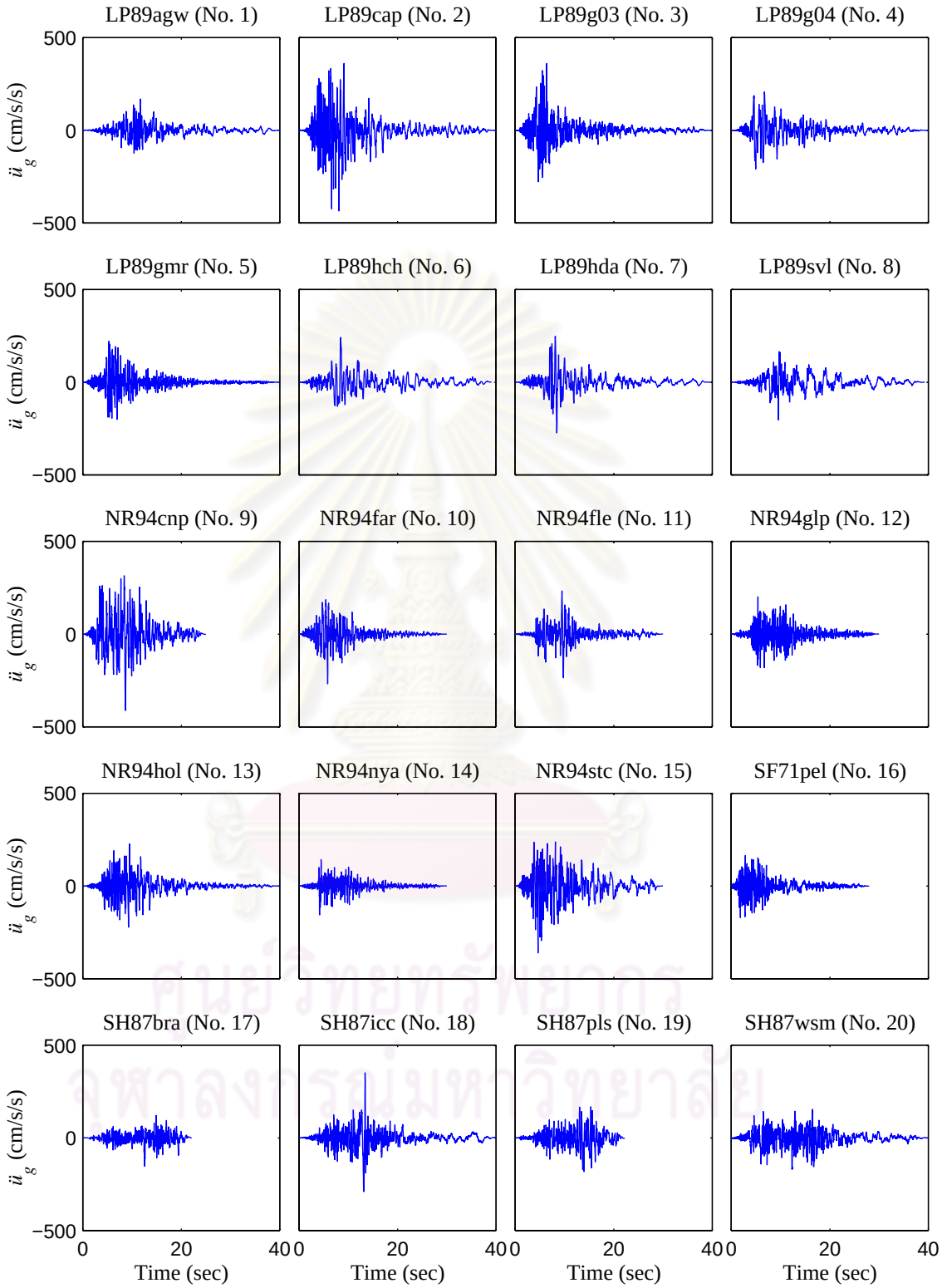

Figure 4.9 Ground accelerations of LMSR ensemble of 20 ground motions.

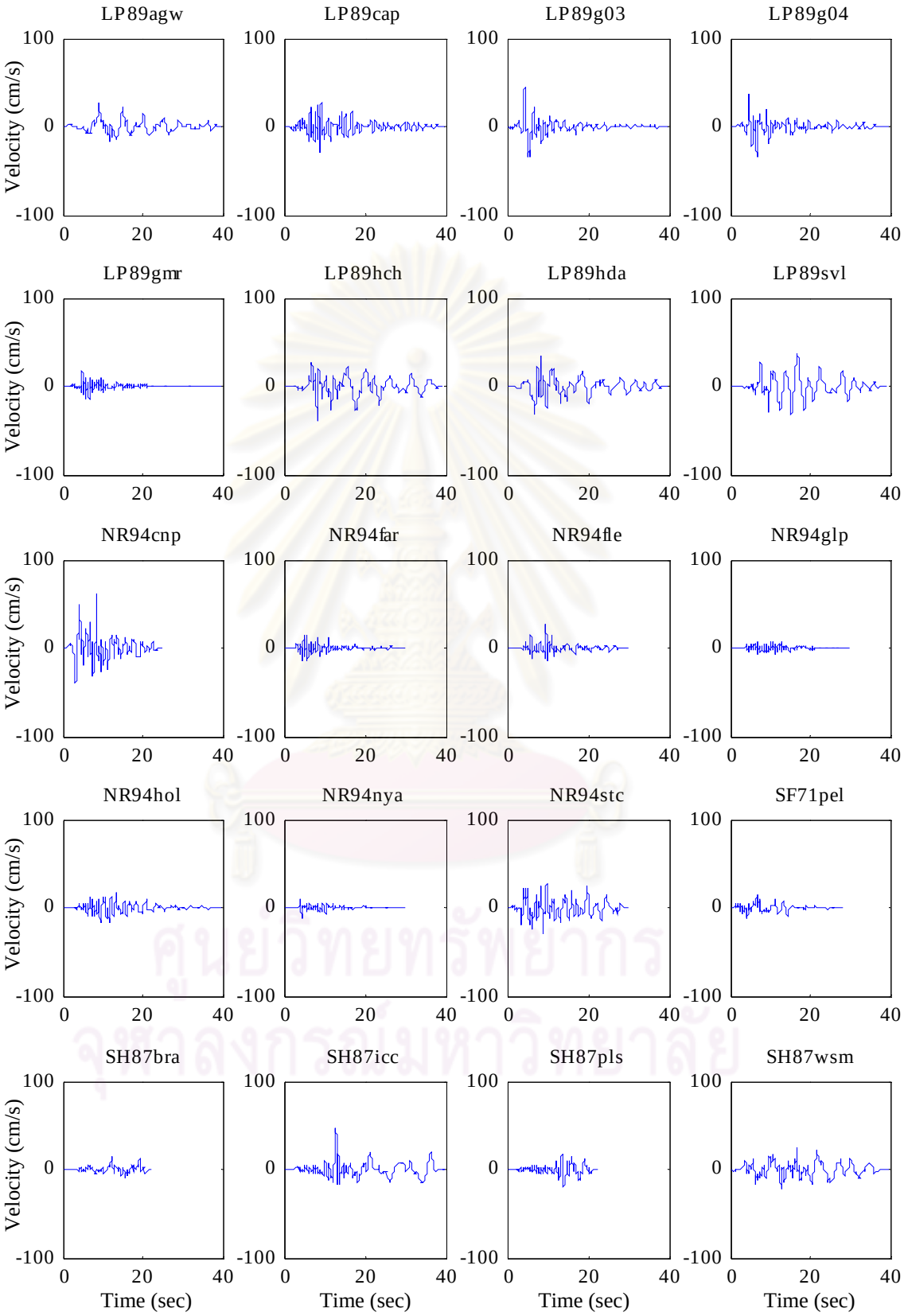

Figure 4.10 Ground velocities of LMSR ensemble of 20 ground motions.

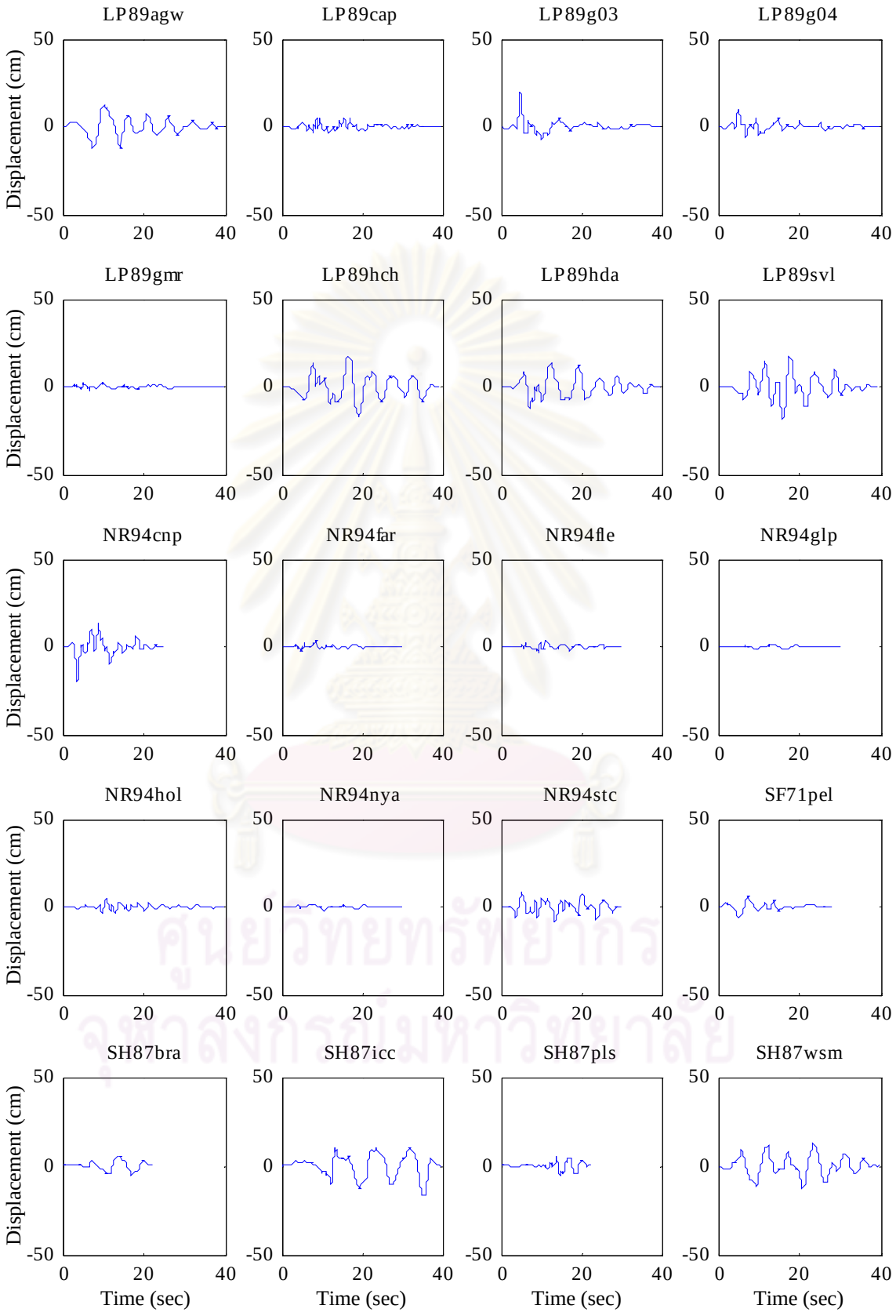

Figure 4.11 Ground displacements of LMSR ensemble of 20 ground motions.

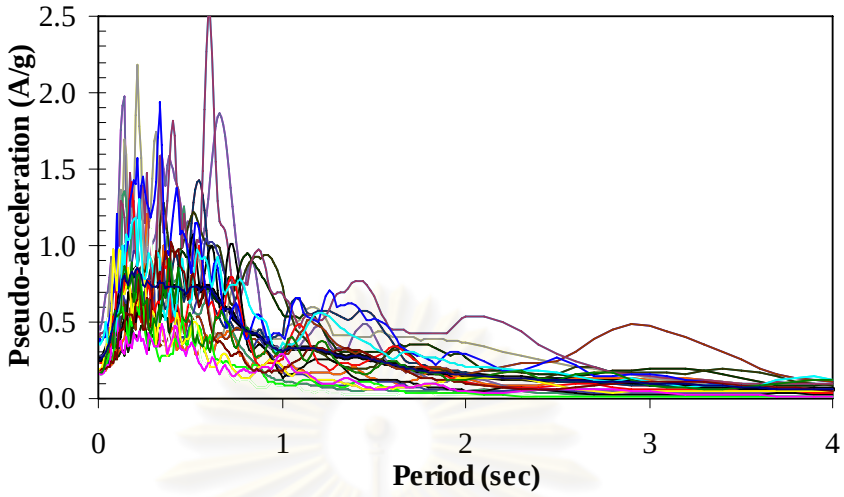

Figure 4.12 Pseudo-acceleration spectra of the set of LMSR, $\varsigma = 2\%$.

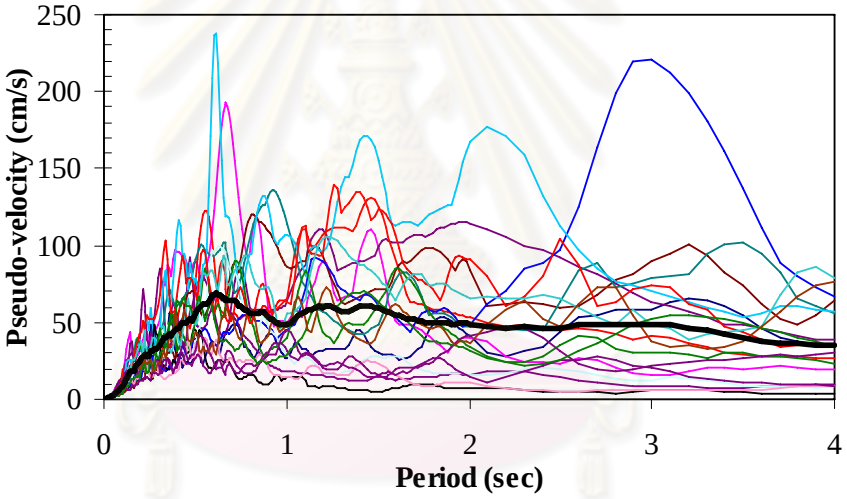

Figure 4.13 Pseudo-velocity spectra of the set of LMSR, $\varsigma = 2\%$.

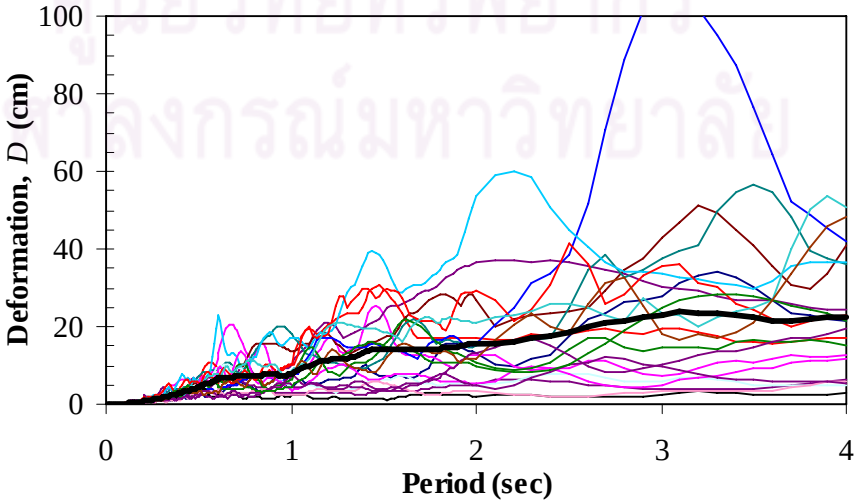

Figure 4.14 Deformation spectra of the set of LMSR, $\varsigma = 2\%$.

4.4 Response Statistics

The dynamic responses of the bridge studied to each of the 20 ground motions are determined by the two procedures described in the previous chapter: nonlinear response history analysis (NL-RHA) (Section 2.2.1), and the proposed extension of MPA procedure (Section 2.3).

The "exact" peak value of structural response, r, determined by NL-RHA is denoted by r_{NL-RHA}, and the approximate value from MPA by r_{MPA}. From these data for each ground motion, a response ratio is calculated from the following equation: $r^*_{MPA} = r_{MPA} / r_{NL-RHA}$. An approximate method is biased if the median of the response ratio differs from one, underestimates the median response if the ratio is less than one, and provides an overestimate if the ratio is larger than one.

The median and the dispersion of r^*_{MPA} were calculated by Equations (3.5) and (3.6) as described in Section 3.4.

CHAPTER V

SEISMIC RESPONSES OF BRIDGE USING THE PROPOSED EXTENSION OF MODAL PUSHOVER ANALYSIS PROCEDURE

5.1 Introduction

The modal pushover analysis (MPA) procedure proposed and developed earlier for estimating seismic demands for buildings (Chopra and Goel, 2002) is adapted for three-dimensional bridges (Section 2.3). The proposed extension of MPA procedure is implemented in estimating seismic demands of the studied bridge due to the set of twenty LMSR ground motions. The bridge selected in this study is an existing continuous steel twin I-girder bridge with PC slab that has structural characteristics of typical highway viaducts in Japan, described in Section 4.2. The bias and dispersion of this procedure are evaluated by comparing its estimates of seismic demands to the results from nonlinear response history analysis (NL-RHA) which are considered as the 'exact' results. The estimates by the conventional pushover analysis are also compared. The response quantities considered in this study are the peak deck displacements, pier (column) drifts, hinge rotations and internal forces which are related to structural damages and serviceability of bridges.

5.2 Bridge Vibration Characteristics

The usual first step in performing a dynamic analysis is determining the natural frequencies and mode shapes of the structure. These results characterize the basic dynamic behaviors of the structure. The number of natural frequencies and associated mode shapes is equal to the number of dynamic degrees-of-freedom of structure. However, among many natural frequencies and associated mode shapes, only some of the first few modes are interesting because of their significant influences in dynamic response of the structure. Presented in this section are vibration properties: periods, mode shapes, and effective modal masses of the selected bridge. These vibration properties are used to identify the modes that contribute significant to the total response.

The first six natural vibration periods and mode shapes of the selected bridge with two types of bearing supports: (a) Steel bearings (SB), and (b) Lead Rubber Bearing (LRB) supports are presented in Figures 5.1 and 5.2, respectively. Also included for each mode are the effective modal mass, as a fraction of the total mass, in the longitudinal, transverse and vertical directions (x-, y-, and z-directions). The bridge natural modes may be categorized by their primary motion: longitudinal, transverse, vertical or torsional, or coupled motion such as longitudinal-vertical or transverse-torsional. Category of a mode shape may be identified from deformed shape of the bridge and effective modal masses. For example, a longitudinal, transverse, and vertical mode shape displays deflection and nonzero value of the effective modal mass in the longitudinal (Figure 5.1a), transverse (Figure 5.1b) and vertical (Figure 5.1e) direction, respectively. A torsional mode displays rotation about the x-axis and nonzero value of the effective modal mass in the transverse direction. A coupled longitudinal-vertical mode displays motions and nonzero values of the effective modal mass in the longitudinal and vertical direction; and a coupled transverse-torsional mode displays transverse and rotational motions about the x-axis but nonzero value of the effective modal mass in the transverse direction. The fundamental modes of the studied bridge display little coupling between longitudinal and vertical motions, transverse and torsional motions (Figures 5.1a and b; Figures 5.2a and b). The coupling of modes are more significant for the higher modes in this study (Appendices B and C). It is noted that, in some cases, it is not easy to classify the mode shapes because of the coupling of modes.

Tables 5.1 and 5.2 show the values of the effective modal mass as proportion of total mass, and the natural periods of the first thirty modes of the bridge studied with two types of bearing supports: (a) Steel bearings (SB), and (b) Lead Rubber Bearing (LRB) supports; respectively. The types of vibration modes of the studied bridges are also listed in these tables. Modes with effective modal masses >0.01 are highlighted with bold font.

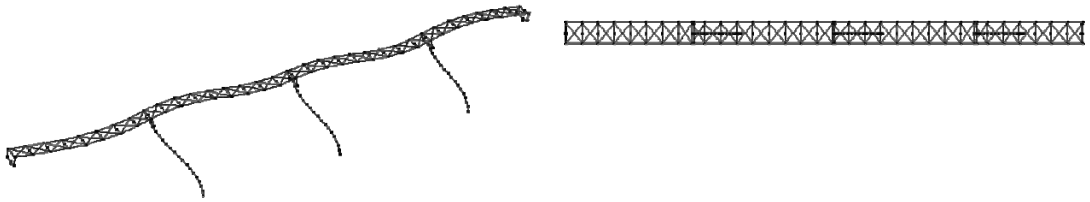

Three-dimensional view Plan view

Elevation view Side view

(a) Mode 1 – The first longitudinal mode (L1): T_1 = 1.750 s, $M_1^* = 0.913, 0.000, 0.000$

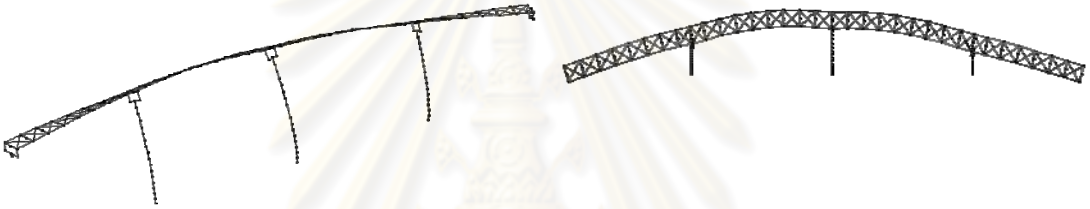

Three-dimensional view Plan view

Elevation view Side view

(b) Mode 2 – The first transverse mode (H1): T_2 = 1.656 s, $M_2^* = 0.000, 0.711, 0.000$

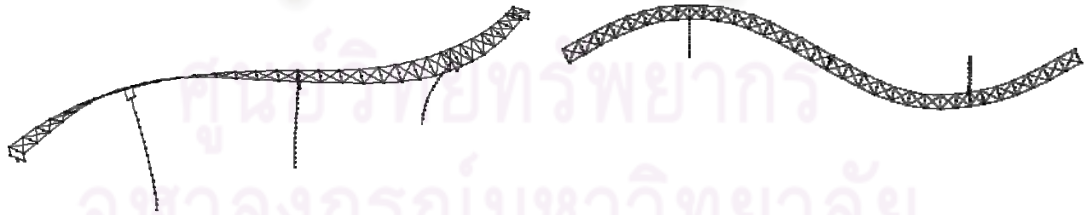

(a) Three-dimensional view (b) Plan view

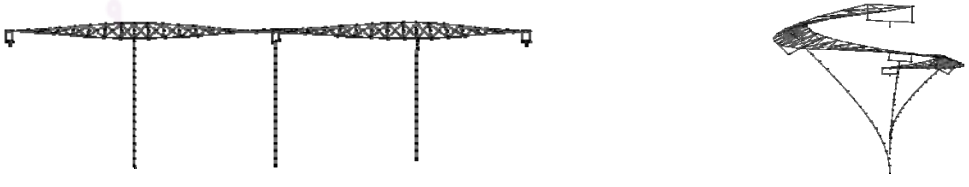

Elevation view Side view

(c) Mode 3 – The second transverse mode (H2): T_3 = 1.025 s, $M_1^* = 0.000, 0.0006, 0.000$

Figure 5.1 Mode shapes, vibration periods, and effective modal masses as a fraction of total mass of the studied bridge supported by steel bearings.

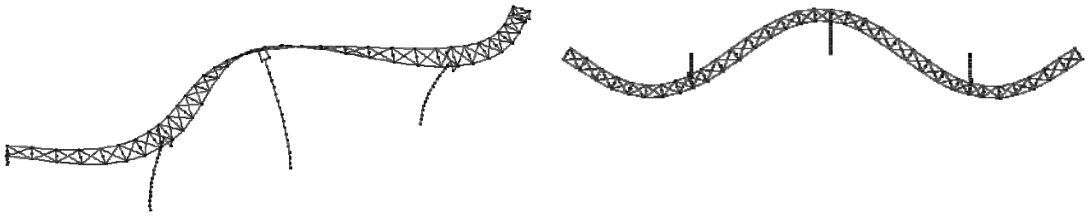

Three-dimensional view Plan view

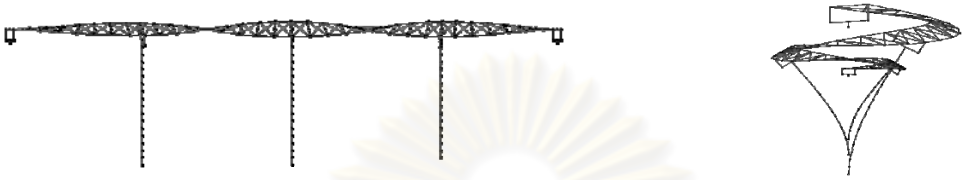

Elevation view Side view

(d) Mode 4 – The third transverse mode (H3): T_4 = 0.619 s, $M_4^* = 0.000, 0.0733, 0.000$

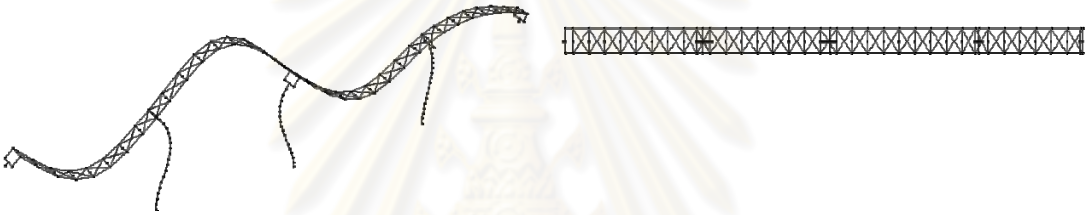

Three-dimensional view Plan view

Elevation view Side view

(e) Mode 5 – The first vertical mode (V1): T_5 = 0.526 s, $M_5^* = 0.0021, 0.0000, 0.0054$

Three-dimensional view Plan view

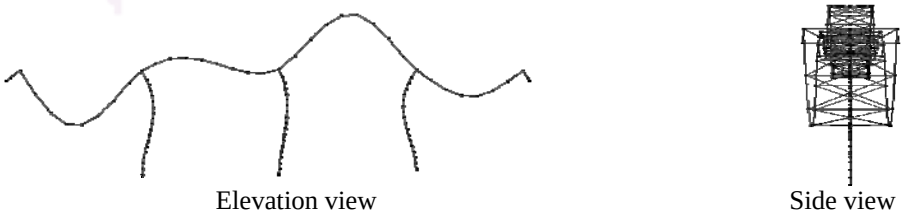

Elevation view Side view

(f) Mode 6 – The second vertical mode (V2): T_6 = 0.455 s, $M_6^* = 0.0003, 0.0000, 0.0014$

Figure 5.1 (Continued) Mode shapes, vibration periods, and effective modal masses as a fraction of total mass of the studied bridge supported by steel bearings.

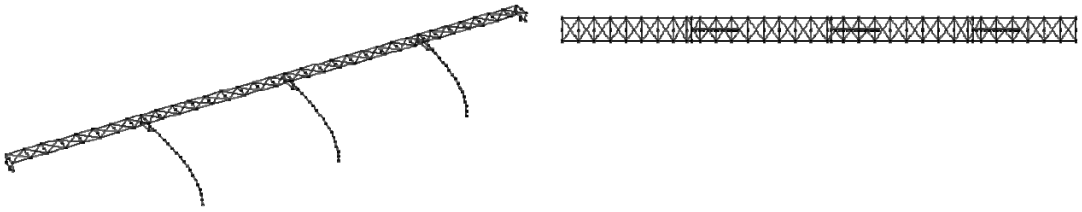

Three-dimensional view Plan view

Elevation view Side view

(a) Mode 1 – The first longitudinal mode (L1): T_1 = 3.019 s, $M_1^* = 0.8977, 0.000, 0.000$

Three-dimensional view Plan view

Elevation view Side view

(b) Mode 2 – The first transverse mode (H1): T_2 = 1.809 s, $M_2^* = 0.000, 0.6998, 0.000$

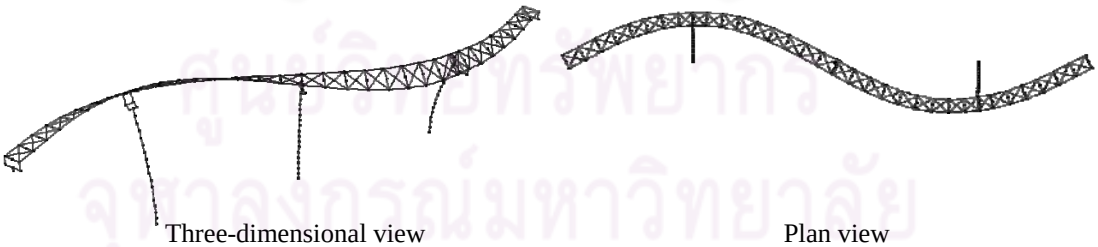

Three-dimensional view Plan view

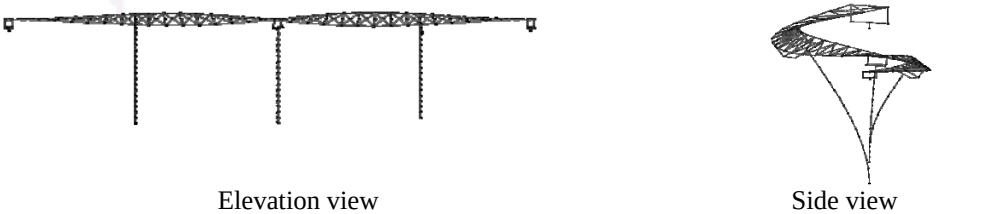

Elevation view Side view

(c) Mode 3 – The second transverse mode (H2): T_3 = 1.062 s, $M_3^* = 0.000, 0.0003, 0.000$

Figure 5.2 Mode shapes, vibration periods, and effective modal masses as a fraction of total mass of the studied bridge with LRB supports.

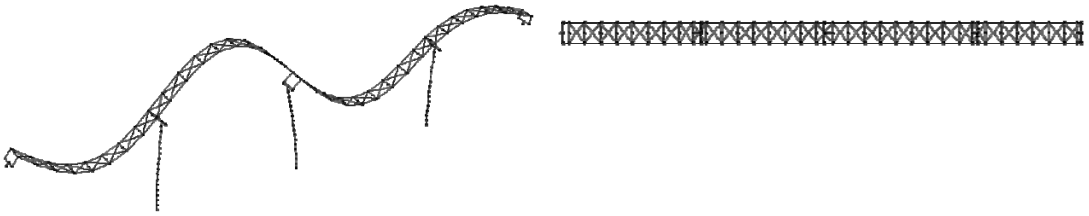

Three-dimensional view Plan view

Elevation view Side view

(d) Mode 4 – The first vertical mode (V1): T_4 = 0.661 s, $M_4^* = 0.000, 0.000, 0.0027$

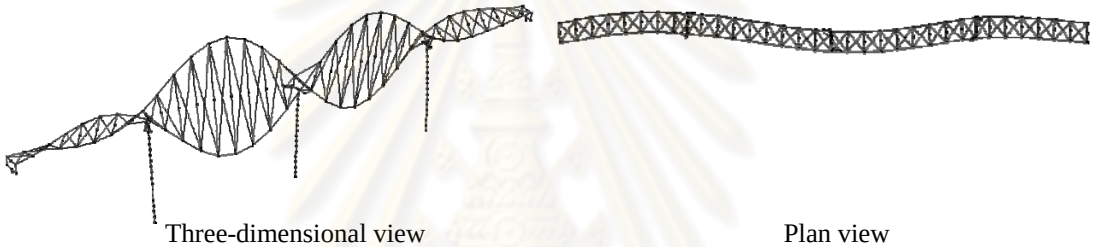

Three-dimensional view Plan view

Elevation view Side view

(e) Mode 5 – The first torsional mode (T1): T_5 = 0.640 s, $M_5^* = 0.000, 0.0022, 0.000$

Three-dimensional view Plan view

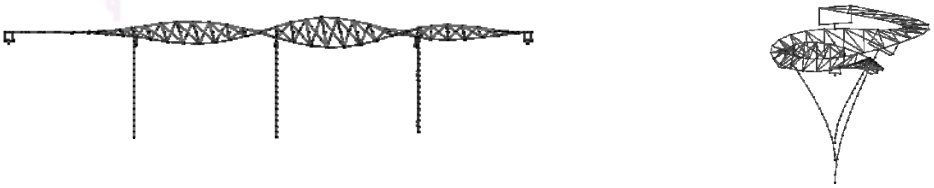

Elevation view Side view

(f) Mode 6 – The third transverse mode (H3): T_6 = 0.624 s, $M_6^* = 0.000, 0.0724, 0.000$

Figure 5.2 (Continued) Mode shapes, vibration periods, and effective modal masses as a fraction of total mass of the studied bridge with LRB supports.

Table 5.1 Dynamic characteristics of the bridge supported by steel bearings.

Mode No.	Period (sec)	Frequency (Hz)	Effective modal mass as proportion of total mass						Type*
			x-direction	y-direction	z-direction	Cumulative x-direction	Cumulative y-direction	Cumulative z-direction	
1	1.75020	0.57136	**0.9132**	0.0000	0.0000	0.9132	0.0000	0.0000	Longitudinal (L1)
2	1.65560	0.60401	0.0000	**0.7106**	0.0000	0.9132	0.7106	0.0000	Transverse (H1)
3	1.02460	0.97599	0.0000	0.0006	0.0000	0.9132	0.7113	0.0000	Transverse (H2)
4	0.61949	1.61423	0.0000	**0.0733**	0.0000	0.9132	0.7846	0.0000	Transverse (H3)
5	0.52634	1.89991	0.0021	0.0000	0.0054	0.9153	0.7846	0.0054	Vertical (V1)
6	0.45473	2.19911	0.0003	0.0000	0.0014	0.9157	0.7846	0.0068	Vertical (V2)
7	0.41634	2.40188	0.0000	0.0000	0.0000	0.9157	0.7846	0.0068	Transverse (H4)
8	0.38541	2.59464	0.0025	0.0000	**0.2311**	0.9181	0.7846	0.2379	Vertical (V3)
9	0.37378	2.67537	0.0000	0.0057	0.0000	0.9181	0.7903	0.2379	Torsional (T1)
10	0.36741	2.72175	0.0000	0.0000	0.0000	0.9181	0.7903	0.2379	Torsional (T2)
11	0.33022	3.02828	0.0020	0.0000	**0.3390**	0.9201	0.7903	0.5769	Vertical/Longitudinal (V4)
12	0.31893	3.13548	0.0000	**0.0296**	0.0000	0.9201	0.8198	0.5769	Transverse/Torsional (H5)
13	0.29526	3.38685	0.0000	0.0002	0.0000	0.9201	0.8200	0.5769	Torsional (T3)
14	0.26122	3.82819	0.0000	0.0010	0.0000	0.9201	0.8210	0.5769	Transverse/Torsional (H6)
15	0.23255	4.30015	0.0000	0.0014	0.0000	0.9201	0.8224	0.5769	Torsional/Transverse (T4)
16	0.22463	4.45177	0.0000	0.0000	0.0000	0.9201	0.8224	0.5769	Transverse/Torsional (H7)
17	0.20301	4.92587	0.0001	0.0000	0.0000	0.9202	0.8224	0.5769	Longitudinal (L2)
18	0.18556	5.38909	**0.0143**	0.0000	0.0005	0.9345	0.8224	0.5774	Longitudinal/Vertical (L3)
19	0.18355	5.44811	0.0000	0.0007	0.0000	0.9345	0.8231	0.5774	Transverse (H8)
20	0.16544	6.04449	0.0000	**0.0102**	0.0000	0.9345	0.8334	0.5774	Transverse/Torsional (H9)
21	0.16495	6.06244	0.0000	0.0000	0.0003	0.9345	0.8334	0.5777	Vertical/ Longitudinal (V5)
22	0.16204	6.17132	0.0000	0.0050	0.0000	0.9345	0.8384	0.5777	Torsional/Transverse (T5)
23	0.15275	6.54664	0.0000	0.0009	0.0000	0.9345	0.8393	0.5777	Torsional/Transverse (T6)
24	0.15059	6.64055	0.0011	0.0000	0.0013	0.9356	0.8393	0.5790	Longitudinal/Vertical (L4)
25	0.14909	6.70736	0.0000	0.0006	0.0000	0.9356	0.8399	0.5790	Torsional/Transverse (T7)
26	0.13841	7.22491	0.0000	**0.0142**	0.0000	0.9356	0.8541	0.5790	Transverse/Torsional (H10)
27	0.13837	7.22700	0.0006	0.0000	0.0024	0.9362	0.8541	0.5814	Vertical/Longitudinal (V6)
28	0.13442	7.43937	0.0000	**0.0204**	0.0000	0.9362	0.8745	0.5814	Transverse/Torsional (H11)
29	0.12896	7.75434	0.0001	0.0000	0.0022	0.9363	0.8745	0.5837	Vertical/ Longitudinal (V7)
30	0.12755	7.84006	**0.0219**	0.0000	0.0015	0.9582	0.8745	0.5851	Longitudinal/Vertical (L5)

*L: Longitudinal; H: Transverse; V: Vertical; and T: Torsional

Table 5.2 Dynamic characteristics of the bridge equipped with LRB supports.

Mode No.	Period (sec)	Frequency (Hz)	Effective modal mass as proportion of total mass						Type*
			x-direction	y-direction	z-direction	Cumulative x-direction	Cumulative y-direction	Cumulative z-direction	
1	3.01860	0.33128	**0.8977**	0.0000	0.0000	0.8977	0.0000	0.0000	Longitudinal (L1)
2	1.80900	0.55279	0.0000	**0.6998**	0.0000	0.8977	0.6998	0.0000	Transverse (H1)
3	1.06200	0.94162	0.0000	0.0003	0.0000	0.8977	0.7001	0.0000	Transverse (H2)
4	0.66053	1.51394	0.0000	0.0000	0.0027	0.8977	0.7001	0.0027	Vertical (V1)
5	0.64041	1.56150	0.0000	0.0022	0.0000	0.8977	0.7023	0.0027	Torsional (T1)
6	0.62386	1.60292	0.0000	**0.0724**	0.0000	0.8977	0.7747	0.0027	Transverse (H3)
7	0.51498	1.94182	0.0000	0.0000	0.0000	0.8977	0.7747	0.0027	Vertical (V2)
8	0.47364	2.11131	0.0000	0.0021	0.0000	0.8977	0.7768	0.0027	Torsional (T2)
9	0.42270	2.36574	0.0000	0.0000	0.0000	0.8977	0.7768	0.0027	Transverse (H4)
10	0.40802	2.45086	0.0001	0.0000	**0.1949**	0.8978	0.7768	0.1976	Vertical (V3)
11	0.34653	2.88575	0.0001	0.0000	**0.4086**	0.8979	0.7768	0.6062	Vertical (V4)
12	0.34109	2.93178	0.0000	0.0035	0.0000	0.8979	0.7802	0.6062	Torsional (T3)
13	0.32322	3.09387	0.0000	**0.0256**	0.0000	0.8979	0.8058	0.6062	Transverse (H5)
14	0.27737	3.60529	0.0000	0.0018	0.0000	0.8979	0.8077	0.6062	Torsional (T4)
15	0.26984	3.70590	0.0021	0.0000	0.0000	0.9000	0.8077	0.6062	Longitudinal (L2)
16	0.26827	3.72759	0.0000	0.0024	0.0000	0.9000	0.8101	0.6062	Transverse (H6)
17	0.26435	3.78286	**0.0105**	0.0000	0.0000	0.9105	0.8101	0.6062	Longitudinal (L3)
18	0.25088	3.98597	**0.0238**	0.0000	0.0003	0.9342	0.8101	0.6065	Longitudinal (L4)
19	0.24137	4.14302	0.0000	0.0084	0.0000	0.9342	0.8185	0.6065	Transverse (H7)
20	0.21585	4.63285	0.0000	0.0006	0.0000	0.9342	0.8191	0.6065	Transverse (H8)
21	0.20865	4.79272	0.0000	0.0009	0.0000	0.9342	0.8200	0.6065	Transverse (H9)
22	0.19507	5.12636	0.0000	0.0071	0.0000	0.9342	0.8271	0.6065	Torsional/ Transverse (T5)
23	0.19289	5.18430	0.0000	**0.0320**	0.0000	0.9342	0.8591	0.6065	Transverse/Torsional (H10)
24	0.18934	5.28150	0.0000	0.0000	0.0000	0.9342	0.8591	0.6065	Longitudinal/Vertical (L5)
25	0.18367	5.44455	0.0007	0.0000	0.0003	0.9350	0.8591	0.6067	Vertical (V5)
26	0.18260	5.47645	0.0000	0.0000	0.0000	0.9350	0.8591	0.6067	Torsional (T6)
27	0.17779	5.62461	0.0000	0.0066	0.0000	0.9350	0.8658	0.6067	Transverse (H11)
28	0.17048	5.86579	0.0000	0.0000	0.0000	0.9350	0.8658	0.6067	Vertical (V6)
29	0.15852	6.30835	0.0000	0.0021	0.0000	0.9350	0.8678	0.6067	Transverse (H12)
30	0.15081	6.63086	0.0000	0.0000	**0.0100**	0.9350	0.8678	0.6167	Vertical (V7)

*L: Longitudinal; H: Transverse; V: Vertical; and T: Torsional

The results presented in Figures 5.1 and 5.2, and Tables 5.1 and 5.2 lead to several observations on the type and number of modes that need to be considered for the modal pushover analysis.

First, it is noticeable that the type of bearing supports have a significant effect on the natural frequencies of the studied bridge especially with the first longitudinal mode. The fundamental natural period of the bridge equipped with isolation bearings is 1.73 times longer than that of the bridge with steel bearings. This value is close to the recommendations of Specifications for Highway Bridges in Japan (JRA, 1996). This first mode corresponds to the mode shape that displaces in the longitudinal direction of the bridge, and the period is significantly influenced by the size of the lead plug inserted in the isolation bearings. For example, short natural period is a result of excessively large lead core and the bridge response can not benefit from isolation effect due to elongation of the fundamental natural period, and therefore, the spectral acceleration is not much reduced during a seismic attack, as described in Section 4.2.2.2.1.

Secondly, as displayed in the Figures 5.1 and 5.2, the mode shapes of the bridge studied are affected by the types of bearings. The order of vibration modes are also affected. However, the first and second modes are always the first longitudinal vibration (L1) and the first transverse one (H1). The second transverse vibration (H2) is the third mode. On the other hand, the order and the properties of torsional and higher modes of the two bridges are different. It is noted that the effective modal mass of the vibration modes are also affected by the type of bearing supports.

Many more modes will be required to accurately estimate the seismic demands in bridges, especially in the transverse direction, compared to the case of buildings. According to the building code, the number of ‘modes’ to be included in response spectrum analysis shall capture at least 90% of the total mass of structure which was adopted in MPA procedure. For the studied bridge, as shown in Tables 5.1 and 5.2, the cumulations of the effective modal mass of the first thirty modes in transverse direction of the bridge equipped with steel bearings and LRB supports are 87.5% and 86.8% of the total mass, respectively. It would need consideration of 50 modes to capture 90% of the total mass in transverse direction of the bridge equipped with steel

bearings and LRB supports considered in this study. The effective modal masses of higher modes are much lower than those of the fundamental modes in both the longitudinal and transverse directions. The effective modal mass of many higher 'modes' are very small (say less than 0.1%) and the contributions in MPA estimate of these modes are not significant as shown in Figure 5.3. Therefore, the contributions of those modes should be neglected in MPA estimate to avoid a large computation.

Finally, the number and types of modes to be included in MPA procedure depend on the response quantity being evaluated. For example, the first longitudinal mode (L1) may be sufficient to estimate the peak displacements and pier drifts of the bridge supported by steel bearings in longitudinal direction, whereas seven 'modes' – second (H1), fourth (H3), ninth (T1), 12th (H5), 20th (H9), 26th (H10), and 28th (H11) – are required to estimate the peak displacements, pier drifts and internal forces of the bridge in the transverse direction.

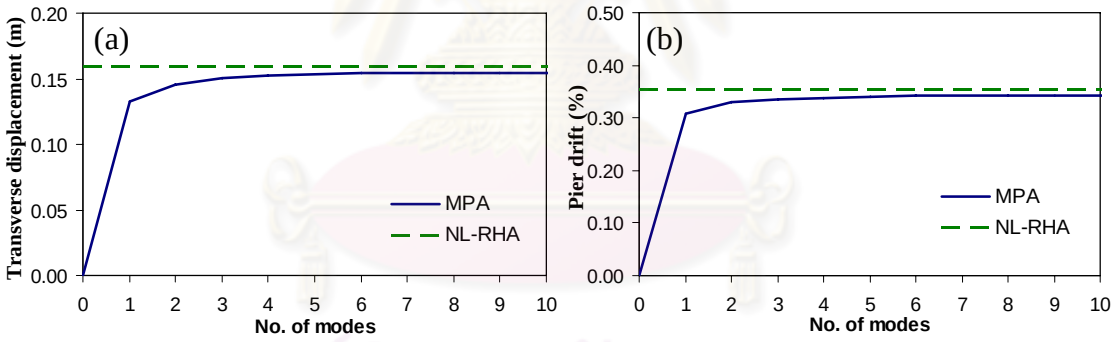

Figure 5.3 (a) The peak transverse displacement at middle of the first span, and (b) the transverse pier drift of pier 1 (P1) of the bridge equipped with LRB supports due to LP89g03 (No. 3) ground motion.

5.3 Pushover Curves

Pushover curves, which show the relationships between base shear force and monitoring displacement, based on spatial modal force distributions were performed in the longitudinal and transverse directions of the bridge. It is noted that unlike the case of buildings where the pushover curve is generally defined in terms of base shear and roof displacement in the direction under consideration, in case of bridges the shape of the pushover curve depends on the location of the monitoring point (Paraskeva *et al.*, 2006). The selection of the monitoring point affects the shape of the pushover curve especially in the inelastic range. For bridges, intuitive selections for the displacement monitoring point are the centre of deck mass as recommended by CEN (2004). It can also be selected as the point of the deck which is determined by using Equation (1.13) recommended by Paraskeva *et al.* (2006). However, the applicability of this approach in structural engineering practice seems to be unsuitable for complicated structures. The selection of the displacement monitoring point for multi-mode pushover analysis of bridge as mentioned above is not able to take into account the contributions of torsional and vertical vibrations of the bridge because the modal force distributions will not cause any displacements at that monitoring point.

As mentioned in Section 2.3, the pushover curve for the *n*th 'mode' used in this study is defined in terms of base shear force and displacement of monitoring point. The displacement monitoring point of the bridge for the *n*th 'mode' is proposed to be at the degree of freedom where mode shape value is maximum in the direction of applied ground motion. This proposal is advantageous because the mode shapes were already computed in Step 1 of MPA procedure and the pushover analysis can be performed for every modes (e.g., to take into account the contributions of torsional and vertical vibrations of bridges). For the bridge considered in this study, the longitudinal and vertical motions are usually coupled while the transverse and torsional vibrations are coupled as shown in Figures 5.1 and 5.2.

Figure 5.4 shows the pushover curves calculated by applying the spatial modal force distributions of the first modes in the longitudinal (L1) and transverse (H1) directions of the studied bridges equipped with steel bearings (SB) and LRB supports. The peak displacements of the deck determined by NL-RHA due to 20 LMSR ground

motions in both longitudinal and transverse directions are also shown in Figure 5.4. The pushover curves are presented in the form of normalized force (V_b/W) versus reference drift (u_{mn}/H_{mn}), where V_b, W and u_{mn} are base shear force, total weight and displacement of monitoring point in the direction under consideration, respectively; and H_{mn} is height from the base of the pier 2 (P2) to the monitoring point. It is observed that the bridge was driven far into the inelastic range in most of cases.

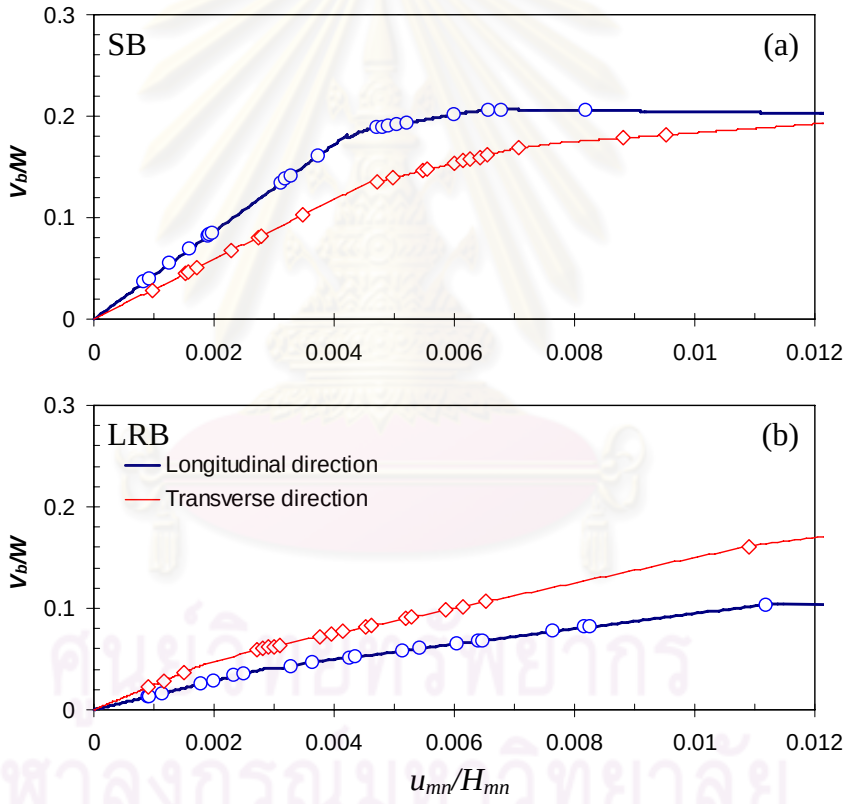

Figure 5.4 First 'mode' pushover curves of the studied bridge with (a) steel bearings; and (b) LRB supports in the longitudinal and transverse directions. The peak displacements of the deck determined by NL-RHA due to 20 LMSR ground motions in both directions are also shown.

Pushover curves presented show that the bearing supports affect the pushover analysis and the inelastic response of the bridge. The pushover curves of the bridge supported by steel bearings are much stiffer than those of the bridge with LRB supports. This trend is clearly noticed in the longitudinal direction as the bridge response is dominated by the first mode where the superstructure slides over the bearing supports.

The pushover curves of the most dominant modes used in this study were performed and shown in Figures 5.5 and 5.6. These curves were derived by applying the spatial modal force distributions with respect to the displacement of monitoring point for each 'mode' (e.g., longitudinal, transverse, tosional and vertical modes). These pushover curves are then idealized as bilinear curves using the procedure described earlier in Step 4, Section 2.3. As discussed in more detail by Paraskeva *et al.* (2006), these curves are not necessarily representative of the actual response of all structural members of the bridge. For example, the pushover curve corresponding the fifth longitudinal mode (L5) or the tenth transverse mode (H10) of the bridge supported by steel bearings is purely linear, for this reason the bridge does not enter the inelastic range when subjected to these modal force distributions, even for very strong ground accelerations.

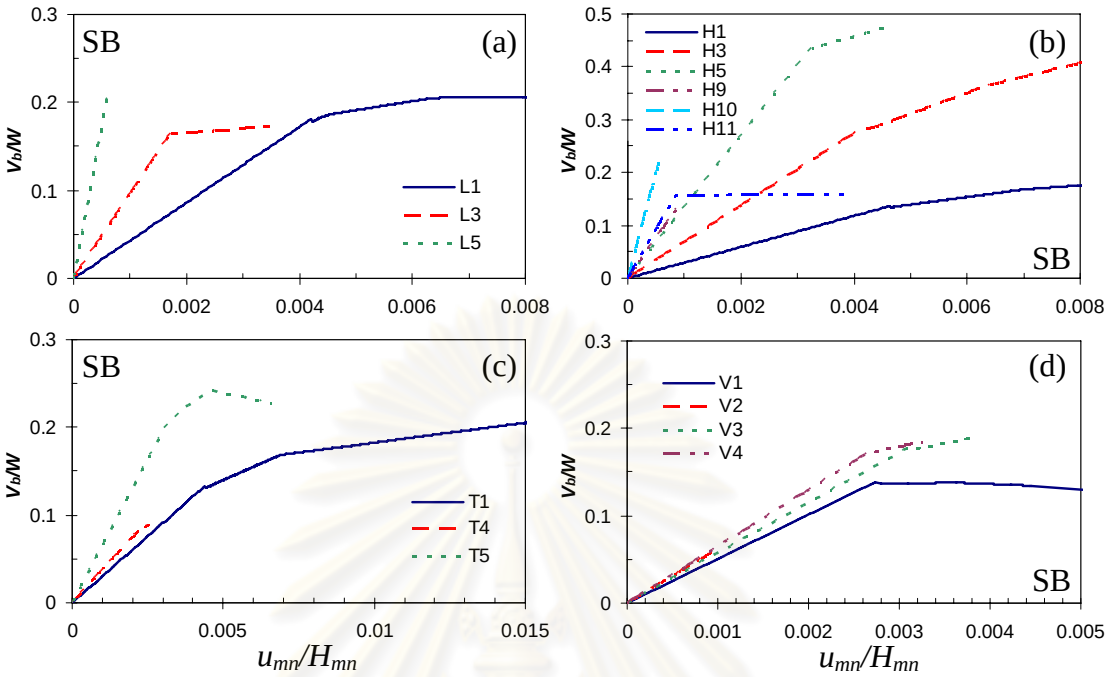

Figure 5.5 Pushover curves of the bridge supported by steel bearings derived by applying modal force distributions: (a) longitudinal, (b) transverse, (c) torsional, and (d) vertical modes.

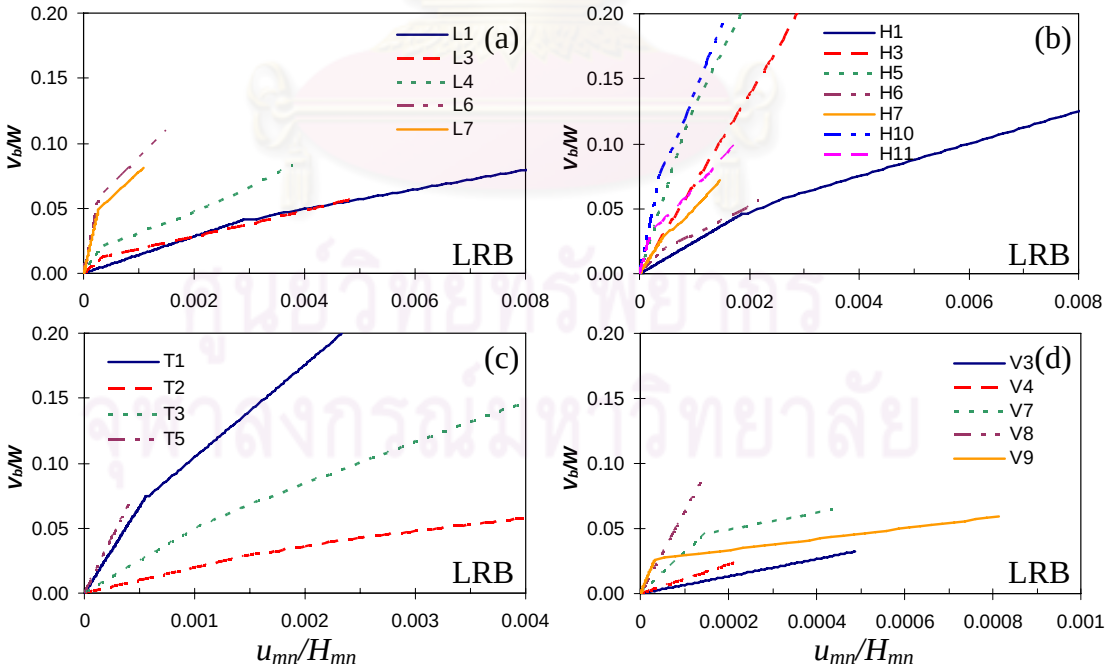

Figure 5.6 Pushover curves of the bridge equipped with LRB supports derived by applying modal force distributions: (a) longitudinal, (b) transverse, (c) torsional, and (d) vertical modes.

5.4 Accuracy of the Proposed Extension of MPA Procedure

The proposed extension of MPA procedure was implemented in estimating seismic demands of the selected bridge due to the set of LMSR ground motions. The bias and accuracy of this procedure are evaluated by a comparison of the response quantities with results from Nonlinear Response History Analysis (NL-RHA), which can be considered as 'exact' results, as well as the conventional pushover analysis (CPA). The response quantities considered in this study are the peak deck displacements, pier (column) drifts, hinge rotations and internal forces. The pier drift, which indicates deformation demand in the column, is defined as the displacement at top of the pier relative to its base displacement divides by its height.

The responses of the studied bridge to the selected ground motions were determined by proposed extension of MPA procedure and also by NL-RHA. For comparison purposes, the conventional pushover analyses (fundamental mode based pushover analysis) were also performed in the longitudinal and transverse directions of the studied bridge, to serve as the reference (i.e., the least involved procedure). The longest-period modes in the longitudinal direction (L1) of the bridges equipped with steel bearings and LRB supports have a period of 1.75 s and 3.02 s; and the participating mass ratios for the longitudinal direction are 91.32% and 89.77% respectively. The participating mass ratios for the transverse direction are zero for both bridges. Similarly, the longest-period modes in the transverse direction (H1) of the bridges equipped with steel bearings and LRB supports have a period of 1.66 s and 1.81 s; and the participating mass ratios for the transverse direction are 71.06% and 69.98%, respectively. The participating mass ratios for the longitudinal direction are zero for both bridges.

As recommended for response spectrum analysis by building code, MPA usually considers as many modes as to include participating mass at least 90% of the total mass (usually the first two or three modes for buildings shorter than 10 stories). However, the number of modes required to capture 90% of the total mass is far too many for the case of bridges, especially in bridges analyzed by very detailed three-dimensional finite element models. As mentioned before, it will need consideration of 50 modes to capture 90% of the total mass in transverse direction of the bridge

considered in this study. It is also found in this study that the contribution of modes whose effective modal mass is very low (say less than 0.1%) is not significant. Therefore, to avoid a large computation, the contribution of five longitudinal 'modes' (L1, L3, L4, L6, and L7) and five vertical 'modes' (V3, V4, V7, V8, and V9) were considered to estimate the seismic demands related to the longitudinal direction of the bridge; whereas six transverse 'modes' and four torsional 'modes' (H1, H3, H5, H7, H10, H11, T1, T2, T3, and T5) were included to estimate the seismic demands related to the transverse direction of the bridge equipped with LRB supports. In the same way, the contributions of six 'modes' in the longitudinal direction (L1, L3, L5, V1, V3, and V4) and nine 'modes' in transverse direction (H1, H3, H5, H9, H10, H11, T1, T4, and T5) whose effective modal mass is larger than 0.1% were considered to estimate the seismic demands of the bridge supported by steel bearings (SB).

For the bridge supported by steel bearings, the 95.6% and 87.04% of the total mass have been included in MPA estimates in the longitudinal and transverse directions, respectively. Similarly, the 95.87% and 85.97% of the total mass have been included in the longitudinal and transverse directions in case of the bridge with LRB bearing supports, respectively.

The total values for desired response quantities calculated by MPA estimates are then determined by combining the peak modal responses using both Square-Root-of-Sum-of-Squares (SRSS) and Complete Quadratic Combination (CQC) rules (these results are denoted as MPA-SRSS, and MPA-CQC). This simple procedure was used for the peak displacements, pier drifts, hinge rotations and internal forces in the present study, which are the main quantities used for assessing the bridges.

5.4.1 Peak Displacements

The median peak displacement responses of the bridges equipped with steel bearings (SB) and LRB supports subjected to LMSR ground motions from two analysis procedures are compared in Figures 5.7 and 5.8, respectively; the results from pushover analysis including only fundamental mode (the conventional pushover analysis) are also shown. Note that for the selected bridge, ground motions applied in the x-direction cause response only in the longitudinal direction of the bridge and

ground motions applied in the y-direction lead to response only in the transverse direction of the bridge. So the responses presented are due to excitation in its corresponding direction. The results show that the contributions of higher modes in estimating the peak displacements in the transverse direction and rotations of the deck are significant, since higher 'modes' participate more actively, particularly towards both ends of the bridges (Figures 5.7b-d, and 5.8b-d). The peak transverse displacements and rotations of the deck predicted by the proposed extension of MPA are closer to the NL- RHA results than the results from fundamental mode pushover analysis. On the contrary, including response contribution of higher modes in estimating the peak longitudinal and vertical displacements is indifferent (Figures 5.7a-c and 5.8a-c). This can easily be understood that the longitudinal vibrations of the bridges equipped with steel bearings (SB) and LRB supports are dominated by the longitudinal fundamental mode whose effective modal masses of the first longitudinal mode alone are 91.32% and 89.77%, respectively; and the bridges behave very much like a SDF system. Consequently, the conventional pushover analysis procedure (one 'mode' pushover analysis) is adequate to predict the peak displacements of the bridges studied in the longitudinal and vertical directions.

Figures 5.9 and 5.10 show the median errors in estimating the peak displacements of the bridges equipped with steel bearings (SB) and LRB supports, respectively. It can be seen that the proposed extension of MPA procedure can accurately estimate the peak displacements of the deck of the studied bridges. In case of the bridge supported by steel bearings, the bias of the proposed extension of MPA procedure is less than 10% in estimating the peak longitudinal, vertical and transverse displacements and generally less than 25% in estimating torsional rotation of the deck. On the contrary, the bias of one 'mode' pushover analysis in estimating transverse displacements or rotation of the deck can be large, especially near both ends of the bridge. The bias of the one 'mode' pushover analysis is less than 25% in estimating the peak displacements in the transverse direction of the bridge and generally less than 30% in predicting the rotation of the deck.

Similarly for the bridge with LRB supports, the bias of the proposed extension of MPA procedure is generally less than 10% in estimating the peak longitudinal,

vertical and transverse displacements and 30% in estimating rotation of the deck, whereas the bias of the one ‘mode’ pushover analysis is 20% in estimating the peak displacements in the transverse direction of the bridge and 30% in predicting the rotation of the deck. However, the bias of the proposed extension of MPA procedure and the one ‘mode’ pushover analysis in estimating the torsional rotation of the deck near both ends of the bridge are large in percentage due to small rotation values.

The MPA estimates combined by CQC are slightly more accurate than by SRSS rule. This is because the modes are coupled. Nevertheless, the couplings of modes are not significant for the first few modes in this case. Both versions of the proposed extension of MPA procedure using SRSS and CQC combination rules (MPA-SRSS, MPA-CQC) can estimate the peak displacement reasonably well with a tendency to slightly underestimate peak displacements compared to NL-RHA.

5.4.2 Pier Drifts

The median pier displacements and median pier drifts of the bridges equipped with steel bearings (SB) and LRB supports determined by the proposed extension of MPA procedure and NL-RHA subjected to the set of twenty LMSR ground motions are compared in Figures 5.11, 5.12, 5.13 and 5.14; also included are the results from pushover analysis including contribution of only the fundamental ‘mode’. The pier drift, which indicates deformation demand in the column, is defined as the displacement at top of the pier relative to its base displacement divided by the pier height.

Similar to investigation of the peak displacements of the bridges considered in this investigation, the presented results show that the pier displacements and pier drifts of the bridges in the transverse direction predicted by both versions of the proposed extension of MPA procedure (i.e., MPA-SRSS, and MPA-CQC) are very close to those from the ‘exact’ NL-RHA procedure, whereas the one ‘mode’ pushover analysis underestimates these values. Nevertheless, the proposed extension of MPA procedure and the conventional pushover analysis predicts well the peak pier displacements and pier drifts in the longitudinal direction of the bridges. The accuracy of this procedure in estimating the pier displacements and pier drifts in the

longitudinal direction of the bridges is not worse than that of the proposed extension of MPA procedure. This implies that the contributions of higher ‘modes’ in estimating these responses are not significant and can be neglected in these cases.

In this section, the errors due to both approximate methods, the conventional pushover analysis (CPA) and the proposed extension of MPA procedure, are investigated by comparing the peak values of the responses determined by approximate procedures and by the NL-RHA, the ‘exact’ approach. Figures 5.15 and 5.16 show the median errors of the pier drifts in the longitudinal and transverse directions of the bridges equipped with steel bearings and LRB supports, respectively. The results presented indicate that all three procedures (the CPA, MPA-SRSS, and MPA-CQC) provide estimates that are essentially identical, and are very close to those from the NL-RHA in estimating the pier drifts of the bridges in the longitudinal direction, which are within about 5% of the exact results for both types of bearings. The bias of the proposed extension of MPA procedure in estimating the pier drifts of the bridges in the transverse direction is generally less than 5%, whereas the bias of the one ‘mode’ pushover analysis can be 17% in predicting the pier drifts of the bridges in the transverse direction.

To demonstrate how bias and dispersion measures relate to the accuracy of the proposed extension of MPA procedure, the pier drift ratios in the longitudinal and transverse directions of the bridges, Δ^{*}_{MPA}, due to the set of 20 LMSR ground motions are shown in Figures 5.17, 5.18, 5.19 and 5.20. The median value and dispersion of the pier drift ratios are also shown in these figures. The pier drift ratio is defined by the following equation: $\Delta^{*}_{MPA} = \Delta_{MPA} / \Delta_{NL-RHA}$, in which Δ_{NL-RHA} is the peak pier drift determined by NL-RHA, and the approximate value from the proposed extension of MPA is Δ_{MPA}. The pier drift value determined by the conventional pushover analysis (CPA) is denoted as Δ_{CPA}. These approximate methods are invariably biased in the sense that the median of the response ratio differs from one, underestimates the median response if the ratio is less than one, and provides an overestimate if the ratio exceeds one. The results presented permit the following observations:

- The proposed extension of MPA procedure accurately estimates the pier drifts of the bridges considered in this investigation in both the longitudinal and transverse directions with the bias is less than 5%.
- The contributions of higher ‘modes’ in estimating the pier drifts in the transverse direction are significant, especially for piers near by the both ends of the bridge. Both versions of proposed extension of MPA procedure are able to capture the NL-RHA results. However, the MPA pier drift results including the contributions of higher ‘modes’ in estimating these responses in the longitudinal direction are close to one ‘mode’ results indicating that the contributions of higher ‘modes’ are not significant and negligible in these cases.
- The dispersions of the pier drift ratios determined by the proposed extension of MPA procedure are smaller than 5% and 10% in the longitudinal and transverse directions, respectively. Dispersion tends to increase for seismic responses in the transverse direction as the contribution from the higher-modes becomes more significant.
- The one ‘mode’ pushover analysis procedure estimates pier drift demands of the studied bridges with less than 5% bias in the longitudinal direction; however, it underestimates pier drift demands of the bridges equipped with steel bearings and LRB supports by 15% and 20% in the transverse direction for certain locations, respectively.
- The dispersions of the pier drift ratio for bridges determined by the one ‘mode’ pushover analysis procedure range from 5% for demand in the longitudinal direction to 20% for demand in the transverse direction.
- These trends in variation of bias and dispersion in the conventional pushover analysis are similar to earlier observations from the proposed extension of MPA results.
- The accuracy of the proposed extension of MPA procedure in predicting pier drift response in the transverse direction can be as large as 30% due to an individual ground motion.

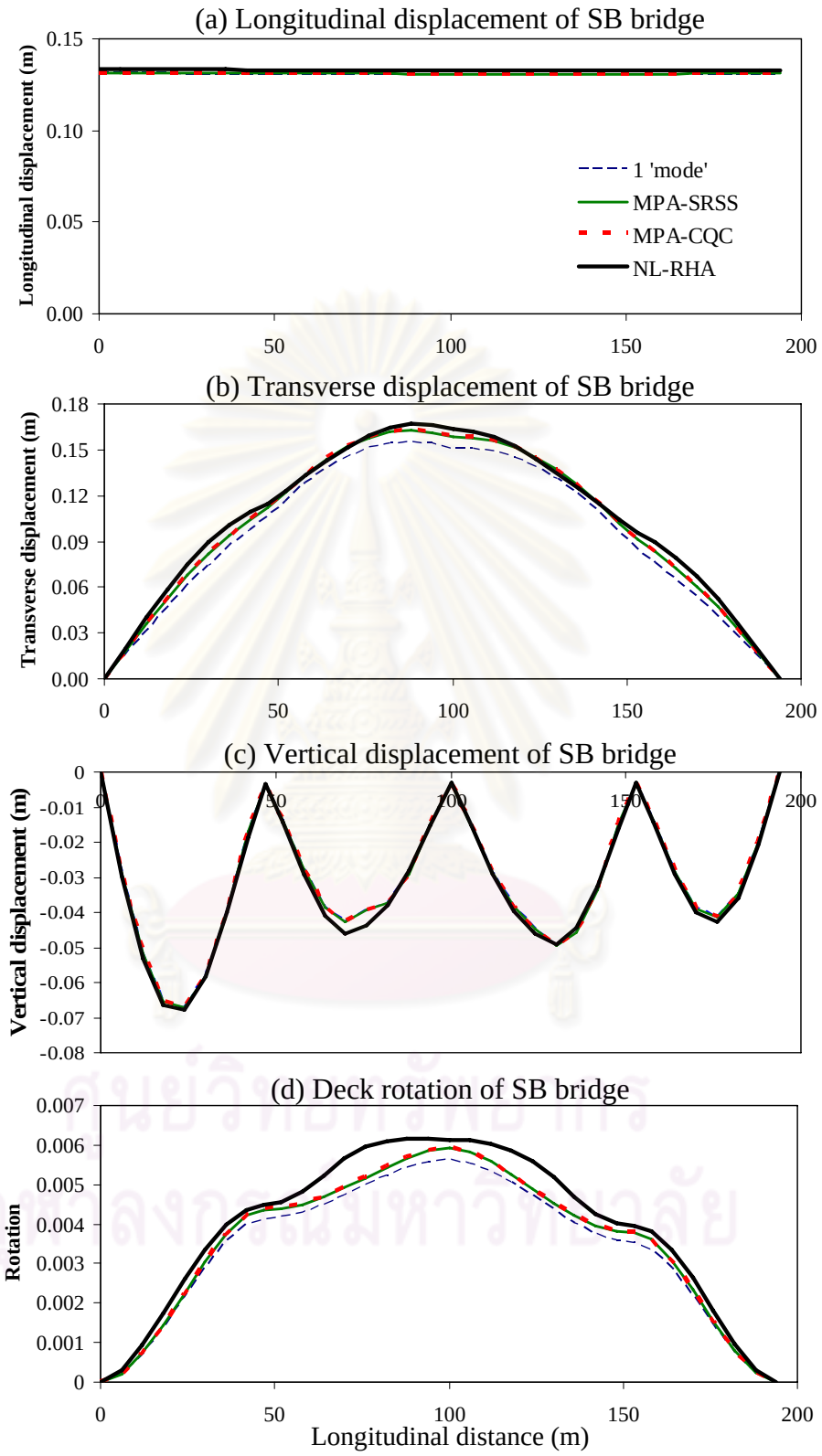

Figure 5.7 Median peak displacements of the bridge supported by steel bearings determined by one ‘mode’ pushover analysis, MPA and NL-RHA due to LMSR ground motions.

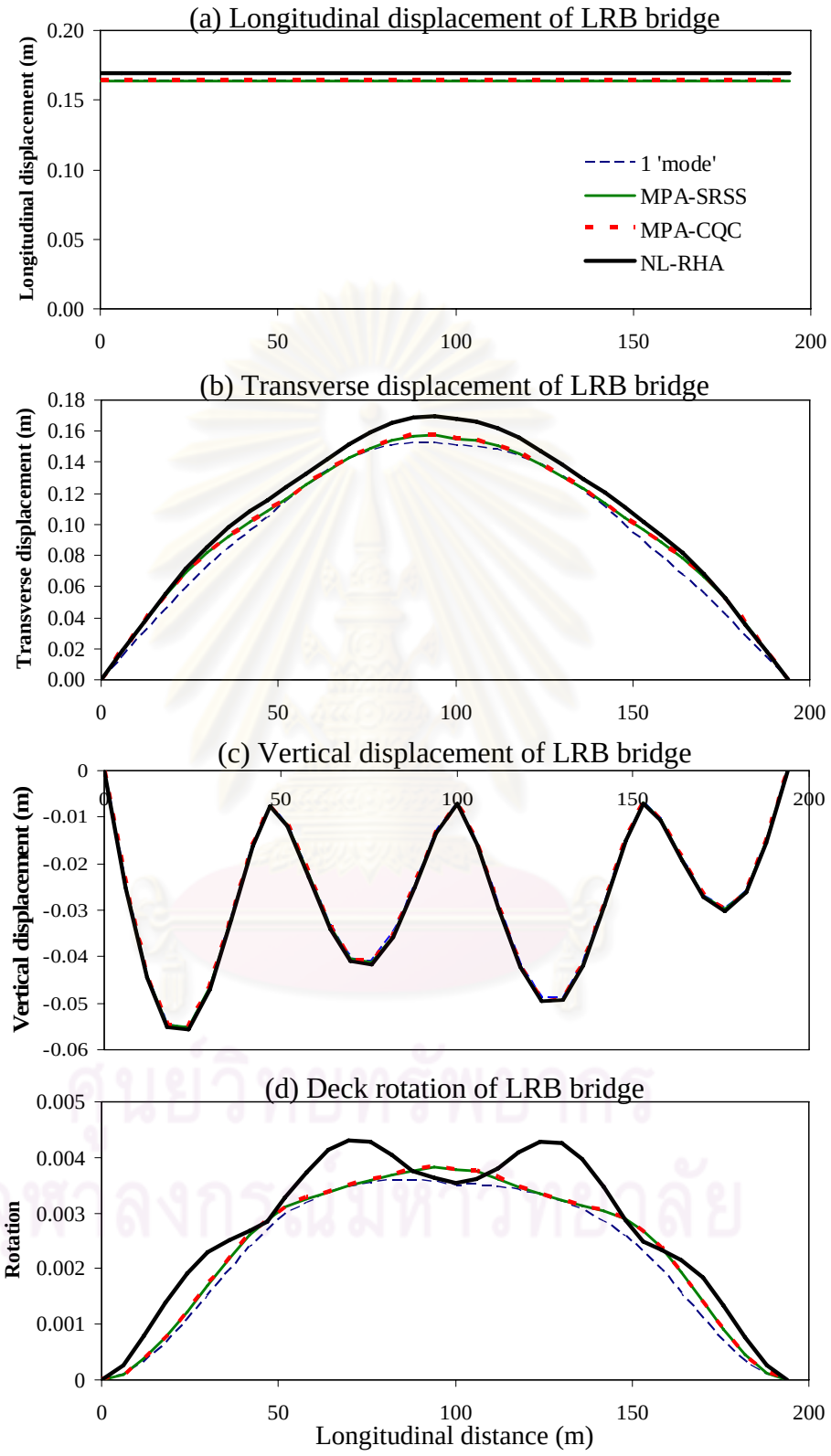

Figure 5.8 Median peak displacements of the bridge equipped with LRB supports determined by one ‘mode’ pushover analysis, MPA and NL-RHA due to LMSR ground motions.

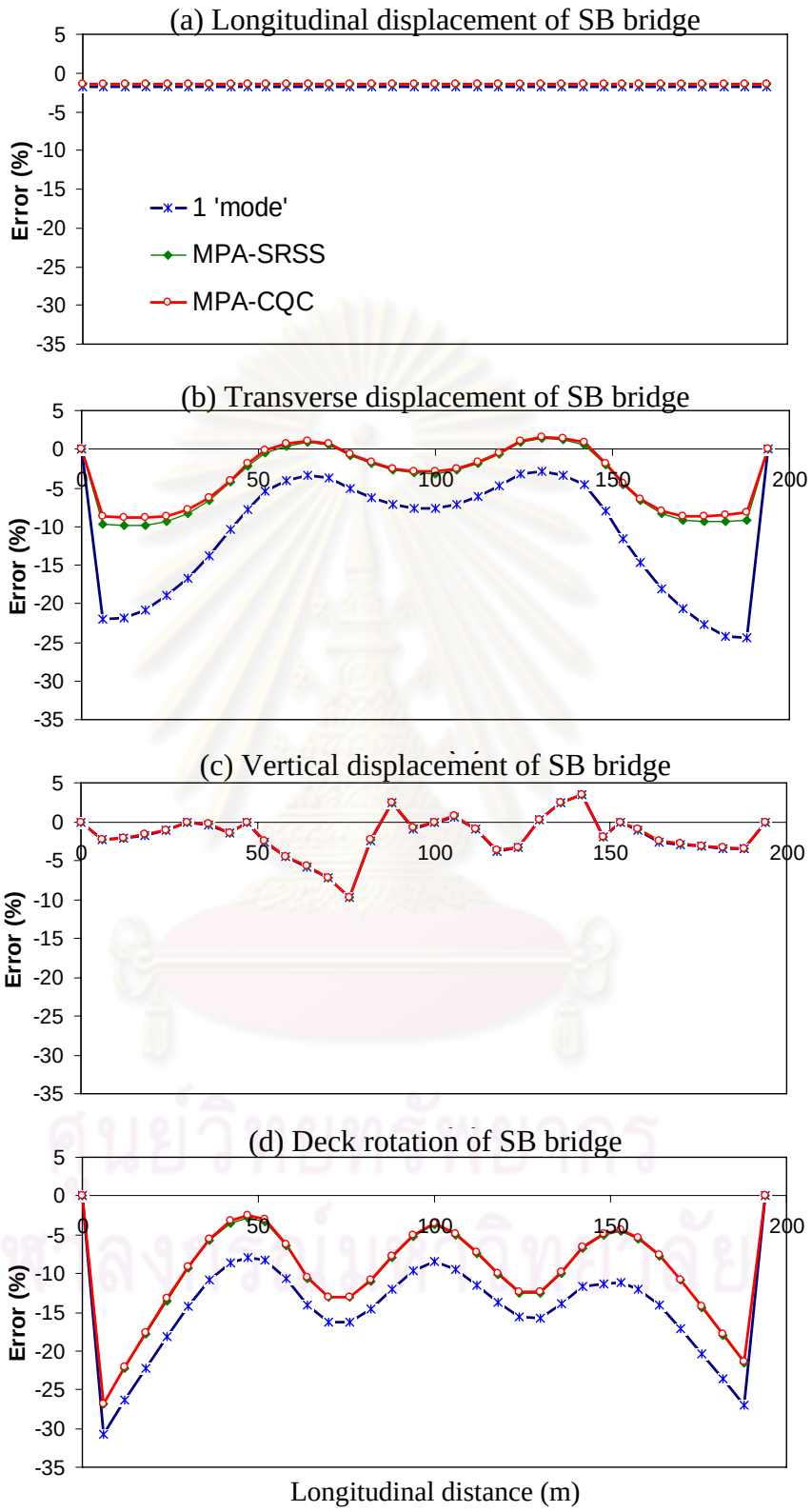

Figure 5.9 Median errors of (a) longitudinal displacements, (b) transverse displacements, (c) vertical displacements and (d) torsional rotations of the deck of the bridge supported by steel bearings.

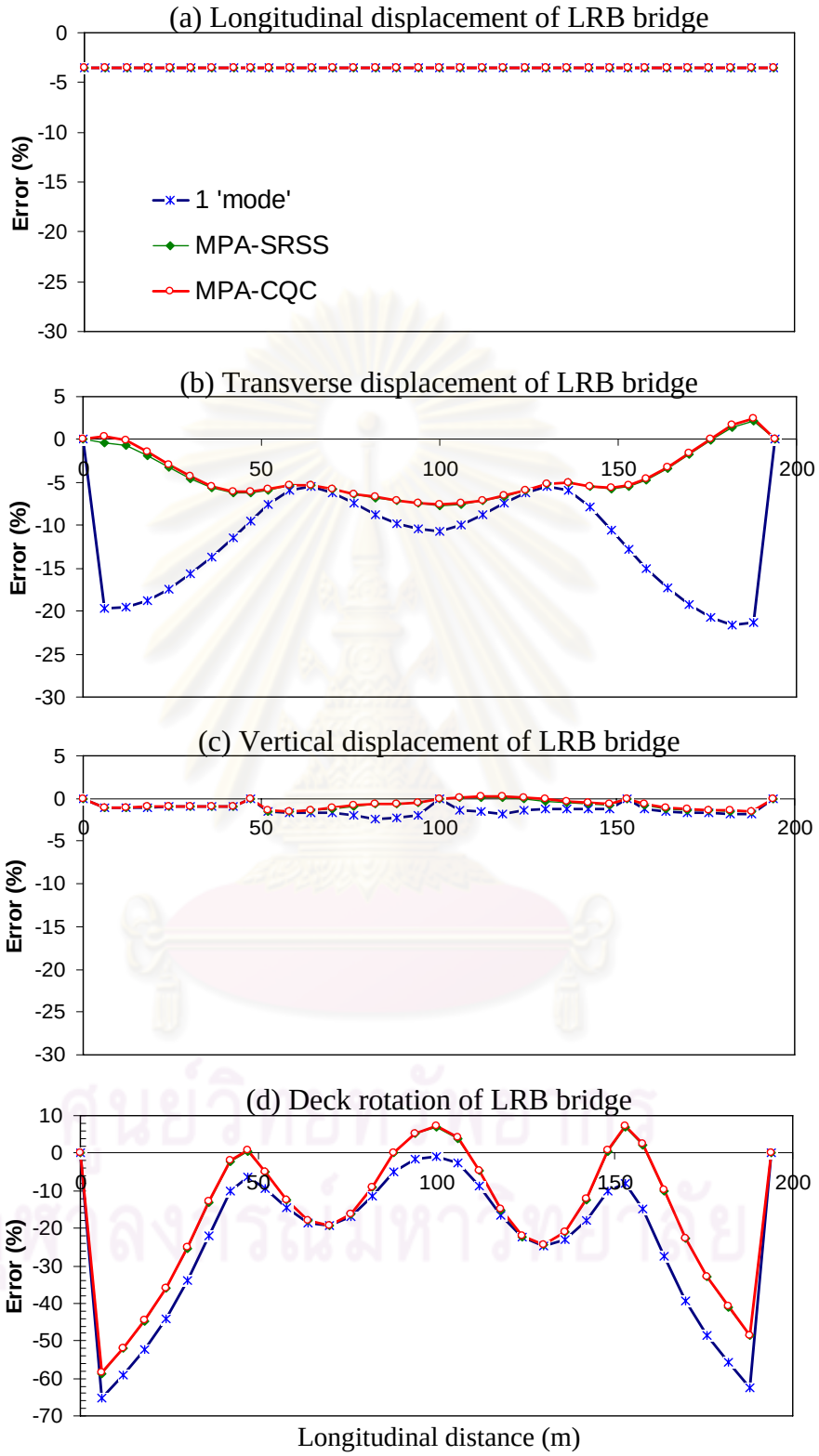

Figure 5.10 Median errors of (a) longitudinal displacements, (b) transverse displacements, (c) vertical displacements and (d) torsional rotations of the deck of the bridge equipped with LRB supports.

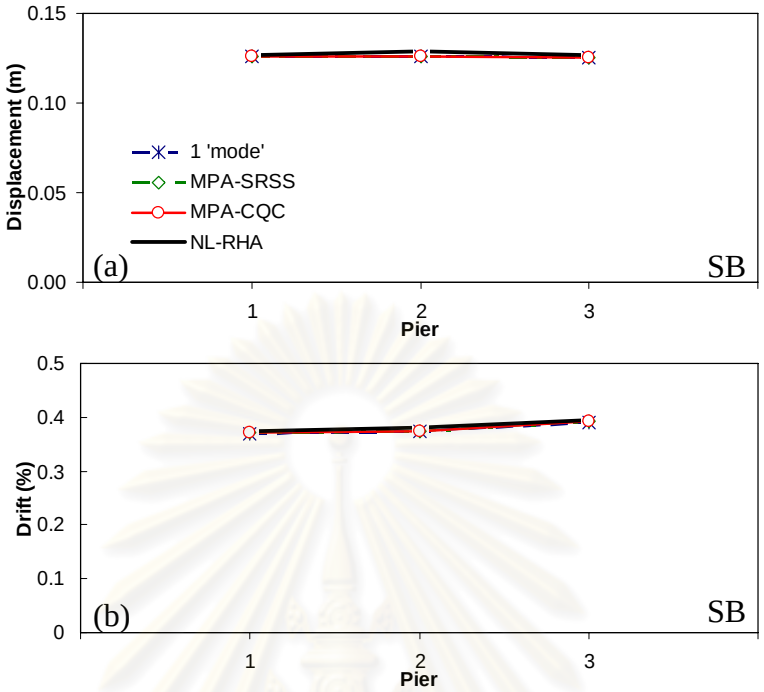

Figure 5.11 Comparison of longitudinal pier (a) displacements and (b) drifts of the bridge supported by steel bearings determined by three analyses: one ‘mode’ pushover analysis, the proposed extension of MPA, and NL-RHA.

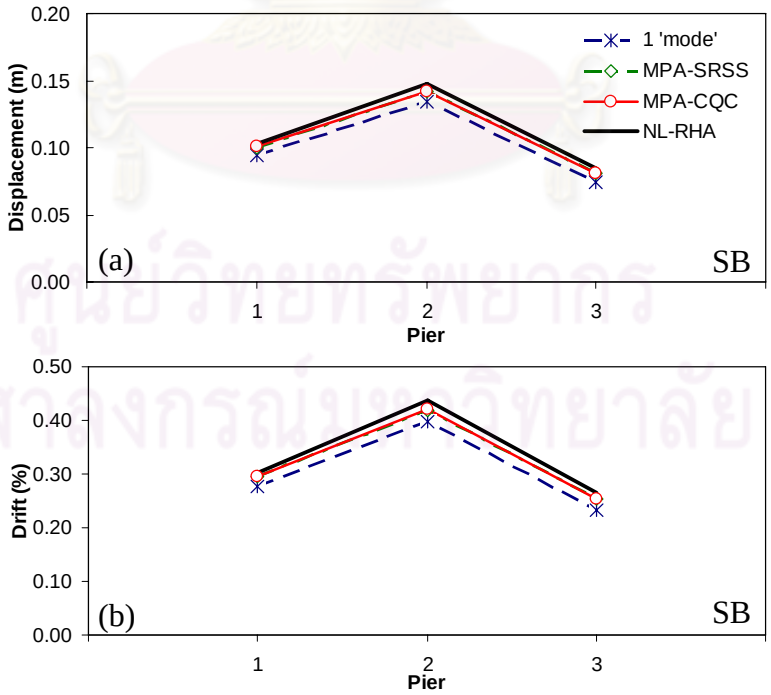

Figure 5.12 Comparison of transverse pier (a) displacements and (b) drifts of the bridge supported by steel bearings determined by three analyses: one ‘mode’ pushover analysis, the proposed extension of MPA, and NL-RHA.

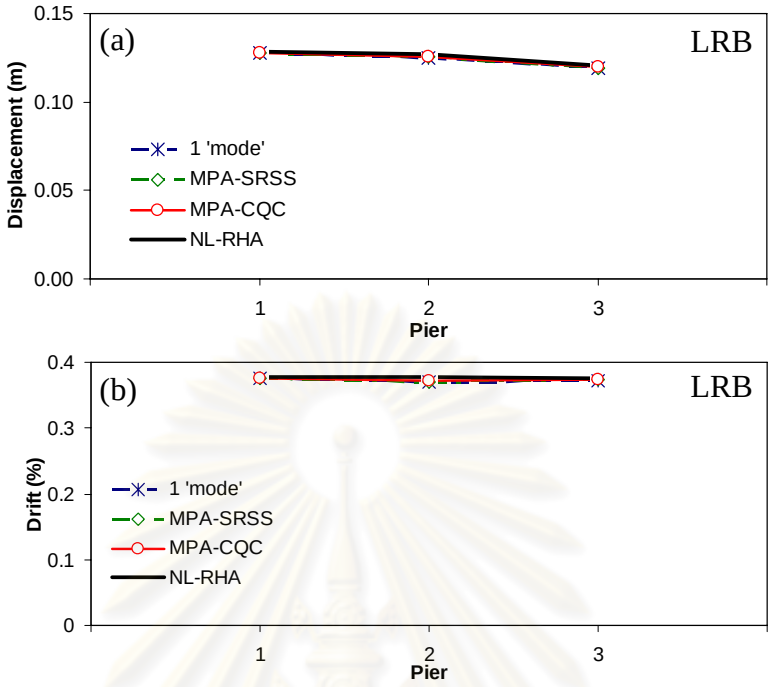

Figure 5.13 Comparison of longitudinal pier (a) displacements and (b) drifts of the bridge equipped with LRB supports determined by three analyses: one ‘mode’ pushover analysis, the proposed extension of MPA, and NL-RHA.

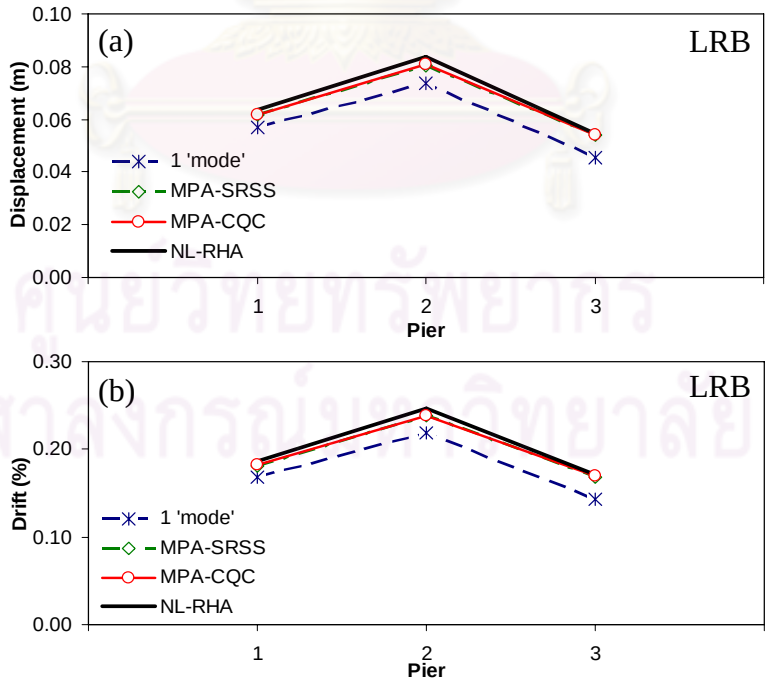

Figure 5.14 Comparison of transverse pier (a) displacements and (b) drifts of the bridge equipped with LRB supports determined by three analyses: one ‘mode’ pushover analysis, the proposed extension of MPA, and NL-RHA.

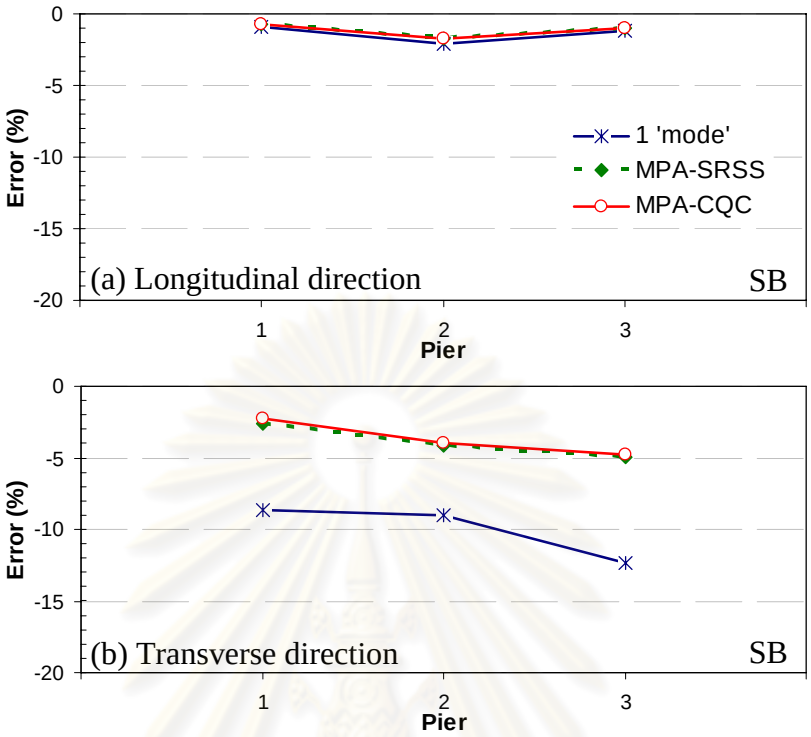

Figure 5.15 Median errors of the pier drifts of the bridge supported by steel bearings in the (a) longitudinal, and (b) transverse directions.

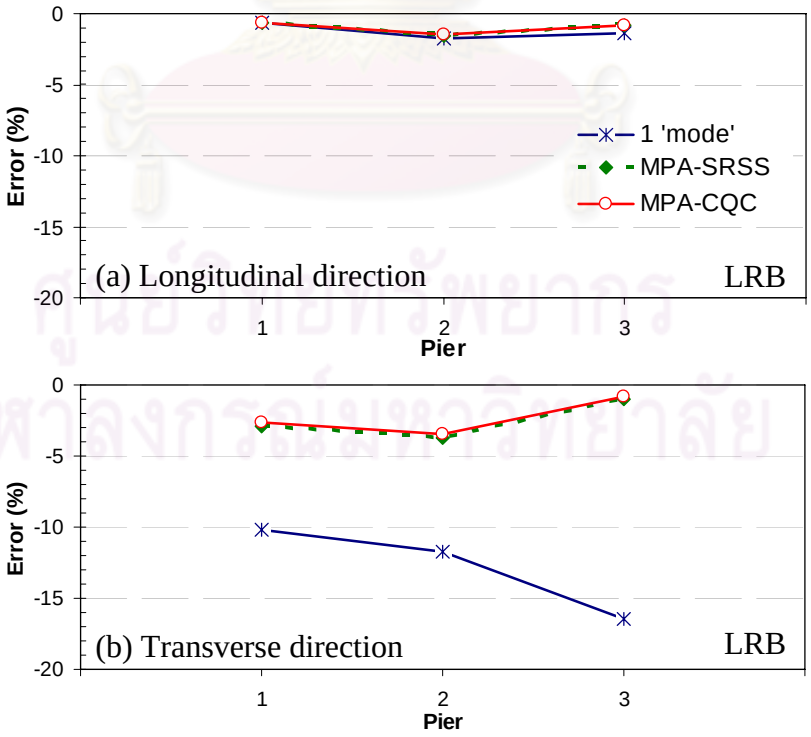

Figure 5.16 Median errors of the pier drifts of the bridge equipped with LRB supports in the (a) longitudinal, and (b) transverse directions.

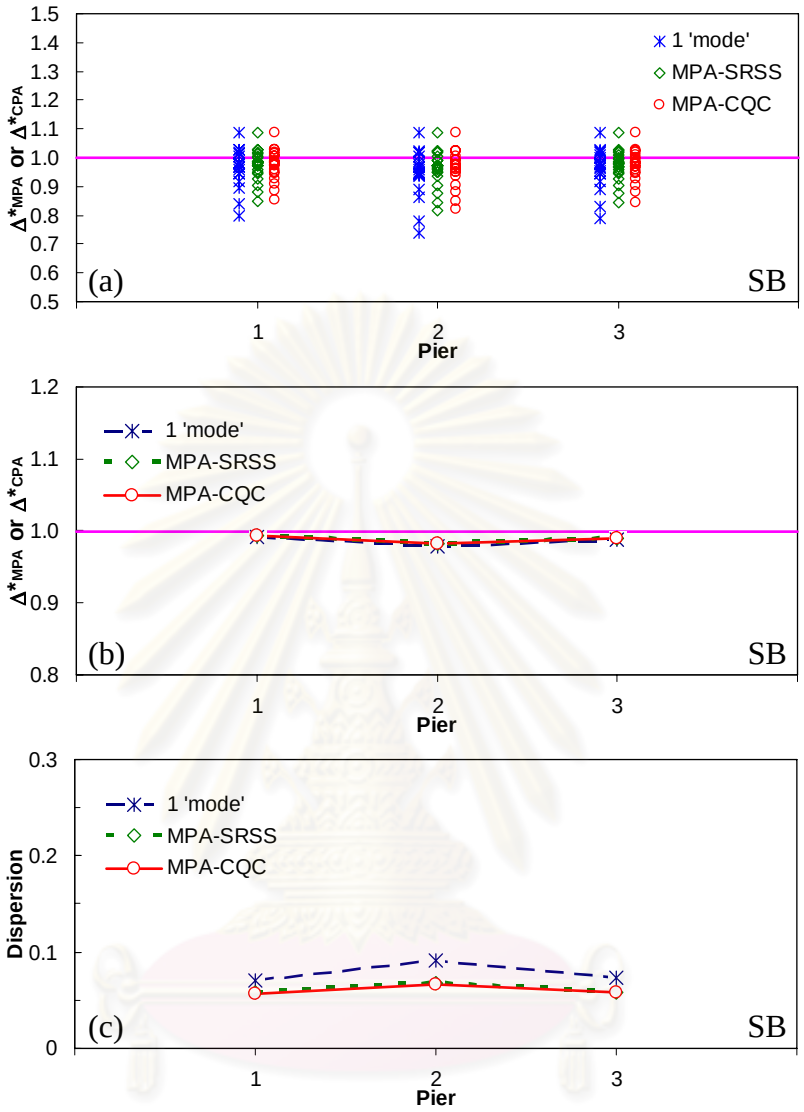

Figure 5.17 (a) Pier drift ratios, Δ^*_{MPA} or Δ^*_{CPA}, (b) median of pier drift ratios, and (c) dispersion of the pier drift ratios in the longitudinal direction of the bridge supported by steel bearings subjected to the set of 20 LMSR ground motions.

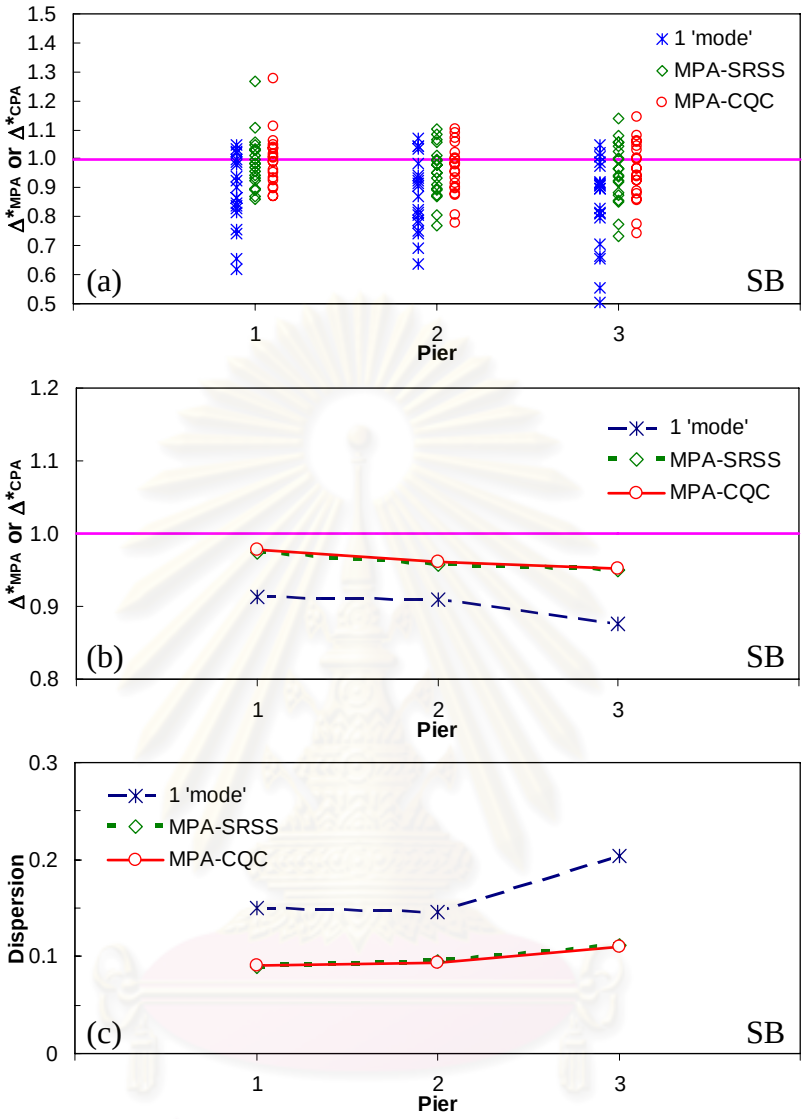

Figure 5.18 (a) Pier drift ratios, Δ^{*}_{MPA} or Δ^{*}_{CPA}, (b) median of pier drift ratios, and (c) dispersion of the pier drift ratios in the transverse direction of the bridge supported by steel bearings subjected to the set of 20 LMSR ground motions.

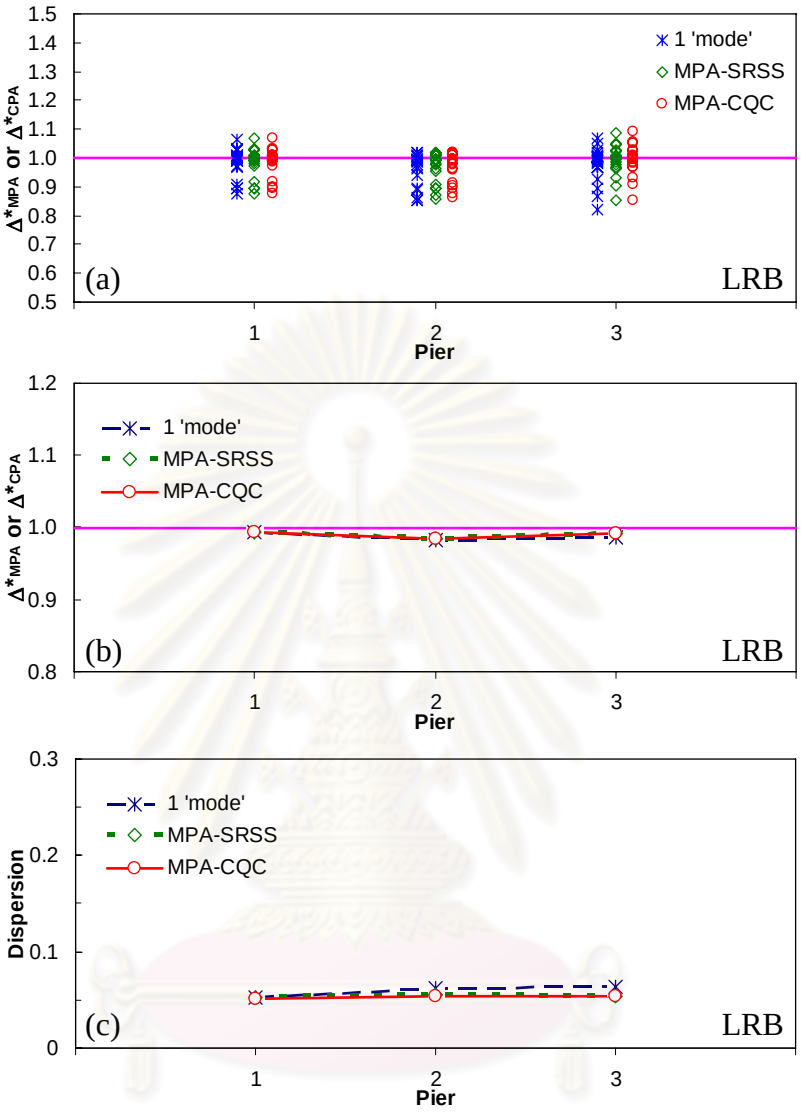

Figure 5.19 (a) Pier drift ratios, Δ^*_{MPA} or Δ^*_{CPA}, (b) median of pier drift ratios, and (c) dispersion of the pier drift ratios in the longitudinal direction of the bridge equipped with LRB supports subjected to the set of 20 LMSR ground motions.

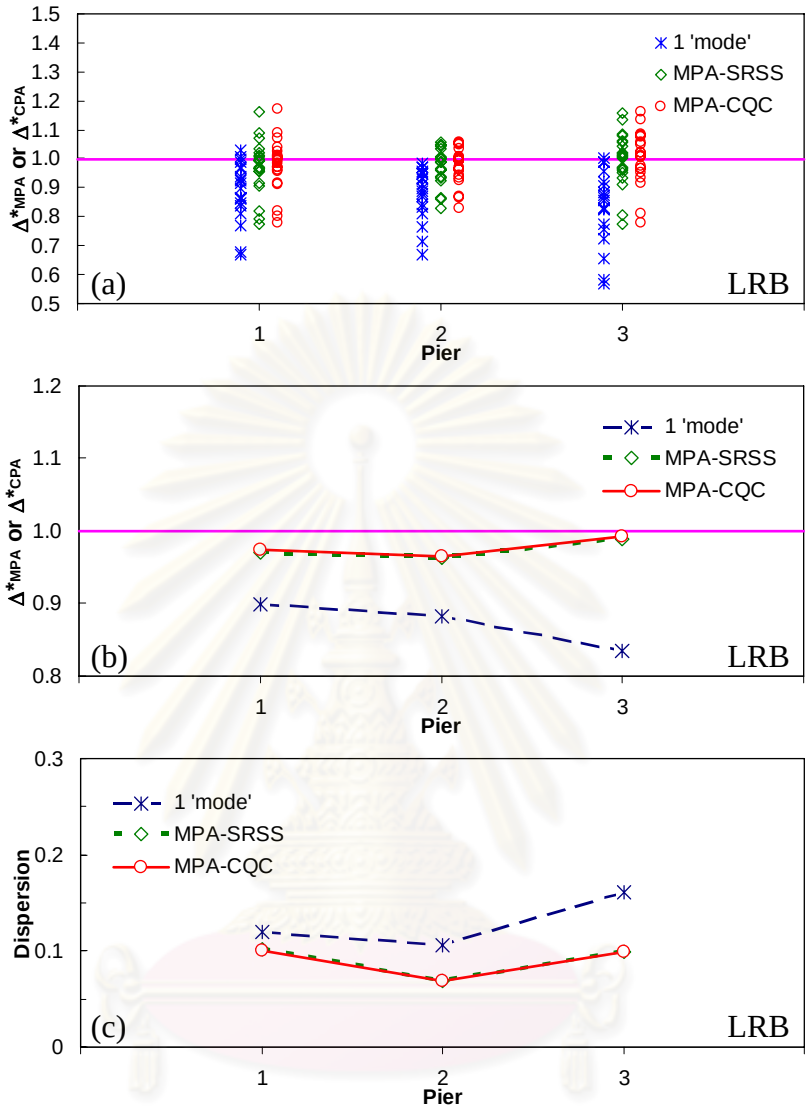

Figure 5.20 (a) Pier drift ratios, Δ^*_{MPA} or Δ^*_{CPA}, (b) median of pier drift ratios, and (c) dispersion of the pier drift ratios in the transverse direction of the bridge equipped with LRB supports subjected to the set of 20 LMSR ground motions.

5.4.3 Internal Forces

The internal forces of the studied bridges, which are the main quantities used for assessing the bridges, due to the set of 20 LMSR ground motions were determined by the proposed extension of MPA procedure and also by NL-RHA. Figures 5.21, 5.22, 5.23 and 5.24 show the median values of bending moments about x- and y-axes at the base of piers, and bending moment ratios, $M^{*}_{MPA} = M_{MPA} / M_{NL-RHA}$ or $M^{*}_{CPA} = M_{CPA} / M_{NL-RHA}$. Note that x-axis is the longitudinal direction and y-axis is the transverse direction. The median and dispersion of moment ratios of the bridges equipped with steel bearings (SB) and LRB supports due to the set of selected ground motions are also shown.

Similar to investigation of the peak deck displacements and pier drifts, the presented results show that the contributions of higher modes in estimating the bending moments about x-axis at the base of piers when subjected to excitation are significant (Figures 5.22a and 5.24a). The MPA-SRSS and MPA-CQC results are very close to those from the NL-RHA procedure. The proposed extension of MPA procedure underestimates slightly the bending moments about x-axis with the bias is less than 10% for both types of bearings of the bridges considered (Figures 5.22c and 5.24c).

The dispersion of the moment about x-axis ratios determined by the proposed extension of MPA procedure is generally smaller than 15%. Comparing the dispersion of the pier drifts in the transverse direction to dispersion of the moment about x-axis predicted by the proposed extension of MPA procedure, we can observe that the pier drifts can be estimated by MPA more accurately than bending moment demands. This is consistent with the intuition that the global response quantities, e.g., pier displacements or pier drifts, are more easily and accurately estimated than local response quantities, e.g., bending moments or plastic hinge rotations; especially when the bridge was driven far into the inelastic range and more inelastic deformations have occurred and led to large bias of MPA.

On the contrary, the one ‘mode’ pushover analysis seems to fail in estimating moment about x-axis. The median and dispersion of the moment about x-axis by one

‘mode’ pushover analysis can be as large as 18%. Figures 5.22d and 5.24c show the cases where both bias and dispersion are large, and clearly the one ‘mode’ pushover analysis procedure does not provide a reasonable estimate for bending moment about x-axis.

The presented results also show that both versions of the proposed extension of MPA procedure (i.e., MPA-SRSS and MPA-CQC) and the conventional pushover analysis procedure slightly underestimates bending moment about y-axis with the bias is less than 5%. This implies that the conventional pushover analysis is adequate to predict the bending moments about y-axis at the base of piers, because the bridges considered in this investigation are dominated by the first longitudinal ‘mode’ whose effective modal masses alone are 91.32% and 89.77% for the bridges equipped with steel bearings and LRB supports, respectively. The dispersion of both approximate procedures, the one ‘mode’ pushover analysis and the proposed extension of MPA procedures, in estimating the moment about y-axis is very small, less than 5% for all cases (Figures 5.21 and 5.23).

Similar results for bias and dispersion of MPA in estimating pier displacements and pier drifts, the bias and dispersion for moment about y-axis is much smaller compared to moment about x-axis, indicating that moment about y-axis can be estimated by MPA more accurately than moment about x-axis demands. This demonstrates that an approximate procedure, such as the proposed extension of MPA procedure, is more likely to be accurate for an individual ground motion if both its bias and dispersion are small. On the other hand, compared to the moment about y-axis, the dispersion tends to increase for moment about x-axis as the contribution from the higher-modes becomes more significant, in particular, for the piers near the both ends of the bridge where higher modes are more active.

Figures 5.25 and 5.26 show the median axial forces at the base of piers of the bridges equipped with steel bearings and LRB supports, respectively; median errors of axial forces are also shown in these figures. The results show that the axial force at the base of piers can be estimated by the proposed extension of MPA procedure as well as the conventional pushover analysis for both types of bearings. The bias is relatively small, less than 5% for the bridge with LRB supports and 10% for bridge

supported by steel bearings, respectively. This is because the axial force at the base at piers is essentially contributed by gravity load.

Median shear forces along x- and y-axes at the base of piers of the bridge supported by steel bearings due to the set of LMSR ground motions are shown in Figures 5.27 and 5.28; median errors of shear force demands are also shown. Similarly, Figures 5.29 and 5.30 show the median shear forces and errors along x- and y-axes at the base of piers of the bridge equipped with LRB supports, respectively. These results lead to the following observations.

Including the response contributions of higher ‘modes’ in estimating the shear forces are significant. Both MPA-SRSS and MPA-CQC can estimate the shear forces along x- and y-axes at the base of piers reasonably well with a tendency to slightly underestimate shear force demands compared to NL-RHA. The bias of the proposed extension of MPA procedure in estimating the shear forces along x- and y-axes is less than 10% for both types of bearings. With several ‘modes’ included, the shear force estimated by MPA is generally similar to the ‘exact’ results from NL-RHA.

On the contrary, the one ‘mode’ pushover analysis is inadequate in estimating shear forces at the base of piers with the bias is relatively large. It underestimates shear force demands by 20% and 30% bias for the bridges equipped with steel bearings and LRB supports, respectively. However, the first ‘mode’ alone is sufficient in estimating the shear force along x-axis at the base of piers of the bridge supported by steel bearings (see Figure 5.27).

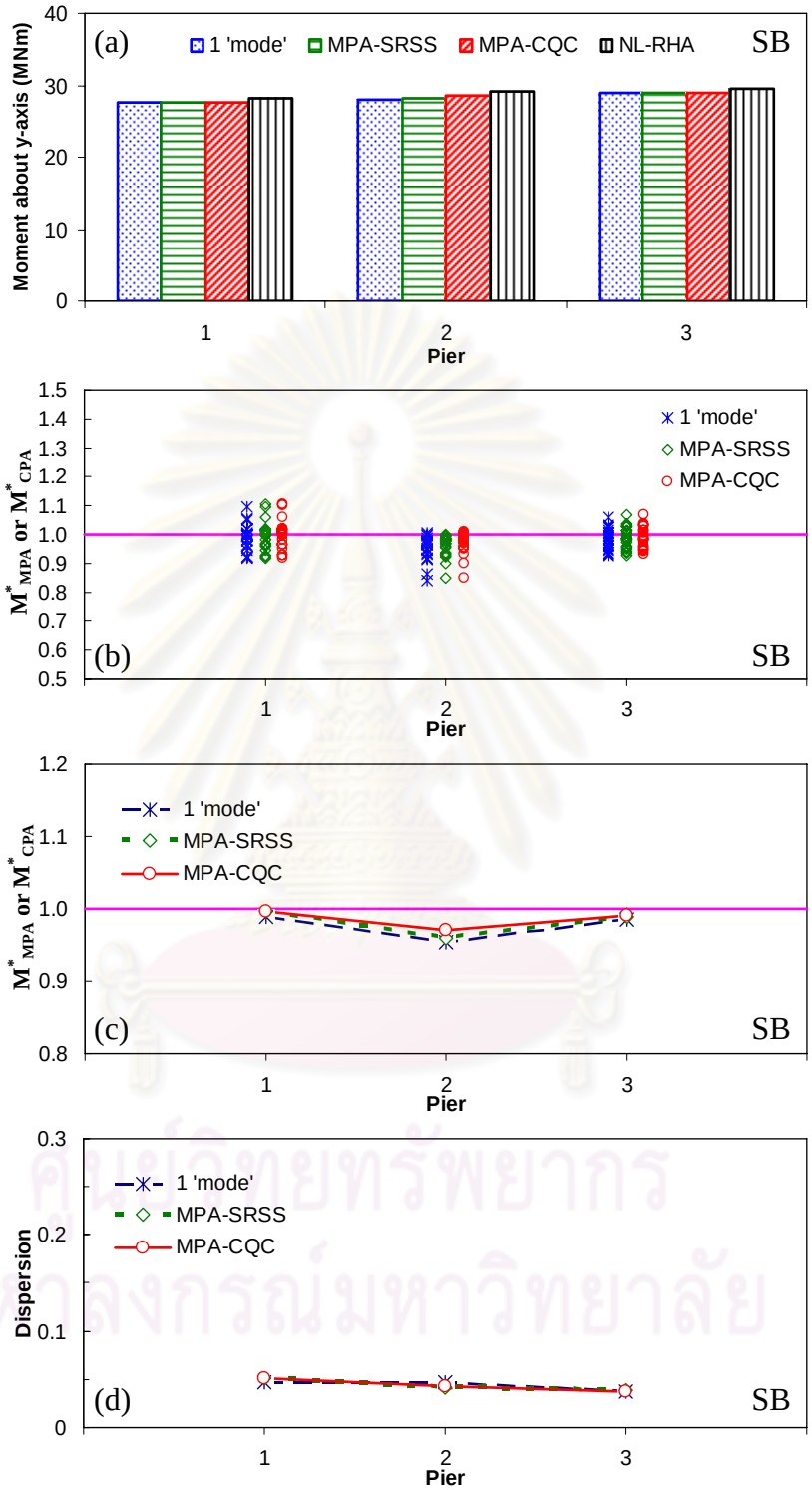

Figure 5.21 (a) Median values of bending moment about y-axis, (b) bending moment about y-axis ratios, M^*_{MPA} or M^*_{CPA}, (c) median of bending moment about y-axis ratios, and (d) dispersion of the bending moment about y-axis ratios at the base of piers of the bridge supported by steel bearings.

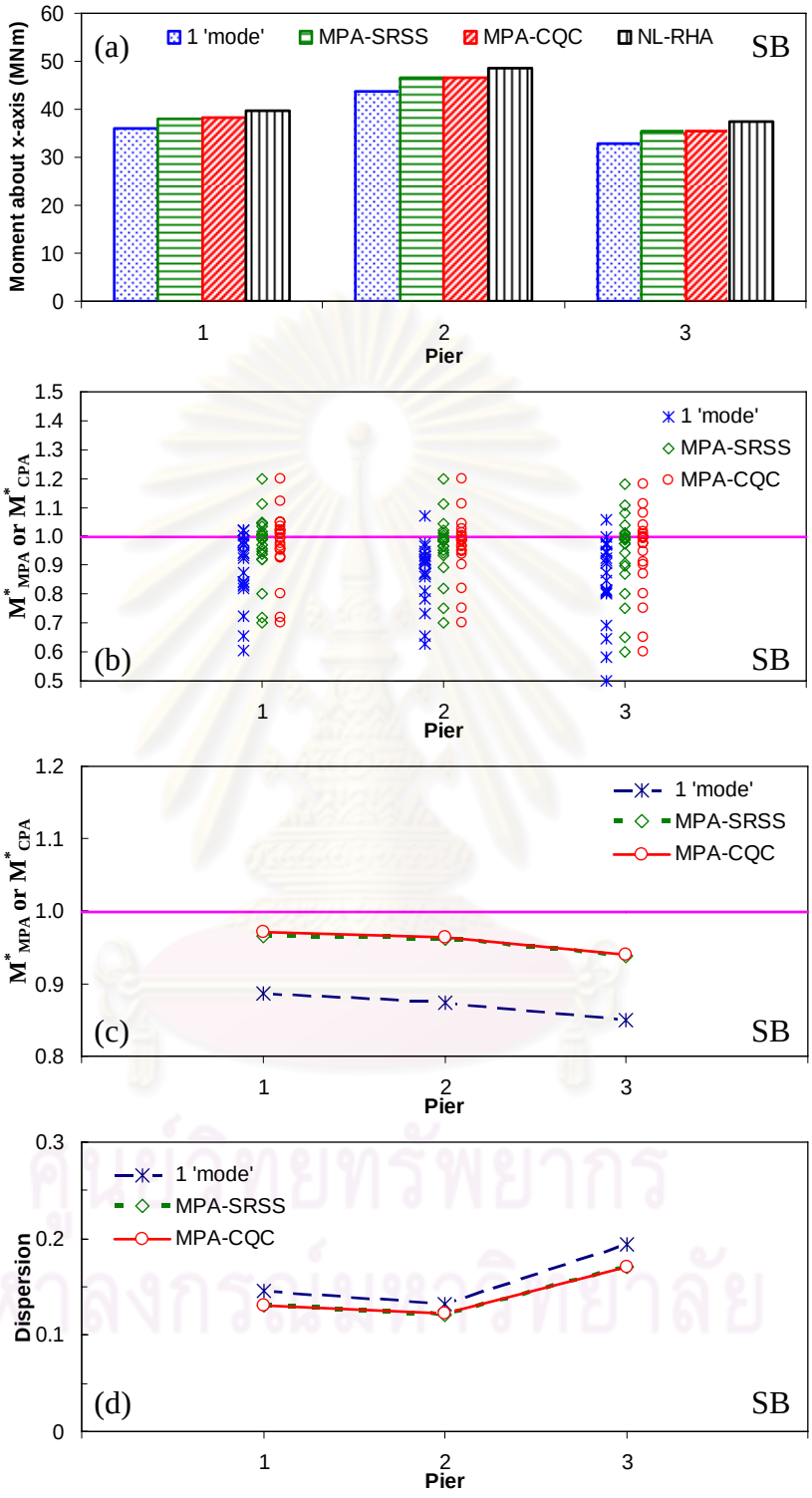

Figure 5.22 (a) Median values of bending moment about x-axis, (b) bending moment about x-axis ratios, M^*_{MPA} or M^*_{CPA}, (c) median of bending moment about x-axis ratios, and (d) dispersion of the bending moment about x-axis ratios at the base of piers of the bridge supported by steel bearings.

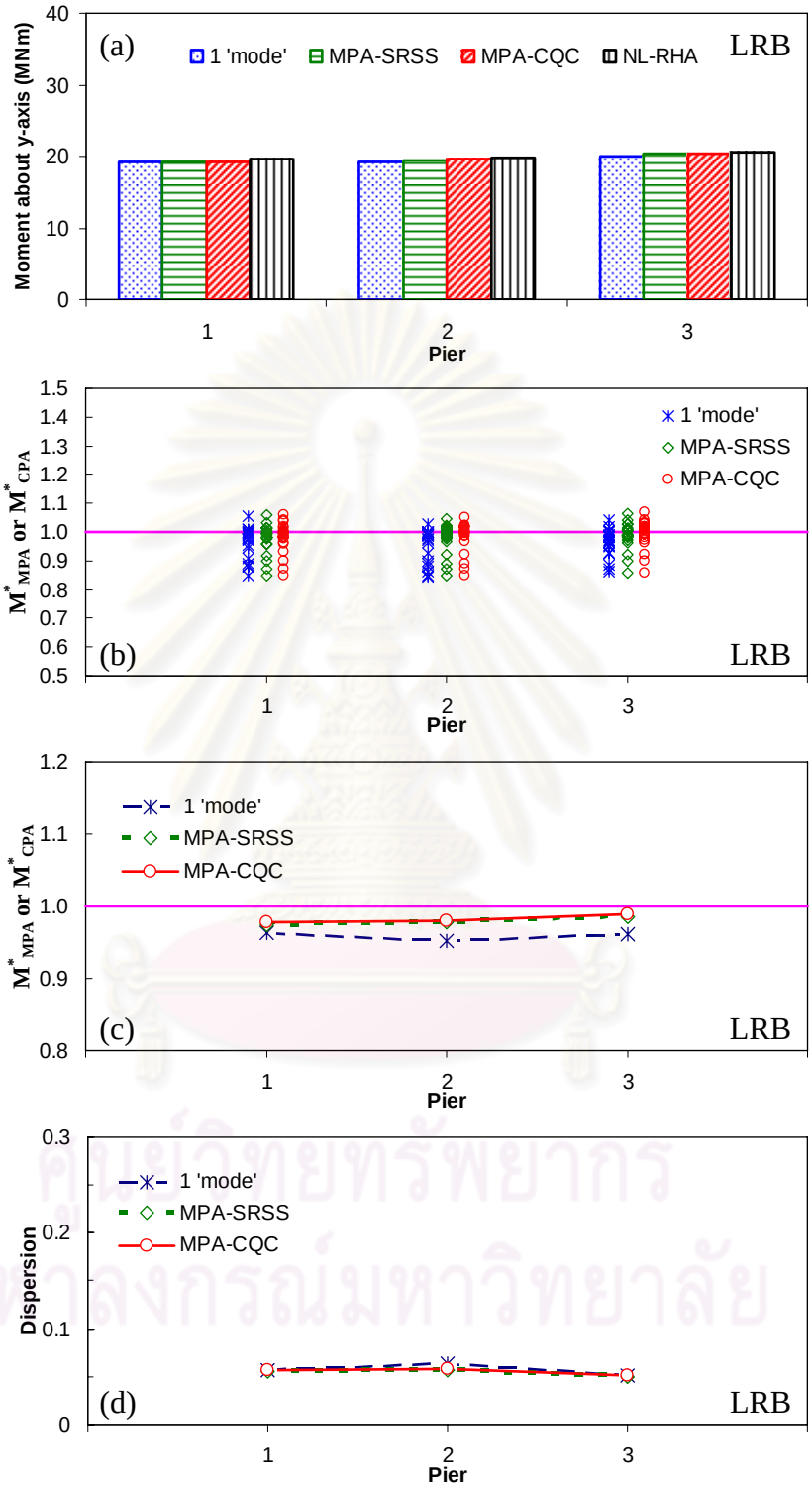

Figure 5.23 (a) Median values of bending moment about y-axis, (b) bending moment about y-axis ratios, M^*_{MPA} or M^*_{CPA}, (c) median of bending moment about y-axis ratios, and (d) dispersion of the bending moment about y-axis ratios at the base of piers of the bridge equipped with LRB supports.

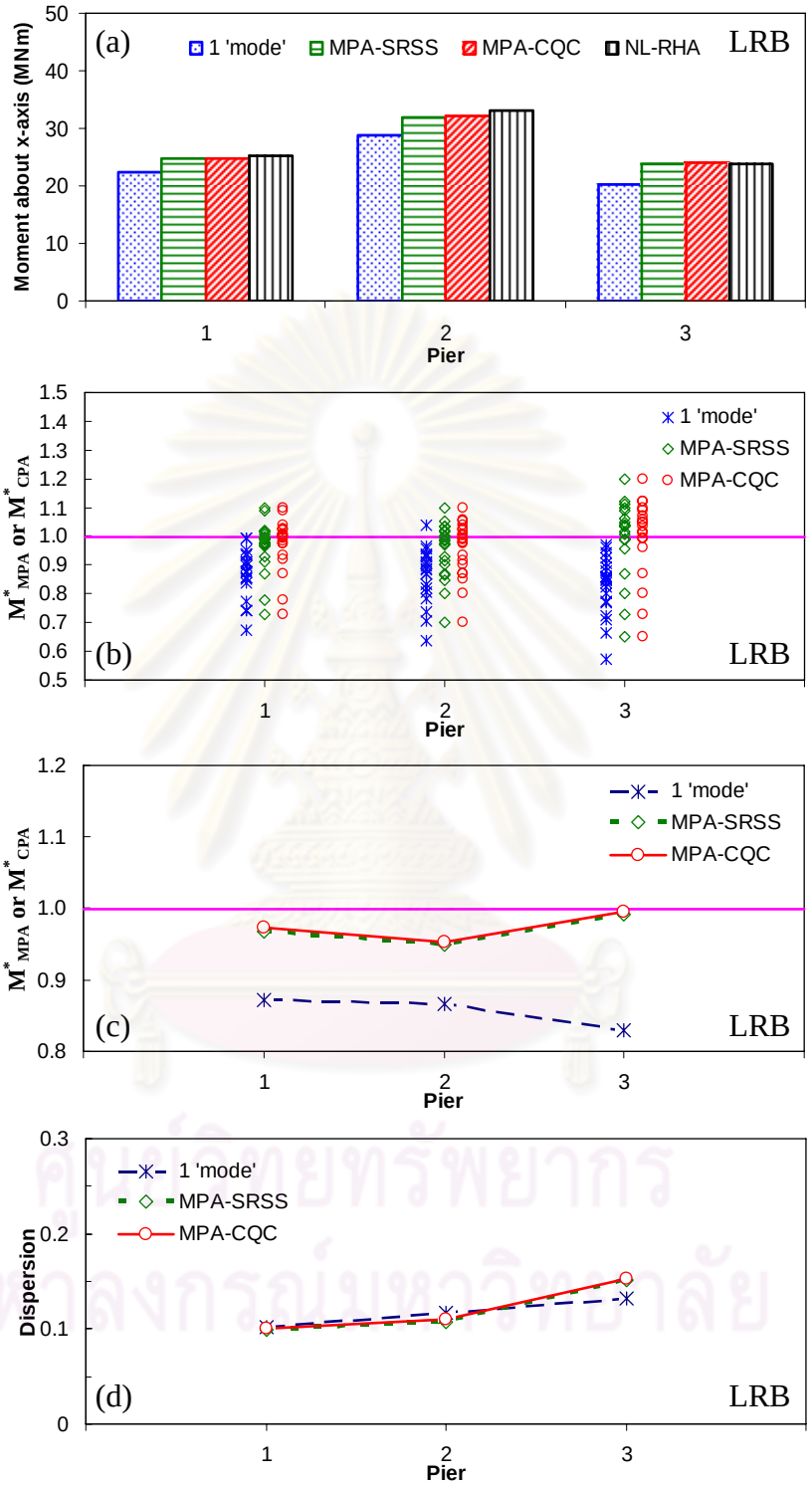

Figure 5.24 (a) Median values of bending moment about x-axis, (b) bending moment about x-axis ratios, M^*_{MPA} or M^*_{CPA}, (c) median of bending moment about x-axis ratios, and (d) dispersion of the bending moment about x-axis ratios at the base of piers of the bridge equipped with LRB supports.

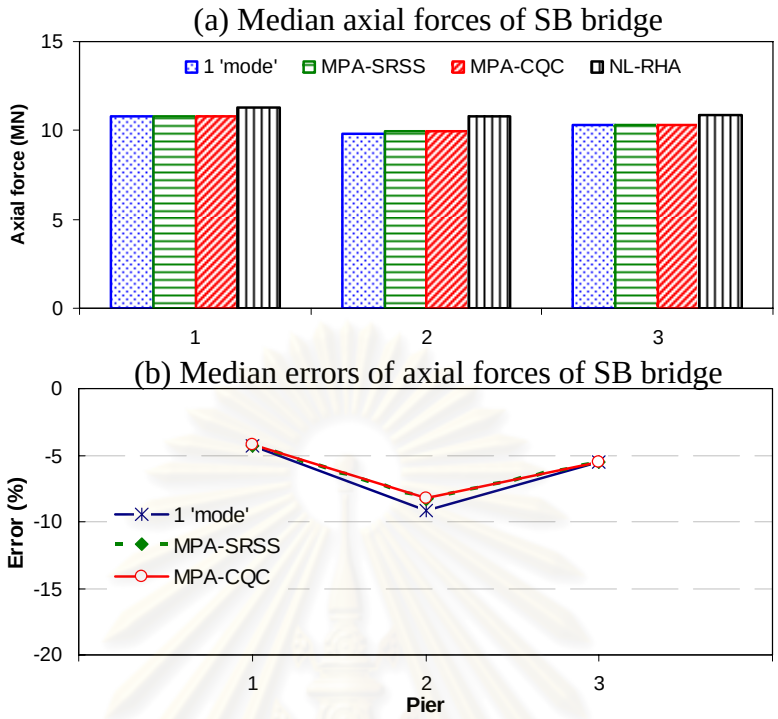

Figure 5.25 (a) Median axial forces, and (b) median errors of axial forces at the base of piers of the bridge supported by steel bearings subjected to the set of 20 LMSR ground motions.

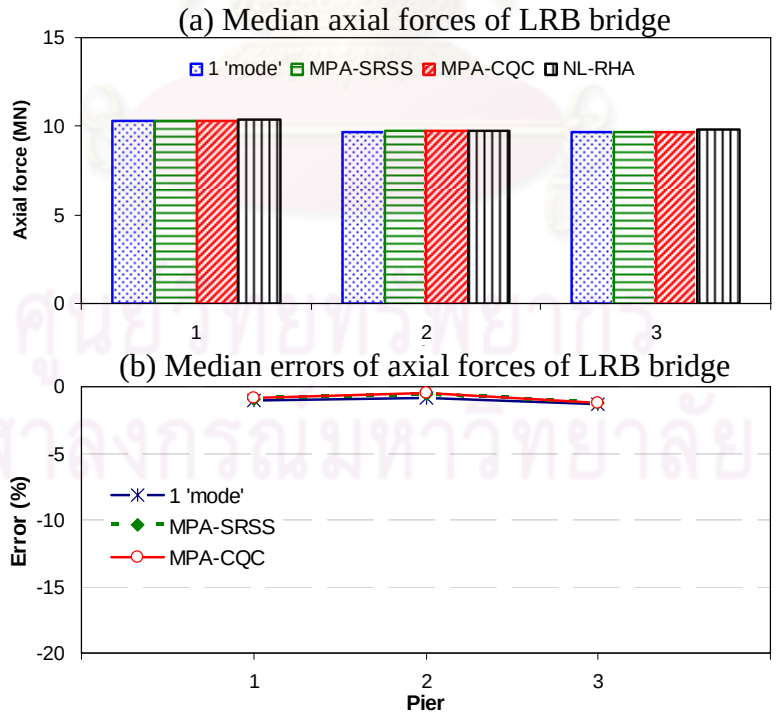

Figure 5.26 (a) Median axial forces, and (b) median errors of axial forces at the base of piers of the bridge equipped with LRB supports subjected to the set of 20 LMSR ground motions.

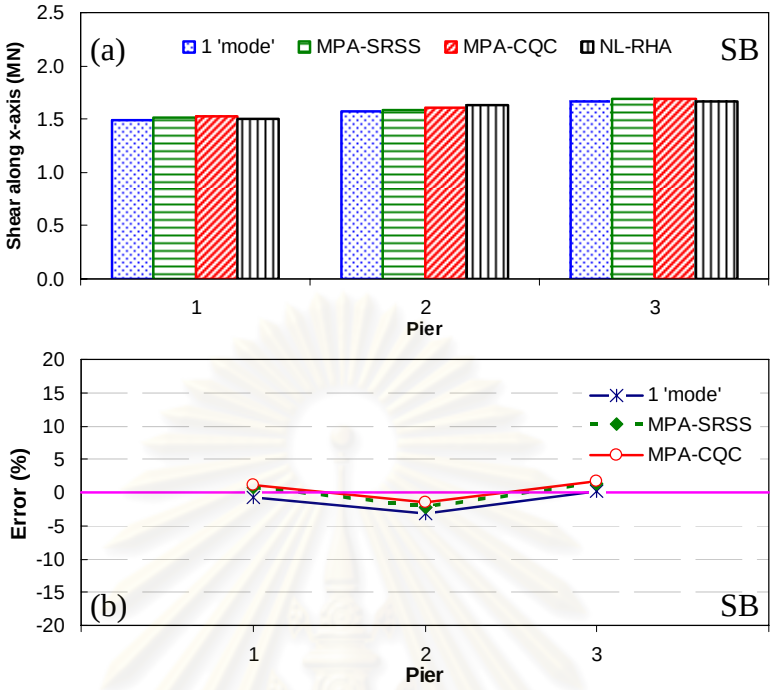

Figure 5.27 (a) Median shear forces along x-axis, and (b) median errors of shear forces along x-axis at the base of piers of the bridge supported by steel bearings subjected to the set of 20 LMSR ground motions.

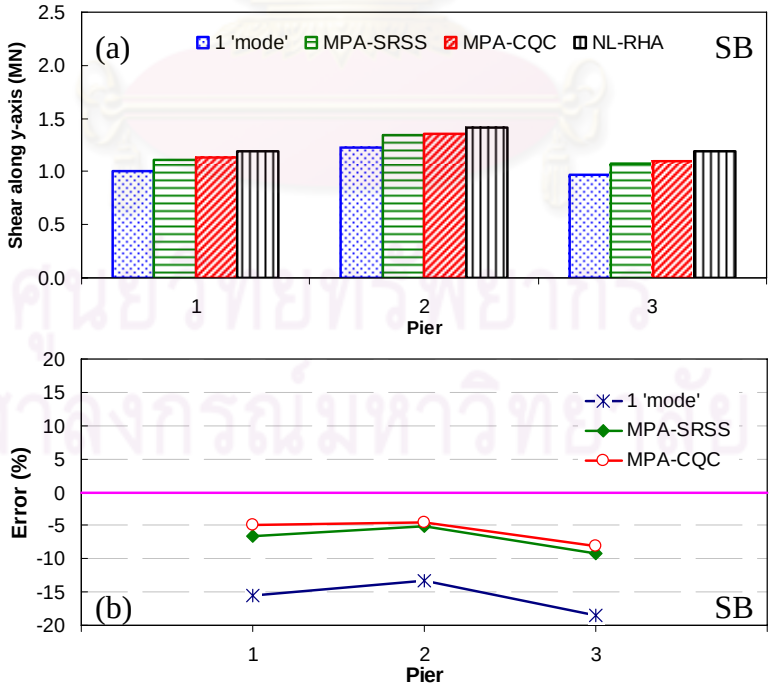

Figure 5.28 (a) Median shear forces along y-axis, and (b) median errors of shear forces along y-axis at the base of piers of the bridge supported by steel bearings subjected to the set of 20 LMSR ground motions.

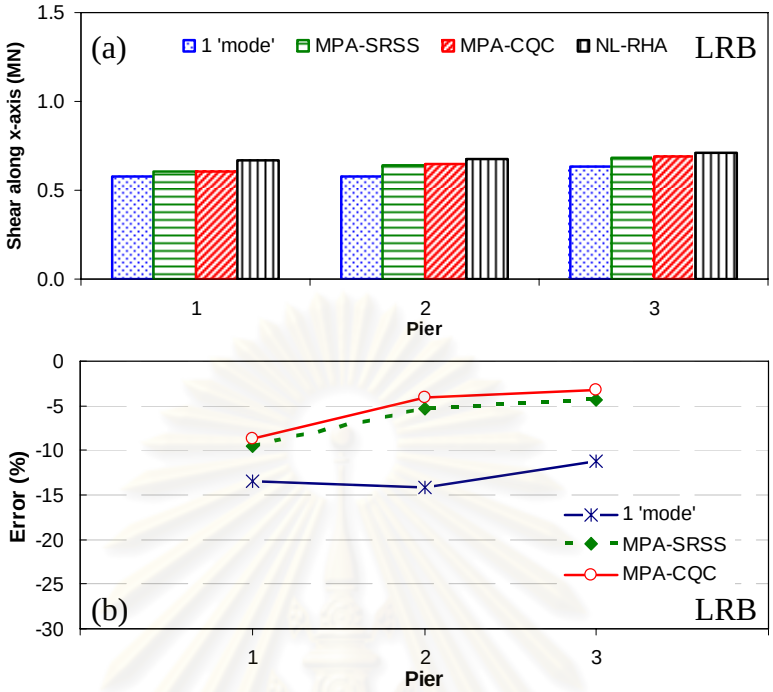

Figure 5.29 (a) Median shear forces along x-axis, and (b) median errors of shear forces along x-axis at the base of piers of the bridge equipped with LRB supports subjected to the set of 20 LMSR ground motions.

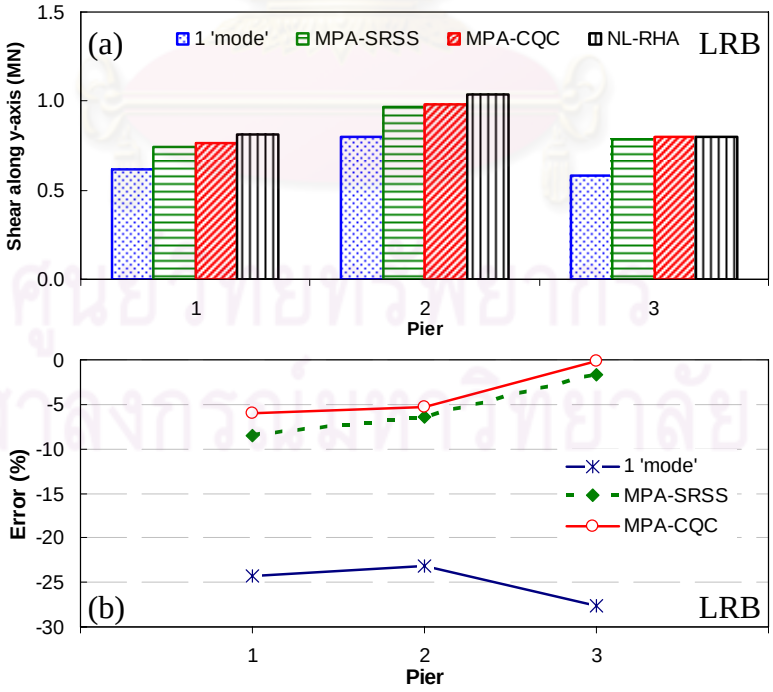

Figure 5.30 (a) Median shear forces along y-axis, and (b) median errors of shear forces along y-axis at the base of piers of the bridge equipped with LRB supports subjected to the set of 20 LMSR ground motions.

5.4.4 Hinge Rotation

The proposed extension of MPA procedure has been implemented for each of the bridges and for each of the 20 LMSR excitations, and contributions from several 'modes' were considered. The combined values of hinge rotations were computed included several 'modes' as mentioned before in Section 5.4. Figures 5.31, 5.32, 5.33, and 5.34 show these median values of hinge rotation demands at the base of piers for the bridges considered, together with the results of NL-RHA. Also included are the results of the conventional pushover analysis procedure, in which pushover analysis considers only the fundamental 'mode'. Hinge rotation ratios, $\theta^*_{MPA} = \theta_{MPA} / \theta_{NL-RHA}$ or $\theta^*_{CPA} = \theta_{CPA} / \theta_{NL-RHA}$, median and dispersion of hinge rotation ratios at the base of piers of the bridges equipped with steel bearings (SB) and LRB supports due to the set of selected ground motions are also shown in these Figures. These results permit the following observations.

The proposed extension of MPA procedure is least biased in estimating hinge rotation demands at the base of piers for the bridge with LRB supports and relatively more biased for the bridge supported by steel bearings (SB). This can easily be understood that the bridge equipped with Lead Rubber Bearings (LRB) are seismically isolated by LRB isolator, and most of piers remain elastic while yielding occurs at LRB systems. On the contrary, the yielding mainly forms at the base of piers of the bridge supported by steel bearings due to intense ground motions.

For the bridge supported by steel bearings, the MPA-SRSS and MPA-CQC procedures can estimate the hinge rotation demands at the base of piers reasonably well with a tendency to slightly underestimate hinge rotations about x-axis and overestimate hinge rotations about y-axis when compared to NL-RHA. The contributions of higher modes in estimating the hinge rotations about x-axis at the base of the piers when subjected to excitation are significant. The bias of the proposed extension of MPA procedure in estimating hinge rotations about x- and y-axes at the base of the piers is generally less than 10%. Conversely, the biases of the one 'mode' pushover analysis in estimating these responses are 10% and 20% for hinge rotations about y- and x-axes, respectively (Figures 5.31 and 5.32).

The bias of the proposed extension of MPA procedure in estimating hinge rotations about x- and y-axes at the base of the piers is relatively small; but the dispersions are quite large, 0.2 for hinge rotation about y-axis and 0.3 for hinge rotation about x-axis, because the data points scatter over a wide range from underestimation to significant overestimation (Figures 5.31b-d, and 5.32b-d). The MPA-SRSS and MPA-CQC estimates are significantly inaccurate for several excitations, although the median values of hinge rotations θ^{*}_{MPA} are very close to 1. This is because the bridge with steel bearings was driven far into the inelastic range by the set of LMSR strong ground motions, and many yields have formed at the base of the piers. Therefore, more inelastic deformations have occurred and led to larger bias of the proposed extension of MPA procedure.

For the bridge equipped with LRB supports, including the response contributions of higher 'modes' in estimating the hinge rotations are significant. The hinge rotations about x- and y-axes at the base of the piers can be accurately estimated by both MPA-SRSS and MPA-CQC with a tendency to slightly underestimate hinge rotation demands compared to NL-RHA. The bias of the proposed extension of MPA procedure in estimating the hinge rotations about x- and y-axes is less than 5%. With several 'modes' included, the hinge rotation estimated by MPA is generally similar to the 'exact' results from NL-RHA (Figure 5.34). The presented results also show that the dispersion of hinge rotations is generally small, less than 0.07 for hinge rotation about y-axis and 0.14 for hinge rotation about x-axis. On the contrary, the bias of the one 'mode' pushover analysis in estimating hinge rotation about x-axis is relatively large (20%). It means that the conventional pushover analysis may be inadequate to estimate hinge rotation demands about x-axis.

Finally, both bias and dispersion of the proposed extension of MPA procedure in estimating the hinge rotations about x- and y-axes of the bridge equipped with LRB supports are small compared to those of the bridge with steel bearings (SB), indicating that MPA-SRSS and MPA-CQC estimate the hinge rotation demands of the bridge with LRB accurately more often than the SB case. As mentioned before, this is because the bridge equipped with LRB are isolated and most of piers remain elastic while yielding occurs at LRB systems due to strong ground motions.

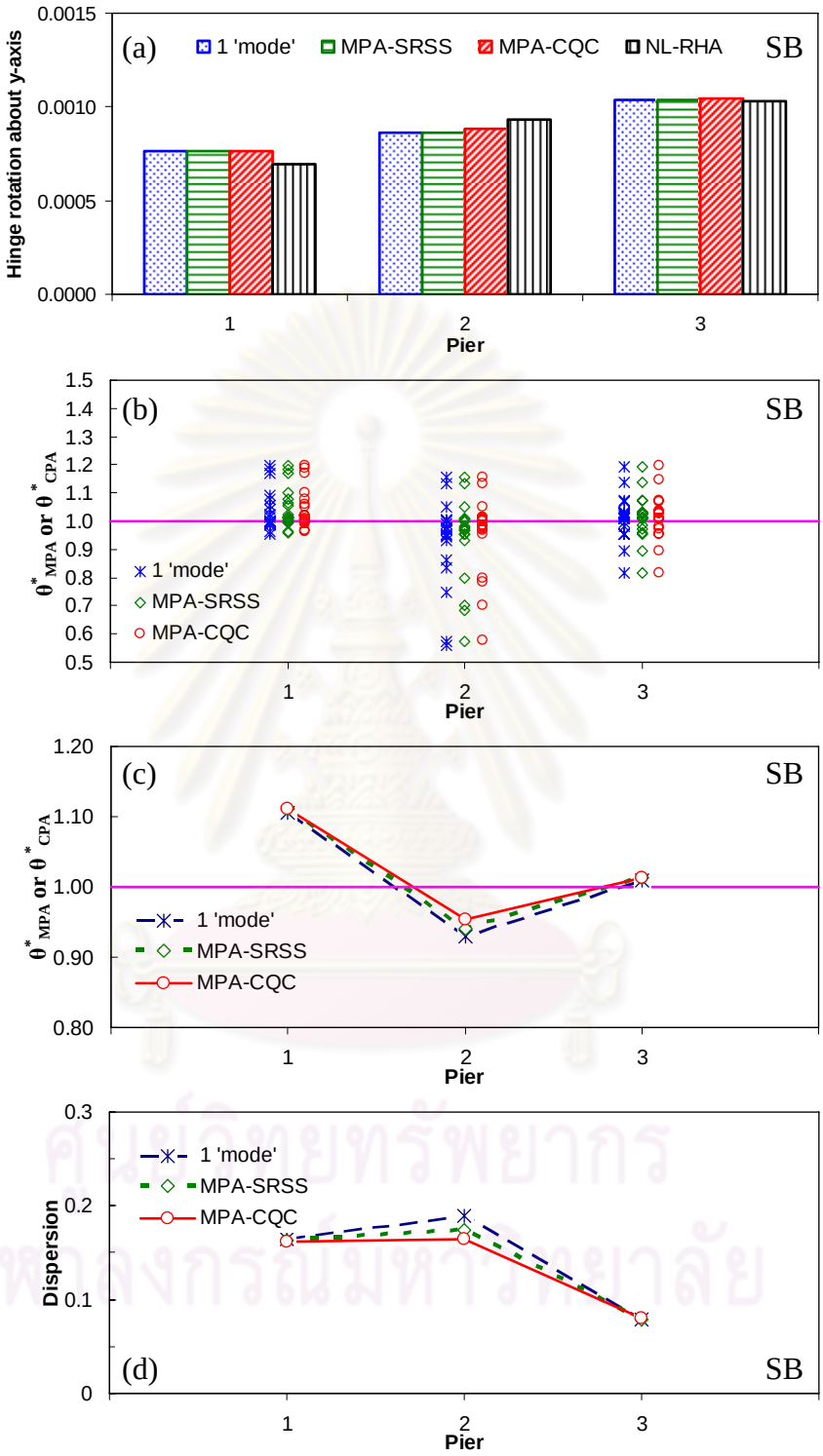

Figure 5.31 (a) Median values of hinge rotation about y-axis, (b) hinge rotation about y-axis ratios, θ^*_{MPA} or θ^*_{CPA}, (c) median of hinge rotation about y-axis ratios, and (d) dispersion of the hinge rotation about y-axis ratios at the base of piers of the bridge supported by steel bearings subjected to the set of 20 LMSR ground motions.

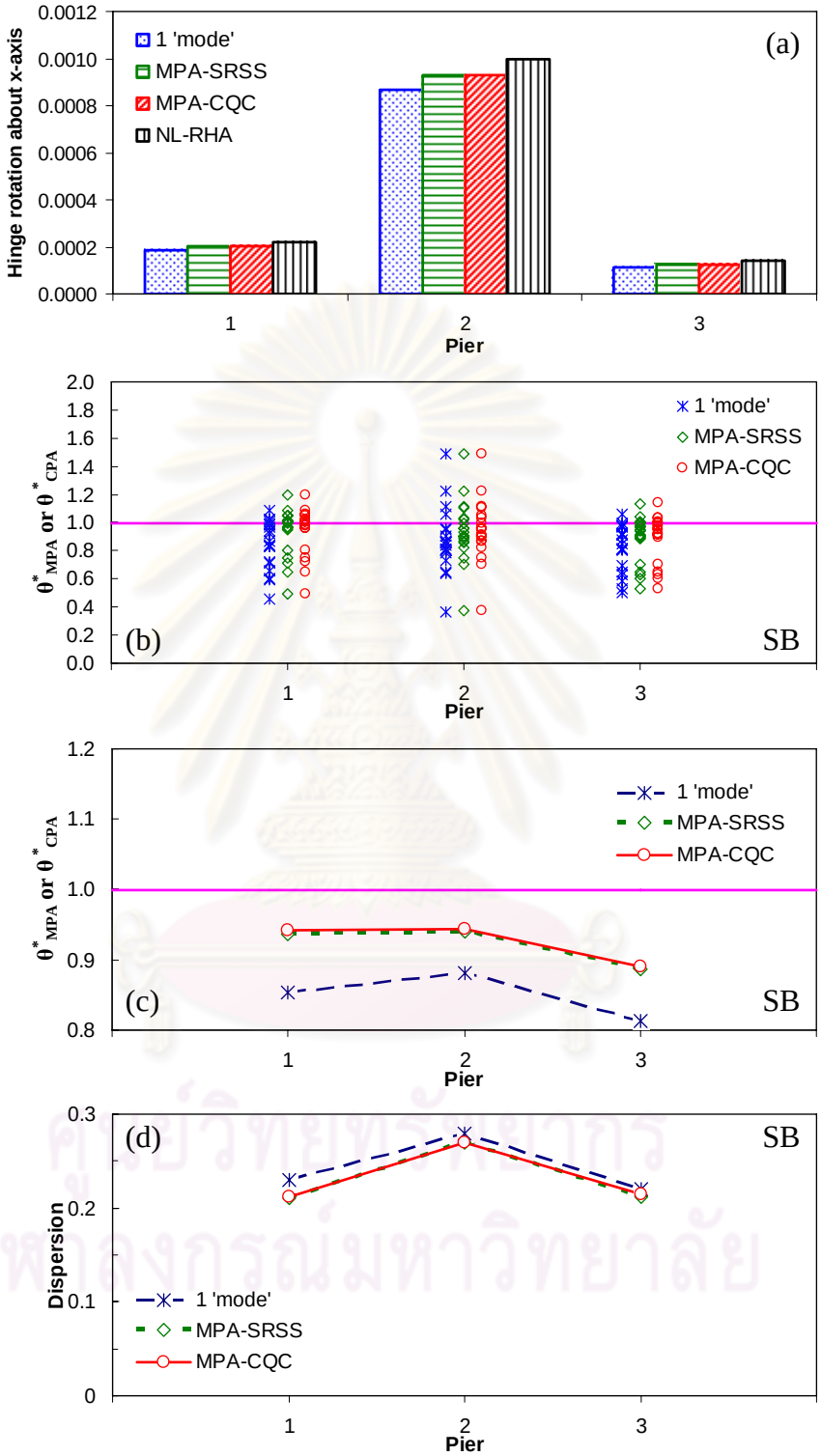

Figure 5.32 (a) Median values of hinge rotation about x-axis, (b) hinge rotation about x-axis ratios, θ^*_{MPA} or θ^*_{CPA}, (c) median of hinge rotation about x-axis ratios, and (d) dispersion of the hinge rotation about x-axis ratios at the base of piers of the bridge supported by steel bearings subjected to the set of 20 LMSR ground motions.

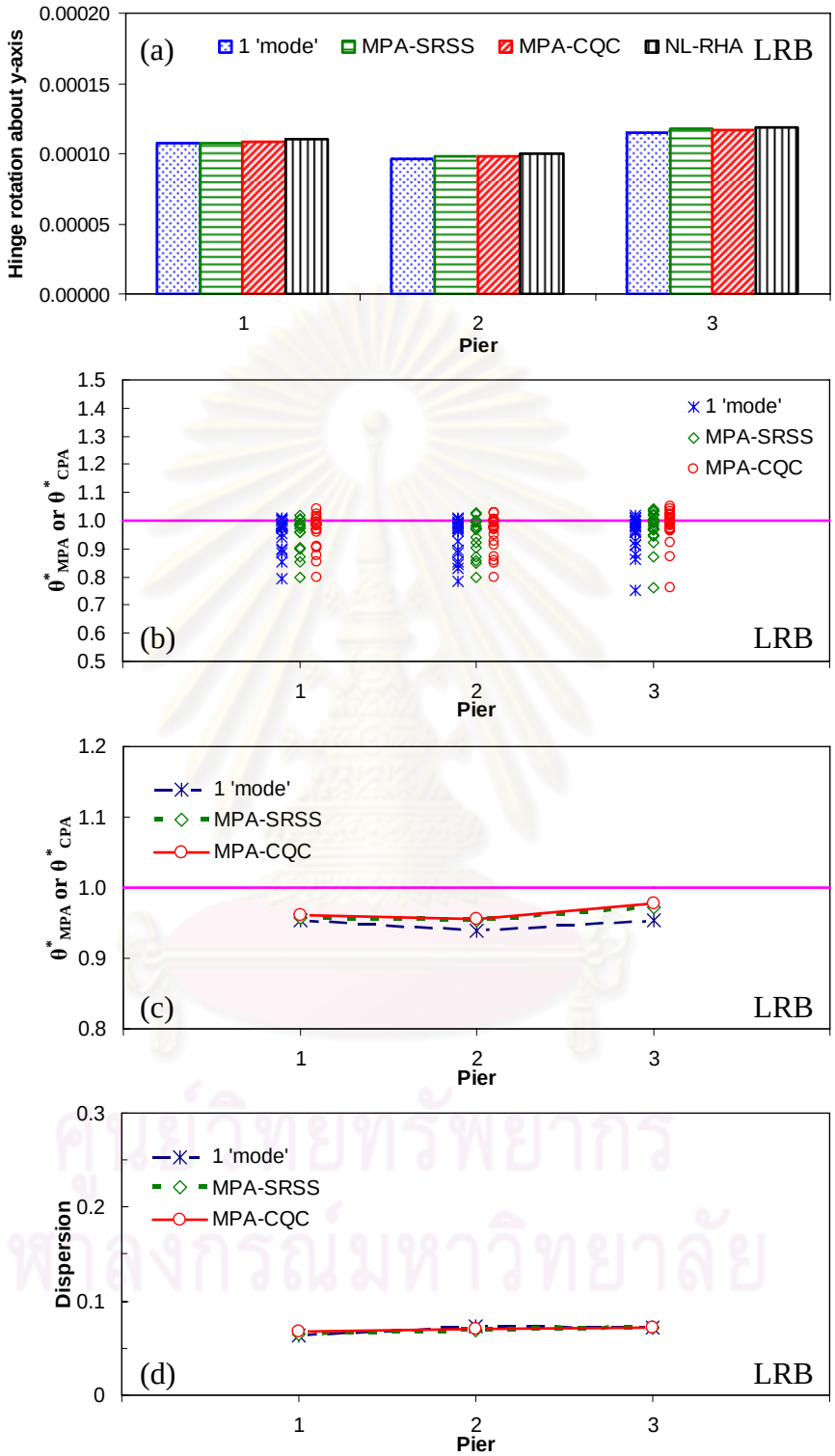

Figure 5.33 (a) Median values of hinge rotation about y-axis, (b) hinge rotation about y-axis ratios, θ^*_{MPA} or θ^*_{CPA}, (c) median of hinge rotation about y-axis ratios, and (d) dispersion of the hinge rotation about y-axis ratios at the base of piers of the bridge equipped with LRB supports subjected to the set of 20 LMSR ground motions.

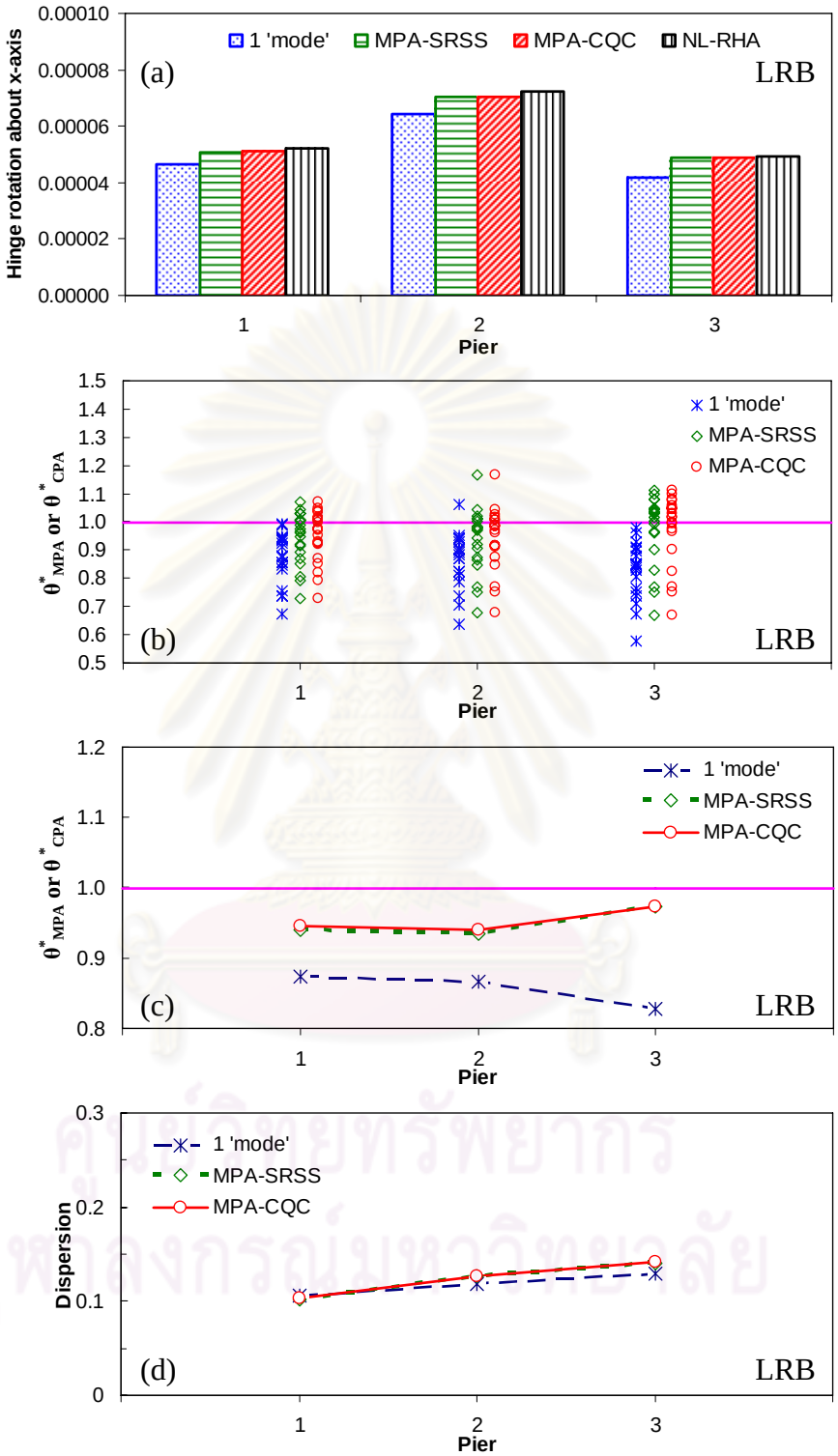

Figure 5.34 (a) Median values of hinge rotation about x-axis, (b) hinge rotation about x-axis ratios, θ^*_{MPA} or θ^*_{CPA}, (c) median of hinge rotation about x-axis ratios, and (d) dispersion of the hinge rotation about x-axis ratios at the base of piers of the bridge equipped with LRB supports subjected to the set of 20 LMSR ground motions.

5.4.5 Bearing Response

To demonstrate how bias and dispersion measures relate to the accuracy of the proposed extension of MPA procedure in estimating bearing responses, Figures 5.35 and 5.36 show the median shear forces along x- and y-axes, shear force ratios, $S^*_{MPA} = S_{MPA} / S_{NL-RHA}$ or $S^*_{CPA} = S_{CPA} / S_{NL-RHA}$; median and dispersion of shear force ratios of LRB supports are also shown in these figures. Similar to investigation the peak displacements and internal forces, the presented results show that the bearing responses predicted by both MPA-SRSS and MPA-CQC are able to follow the NL-RHA results whereas the first 'mode' alone is inadequate. With several 'modes' included as discussed early in this section, the shear forces along x- and y-axes of LRB systems estimated by the proposed extension of MPA procedure is generally similar to the results from NL-RHA.

The bias of MPA-SRSS and MPA-CQC in estimating shear forces along x- and y-axes of LRB systems is less than 10% for LMSR ground motions. Conversely, the bias of the one 'mode' pushover analysis in shear force estimation at an individual pier can be as large as 20%. However, the dispersion of three these procedures (the one 'mode' pushover analysis, MPA-SRSS, and MPA-CQC) in estimating LRB shear force demands is relatively large, 0.25 and 0.2 for shear forces along x- and y-axes, respectively. This is because the data points scatter over a wide range from significant underestimation to overestimation (Figures 5.35b-d, and 5.36b-d). The MPA-SRSS and MPA-CQC estimates are significantly inaccurate for several excitations, although the median values of shear forces S^*_{MPA} are close to 1. This is understood that the LRB system was driven far into the inelastic range by the set of LMSR strong ground motions. Consequently, more inelastic deformations have occurred and led to larger bias of the proposed extension of MPA procedure.

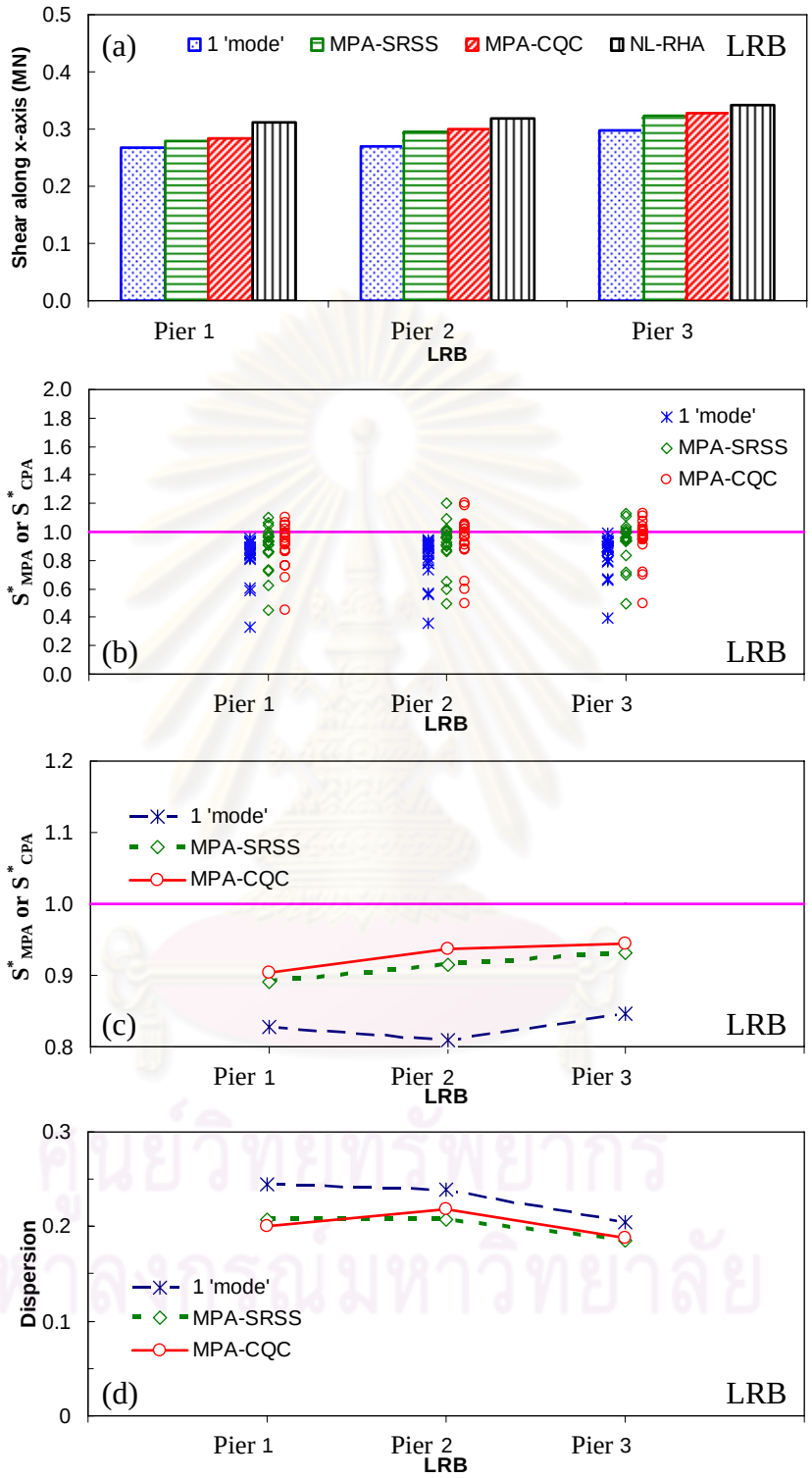

Figure 5.35 (a) Median shear forces along x-axis, (b) shear force along x-axis ratios, S^*_{MPA} or S^*_{CPA}, (c) median of shear force along x-axis ratios, and (d) dispersion of shear force along x-axis ratios of LRB supports subjected to the set of 20 LMSR ground motions.

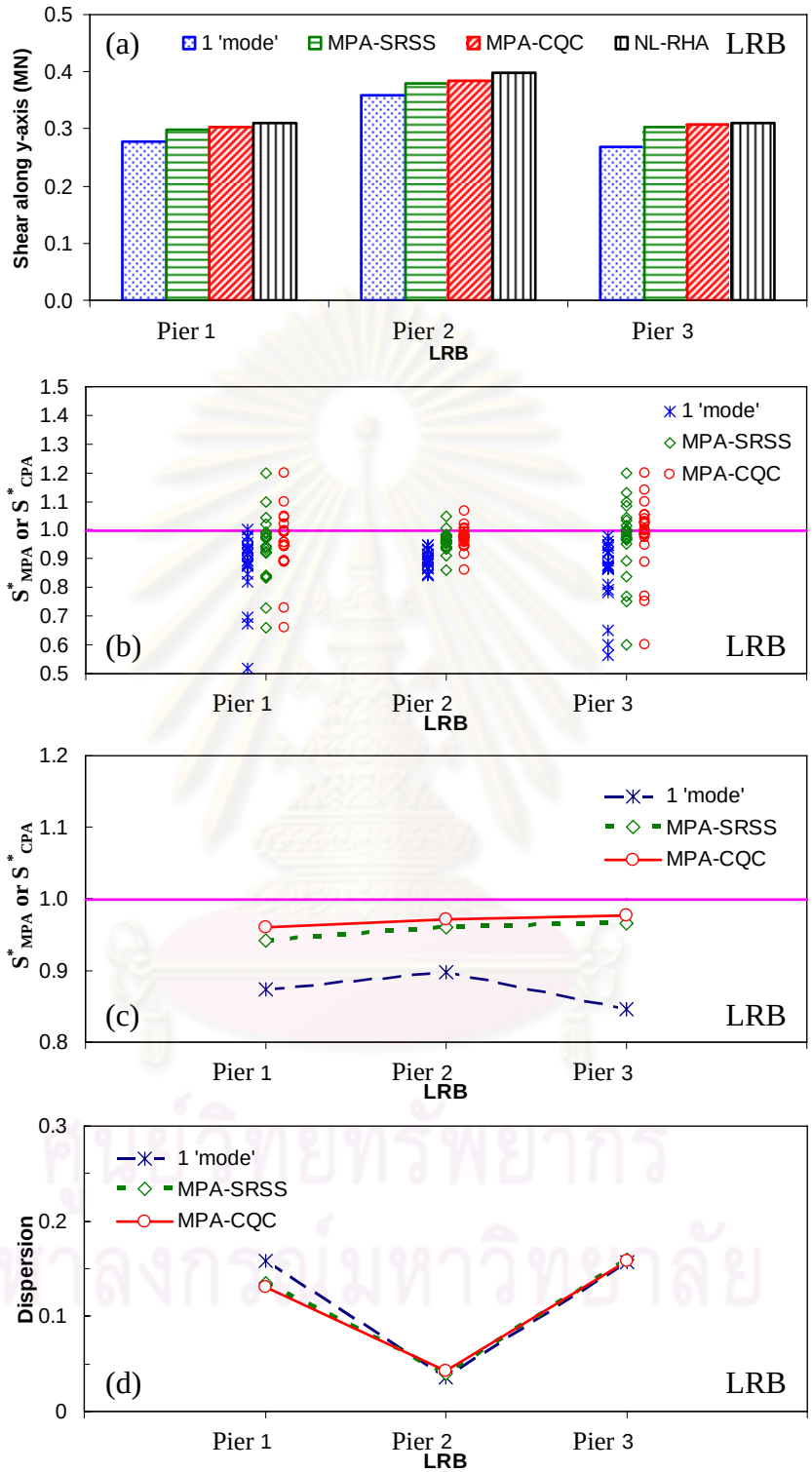

Figure 5.36 (a) Median shear forces along y-axis, (b) shear force along y-axis ratios, S^*_{MPA} or S^*_{CPA}, (c) median of shear force along y-axis ratios, and (d) dispersion of shear force along y-axis ratios of LRB supports subjected to the set of 20 LMSR ground motions.

CHAPTER VI

CONCLUSIONS AND RECOMMENDATIONS

6.1 Conclusions

6.1.1 Accuracy of Current Nonlinear Static Procedures for Seismic Analysis of BRBF Buildings

The following conclusions are obtained from the accuracy assessment of nonlinear static procedures (MPA, IMPA, and MPP) in estimating the seismic demands of buckling-restrained braced frame buildings using LA10/50 and LA2/50 sets of intense ground motions. These conclusions are based on a comparison of NSP estimates of seismic demands and the corresponding values determined by NL-RHA for 3-, 6-, 10-, and 14-story BRBF buildings which were designed to meet seismic code criteria.

(1) The equivalent bilinear SDF systems of nonlinear static procedures can estimate the peak roof displacement quite accurately with a bias no larger than 15% and 19% for LA10/50 and LA2/50 sets of ground motions, respectively. The IMPA tends to predict the median and dispersion of target roof displacements more accurately than MPA; however, the difference is not significant while the MPP tends to estimate the maximum roof displacements slightly more accurately than both MPA and IMPA for set of LA10/50 but less accurate for the stronger records LA2/50.

(2) The story drift demands predicted by MPA and IMPA are able to follow the NL-RHA results. However, the higher ‘modes’ contributions of these procedures in the response of 3-, and 6-story BRBF buildings are generally not significant, so the first ‘mode’ alone may be adequate.

(3) Despite considering the redistribution of inertia forces after structure yields, the pushover curve of IMPA is similar to MPA, resulting in nearly identical estimates of target roof displacements by both procedures. The IMPA tends to overlap the MPA in estimating story drifts with slight differences.

(4) The MPP tends to significantly overestimate seismic demands for lower stories but underestimates story drifts for upper stories with increasing bias when the building height increases. Moreover, the story drifts predicted by the MPP procedure seem to be uniform in upper stories, especially for 10- and 14-story BRBF buildings considered in this study.

(5) The bias and dispersion of nonlinear static procedures in estimating seismic demands tends to increase for taller BRBF buildings and stronger excitations. The height-wise variation of bias primarily depends on the structural properties, e.g., building height, rather than the intensity of ground motions.

(6) The bias of MPA and IMPA procedures in estimating the maximum story drift over all stories is generally small; however, the bias of these procedures in estimating peak story drift at an individual story can be considerable for certain cases. Both of these procedures provide practically similar results whereas MPA is slightly simpler and more practical than IMPA as it involves an invariant load pattern. On the contrary, the bias in estimating maximum story drifts over all stories of MPP can be large.

6.1.2 Accuracy of the Proposed Extension of MPA Procedure for Seismic Evaluation of Bridge

The median seismic demands for an existing continuous twin I-girder bridge due to an ensemble of 20 LMSR ground motions were computed by the conventional pushover analysis, the proposed extension of MPA and NL-RHA procedures and compared. The bias and dispersion of the proposed extension of MPA procedure are evaluated over a wide range of bridge responses from essentially within the linearly elastic range to far into the inelastic range. The presented results have led to the following conclusions:

(1) Types of bearings have a significant effect on the natural frequencies of the studied bridge especially with the first longitudinal mode. Mode shapes,

effective modal masses, and the order of vibration modes of bridges studied are also affected by the types of bearing supports.

(2) Many more modes may be required to accurately estimate the seismic demands in bridges, especially in transverse direction, compared to the case of buildings. The effective modal masses of higher modes are much lower than those of the fundamental modes in both the longitudinal and transverse directions. Additionally, the effective modal mass of many higher ‘modes’ are very small (say less than 0.1%) and the contributions of these modes are not significant. Therefore, the contributions of those modes should be neglected in MPA estimate to avoid a large computation.

(3) The number and types of modes to be included in MPA procedure depend on the response quantities of interest.

(4) Bearing supports have significant influence on the results of analyses. Pushover curves of the bridge supported by steel bearings are much stiffer than those of the bridge with LRB supports. This trend is clearly noticed in the longitudinal direction as the bridge response is dominated by the first mode where the superstructure slides over the bearings.

(5) The one ‘mode’ pushover analysis predicts the peak displacements and internal forces well in the longitudinal direction only (first longitudinal mode dominates), but it fails to accurately predict seismic demands in the transverse direction of the bridges studied. It is also demonstrated that the conventional pushover analysis procedure currently used by bridge engineers is inadequate for estimating seismic demands in the transverse direction of bridges.

(6) The contributions of higher modes in estimating seismic demands in the transverse direction of the bridges considered are significant, since higher ‘modes’ participate more actively, particularly towards both ends of the bridges. The seismic responses of the bridges predicted by the proposed extension of MPA procedure are able to capture the NL- RHA results, whereas the one ‘mode’ pushover analysis is inadequate. Both the MPA-SRSS and

MPA-CQC procedures can estimate the peak displacements and internal forces reasonably well with a tendency to slightly underestimate responses when compared to NL-RHA.

(7) Including response contribution of higher modes in estimating the peak responses in the longitudinal direction of the studied bridges is unaffected. Consequently, both the conventional pushover analysis and the proposed extension of MPA procedures provide estimates that are essentially identical, and are very close to those from the NL-RHA in estimating the median seismic demands of the bridges in the longitudinal direction.

(8) The bias of the proposed extension of MPA procedure is relatively small in estimating the peak longitudinal, vertical and transverse displacements of the bridges. However, the biases of the proposed extension of MPA procedure and the one ‘mode’ pushover analysis in estimating the torsional rotation of the deck near both ends of the bridge can be large in percentage.

(9) The bias of the proposed extension of MPA in estimating the peak displacements, pier drifts is generally small; conversely, the bias of the proposed extension of MPA in estimating hinge rotations at the base of piers of the bridge supported by steel bearings can be large for certain locations.

(10) The dispersion of the one ‘mode’ pushover analysis, MPA-SRSS, and MPA-CQC in estimating LRB shear force demands is relatively large, 0.25 and 0.2 for shear forces along x- and y-axes, respectively.

(11) The dispersions of the pier drift ratios for bridges determined by the one ‘mode’ pushover analysis procedure range from 5% for demand in the longitudinal direction to 20% for demand in the transverse direction. The dispersions of the pier drift ratios determined by the proposed extension of MPA procedure are smaller than 5% and 10% in the longitudinal and transverse directions, respectively. Dispersion tends to increase for seismic responses in the transverse direction as the contribution from the higher-modes becomes more significant.

(12) Comparing the bias and dispersion of the pier drifts, the internal forces in the transverse direction predicted by the proposed extension of MPA procedure, it is observed that the pier drifts can be estimated by MPA more accurately than internal force demands. It is shown that both the MPA-SRSS and MPA-CQC procedures provide estimates of peak total response that are very close to the peak response determined by exact NL-RHA.

(13) The proposed extension of MPA procedure is least biased in estimating hinge rotation demands for the bridge with LRB supports and relatively more biased for the bridge supported on steel bearings.

(14) The bias of the proposed extension of MPA procedure in estimating hinge rotations about x- and y-axes at the base of the piers of the bridge supported by steel bearings (SB) is relatively small; but the dispersions are quite large, 0.3 and 0.2 for hinge rotations about x- and y-axes, respectively. Both bias and dispersion of the proposed extension of MPA procedure in estimating the hinge rotations about x- and y-axes of the bridge equipped with LRB supports are small compared to those of the bridge with steel bearings, indicating that MPA-SRSS and MPA-CQC estimate the hinge rotation demands of the bridge with LRB accurately more often than the SB case.

(15) The MPA estimates combined by CQC are slightly more accurate than by SRSS rule. This is because the modes are coupled. Nevertheless, the couplings of modes are not significant for the first few modes in this case. Both versions of the proposed extension of MPA procedure using SRSS and CQC combination rules (MPA-SRSS, MPA-CQC) can accurately estimate the seismic demands of the bridges considered in this investigation.

6.2 Recommendations

Being an approximate method, the proposed extension of MPA procedure should obviously be evaluated comprehensively before practical application to bridge evaluation and design. More work is clearly required to further investigate the

accuracy and effectiveness of the MPA procedure for a wide range of bridges with different configuration, degree of irregularity, dynamic characteristics (in terms of higher mode significance, in particular bridges with important anti-symmetric and torsion modes), and ground motion ensembles. Since the MPA is expected to be even more valuable for the assessment of the actual inelastic response of bridges with significant higher modes.

REFERENCES

Abeysinghe, R.S., Gavaise, E., Rosignoli, M., and Tzaveas, T., 2002. Pushover analysis of inelastic seismic behaviour of Greveniotikos bridge. *Journal of bridge engineering*, ASCE 7(2): 115-126.

ADINA, 2000. *ADINA user interface (AUI) users guide, 900 node version*. Watertown (MA): ADINA R & D.

Ali, H. M., and Abdel-Ghaffar, A. M., 1995. Modeling the nonlinear seismic behavior of cable-stayed bridges with passive control bearings. *Computers and Structures* 54(3): 461-492.

Akkar, S., and Metin, A., 2007. Assessment of improved nonlinear static procedures in FEMA-440. *Journal of structural engineering,* ASCE 133(9): 1237-1246.

American Society of Civil Engineers (ASCE), 2000. *Prestandard and commentary for the seismic rehabilitation of buildings*. Washington, D.C: Federal Emergency Management Agency, FEMA-356.

Applied Technology Council (ATC), 1996. *Seismic evaluation and retrofit of concrete buildings: Volumes 1 and 2*. *Report no. ATC-40*. California: Redwood City.

Applied Technology Council (ATC), 1997. *NEHRP Guidelines for the seismic rehabilitation of buildings (FEMA-273), and NEHRP Commentary on the guidelines for seismic rehabilitation of buildings (FEMA-274)*. Washington, D.C: Building Seismic Safety Council, Federal Emergency Management Agency.

Applied Technology Council (ATC), 2005. *Improvement of inelastic seismic analysis procedures*. *Report FEMA-440*. Washington, D.C: Federal Emergency Management Agency.

Asgarian, B. and Shokrgozar, H.R., 2009. BRBF response modification factor. *Journal of constructional steel research* 65(2): 290-298.

ATC-32 1996a. *Improved seismic design criteria for California bridges: Provisional recommendation*. Applied Technology Council, Redwood City, California.

ATC-32 1996b. *Improved seismic design criteria for California bridges: Resource document*. Applied Technology Council, Redwood City, California.

Aydinoglu, M.N, 2004. An improved pushover procedure for engineering practice: incremental response spectrum analysis IRSA. *Proceedings of the international workshop: performance-based seismic design concepts and implementation*, Blend, Slovenia, 345-356.

Banerjee, S., and Shinozuka, M., 2007. Nonlinear Static Procedure for Seismic Vulnerability Assessment of Bridges. *Computer-Aided Civil and Infrastructure Engineering* 22: 293-305.

Barros, R.C., and Almeida, R., 2005. Pushover analysis of asymmetric three-dimensional building frames. *Journal of civil engineering and management* 11(1): 3-12.

Bessason, B., and Haflidason, E., 2004. Recorded and numerical strong motion response of a base-isolated bridge. *Earthquake Spectra* 20(2): 309-332.

Bobadilla, H., and Chopra, A.K., 2007. *Modal pushover analysis for seismic evaluation of reinforced concrete special moment resisting frame buildings. Report no. EERC 2007-01, Earthquake engineering research center*. California: University of California, Berkeley.

Bracci, J.M., Kunnath, S.K., and Reinhorn, A.M., 1997. Seismic performance and retrofit evaluation for reinforced concrete structures. *Journal of structural engineering*, ASCE 123(1): 3-10.

CEN, 2004a. *EC8/1-Eurocode 8: Design of structures for earthquake resistance – part 1: general rules, seismic actions and rules for buildings*. EN 1998-1:2004, CEN, Brussels.

CEN, 2004b. *EC8/2-Eurocode 8: Design of structures for earthquake resistance – part 2: bridges.* prEN 1998-2:200X draft 5(pr Stage 51), CEN, Brussels.

Chandrasekaran, S., and Roy, A., 2006. Seismic evaluation of multi-story RC frame using modal pushover analysis. *Nonlinear dynamics* 43: 329-342.

Chang, S. E., and Nojima, N., 2001. Measuring post-disaster transportation system performance: the 1995 Kobe earthquake in comparative perspective. *Transportation Research Part A* 35(6): 475-494.

Chen, Y., 1996. Modeling and analysis methods of bridges and their effects on seismic responses: I-Theory, *Computers & Structures* 59(1): 81-98.

Chintanapakdee, C. and Chopra, A.K., 2003a. Evaluation of modal pushover analysis using generic frames. *Earthquake engineering and structural dynamics* 32(3): 417-442.

Chintanapakdee, C. and Chopra, A.K., 2003b. *Evaluation of the modal pushover analysis procedure using vertically "regular" and irregular generic frames. Report no. EERC 2003-03, Earthquake Engineering and Research Center*. California: University of California, Berkeley.

Chintanapakdee, C., Nguyen, A.H., and Hayashikawa, T., 2009. Assessment of modal pushover analysis procedure for seismic evaluation of buckling-restrained braced frames. *The IES journal Part A: Civil & Structural Engineering* 2(3): 174-186.

Chopra, A.K., 2007. *Dynamics of Structures: Theory and Applications to Earthquake Engineering*. Third edition, Prentice Hall, Upper Saddle River, New Jersey, 876pp.

Chopra, A.K. and Chintanapakdee, C., 2004a. Evaluation of modal and FEMA pushover analyses: vertically "regular" and irregular generic frames. *Earthquake spectra* 20(1): 255-271.

Chopra, A.K., and Chintanapakdee, C., 2004b. Inelastic deformation ratios for design and evaluation of structures: single-degree-of-freedom bilinear system. *Journal of structural engineering,* ASCE 130(9): 1309-1319.

Chopra, A.K and Goel, R.K., 1999a. *Capacity-demand-diagram methods for estimating seismic deformation of inelastic structures: SDF systems. Report no. PEER-1999/02*, Pacific Earthquake Engineering Research Center, University of California, Berkeley.

Chopra, A.K and Goel, R.K., 1999b. Capacity-demand-diagram methods based on inelastic design spectrum. *Earthquake spectra* 15(4): 637-656.

Chopra, A.K. and Goel, R.K., 2000. Evaluation of NSP to estimate seismic deformation: SDF system. *Journal of structure engineering,* ASCE 126(4): 482-490.

Chopra, A.K. and Goel, R.K., 2002. A modal pushover analysis procedure for estimating seismic demands for buildings. *Earthquake engineering and structural dynamics* 31(3): 561-582.

Chopra, A.K. and Goel, R.K., 2004. A modal pushover analysis procedure to estimate seismic demands for unsymmetric-plan buildings. *Earthquake engineering and structural dynamics* 33(8): 903-927.

Chopra, A.K., Goel, R.K., and Chintanapakdee, C., 2001. *Statistics of SDF-system estimate of roof displacement for pushover analysis of buildings. PEER report no. 2001/16.* Pacific earthquake, Engineering research center, University of California, Berkeley, Calif.

Chopra, A.K., Goel, R.K., and Chintanapakdee, C., 2003. Statistics of single-degree-of-freedom estimate of displacement for pushover analysis of buildings. *Journal of structural engineering,* ASCE 129(4): 459-469.

Chopra, A.K.., Goel, R.K., and Chintanapakdee, C., 2004. Evaluation of a modified MPA procedure assuming higher modes as elastic to estimate seismic demands. *Earthquake spectra* 20(3): 757-778.

Computers and Structures Inc. (CSi), 1997. *SAP2000 analysis reference*. Computers and Structures: Berkeley, California.

Computers and Structures Inc. (CSi), 2006. *PERFORM 3D: Nonlinear Analysis and Performance Assessment for 3D Structures*. Computers and Structures: Berkeley, California.

DASSE DESIGN INC., 2007. Cost advantages of buckling restrained braced frame buildings. *Report no. 06B260,* San Francisco, California.

DesRoches, R., Choi, E., Leon, R. T., Dyke, S. J., and Aschheim, M., 2004. Seismic response of multiple span steel bridges in central and southeastern United States. I: As built. *Journal of Bridge Engineering,* ASCE 9(5): 464-472.

Dicleli, M., and Bruneau, M., 1995. Seismic performance of multispan simply supported slab-on-girder steel highway bridges. *Engineering Structures* 17(1): 4-14.

El-Tawil, S., and Deierlein, G.G., 2001a. Nonlinear analyses of mixed steel-concrete moment frames, Part I: Beam-column element formulation. *Journal of Structural Engineering,* ASCE 127(6): 647-655.

El-Tawil, S., and Deierlein, G.G., 2001b. Nonlinear analyses of mixed steel-concrete moment frames, Part II: Implementation and verification. *Journal of Structural Engineering*, ASCE 127(6): 656-665.

Erduran, E., 2008. Assessment of current nonlinear static procedures on the estimation of torsional effects in low-rise frame buildings. *Engineering structures* 30(9): 2548-2558.

Fajfar, P., 1999. Capacity spectrum method based on inelastic demand spectra. *Earthquake engineering and structural dynamics* 21: 837-848.

Fajfar, P., 2000a. A nonlinear analysis method for performance-based seismic design. *Earthquake spectra* 16 (3): 573-592.

Fajfar, P., 2000b. A practical nonlinear method for seismic performance evaluation. Advanced Technology in Structural Engineering. *Proceedings of Structural Congress*.

Fajfar, P., and Fischinger, M., 1987. Nonlinear seismic analysis of RC buildings: Implications of a case study. *European earthquake engineering* 1: 31-43.

Fajfar, P., and Fischinger, M., 1989. N2 - A method for nonlinear seismic analysis of regular buildings. *Proceeding of the ninth world conference on earthquake engineering*, Tokyo-Kyoto, Japan, 5: 111-116.

Fajfar, P., and Gaspersic, P., 1996. The N2 method for the seismic damage analysis of RC buildings. *Earthquake engineering and structural dynamics* 25: 23-67.

Fajfar, P., Gaspersic, P., and Drobnic, D., 1997. A simplified nonlinear method for seismic damage analysis of structures. *Seismic design methodologies for the next generation of codes*, Balkema, Rotterdam, 183-194.

Fajfar, P., Marusic, D., and Peruc, I., 2005. Torsional effects in the pushover-based seismic analysis of buildings. *Journal of earthquake engineering* 9(6): 831-854.

Freeman, S.A., Nicoletti, J.P., and Tyrell, J.V., 1975. Evaluations of existing buildings for seismic risk - A case syudy of Puget Sound Naval Shipyard, Bremerton, Washington. *Proceedings of 1st U.S. National Conference on Earthquake Engineering*, EERI, Berkeley, 113-122.

Freeman, S.A., 1978. Prediction of response of concrete buildings to serve earthquake motion. *Publication* SP-55, American Concrete Institute, Detroit, MI, 589-606.

Fumoto, K., Murakoshi, J., and Miyazaki, M., 2006. *Experimental Study on Vibration Characteristics of Steel Two Girder Bridges*. Report of the Structures Research Group, Public Works Research Institute, Tsukuba.

Goel, R.K., and Chopra, A.K., 2004a. Evaluation of modal and FEMA pushover analyses: SAC buildings. *Earthquake spectra* 20(1): 225-254.

Goel, R.K., and Chopra, A.K., 2004b. Extension of modal pushover analysis to compute member forces. *Earthquake spectra* 21(1): 125-139.

Goel, R.K., and Chopra, A.K., 2005. Modal pushover analysis for unsymmetric buildings. *Proceedings of the 2005 Structures Congress and the 2005 Forensic Engineering Symposium*, New York.

GT-STRUDL, 2000. *GT-STRUDL users manual, version 25*. Atlanta (GA): Georgia Tech Research Corporation.

Gupta, A., and Krawinkler, H., 1999. *Seismic demands for performance evaluation of steel moment resisting frame structures (SAC Task 5.4.3). Report No. 132, John A. Blume Earthquake Engineering Center*. California: Stanford University.

Gupta, B. and Kunnath, S.K., 2000. Adaptive spectra-based pushover procedure for seismic evaluation of structures. *Earthquake spectra* 16(2): 367-391.

Hashimoto, S., Abe, M., and Fujino, Y., 2005. Damage analysis of Hanshin Expressway viaducts during 1995 Kobe earthquake. III: Three-span continuous girder bridges. *Journal of Bridge Engineering,* ASCE 10(1): 61-68.

Hsu, H. L., and Chang, D. L., 2001. Upgrading the performance of steel box piers subjected to earthquakes. *Journal of Constructional Steel Research* 57(9): 945-958.

Hwang, J. S., and Chiou, J. M., 1996. An equivalent linear model of lead-rubber seismic isolation bearings. *Engineering Structures* 18(7): 528-536.

Huang, W., and Gould, P.L., 2007. 3-D pushover analysis of a collapsed reinforced concrete chimney. *Finite elements in analysis and design* 43(11-12): 879 – 887.

Irtem, E., and Hasgul, U., 2009. Investigation of effects of nonlinear static analysis procedures to performance evaluation on low-rise RC buildings. *Journal of Performance for Constructed Facilities*, ASCE 23(6): 456-466.

Isakovic, T., and Fischinger, M., 2006. Higher modes in simplified inelastic seismic analysis of single column bent viaducts. *Earthquake engineering and structural dynamics* 35: 95-114.

Isakovic, T., Lazaro, M.P.N., and Fischinger, M., 2008. Applicability of pushover methods for the seismic analysis of single column bent viaducts. *Earthquake engineering and structural dynamics* 37: 1185-1202.

Itani, A. M., Bruneau, M., Carden, L., and Buckle, I. G., 2004. Seismic behavior of steel girder bridge superstructures. *Journal of Bridge Engineering*, ASCE 9(3): 243-249.

Jangid, R.S., 2004. Seismic Response of Isolated Bridges. *Journal of Bridge Engineering*, ASCE 9(2): 156-166.

Japan Road Association (JRA), 1996. *Specification for Highway Bridges - Part V Seismic Design*. Tokyo, Maruzen.

Japan Society of Civil Engineers (JSCE), 1996. Committee of Earthquake Engineering: *The 1995 Hyogoken-Nanbu Earthquake, Investigation into Damage to Civil Engineering Structures*.

Jianmeng, M., Changhai, Z., and Lili, X., 2008. An improved modal pushover analysis procedure for estimating seismic demands of structures. *Earthquake engineering and Engineering vibration* 7(1): 25-31.

Julian, F.D.R., 2005. *Seismic performance of isolated curved highway viaducts equipped with unseating prevention cable restrainers*. Doctoral thesis, Hokkaido University, Sapporo, Japan.

Julian, F.D.R., Hayashikawa, T., and Obata, T. 2007. Seismic performance of isolated curved steel viaducts equipped with deck unseating prevention cable restrainers. *Journal of Constructional Steel Research* 63(2): 237-253.

Kalkan, E., and Kunnath, S.K., 2006. Adaptive modal combination procedure for nonlinear static analysis of building structures. *Structural Engineering* 132(11): 1721-1731.

Kalkan, E., and Kunnath, S.K., 2007. Assessment of current nonlinear static procedures for seismic evaluation of buildings. *Engineering Structures* 29(3): 305-316.

Keady, K. I., Alameddine, F., and Sardo, T. E., 1999. Chapter 43: Seismic retrofit technology. In: Chen, W. F., and Duan, editors. *Bridge Engineering Handbook*, Boca Raton, CRC Press.

Kilar, V., and Fajfar, P., 1997. Simple pushover analysis of asymmetric buildings. *Earthquake engineering and structural dynamics* 26: 233-249.

Kiggins, S., and Uang, C.M., 2006. Reducing residual drift of buckling-restrained braced frames as a dual system. *Engineering structures* 28(11): 1525-1553.

Kim, S.P., and Kurama, Y.C., 2008. An alternative pushover analysis procedure to estimate seismic displacement demands. *Engineering structures* 30(12): 3793-3807.

Kim, H., and Goel, S., 1992. Seismic evaluation and upgrading of braced frame structures for potential local failures. *UMCEE 92-24*, Dept. of Civil Engineering and Environmental Engineering, Univ. of Michigan, Ann Arbor.

Krawinkler, H., Alali, A., and Dunlea, J.M., 1995. Analysis of a damaged 4-story building and an undamaged 2-story building, SAC 95-04, part 1. *Technical report: Analytical and field investigations of buildings affected by the Northridge earthquake of January 17, 1994*, SAC Joint Venture.

Krawinkler, H., and Seneviratna, G.D.P.K., 1998. Pros and cons of a pushover analysis of seismic performance evaluation. *Engineering structures* 20(4-6): 452-464.

Kumar, G.R., Kumar, S.R.S., and Kalyanaraman, V., 2007. Behaviour of frames with non-buckling bracings under earthquake loading. *Journal of Constructional Steel Research* 63(2): 254-262.

Kunnath, S.K., and Kalkan, E., 2004. Evaluation of seismic deformation demands using nonlinear procedures in multistory steel and concrete moment frames. *ISET Journal of Earthquake Technology* 41(1): 159–182.

Mahin, S.A., 1998. Lessons from damage to steel buildings due to the Northridge earthquake. *Engineering structures* 20(4-6): 261-270.

MATLAB, 2007. *The Language of Technical Computing*. Version R2007a, The Mathworks Inc., Natick, Massachusetts.

Menoni, S., 2001. Chains of damages and failures in a metropolitan environment: some observations on the Kobe earthquake in 1995. *Journal of Hazardous Materials* 86(1-3): 101-119.

Moehle, J.P., 1995. Northridge earthquake of January 17, 1994: reconnaissance report, volume 1 - highway bridges and traffic management. *Earthquake Spectra* 11: 287-372.

Morishita, N., Maeno, H., Mori, N., and Ouchi, H., 2002. Experiments and applications of seismic characteristics of isolation bearings in urban highway viaducts. *Bridge and Foundations* 3: 39-46 (in Japanese).

Murakoshi, J., Fumoto, K., Ashizuka, K., Kiyota, R., and Miyazaki, M., 2006. *Experimental Study on Aerodynamic stability and vibration characteristics of steel two-girder bridges*. Report of the Structures Research Group, Public Works Research Institute, Tsukuba.

Nasim, K.S., Michael, D.S., David, I.M., and William, F.C., 2008. Evaluation of nonlinear static analysis methods and software tools for seismic analysis of highway bridges. *Engineering Structures* 30: 1335–1345.

Ngo-Tran, T.L., Hayashikawa, T., and Matsumoto, T., 2008. Three-dimensional bridge-vehicle interaction analysis of simply supported twin I-girder bridge. *Journal of Structural Engineering*, JSCE 54(A): 181-188.

Nguyen, A.H., Chintanapakdee, C., and Hayashikawa, T., 2010. Assessment of current nonlinear static procedures for seismic evaluation of BRBF buildings. *Journal of Constructional Steel Research* 66(8-9): 1118-1127.

Osteraas, J., and Krawinkler, H., 1989. The Mexico earthquake of September 19, 1985—behavior of steel buildings. *Earthquake spectra* 5(1): 51–88.

Pan, P., Zamfirescu, D., Nakashima, M., Nakayasu, N., and Kashiwa, H., 2005. Base-isolation design practice in Japan: Introduction to the post-Kobe approach. *Journal of Earthquake Engineering* 9(1): 147-171.

Paraskeva, T.S., Kappos, A. J., and Sextos, A. G., 2006. Extension of modal pushover analysis to seismic assessment of bridges. *Earthquake engineering and structural dynamics* 35(3): 1269–1293.

Pinho, R., Antoniou, S., Casarotti, C., and Lopez, M., 2006. A displacement-based adaptive pushover for assessment of buildings and bridges. *Advances in earthquake engineering for urban risk reduction* 66: 79-94.

Prakash, V., Powell, G.H. and Campbell, S., 1993. *DRAIN-2DX: Base program description and user guide. Report no. UCB/SEMM-93/17*. California: Department of Civil Engineering, University of California, Berkeley.

Rashidi, S., and Saadeghvaziri, A.M., 1997. Seismic modeling of multi-span simply-supported bridges using Adina. *Computers & Structures* 64(5-6): 1025-1039.

Roberts, J. M., 2005. Caltrans structural control for bridges in high-seismic zones. *Earthquake Engineering and Structural Dynamics* 34: 449-470.

Robinson, W. H., 1982. Lead rubber hysteretic bearings suitable for protecting structures during earthquakes. *Earthquake Engineering and Structural Dynamics* 10(4): 593-604.

Rose, A., and Lim, D., 2002. Business interruption losses from natural hazards: conceptual and methodological issues in the case of the Northridge earthquake. *Environmental Hazards* 4: 1-14.

Sabelli, R., Mahin, S.A. and Chang, C., 2003. Seismic demands on steel braced frame buildings with buckling restrained braces. *Engineering structures* 25(5): 655-666.

Salomon, O., Oller, S., and Barbat, A., 1999. Finite element analysis of base isolated buildings subjected to earthquake loads. *International Journal for Numerical Methods in Engineering* 46: 1741-1761.

Saiidi, M., and Sozen, M.A., 1981. Simple nonlinear seismic analysis of RC structures. *Journal of structural engineering*, ASCE 107: 937-952.

Sasaki, K.K., Freeman, S.A., and Paret, T.F., 1998. Multimode pushover procedure (MMP) – a method to identify the effects of higher modes in a pushover analysis. *Proceedings of the 6th US National Conference on Earthquake Engineering*, Seattle.

Sato, N., Kato, A., Fukushima, Y., and Iizuka, M., 2002. Shaking table tests on failure characteristics of base isolation system for a DFBR plant. *Nuclear Engineering and Design* 212: 293-305.

SC Solutions, 1998. *SC-Push3D user's guide*. Santa Clara (CA): SC solutions.

SEAOC, 2001. *Recommended Provision for Buckling-restrained braced frames*. Seismology and structural committee, Structural Engineers Association of Northern California: San Francisco, California.

Shattarat, N.K., Symans, M.D., McLean, D.I., and Cofer, W.F., 2008. Evaluation of nonlinear static analysis methods and software tools for seismic analysis of highway bridges. *Engineering structures* 30 (5): 1335-1345.

Shome, N. and Cornell, C.A., 1997. *Probabilistic Seismic Demand Analysis of Nonlinear Structures*. *Report No. RMS-35*. California: Stanford University.

Somerville, P., Smith, N., Punyamurthula, S. and Sun, J., 1997. *Development of ground motion time histories for phase 2 of the FEMA/SAC steel project*. *Report no. SAC/BD-97/04*. California: SAC Joint Venture, Sacramento.

Tamura, Y., Kawashiri, K., Ohgaki, K., and Sakugawa, K., 1998. Design of Chidorinosawa river bridge – A continuous composite two-girder bridge with PC slab. *Bridge and Foundation* 9: 18-22 (in Japanese).

Tanimura, S., Sato, T., Umeda, T., Mimura, K. and Yoshikawa, O., 2002. A note of dynamic fracture of the bridge bearing due to the great Hanshin-Awaji earthquake. *International Journal of Impact Engineering* 27(2): 153-160.

Tremblay, R., Bruneau, M., Nakashima, M., Prion, H.G.L., Filiatrault, A., and Devall, R., 1996. Seismic design of steel buildings: lessons from the 1995 Hyogo-ken Nanbu earthquake. *Canadian journal of civil engineering* 23(3): 727–756.

Turkington, D. H., Carr, A. J., Cooke, N., and Moss, P.J., 1989. Seismic design of bridges on lead-rubber bearings. *Journal of Structural Engineering*, ASCE 115(12): 3000-3016.

Uang, C.M., and Nakashima, M., 2003. *Steel buckling-restrained braced frames*. Earthquake engineering: Recent advances and applications, CRC Press, Boca Raton, FL.

Unjoh, S., 1999. Chapter 44: Seismic design practice in Japan. In: Chen, W. F., and Duan, editors. *Bridge Engineering Handbook*, Boca Raton, CRC Press.

Usami, T., and Kumar, S., 1998. Inelastic seismic design verification method for steel bridge piers using a damage index based hysteretic model. *Engineering Structures* 20(4-6): 472-480.

Yoshikawa, M., Hayashi, H., Kawakita, S., and Hayashida, M., 2000. Construction of Benten viaduct, rigid-frame bridge with seismic isolators at the foot of piers. *Cement and Concrete Composites* 22: 39-46.

Zhang, R., 1999. Chapter 41: Seismic isolation and supplemental energy dissipation. In: Chen, W. F., and Duan, editors. *Bridge Engineering Handbook*, Boca Raton, CRC Press.

Wilson, J. C., 2003. Repair of new long-span bridges damaged by the 1995 Kobe earthquake. *Journal of Performance of Constructed Facilities,* ASCE 17(4): 196-205.

APPENDICES

APPENDIX A

BILINEAR IDEALIZATION

In the MPA procedure presented in Chapter 2, the force-deformation $\left(F_{sn}/L_n - D_n\right)$ relation of equivalent inelastic SDF system is obtained from the pushover curve, the relationship between base-shear and displacement of the monitoring point ($V_{bn} - u_{rn}$). The pushover curve often consists of multi-linear segments as a result of successive yielding at different locations in the structure. Such multi-linear curve is usually idealized as bilinear curve to facilitate solution of Equation (2.14). The implementation of bilinear idealization in this study was presented by Chintanapakdee and Chopra, (2003b) adopted the criterion specified in FEMA-356 that the first linear segment shall intersect the actual curve at 60% of the (idealized) yield force; however, this criterion alone can not uniquely define a bilinear curve. Therefore, another widely used criterion was adopted that the strain energy (area under the curve) associated with the peak response has to be the same as for the actual curve. To impose the second criterion, the target roof displacement is needed, but not yet known, so the idealization process needs to implemented iteratively:

(1) Assume a trial target displacement of pushover analysis so that area under the pushover curve can be calculated.

(2) Obtain a bilinear curve that satisfies the two criteria (by any optimization algorithm, e.g., *fminsearch.m* function in MATLAB, 2007).

(3) Convert the idealized pushover curve to the $F_{sn}/L_n - D_n$ relation (Figure 2.2b) by utilizing Equation (2.23).

(4) Compute the peak deformation, D_n, of the *n*th-"mode" inelastic SDF system (Figure 2.2b) with force-deformation relation of Figure 2.2b by solving Equation (2.14), or from the inelastic response (or design) spectrum.

(5) Calculate the peak roof displacement u_{rno} associated with the nth-"mode" inelastic SDF system from Equation (2.21).

(6) Repeat steps (2)-(5) until the peak roof displacement is equal to the value in the previous iteration.

It was found that the idealized bilinear curve is sensitive to the target roof displacement assumed in Step 1, implying that, without the iteration presented above, target displacement varies randomly with the arbitrarily assumed target displacement in bilinear curve idealization; therefore the iteration should be implemented (Chintanapakdee and Chopra, 2003b).

APPENDIX B

MODE SHAPES OF THE STEEL BEARING BRIDGE

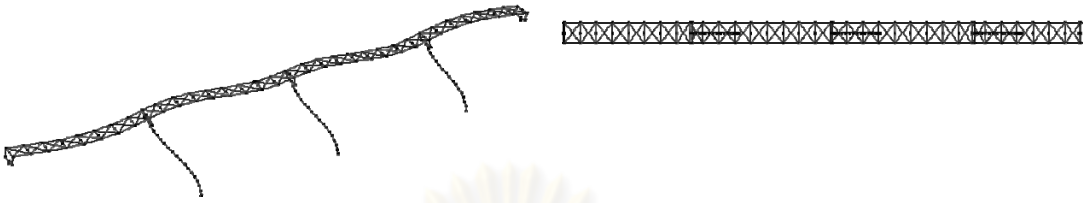

Three-dimensional view Plan view

Elevation view Side view

Mode 1 – The first longitudinal mode (L1): $T_1 = 1.750$ s, $M_1^* = 0.913, 0.000, 0.000$

Three-dimensional view Plan view

Elevation view Side view

Mode 2 – The first transverse mode (H1): $T_2 = 1.656$ s, $M_2^* = 0.000, 0.711, 0.000$

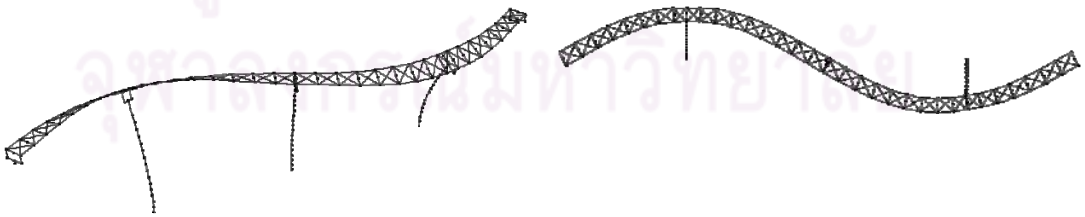

(a) Three-dimensional view (b) Plan view

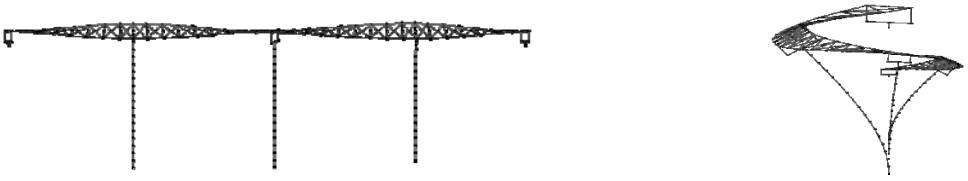

Elevation view Side view

Mode 3 – The second transverse mode (H2): $T_3 = 1.025$ s, $M_1^* = 0.000, 0.0006, 0.000$

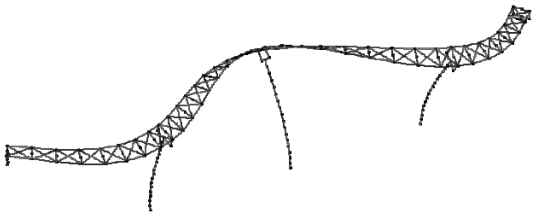

Three-dimensional view

Plan view

Elevation view

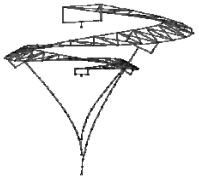

Side view

Mode 4 – The third transverse mode (H3): $T_4 = 0.619$ s, $M_4^* = 0.000, 0.0733, 0.000$

Three-dimensional view

Plan view

Elevation view

Side view

Mode 5 – The first vertical mode (V1): $T_5 = 0.526$ s, $M_5^* = 0.0021, 0.0000, 0.0054$

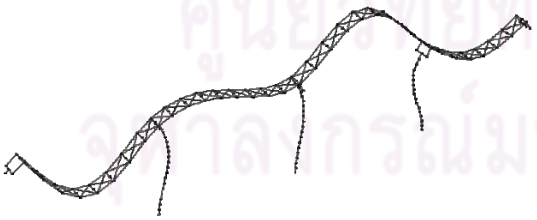

Three-dimensional view

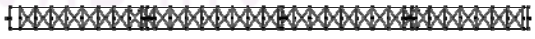

Plan view

Elevation view

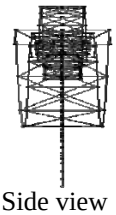

Side view

Mode 6 – The second vertical mode (V2): $T_6 = 0.455$ s, $M_6^* = 0.0003, 0.0000, 0.0014$

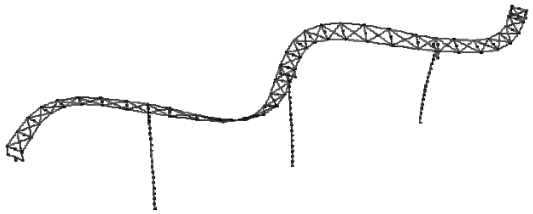

Three-dimensional view

Plan view

Elevation view

Side view

Mode 7 – The fourth transverse mode (H4): $T_7 = 0.416$ s, $M_7^* = 0.000, 0.000, 0.000$

Three-dimensional view

Plan view

Elevation view

Side view

Mode 8 – The third vertical mode (V3): $T_8 = 0.385$ s, $M_8^* = 0.0025, 0.0000, 0.2311$

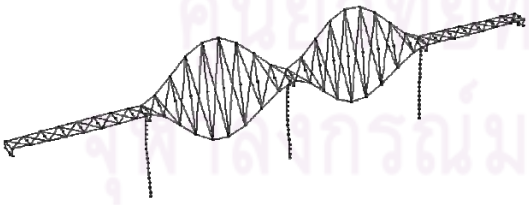

Three-dimensional view

Plan view

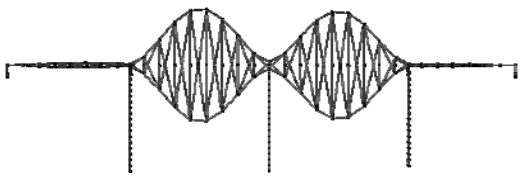

Elevation view

Side view

Mode 9 – The first torsional mode (T1): $T_9 = 0.374$ s, $M_9^* = 0.0000, 0.0057, 0.0000$

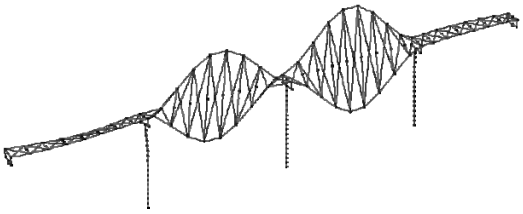

Three-dimensional view

Plan view

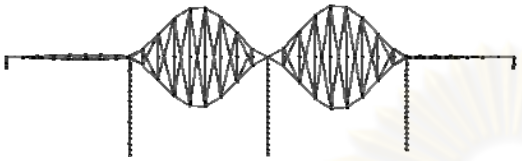

Elevation view

Side view

Mode 10 – The second torsional mode (T2): T_{10} = 0.367 s, $M_{10}^{*} = 0.0000, 0.0000, 0.0000$

Three-dimensional view

Plan view

Elevation view

Side view

Mode 11 – The fourth vertical mode (V4): T_{11} = 0.330 s, $M_{11}^{*} = 0.0020, 0.0000, 0.3390$

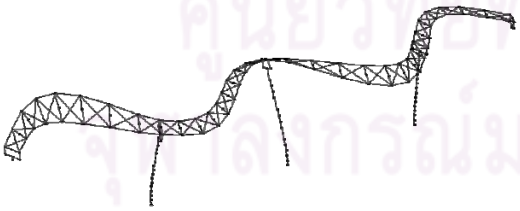

Three-dimensional view

Plan view

Elevation view

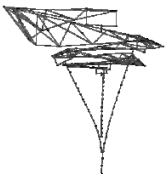

Side view

Mode 12 – The fifth transverse mode (H5): T_{12} = 0.319 s, $M_{12}^{*} = 0.0000, 0.0296, 0.0000$

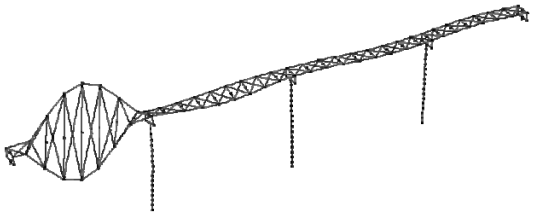

Three-dimensional view

Plan view

Elevation view

Side view

Mode 13 – The third torsional mode (T3): T_{13} = 0.295 s, $M_{13}^{*} = 0.0000, 0.0002, 0.0000$

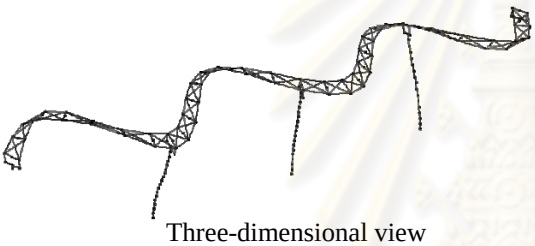

Three-dimensional view

Plan view

Elevation view

Side view

Mode 14 – The sixth transverse mode (H6): T_{14} = 0.261 s, $M_{14}^{*} = 0.0000, 0.0010, 0.0000$

Three-dimensional view

Plan view

Elevation view

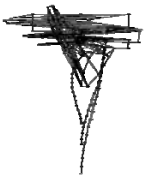

Side view

Mode 15 – The fourth torsional mode (T4): T_{15} = 0.233 s, $M_{15}^{*} = 0.0000, 0.0014, 0.0000$

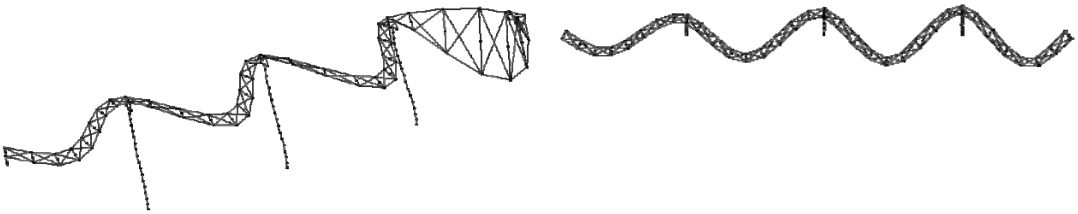

Three-dimensional view Plan view

Elevation view Side view

Mode 16 – The seventh transverse mode (H7): $T_{16} = 0.225$ s, $M_{16}^{*} = 0.0000, 0.0000, 0.0000$

Three-dimensional view Plan view

Elevation view Side view

Mode 17 – The second longitudinal mode (L2): $T_{17} = 0.203$ s, $M_{17}^{*} = 0.0001, 0.0000, 0.0000$

Three-dimensional view Plan view

Elevation view Side view

Mode 18 – The third longitudinal mode (L3): $T_{18} = 0.186$ s, $M_{18}^{*} = 0.0143, 0.0000, 0.0000$

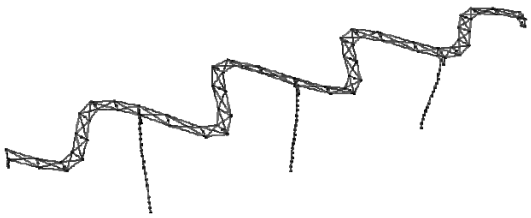

Three-dimensional view

Plan view

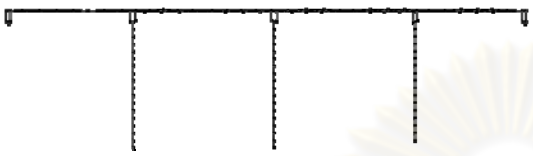

Elevation view

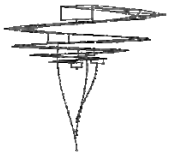

Side view

Mode 19 – The eighth transverse mode (H8): T_{19} = 0.184 s, $M_{19}^{*} = 0.0000, 0.0007, 0.0000$

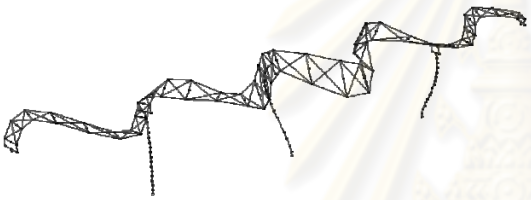

Three-dimensional view

Plan view

Elevation view

Side view

Mode 20 – The ninth transverse mode (H9): T_{20} = 0.165 s, $M_{20}^{*} = 0.0000, 0.0102, 0.0000$

Three-dimensional view

Plan view

Elevation view

Side view

Mode 21 – The fifth vertical mode (V5): T_{21} = 0.165 s, $M_{21}^{*} = 0.0000, 0.0000, 0.0003$

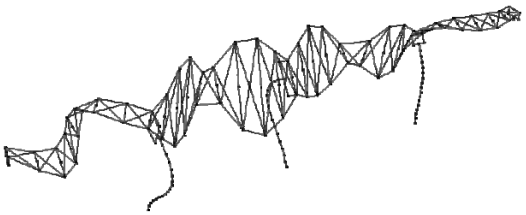

Three-dimensional view

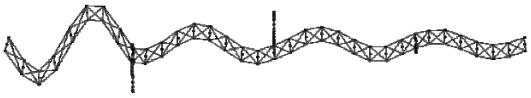

Plan view

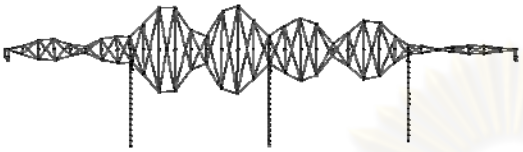

Elevation view

Side view

Mode 22 – The fifth torsional mode (T5): T_{22} = 0.162 s, $M_{22}^{*} = 0.0000, 0.0050, 0.0000$

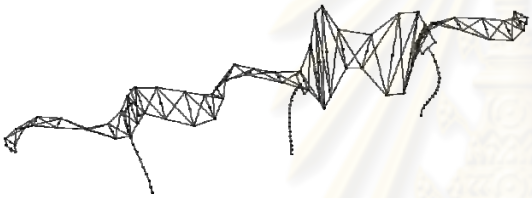

Three-dimensional view

Plan view

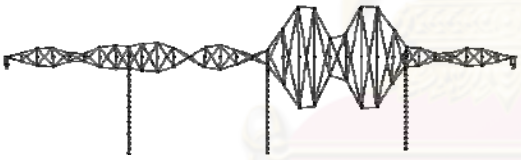

Elevation view

Side view

Mode 23 – The sixth torsional mode (T6): T_{23} = 0.153 s, $M_{23}^{*} = 0.0000, 0.0009, 0.0000$

Three-dimensional view

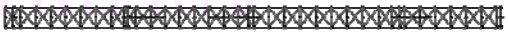

Plan view

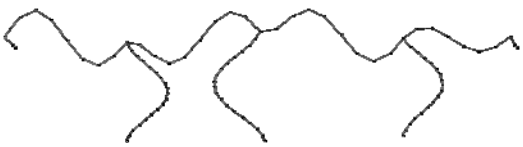

Elevation view

Side view

Mode 24 – The fourth longitudinal mode (L4): T_{24} = 0.151 s, $M_{24}^{*} = 0.0011, 0.0000, 0.0013$

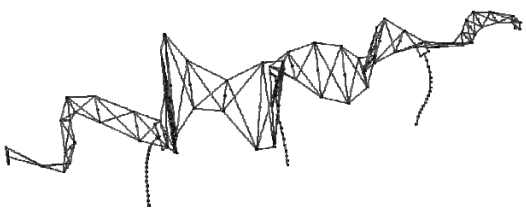

Three-dimensional view

Plan view

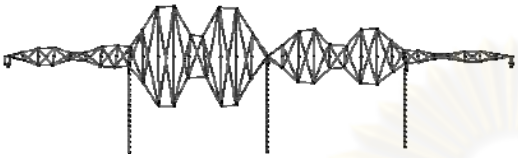

Elevation view

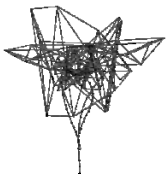

Side view

Mode 25 – The seventh torsional mode (T7): T_{25} = 0.149 s, $M_{25}^{*} = 0.0000, 0.0006, 0.0000$

Three-dimensional view

Plan view

Elevation view

Side view

Mode 26 – The tenth transverse mode (H10): T_{26} = 0.138 s, $M_{26}^{*} = 0.0000, 0.0142, 0.0000$

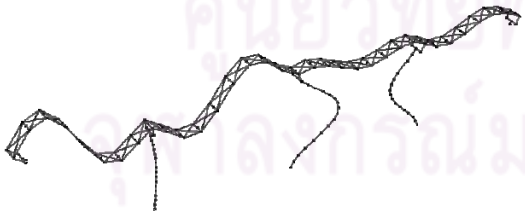

Three-dimensional view

Plan view

Elevation view

Side view

Mode 27 – The sixth vertical mode (V6): T_{27} = 0.138 s, $M_{27}^{*} = 0.0006, 0.0000, 0.0024$

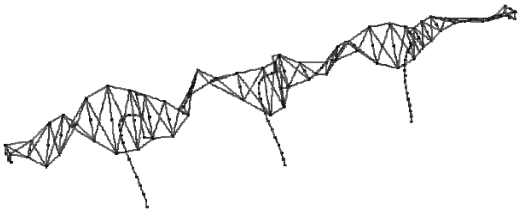

Three-dimensional view

Plan view

Elevation view

Side view

Mode 28 – The eleventh transverse mode (H11): T_{28} = 0.134 s, $M_{28}^{*} = 0.0000, 0.0204, 0.0000$

Three-dimensional view

Plan view

Elevation view

Side view

Mode 29 – The seventh vertical mode (V7): T_{29} = 0.129 s, $M_{29}^{*} = 0.0001, 0.0000, 0.0022$

Three-dimensional view

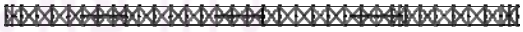

Plan view

Elevation view

Side view

Mode 30 – The fifth longitudinal mode (L5): T_{30} = 0.128 s, $M_{30}^{*} = 0.0219, 0.0000, 0.0015$

APPENDIX C

MODE SHAPES OF THE LRB BRIDGE

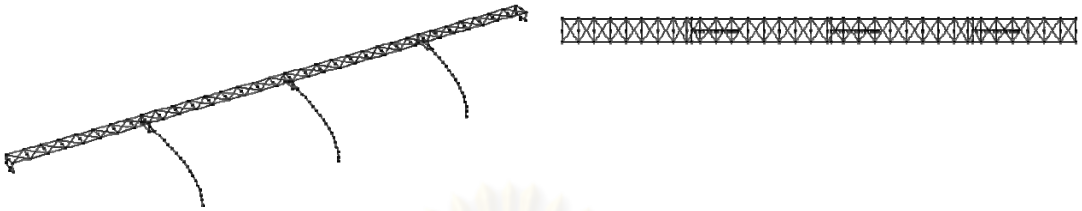

Three-dimensional view Plan view

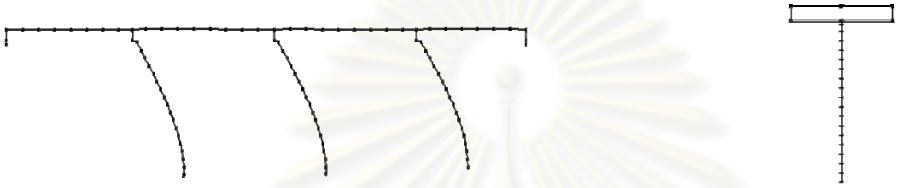

Elevation view Side view

Mode 1 – The first longitudinal mode (L1): $T_1 = 3.019$ s, $M_1^* = 0.8977, 0.000, 0.000$

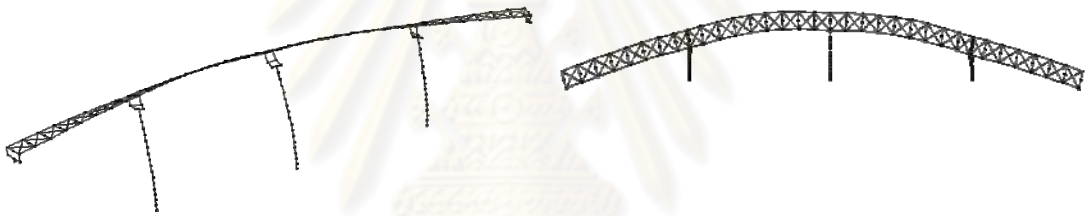

Three-dimensional view Plan view

Elevation view Side view

Mode 2 – The first transverse mode (H1): $T_2 = 1.809$ s, $M_2^* = 0.000, 0.6998, 0.000$

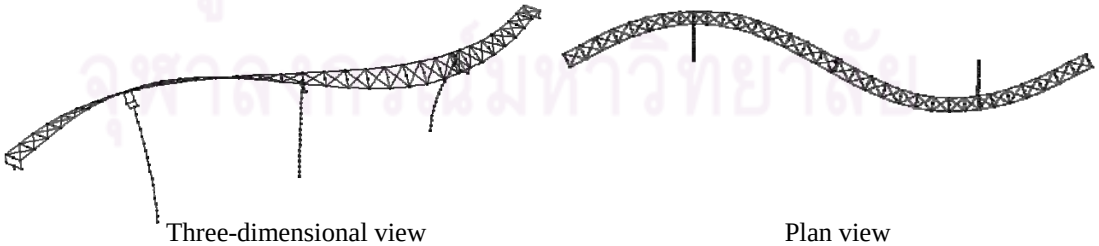

Three-dimensional view Plan view

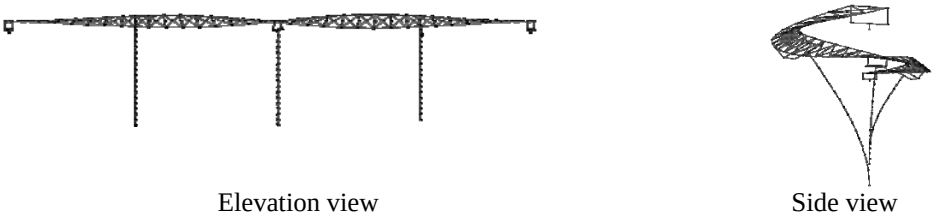

Elevation view Side view

Mode 3 – The second transverse mode (H2): $T_3 = 1.062$ s, $M_3^* = 0.000, 0.0003, 0.000$

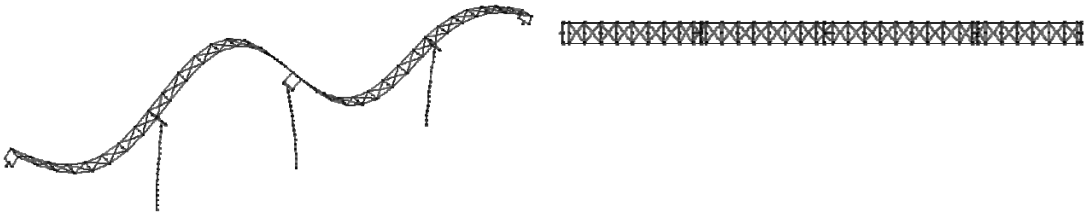

Three-dimensional view Plan view

Elevation view Side view

Mode 4 – The first vertical mode (V1): $T_4 = 0.661$ s, $M_4^* = 0.000, 0.000, 0.0027$

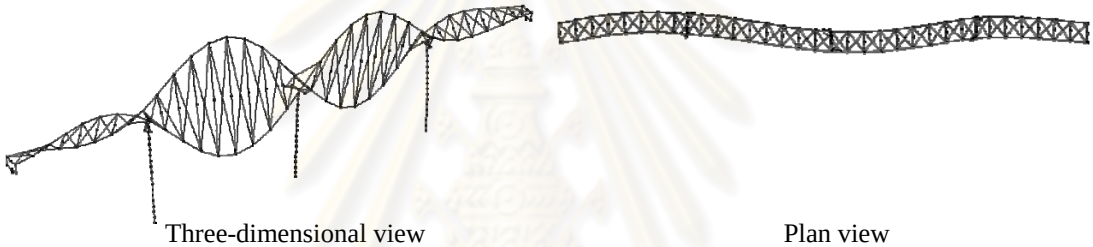

Three-dimensional view Plan view

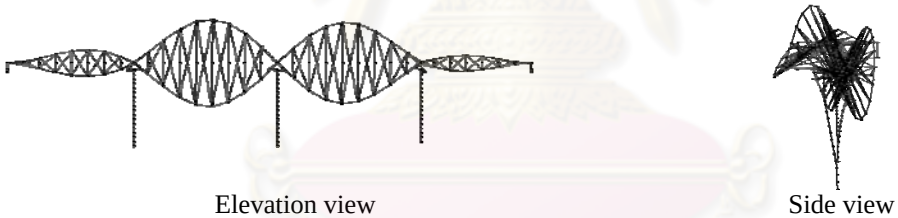

Elevation view Side view

Mode 5 – The first torsional mode (T1): $T_5 = 0.640$ s, $M_5^* = 0.000, 0.0022, 0.000$

Three-dimensional view Plan view

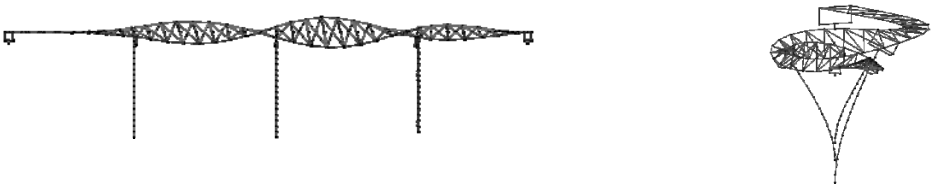

Elevation view Side view

Mode 6 – The third transverse mode (H3): $T_6 = 0.624$ s, $M_6^* = 0.000, 0.0724, 0.000$

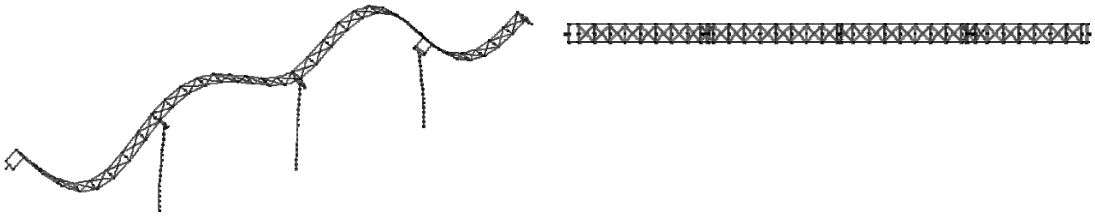

Three-dimensional view Plan view

Elevation view Side view

Mode 7 – The second vertical mode (V2): $T_7 = 0.515$ s, $M_7^* = 0.0000, 0.0000, 0.0000$

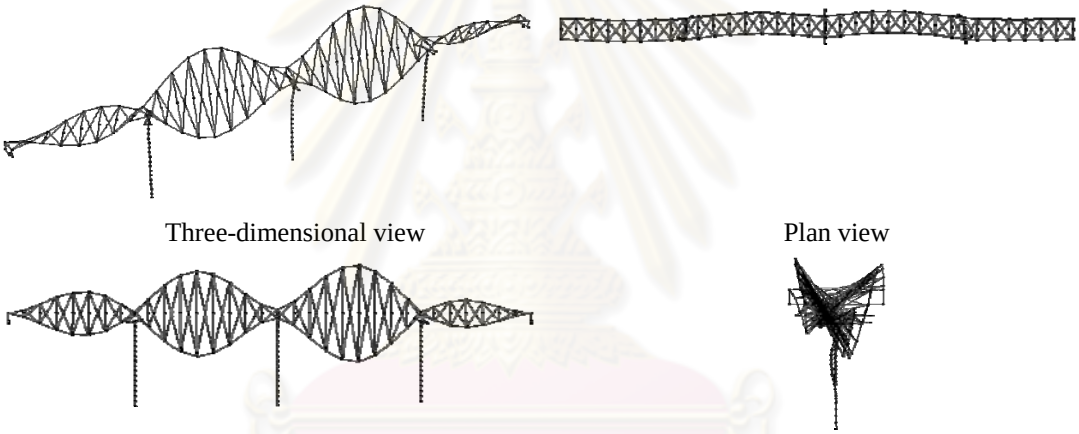

Three-dimensional view Plan view

Elevation view Side view

Mode 8 – The second torsional mode (T2): $T_8 = 0.474$ s, $M_8^* = 0.0000, 0.0021, 0.0000$

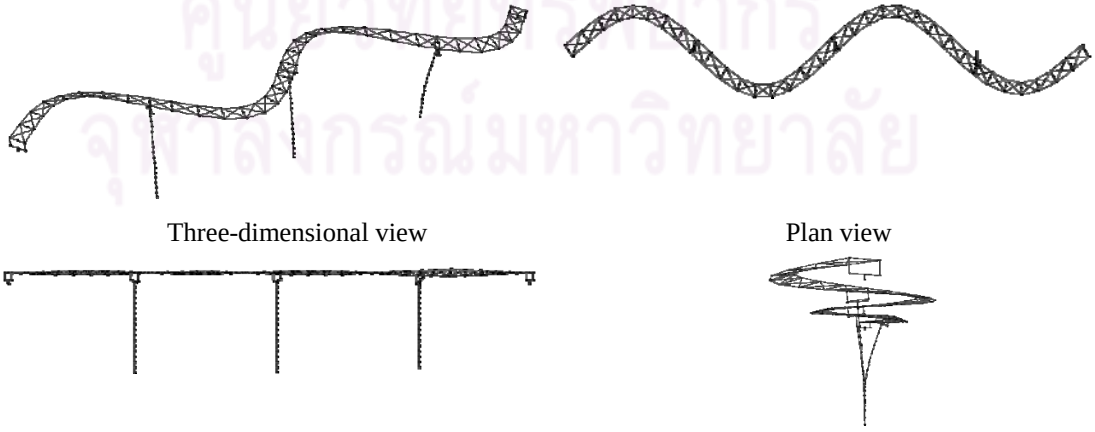

Three-dimensional view Plan view

Elevation view Side view

Mode 9 – The fourth transverse mode (H4): $T_9 = 0.423$ s, $M_9^* = 0.0000, 0.0000, 0.0000$

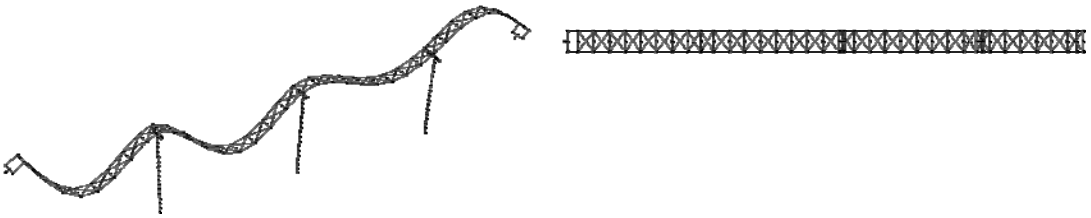

Three-dimensional view Plan view

Elevation view Side view

Mode 10 – The third vertical mode (V3): T_{10} = 0.408 s, $M_{10}^{*} = 0.0001, 0.0000, 0.1949$

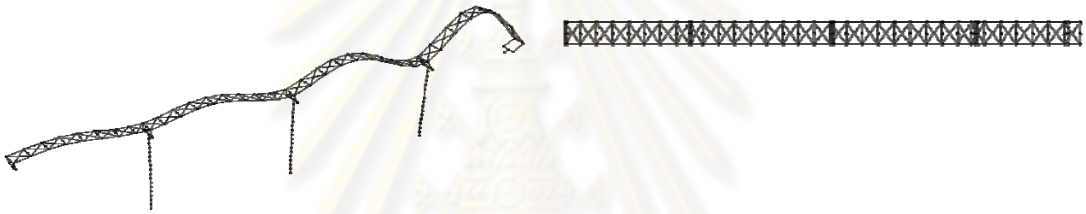

Three-dimensional view Plan view

Elevation view Side view

Mode 11 – The fourth vertical mode (V4): T_{11} = 0.347 s, $M_{11}^{*} = 0.0001, 0.0000, 0.4086$

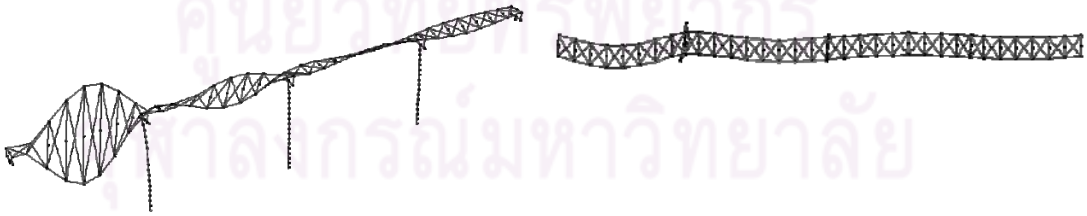

Three-dimensional view Plan view

Elevation view Side view

Mode 12 – The third torsional mode (T3): T_{12} = 0.341 s, $M_{12}^{*} = 0.0000, 0.0035, 0.0000$

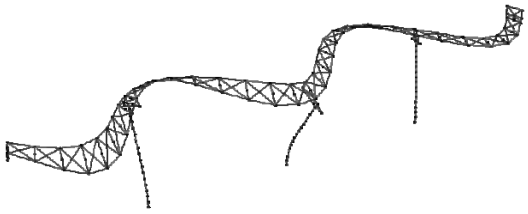

Three-dimensional view

Plan view

Elevation view

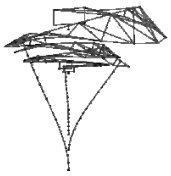

Side view

Mode 13 – The fifth transverse mode (H5): T_{13} = 0.323 s, $M_{13}^{*} = 0.0000, 0.0256, 0.0000$

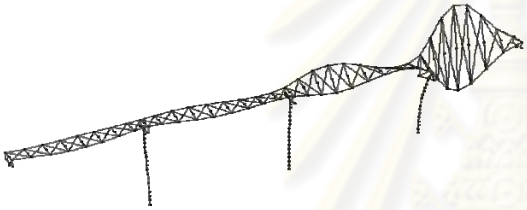

Three-dimensional view

Plan view

Elevation view

Side view

Mode 14 – The fourth torsional mode (T4): T_{14} = 0.277 s, $M_{14}^{*} = 0.0000, 0.0018, 0.0000$

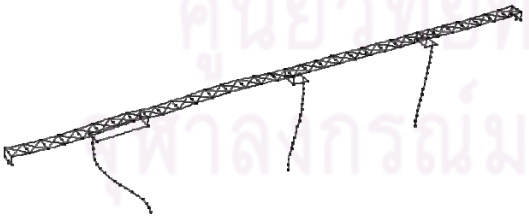

Three-dimensional view

Plan view

Elevation view

Side view

Mode 15 – The second longitudinal mode (L2): T_{15} = 0.270 s, $M_{15}^{*} = 0.0021, 0.0000, 0.0000$

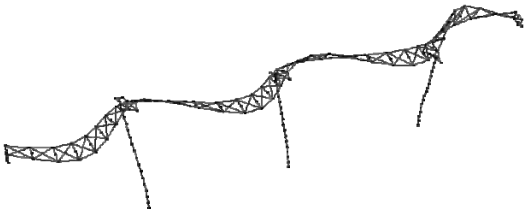

Three-dimensional view

Plan view

Elevation view

Side view

Mode 16 – The sixth transverse mode (H6): T_{16} = 0.268 s, $M_{16}^{*} = 0.0000, 0.0024, 0.0000$

Three-dimensional view

Plan view

Elevation view

Side view

Mode 17 – The third longitudinal mode (L3): T_{17} = 0.264 s, $M_{17}^{*} = 0.0105, 0.0000, 0.0000$

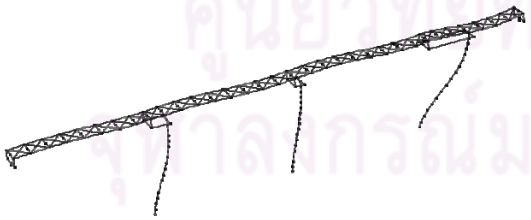

Three-dimensional view

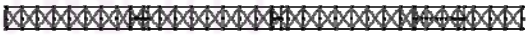

Plan view

Elevation view

Side view

Mode 18 – The fourth longitudinal mode (L4): T_{18} = 0.251 s, $M_{18}^{*} = 0.0238, 0.0000, 0.0003$

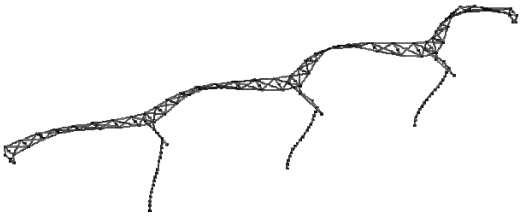

Three-dimensional view

Plan view

Elevation view

Side view

Mode 19 – The seventh transverse mode (H7): T_{19} = 0.241 s, $M_{19}^{*} = 0.0000, 0.0084, 0.0000$

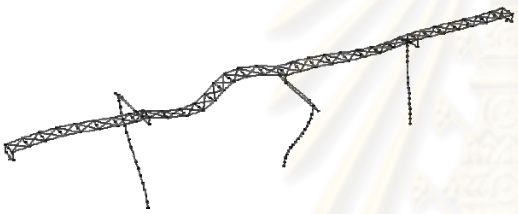

Three-dimensional view

Plan view

Elevation view

Side view

Mode 20 – The eighth transverse mode (H8): T_{20} = 0.216 s, $M_{20}^{*} = 0.0000, 0.0006, 0.0000$

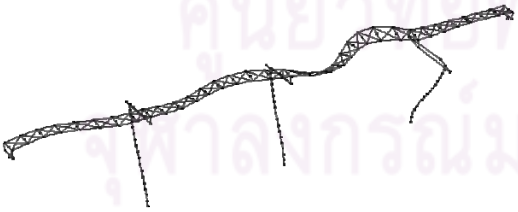

Three-dimensional view

Plan view

Elevation view

Side view

Mode 21 – The ninth transverse mode (H9): T_{21} = 0.209 s, $M_{21}^{*} = 0.0000, 0.0009, 0.0000$

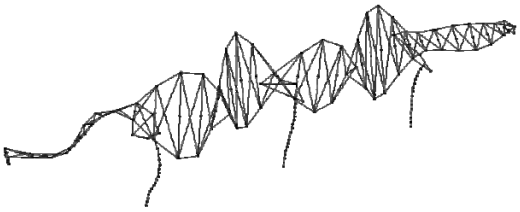

Three-dimensional view

Plan view

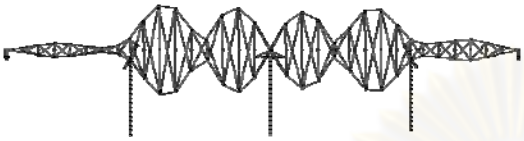

Elevation view

Side view

Mode 22 – The fifth torsional mode (T5): T_{22} = 0.195 s, $M_{22}^{*} = 0.0000, 0.0071, 0.0000$

Three-dimensional view

Plan view

Elevation view

Side view

Mode 23 – The tenth transverse mode (H10): T_{23} = 0.193 s, $M_{23}^{*} = 0.0000, 0.0320, 0.0000$

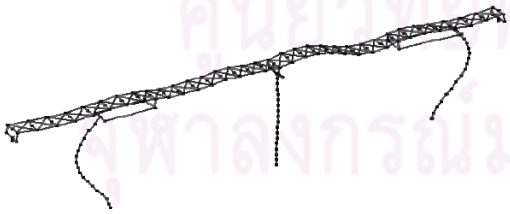

Three-dimensional view

Plan view

Elevation view

Side view

Mode 24 – The fifth longitudinal mode (L5): T_{24} = 0.189 s, $M_{24}^{*} = 0.0000, 0.0000, 0.0000$

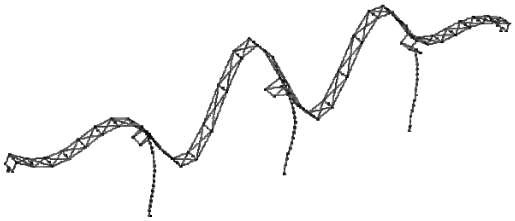

Three-dimensional view

Plan view

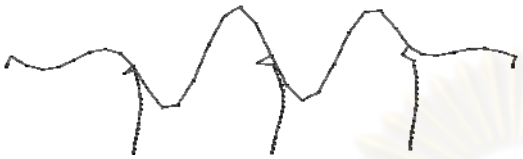

Elevation view

Side view

Mode 25 – The fifth vertical mode (V5): T_{25} = 0.184 s, $M_{25}^{*} = 0.0007, 0.0000, 0.0003$

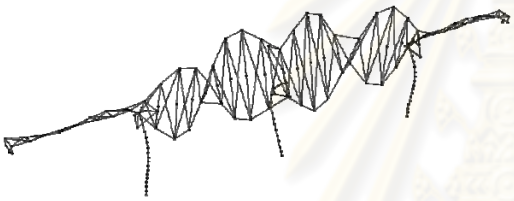

Three-dimensional view

Plan view

Elevation view

Side view

Mode 26 – The sixth torsional mode (T6): T_{26} = 0.183 s, $M_{26}^{*} = 0.0000, 0.0000, 0.0000$

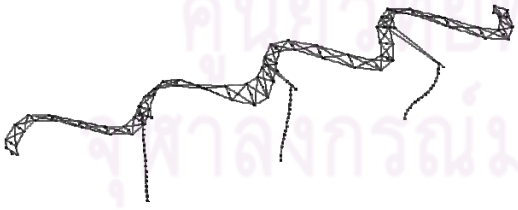

Three-dimensional view

Plan view

Elevation view

Side view

Mode 27 – The eleventh transverse mode (H11): T_{27} = 0.178 s, $M_{27}^{*} = 0.0000, 0.0066, 0.0000$

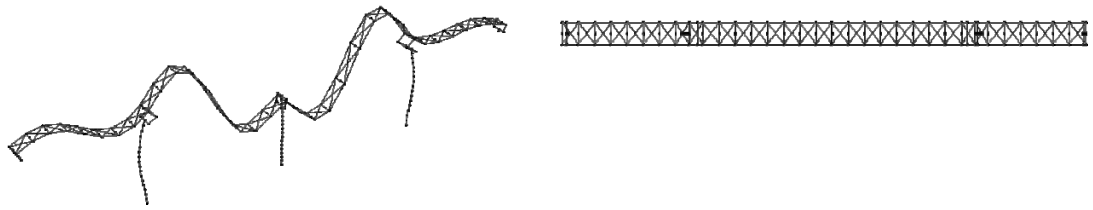

Three-dimensional view Plan view

Elevation view Side view

Mode 28 – The sixth vertical mode (V6): T_{28} = 0.170 s, $M_{28}^{*} = 0.0000, 0.0000, 0.0000$

Three-dimensional view Plan view

Elevation view Side view

Mode 29 – The twelfth transverse mode (H12): T_{29} = 0.159 s, $M_{29}^{*} = 0.0000, 0.0021, 0.0000$

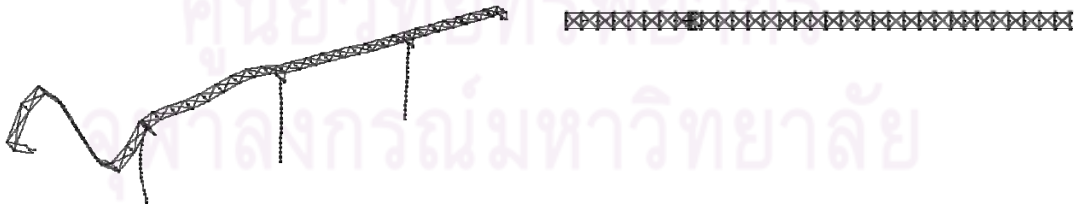

Three-dimensional view Plan view

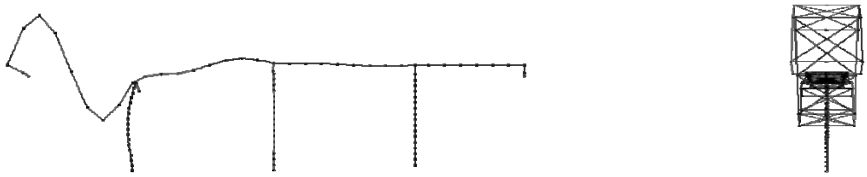

Elevation view Side view

Mode 30 – The seventh vertical mode (V7): T_{30} = 0.151 s, $M_{30}^{*} = 0.0000, 0.0000, 0.0100$

BIOGRAPHY

Mr. An Hong Nguyen was born in Dong Thap, Vietnam on July 20th, 1979. He graduated high school from senior high Nguyen Du located in Ninh Thuan province. He then entered Ho Chi Minh City University of Technology, Vietnam and obtained Bachelor Degree with honor in Civil Engineering in 2002. During these years in university, he had won several national prizes: a bronze medal in Strength of Materials and a silver medal in Structural Mechanics at the National Mechanics Olympic Competition in 2000 and 2001, respectively. He worked as an assistant lecturer of Department of Civil Engineering after the graduation at the same school.

In 2005, concurrent with his position at University of Technology, Mr. An Hong Nguyen received a M.Eng. degree in Civil Engineering from University of Technology under Sandwich program sponsored by Osaka Sangyo University, Japan. He became a lecturer at Department of Civil Engineering in that university.

In 2007, with the sponsorship from Japan International Cooperation Agency (JICA) through the ASEAN University Network/ Southeast Asia Engineering Education Development Network (AUN/SEED-Net), Mr. An Hong Nguyen continued to pursue his goal in education by entering in Ph.D. program in his major of Civil Engineering. He spent most of his time researching in Chulalongkorn University, Thailand and 10 months (Aug., 2009 – Jun., 2010) in Hokkaido University, Japan. His research interests include various areas of earthquake engineering and vibration.